DEVELOPMENT OF THULIUM-DOPED AND CO-DOPED FIBER LASERS FOR 1.9 MICRON REGION OPERATION

NORAZLINA BINTI SAIDIN

THESIS SUBMITTED IN FULFILLMENT OF THE REQUIREMENT FOR THE DEGREE OF DOCTOR OF PHILOSOPHY

FACULTY OF ENGINEERING
UNIVERSITY OF MALAYA
KUALA LUMPUR

2015

UNIVERSITI MALAYA

ORIGINAL LITERARY WORK DECLARATION

Name of Candidate: **Norazlina binti Saidin**

Registration/Matric No: **KHA 100086**

Name of Degree: **Doctor of Philosophy**

Title of Project Paper/Research Report/Dissertation/Thesis ("this Work"):

Development of Thulium-doped and Co-doped Fiber Lasers for 1.9 micron Region Operation

Field of Study: **Fiber Optics**

I do solemnly and sincerely declare that:

(1) I am the sole author/writer of this Work;
(2) This Work is original;
(3) Any use of any work in which copyright exists was done by way of fair dealing and for permitted purposes and any excerpt or extract from, or reference to or reproduction of any copyright work has been disclosed expressly and sufficiently and the title of the Work and its authorship have been acknowledged in this Work;
(4) I do not have any actual knowledge nor do I ought reasonably to know that the making of this work constitutes an infringement of any copyright work;
(5) I hereby assign all and every rights in the copyright to this Work to the University of Malaya ("UM"), who henceforth shall be owner of the copyright in this Work and that any reproduction or use in any form or by any means whatsoever is prohibited without the written consent of UM having been first had and obtained;
(6) I am fully aware that if in the course of making this Work I have infringed any copyright whether intentionally or otherwise, I may be subject to legal action or any other action as may be determined by UM.

Candidate's Signature Date

Subscribed and solemnly declared before,

Witness's Signature Date

Name:
Designation:

ABSTRACT

1.9 μm fiber lasers offer numerous applications in the area of spectroscopy, military and medical field. Thulium doped fiber has been used in order to realize laser applications in this region. Various methods have been implemented to achieve high output power as well as low threshold pump power for the laser's applications. Other than being used for continuous wave operation, pulse lasers are also important in various fields of applications including high-precision material processing, bio-medicine and ranging. This thesis thoroughly describes the development of 1.9 μm fiber lasers based on thulium doped and co-doped fibers as the gain medium. Two different co-doped fibers; ytterbium-thulium co-doped fiber (YTDF) and thulium-bismuth co-doped fiber (TBF) is investigated.

A lasing action was successfully obtained at the 1901.6 nm wavelength using two YTDF samples with different Ytterbium and Thulium concentration based on the cladding pumping technique. Higher ytterbium to thulium concentration ratio exhibits better lasing efficiency and threshold pump power which utilizes a linear configuration device pumped by a 931 nm pumping wavelength. The enhancement of lasing performance has been identified in TBF compared to YTDF and commercial thulium doped fiber (TDF). By using three TBF samples (TB1, TB2, TB3), TB2 which contains the highest amount of active bismuth and thulium concentrations, exhibit the best lasing efficiency of 42.2% at a threshold pump power of 92 mW by employing a 0.4 m long fiber. The energy transfer process can be optimized by adjusting the dopants compositions thus increasing the efficiency of the stepwise energy transfer.

An all-fiber 1.9 μm Q-switched laser has been successfully constructed using commercial TDF and TBF as the gain medium in a ring cavity configuration. Reliable self-starting Q-switched lasers based on graphene saturable absorber (GSA) and multi-walled carbon nanotube saturable absorber (MWCNT-SA) were observed. Both of the

GSA and MWCNT-SA were fabricated in-house using new preparation method. The best Q-switched laser was generated by a 1.5 m long TB2 in conjunction with the MWCNT-SA. A wide pump power range of 500 mW to 800 mW with the highest repetition rate and lowest pulse duration of 61.99 kHz and 4.0 μs, respectively have been achieved using a 1552 nm pumping wavelength. Besides that, an all-fiber ring cavity configuration is significant for the compatibility of silica host with standard optical components. Compared to the other 2 μm Q-switched fiber laser, the proposed laser configuration is simpler and more compact.

ABSTRAK

Peranti laser gentian pada gelombang 1.9 μm menawarkan pelbagai aplikasi dalam pelbagai bidang seperti spektroskopi, ketenteraan dan perubatan. Gentian thulium dop telah digunakan bagi merealisasikan aplikasi laser pada gelombang ini. Pelbagai kaedah telah digunakan untuk menghasilkan kuasa keluaran yang tinggi dan had kuasa yang rendah untuk penghasilan laser. Selain gelombang berterusan, denyut laser juga penting dalam pelbagai bidang aplikasi seperti aplikasi menggunakan ketepatan tinggi dalam bidang pemprosesan bahan, bio-perubatan dan juga pengesanan. Tesis ini menghuraikan tentang penghasilan 1.9 μm laser gentian dengan menggunakan gentian thulium dop dan gentian thulium dop-bersama yang lain sebagai medium gandaan. Dua jenis gentian yang digunakan iaitu gentian ytterbium-thulium dop-bersama (YTDF) dan gentian thulium-bismuth dop-bersama (TBF) telah diselidiki.

Laser gentian telah berjaya diperolehi pada gelombang 1901.6 nm dengan menggunakan dua sampel YTDF yang mempunyai perbezaan kepekatan ion ytterbium dan thulium berdasarkan teknik '*cladding pumping*'. Nisbah ytterbium kepada thulium yang tertinggi telah menghasilkan kecekapan laser dan had kuasa penghasilan laser yang lebih baik. Penghasilan laser ini menggunakan konfigurasi linear yang di jana oleh 931 nm pam. Peningkatan prestasi laser gentian telah dikenal pasti dengan menggunakan TBF berbanding YTDF dan gentian thulium dop konvensional (TDF). Dengan menggunakan tiga sampel TBF (TB1, TB2, TB3), TB2 yang mempunyai jumlah kepekatan ion tertinggi dalam bismuth aktif dan juga thulium menghasilkan kecekapan tertinggi iaitu 42.2% dengan had kuasa pam 92 mW menggunakan 0.4 m panjang gentian. Proses pemindahan tenaga boleh dioptimumkan dengan menyesuaikan komposisi doping dan seterusnya meningkatkan kecekapan pemindahan tenaga.

1.9 μm denyut laser gentian telah berjaya diselidiki dengan menggunakan dua jenis medium gandaan yang berbeza iaitu TDF komersial dan TBF dalam konfigurasi

gelang resonator. Denyut laser gentian diperolehi dengan menggunakan graphene penyerap saturable (GSA) dan tiub nano-karbon '*multi-wall'* penyerap saturable (MWCNT-SA). Kedua-dua penyerap saturable GSA dan MWCNT di fabrikasikan di makmal menggunakan teknik terkini. Prestasi laser terbaik telah dihasilkan oleh gentian TB2 yang mempunyai panjang 1.5 m menggunakan MWCNTs-SA. Julat kuasa pam yg besar iaitu 500 mW ke 800 mW dengan kadar pengulangan yang tinggi sebanyak 61.99 kHz serta masa denyutan yang pendek iaitu 4.0 μs telah dicapai dengan menggunakan 1552 nm pam. Di samping itu, konfigurasi gelang gentian resonator adalah penting untuk penggunaan bersama komponen optik yang sedia ada, berbanding dengan konfigurasi 2 μm denyut laser gentian yang lain, konfigurasi laser yang dicadangkan ini adalah lebih mudah dan lebih padat.

ACKNOWLEDGEMENTS

Praise be to The Almighty for the successful completion of this study. I would like to express my sincere and deepest gratitude to my supervisor, Prof. Dr. Sulaiman Wadi Harun for all of his support, help and guidance throughout my PhD studies. His infinite knowledge and enthusiasm has transformed the way I view and conduct research and for that I am also extremely grateful.

My sincere and heartfelt gratitude goes to Sarah, Muni, Dess and Fauzan for your selflessness and generous help in doing our lab works and precious discussions throughout our studies. My appreciation also goes to the members of the Photonic Research Center especially Kak Husna, Tan, Malathy, Kak Wati, Asiah, Amirah, Timah, Ann, Nabilah, Ninik, Arni, Ali, Kak Zura, Fatin and Nurul. You have made the lab most enjoyable place to work; despite of the many challenges we have to put up with. We have gone through the hard times and good times together.

I am also extremely grateful to the team at the CGCRI, India, in particular, Dr. Paul Chandra Mukul for providing us with the new fabricated fiber. To Dr. Norfizah and Prof. Dr. Hamzah Arof, thank you both for your kind assistance in checking my research papers and thesis writing. Also to those who have directly or indirectly contributed to the completion of this thesis, my gratitude goes to you.

My entire study has been sponsored by the Skim Latihan Bumiputra (SLAB) from the Ministry of Tertiary Education and International Islamic University Malaysia (IIUM). I thank them for their generosity, which helped me to achieve my PhD.

Last but not least, to my beloved parents and families, thank you for your encouragement, prayers and for believing in me. Most of all, to my husband Hafiz, I could not have done this without you, also to my daughters, Syafiqah and Safiyyah, thank you for your love, patience, understanding and continuous supports throughout my studies. This precious work means nothing without you.

TABLE OF CONTENTS

LIST OF FIGURES

LIST OF TABLES

LIST OF SYMBOLS AND ABBREVIATION

d_{core}	Diameter of a fiber's core
d_{clad}	Diameter of a fiber's cladding
A_{core}	Core area
A_{clad}	Inner cladding area
θ_i	Maximum acceptance angle
n	Refractive index
E_0	Energy of a ground state
h	Plank's constant
v_{10}	Frequency of the incoming photon for level 0 and 1
N	Ion populations
W_{ij}	Stimulated absorption and emission rate
A_{ij}	Spontaneous decay rate for the radiative and non-radiative decay
A_i^{nr}	Spontaneous decay rate for the non-radiative decay
L	Cavity length
γ	Measured loss in a single passage
β	Amplification coefficient
P_{out}	Output power of the laser
P_{in}	Absorbed pump power
η_s	Slope efficiency
Q	Quality of the laser resonator
τ_p	Pulse width
P_{avg}	Average power
f_{rep}	Repetition rate
E_p	Pulse energy

ACCVD	Alcohol catalytic CVD
ASE	Amplified Spontaneous Emission
Bi	Bismuth
CCD	Charge-coupled device
CNTs	Carbon nanotubes
CVD	Chemical Vapour Deposition
CW	Continuous wave
EDFL	Er^{3+}-doped fiber laser
EPMA	Electron probe microscopic analysis
Er	Erbium
ET	Energy transfer
FBG	Fiber Bragg grating
FWHM	Full-width at half-maximum
GSA	Graphene Saturable Absorber
HeNe	Helium neon
IR	Infrared
LAGS	Lithium-alumino-germano-silicate
LIDAR	Light Detection and Ranging
MCVD	Modified chemical vapour deposition
MMC	Multimode Combiner
MOPA	Master Oscillator/Power Amplifier
MWCNTs	Multi-walled carbon nanotubes
NA	Numerical aperture
OSA	Optical spectrum analyzer
OSNR	Optical signal to noise ratio
PEO	Polyethylene oxide

PM	Power meter
PVA	Polyvinyl alcohol
RF	Radio Frequency
RI	Refractive index
SA	Saturable absorber
SD	Solution doping
SDS	Sodium dodecyl sulphate
SESAM	Semiconductor saturable-absorber mirror
SNR	Signal to noise ratio
SPM	Self-phase modulation
TBF	Thulium-Bismuth fiber
TBFL	Thulium-Bismuth co-doped fiber laser
TDF	Thulium doped fiber
TDFL	Thulium doped fiber laser
Tm	Thulium
WDM	Wavelength Division Multiplexing
XPM	Cross-phase modulation
Yb	Ytterbium
YDFL	Yb^{3+}-doped fiber lasers
YTDFL	Yb^{3+}/ Tm^{3+} co-doped fiber lasers

CHAPTER 1

INTRODUCTION

1.1 Background of fiber laser

A study of light amplification by stimulated emission of radiation (LASER) has been realized by Gould, where the basic idea was to emit or amplify light through a stimulated emission process (Gould, 1959). The lasers research areas has grown rapidly since Planck discovered that energy could be emitted or absorbed only in discrete amounts which are called quanta. The study of quantum electronics relates the rare-earth ions such as Erbium (Er), Neodymium (Nd), Ytterbium (Yb) and Thulium (Tm) which are used as the gain medium to generate lasers over a wide wavelength range covering from visible to the near-infrared wavelength. In 1960, Maiman et. al (Maiman, 1960) introduced the first experimental demonstration of laser using ruby crystal pumped by flash lamp. Since then, several types of lasers were demonstrated using Nd-glass laser (Snitzer, 1961), helium neon (HeNe) (Javan *et al.*, 1961), carbon dioxide (CO_2) and Argon laser.

In 1970's, most of the research works have been focused on the pumping methods and its glass composition (Burrus *et al.*, 1976; Stone *et al.*, 1974; Stone *et al.*, 1976). The most important achievement was the development of low absorption loss silica (SiO_2) host glass fibers, which is the key enabling technology of the modern communication (Stone *et al.*, 1973). In 1980's, as the interest in fiber-optic research increased steadily, many new materials and fabrication techniques on optical fibers have been proposed and improved. For instance, modified chemical vapour deposition (MCVD) and solution doping process have been developed to fabricate low loss rare-earth doped fiber (Poole *et al.*, 1986; Townsend *et al.*, 1987). This great development

became an essential step towards realizing the practical rare-earth ion doped fiber lasers with controllable doping concentration. Soon after that, novel active fibers doped with Er, Yb, and Tm were developed and fabricated. A new optical amplifier was also introduced based on Erbium-doped fiber amplifier (EDFA) for amplifying optical signals in optical communication networks (Mears *et al.*, 1987). At this time, most of the proposed fiber lasers were based on core pumping approach and produce single mode continuous wave (CW) output. This approach was the best choice due to its extremely low threshold pump power, however, it suffered from a very low laser output power due to the low coupling efficiency (Mears *et al.*, 1985).

Despite the tremendous advances in fiber lasers, the output power was still limited by the availability of single transverse mode pump power launched into the single mode fiber core. Owing to this limitation, E. Snitzer et al found a way to overcome this limitation (Snitzer *et al.*, 1988) by allowing the use of a double-clad fiber in order to inject the high-power pump light (in a kilowatt based) to the doped fiber. They designed a fiber with two types of cladding consisting of the inner cladding and outer cladding. Mostly, the inner cladding was not round in shape in order to improve pump absorption (Muendel, 1996). The new invention has led to the increase in the laser's output power which is typically limited by the power level of the laser diode. As mentioned earlier, the pioneering work of double-clad fiber was proposed by E. Snitzer in late 80s (Po *et al.*, 1989). The gain medium used in this work was Nd^{3+}-doped fiber pumped by the GaAlAs phased array. The development of cladding pumping Yb^{3+}-doped fiber lasers (YDFL) followed slightly after. The demonstration of YDFL has been proposed by Hanna and co-worker in the 90s (Hanna *et al.*, 1990a; Pask *et al.*, 1995). The accelerating pace can be seen in successive publications afterwards. The used of double clad fiber has successfully achieved a CW output power of several kW level (Jeong *et al.*, 2004) which was generated from 12 m length of double-clad Yb^{3+}-doped fiber. Due

to the high achievement of fiber lasers in terms of its output power and efficiency, interest was then focused on the Er^{3+}-doped fiber laser (EDFL) which has an operating wavelength of 1550 nm that falls within the low-loss telecommunication window. Since the introduction of double clad fibers, the maximum reported output power of a CW EYDFL has reached 297 W at 1567 nm using a 6 m long Er-Yb co-doped double-clad fiber (Jeong *et al.*, 2007) within a very short time span.

Many applications require the use of modulated lasers or in other words pulsed lasers. There are a variety of pulsed laser applications in the area of optical communication, range finding, spectroscopy and micromachining. The pulsed laser has been proposed soon after the first demonstration of a single mode CW fiber laser. The first Q-switched and mode-locked fiber were reported by Alcock et. al. (Alcock *et al.*, 1986a; Alcock *et al.*, 1986b). The pulse formation has been realized by using acousto-optic modulator which generated a pulse width of 200 ns and ~1 ns for Q-switching and mode-locking, respectively. Pulsed formation can be achieved using several techniques and the simplest way is to directly modulate the CW lasers. Light can escape from the cavity for a very short period of time by placing the fast modulator into the cavity. However, by using this method, the loss of the produced light is high when the modulator is in closed state. Thus, more sophisticated techniques have been used such as cavity dumping, gain switching, mode-locking and Q-switching. The two latter techniques provide more reliable, robust and superior technique for pulsing the lasers.

In 1989, the first mode locked fiber laser based on soliton pulse shaping was reported (Kafka *et al.*, 1989) which demonstrate ~4 ps pulses. A year later, sub-picosecond pulses shorter than 500 fs were reported from Nd^{3+}-doped fiber laser by pulse compression mode-locking. In contrast with mode-locking, Q-switching typically produces a giant pulse formation which is high in pulse energy and peak powers while the repetition rate is in the range of hertz to kilohertz. One of a few best Q-switching

performances was indicated in 1999 by Paschotta et. al. (Paschotta *et al.*, 1999) generating pulses with as much as 0.1 mJ pulse energy at 1.53 μm and a repetition rate of higher than 1 kHz using a semiconductor saturable-absorber mirror (SESAM). In the following year, (Alvarez-Chavez *et al.*, 2000) reported on the actively Q-switched Yb^{3+}-doped fiber laser which is capable of generating a 2.3 mJ of output pulse energy at a 500 Hz repetition rate and more than 5 W of average output power at higher repetition rates. In 2007, Schmidt et. al. demonstrated a Q-switched employing a short-length Yb-doped photonic crystal fiber producing 100 W of average output power with up to 2 mJ of pulse energy and a sub-10 ns pulse duration was extracted at lower repetition rates (Schmidt *et al.*, 2007).

1.2 Fiber laser at 2 micron region

Thulium is one of the rare earth ions which provide a lot of interesting applications based on fiber laser. Its broad emission ranging from 1400 nm to 2400 nm make it possible to be used in spectroscopy, military and medical field (Scholle *et al.*, 2010). Interestingly, its emission at the 2 μm region has strong water and biological tissue absorption coefficients, thus making it possible for medical application. Several works on thulium-doped fiber laser (TDFL) has been demonstrated using different glass host such as ZBLAN (Allain *et al.*, 1989), tellurite (Wu *et al.*, 2005), germanate (Wu *et al.*, 2007) and silica (Hanna *et al.*, 1990c; Jackson *et al.*, 1998). Thulium doped fiber with silica based glass exhibit higher non-radiative decay (Layne *et al.*, 1975; Layne *et al.*, 1977). The high phonon energy in silica fiber limits the quantum efficiency of the respective level which leads to low efficiency. Yet, silica based materials are needed for the integration into standard communication systems as well as for robustness in applications. Nevertheless, the use of other glasses to avoid high phonon energy such as fluoride or tellurite glass gives some disadvantages in terms of low melting temperature;

low durability and strength thus contribute to the problem in splicing. Another problem associated with thulium ions is the lack of pumping source at their high absorption band of 1.2 μm, thus several works have reported on the sensitization of Ytterbium ion in Thulium doped fiber to realize the absorption at this wavelength. In this work, two different co-doping elements which are Ytterbium-Thulium doped fiber (YTDF) and Thulium-Bismuth doped fiber (TBF) are used as a gain medium. Both fibers are newly fabricated and the spectroscopic properties as well as energy transfer processes and lasing performances have been investigated.

Ytterbium thulium doped fiber lasers (YTDFLs) rely on the indirect pumping from the Yb^{3+} usually over the wavelength region from 910 nm to 980 nm to allow the energy transfer between the Yb^{3+} to Tm^{3+} (Jackson, 2003). Ytterbium co-doping enhanced the pump absorption and could facilitate population inversion between the energy level. Spectroscopic properties, namely up-conversion (UC) has also been extensively studied for YTDF since the 90's in order to realize the laser emission at the visible wavelength (Hanna *et al.*, 1990b; Zhang *et al.*, 1995). Previous works reported on the alternative methods such as nonlinear frequency conversion which employs energy up-conversion, absorption, refraction or second harmonic generation; however it is very much complicated. Thus, sensitization of Yb^{3+} will ease the difficulties. Nevertheless, the UC via Yb^{3+}-sensitized still suffers from quenching of the excited state population at its amplifying level (Gomes *et al.*, 1990). Due to the limitation, YTDFLs are significantly less efficient compared to other thulium-doped silica fiber lasers. In this work, the up-conversion and the lasing performances at 1.9 μm region of YTDF on various length and doping concentration will be investigated and discussed.

A study of Thulium-Bismuth co-doped fiber laser (TBFL) seems limited in terms of publications and research works. The most common reported works usually focus on the broadband light sources based on the emission properties from the energy

structure of dopant ions in the glass host that are thulium and bismuth (Zhou *et al.*, 2011). The amplified spontaneous emission (ASE) sources operating around the 1900 nm spectral region have gained tremendous interest for possible applications in spectroscopy, gas sensing, low coherence interferometer and medical imaging via optical coherence tomography. Tm^{3+} has a broad ASE between 1650 nm to 2100 nm (Agger *et al.*, 2006) and therefore, is suitable to be a broadband ASE source which is doped with active Bismuth ions to realize broad emission wavelength via energy transfer (Ruan *et al.*, 2009). Based on previously reported work, countless publications have been reported on the high output power using double-clad fiber as mentioned earlier. However, considerable amounts of output power as well as laser efficiency at 1.9 μm regions is suitable in some applications, such as sensor, where only low amount of energy and power are needed (Coté, 2001) owing to their specific IR absorption at the 1900 nm region. The use of single mode fiber instead of double-clad fiber brings significant advantages in term of laser performance such as low threshold power. Very few research works have been done to investigate the 2 μm emission from thulium rare earth ions using single mode silica fiber with comparatively high laser efficiency and low threshold power.

1.3 Recent development on 2 μm pulsed fiber laser based on graphene and multi-walled carbon nanotubes saturable absorber

Lasers at the 2 μm wavelength region have gained tremendous attention due to the strong absorption of water and biological tissue at the 2 μm wavelength which makes the laser transitions possible for various applications such as spectroscopy, LIDAR, and medical. Considering the useful applications, Q-switching and mode locking lasers are crucial. Apart from the previously discussed pulse laser in section 1.1, this section provides additional information regarding the use of graphene saturable

absorber (GSA) and multi-walled carbon nanotubes saturable absorber (MWCNTs) as a passive Q-switching element in their implementation on 2 μm pulsed fiber laser. Pulse lasers have been demonstrated based on various host media such as silica, tellurite (Richards *et al.*, 2008), germanate (Fang *et al.*, 2012) and fluoride (Yang *et al.*, 1996) fibers. Among the host materials used, silica is preferred because of its compatibility with standard optical components. The use of passive elements to generate pulse lasers are favourable due to their flexibility of configurations. The lasers have been successfully demonstrated using different kinds of saturable absorbers (SAs), such as semiconductor saturable absorber mirrors (SESAMs), nonlinear polarization rotation (NPR), graphene and carbon nanotubes.

To date, few works on the generation of Q-switched fiber laser near the 2 μm wavelength region have been reported. For instance, Wang et. al. (Wang *et al.*, 2012b) reported on the Q-switched generation with maximum pulse energy of 69 nJ and a repetition rate of 26 kHz using 1560 nm CW laser source and graphene saturable absorber (GSA). More recently, Jiang et. al. (Jiang *et al.*, 2013) achieved laser with a short pulse duration of 760 ns and a repetition rate of 202 kHz using graphene that is being transferred to the HR mirror to function as SA. Works on GSA based Q-switched TDFLs are mostly related to the free-space arrangement (Wang *et al.*, 2012c) and linear configuration (Lu *et al.*, 2013). Nevertheless, a number of publications have been reported on the Q-switched lasers at other wavelength regions using SWCNT as SA. For instance, Zhang et. al (Zhang *et al.*, 2011a) demonstrated a passive Q-switched and mode locked Nd:YVO_4 laser using SWCNT-SA to generate a Q-switched repetition rate and pulse width of 33 kHz and 5.6 μs, respectively. Yu et al. (Yu *et al.*, 2012) proposed a Q-switched Ytterbium-doped double-cladding fiber laser based on SWCNT-SA in a linear-cavity. The pulse-repetition rates were tuned from 9.1 kHz to 60 kHz when the pump powers were changed from 1.85 W to 10 W and the shortest pulse duration was

around 600 ns. More recently, (Tan *et al.*, 2013) demonstrated a Q-switched multi-wavelength Brillouin erbium fiber laser using SWCNT–SA with a repetition rate of 105.2 kHz and a pulse width of 0.996 μs. To the best of our knowledge, there are only a few reported works on the use of MWCNTs as a saturable absorber for the generation of a mode locked Nd:YVO_4 laser (Lin *et al.*, 2013; Zhang *et al.*, 2011b). The Q-switched laser generation at 2 μm regions using MWCNTs can hardly be found.

1.4 Objective of the thesis

The scope of this thesis focuses on the development of new fiber lasers, which incorporates Thulium as the gain medium to generate CW and pulse laser output at 1.9 μm regions. The main objective of this work is to evaluate the effect of co-doping ytterbium and bismuth ions into the thulium fiber in order to enhance the performance at 1.9 μm region for CW and Q-switched laser, respectively. To achieve this, few objectives have been proposed to guide the research direction, i.e.:

- To construct fiber laser devices operating at 1.9 μm region and evaluate the performance of these lasers in term of lasing efficiency and the lasing pump power threshold.
- To investigate the spectroscopy in terms of the energy transfer ability between the co-doping elements to the Tm^{3+} ions.
- To enhance the lasing performance of the proposed lasers by employing the best amount of ions concentration between the co-doping elements and Tm^{3+} ions.
- To construct Q-switched fiber laser devices using commercially available TDF and the newly developed TBF in conjunction with the homemade graphene and MWCNTs film based saturable absorber as a Q-switcher.

1.5 Work contributions

Some of the contributions of this thesis work are highlighted below:

1. Development of YTDFL based on higher ytterbium to thulium concentration ratio exhibits efficient energy transfer between the co-doping elements in conjunction with appropriate pumping wavelength.
2. Demonstration of broadband ASE generation in the 1900 nm region using a Tm-Bi co-doped fiber as the gain medium for the first time. The 10 dB bandwidth of the ASE spectrum covers from 1735 nm to 2077 nm.
3. To the best of our knowledge, the generation of CW fiber laser from the newly develop TBFL exhibits the highest CW laser efficiency from single mode fibers and comparatively low threshold pump power with the assistance from active bismuth ions. Furthermore, a comparative analysis on the lasing performance between commercial TDFL and TBFL has been performed.
4. Development of Q-switched fiber laser using GSA with pump wavelength of 800 nm shows that the V-shaped curve of pulse duration is contributed by heat transfer to the GSA.
5. The generated fiber laser is the first reported Q-switched laser at 1.9 μm using MWCNT-SA in conjunction with TBF as the gain medium. The pulse has been observed to generate a wide pump power range of 500 mW to 800 mW with the highest repetition rate and lowest pulse duration of 61.99 kHz and 4.0 μs, respectively using a 1552 nm pump wavelength.
6. The use of passive elements which are GSA and MWCNTs-SA proposed in this work is simpler, cost-effective and more compact due to the all-fiber ring configuration compared to the existing research work.

1.6 Thesis outline

This thesis consists of six chapters including this chapter which serves as an introduction. The current chapter presents an introduction to the fiber laser field and the objectives of this thesis. Chapter 2 explains the theoretical background and basic equations for the generation of CW and Q-switched fiber laser and provides literature on the Thulium energy transitions, gain characteristics and basic rate equations which serves as a key element in this thesis. It is then followed by the literature on the cladding pumping technique involved in this work. Moreover, the use of GSA and MWCNTs-SA as a Q-switcher is briefly discussed.

Chapter 3 describes the fabrication and spectroscopy of the newly fabricated double-clad Tm^{3+}/Yb^{3+} co-doped yttria alumina silicate fibers (YTDFs). The performance of 1.9 μm fiber lasers based on cladding pumping technique using various pumping wavelengths and two different cavity configurations are investigated. The effect of various lengths and doping concentration on the lasing efficiency and threshold pump power are demonstrated. Thereafter, an investigation is carried out for the enhancement of laser efficiency using the dual-pumping method.

Chapter 4 proposes new, efficient fiber lasers operating at 1.9 μm based on core-pumping approach using a newly developed single mode Thulium-Bismuth co-doped lithium-alumino-germano-silicate (LAGS) fiber (TBF) as the gain medium. The energy transfer between Tm^{3+} and active Bismuth has been investigated based on the ASE emission and pump wavelength. Broad ASE generation employing TBF is also discussed. Two laser cavity designs are being presented, which are ring and linear cavity configuration. Discussion on the effect of different dopants concentration of active Bismuth and Tm^{3+} ions on the lasing performance has been included. Next, the proposed TBF laser (TBFL) is compared with the one obtained using a commercial

TDF. Finally, dual-pumping operation to enhance the laser efficiency has been proposed.

In chapter 5, Q-switched fiber laser with longer emission wavelengths of around 1.9 μm has been constructed using a passive Q-switcher, which are graphene and MWCNTs saturable absorber. The gain media used are TDF and TBF. Both graphene and MWCNTs are embedded in the polymer composite film before it is integrated into a ring laser cavity by sandwiching it between two fiber connectors. Discussion on the different pumping wavelengths of 800 nm and 1552 nm has been carried out. The Q-switched performance of the proposed Q-switched TBFL with a Q-switched TDFL is then compared, which was obtained by using a commercial TDF and the same MWCNT-SA.

Finally, chapter 6 summarizes all of the results and analysis obtained from this work. Future work suggestions are also provided as an extension of the work presented in this thesis.

CHAPTER 2

LITERATURE REVIEW OF FIBER LASERS

2.1 Fundamental of Fiber Lasers

Fiber laser technology has played an important role in the modern telecommunication systems. The advent of low-loss optical fibers becomes a major achievement to the great era of optical fiber communications. Despite the high propagation loss which is 1000 dB/km at the telecommunication wavelength of 1.5 μm at early 60s, the fast growing fiber optics technology made it possible to reduce it until 20 dB/km in the early 70s (Kapron *et al.*, 1971) and soon was further reduced to 0.2 dB/km (Miya *et al.*, 1979). The revolution in the field of telecommunications was started as soon as fibers for long-distance optical signal transmission were ready and long haul optical networks became practical (Kato *et al.*, 1999).

The transmission of light in the fiber optics is based on the principle called total internal reflection (TIR) (Hecht, 2004; Snitzer, 1961). Figure 2.1 shows an optical fiber in its simplest form, which consists of a cylindrical core (d_{core}, with diameter of around 9 μm) that is surrounded by a cladding (d_{clad}, diameter of around 125 μm). The condition of TIR at the core-cladding interface must be satisfied for the light propagation, thus the refractive index of the core (n_{core}) should be slightly higher than that of the cladding (n_{clad}). Therefore, ideally, light can be confined inside the core without any propagation loss. For a step-index fiber, the index distribution along its radial direction is:

$$n(r) = \begin{cases} n_{core} & (0 < r < R_{core}) \\ n_{clad} & (R_{core} < r < R_{clad}) \end{cases} \quad (2\text{-}1)$$

where r is the radial coordinate, R_{core} is the core radius and R_{clad} is the cladding radius. The numerical aperture (NA) of the fiber, which represents the maximal acceptance angle ($NA = \sin\theta_i$) within which the TIR condition can be satisfied by:

$$NA = \sqrt{{n_{core}}^2 - {n_{clad}}^2} \approx n_{core}\sqrt{2\Delta} \tag{2-2}$$

where $\Delta = (n_{core} - n_{clad})/n_{core}$ and $n_{core} \approx n_{clad}$.

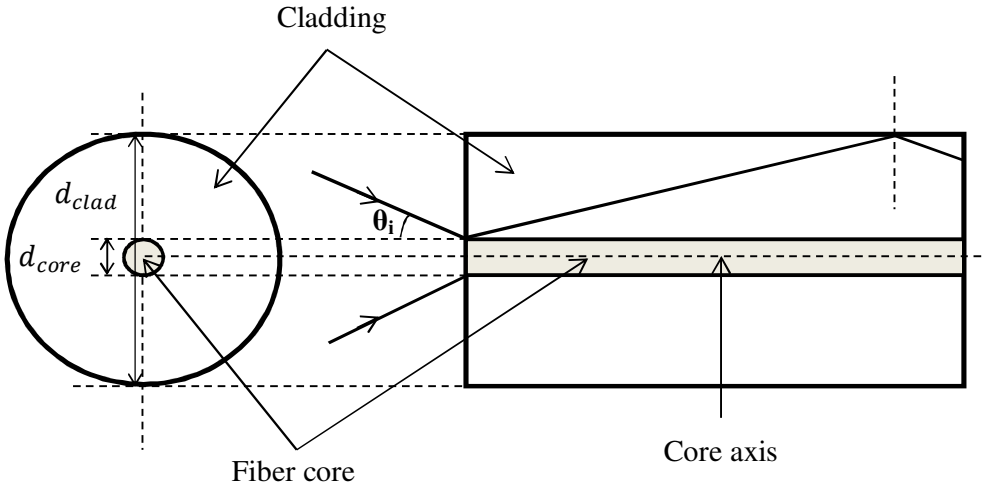

Figure 2.1: Illustration of an optical fiber with single layer of cladding.

The initial purpose of fiber optics is merely to transmit light, however due to their ability to confine light with very minimal loss and robust mechanical strength have attracted them to other applications. The most important application is to fabricate the light amplification and lasing devices by doping the fiber core with rare-earth ion. The fiber core doped with rare earth ions (gain medium) which confined light exhibit high optical power densities, hence open the possibilities to realize compact low-threshold high-gain amplifiers and lasers. The invention of the laser was first demonstrated by Theodore H. Maiman in 1960 using a photographic flash lamp as the pump source (Maiman, 1960). In 1964, Elias Snitzer reported the first operation of laser amplification using a neodymium doped glass (Nd:glass) which became the pioneering work in the

generation of laser employing a gain medium (Koester *et al.*, 1964). A decade after, the first fiber lasers were realized in both pulsed and continuous-wave (CW) forms (Stone *et al.*, 1974).

The terms fiber lasers are usually associated with the gain media of optical fibers. The active gain medium is an optical fiber core doped with one or more rare-earth ions, precisely known as lanthanides in the periodic table (but not restricted to the lanthanide) (Digonnet, 2002). A simple fiber laser setup is shown in Figure 2.2. The optical laser cavity is formed with the input coupler which provides feedback to form a standing wave for light amplification produced by the gain medium. The light confinement and low propagation loss in optical fibers are an advantage for the use of longer active gain medium which can provide higher gain. Nevertheless, the higher dopant concentration of the active gain medium as short as 2 cm long can produce laser using the erbium-concentration of 2500 ppm (Zyskind *et al.*, 1992). Due to the short cavity length, a high concentration of active ions must be introduced into the fiber core to facilitate sufficient pump power to reach threshold.

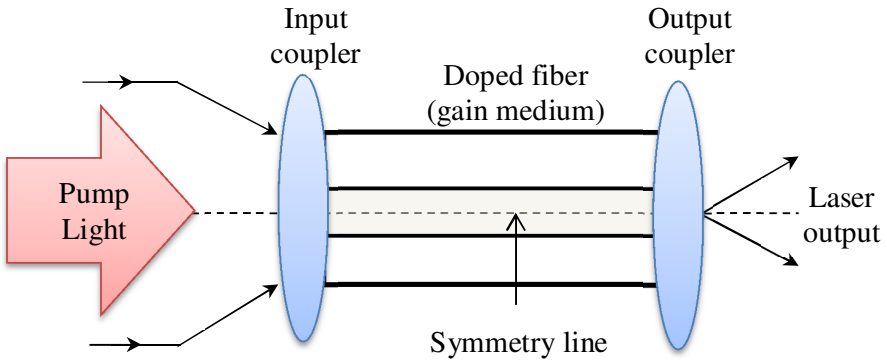

Figure 2.2: Schematic diagram of the simplest fiber laser with Fabry-Perot resonator.

2.2 Reviews in related areas

2.2.1 Rare earth material

A periodic table contains a group of fourteen chemical elements called rare earth. The term 'rare earth' is derived consist of the word 'rare' which refers to the idea that only a small amount of the discovered element was present in the earth's crust, while 'earth' comes from the earthy appearance of oxide based element. The first invention to apply rare earth was suggested in the late 19th century by an Austrian scientist, Carl Auer von Welsbach. He discovered a useful development in the production of light by generating white light (gas lamp) when heated by a flame (Greinacher, 1980) which is still being used today as a lantern. Nowadays, rare earth elements become an important role in various fields. Most lanthanides are widely used in lasers, and as co-dopants in doped-fiber optical amplifiers and lasers as well as in life science applications (Bünzli *et al.*, 2005). The rare earth elements when embedded in the host glass forms trivalent (+3) rare earth ionization state of these elements, which has an electronic configuration of xenon plus a certain number; $[Xe]4f^N5s^25p^66s^0$, where $N = 1 \ldots 14$ (Digonnet, 2002). All existing trivalent rare earth elements are 4-level lasers. Its N inner electrons of $4f$ shell are shielded from the external electromagnetic field by the outmost shell $5s$ and $5p$. Since the optically active electrons in rare earths are well shielded, the energy levels remain fairly constant when comparing the levels in different hosts. Figure 2.3 (Reisfeld *et al.*, 1977) shows the extended and modified version of a Dieke's diagram (Dieke *et al.*, 1963) for the energy level of the trivalent lanthanides (except for cerium and promethium) in the crystal.

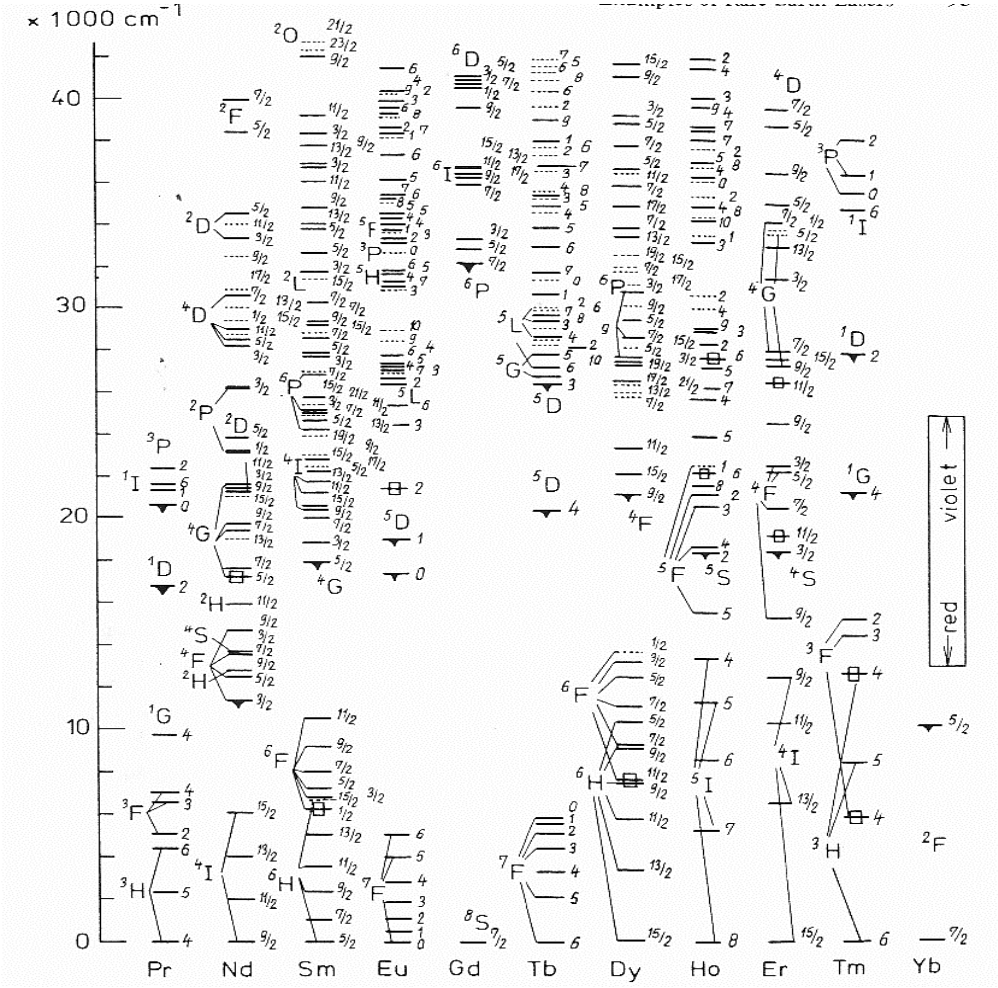

Figure 2.3: Principle energy levels of all the trivalent rare earth ions (Reisfeld *et al.*, 1977).

2.2.2 Interaction between photons and electrons

The lowest energy level of an electron configuration of an atom is defined as a ground state. In thermal equilibrium, the electron stays in the ground state with energy, E_0. If the electron excites to a higher energy level, it will decays and emits the photon. This may happen spontaneously or by stimulation. Spontaneous emission happens naturally and incoherent. Stimulated emission on the other hand needs certain perturbation in the form of light from arc lamps, flash lamps or laser diode which acts as a source to supply photons to the ions. The photon released from stimulation emission

process has the same frequency, energy and direction as the incoming photon. Referring to Figure 2.4, electrons in the ground state excites to the higher energy level, E_1 after absorbing the energy of the incoming photon. The injected light, should carry energy almost similar to the energy difference between E_1 and E_0, $\Delta E = hv_{10}$, where h is the Plank's constant and v_{10} is the frequency of the incoming photon for level 0 and 1. As the stimulated electrons occupy higher energy level, population inversion occurs. The term population inversion refers to the concept in which the number of electrons in the excited state, N_1 is greater than those in the lower state, N_0. This is the fundamental concept in the generation of standard laser devices.

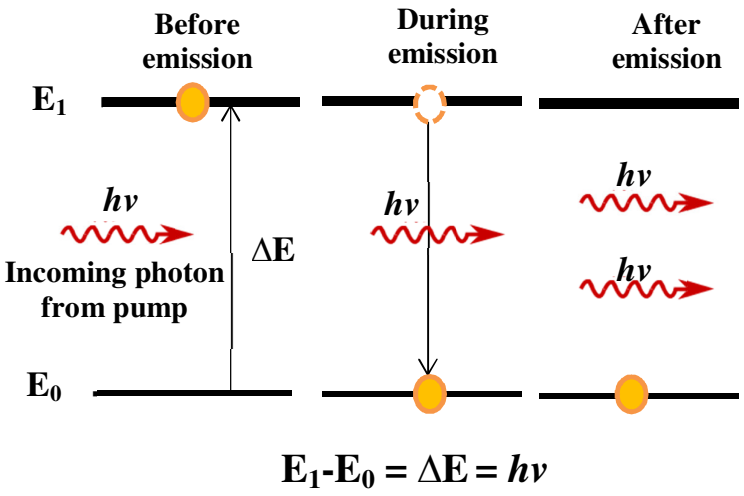

Figure 2.4: Process of stimulated emission of radiation.

2.2.3 Energy transition and gain characteristic in Tm ions

Based on the periodic table, Thulium has an atomic number of 69, discovered by Per Theodor Cleve in 1879. He found that the residue from erbia; the oxide of erbium (Er_2O_3) varies in weight, thus it contains other elements which are found to be Holmium and Thulium (James, 1911). Like the other lanthanides, the most common oxidation state is +3, seen in its oxide and other compounds. The energy level diagram of Tm^{3+} is

shown in Figure 2.5. Thulium presents three major absorption bands in the infrared region from the ground state absorption (GSA) shown in Figure 2.5 which are $^3H_6$ to $^3F_4$ (~1550 nm), $^3H_5$ (~1210 nm) and $^3H_4$ (~790 nm) (Moulton *et al.*, 2009). Other possible transitions are provided in the figure which consists of GSA and excited state absorption (ESA). The electronic transition of $^3F_4 \rightarrow {}^3H_6$ is a well known energy transition of Tm^{3+} ions used for 2 μm light emission. The transition of $^3H_6 \rightarrow {}^3H_4$ exhibits broad emission, ~130 nm. This is due to the fiber absorption peak which coincides with the laser diode operating wavelength of 790 nm. Therefore, it is suitable to be used in tunable laser source for broadband application.

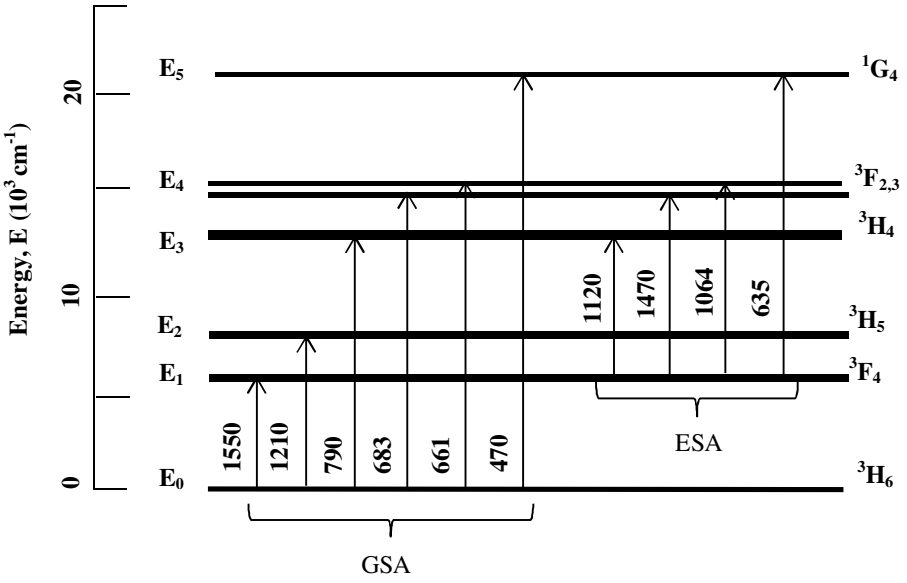

Figure 2.5: Possible ground state absorption (GSA) and excited state absorption (ESA) of Tm^{3+} ions. All transitions are in nm scale.

The gain of the Tm^{3+} ions can be modelled in terms of an atomic rate equation depending on their respective energy level of transitions. Figure 2.6 denotes the possible Tm^{3+} ions transition according to (Peterka *et al.*, 2011). The left hand side shows the

energy level of thulium while the right hand side indicates the number of levels associated with it.

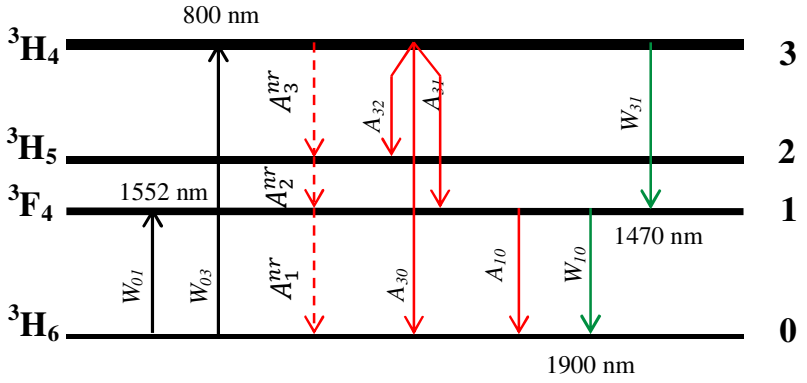

Figure 2.6: The possible laser transition of Tm^{3+} ions in a silica based fiber.

The energy level diagram shown in Figure 2.6 includes some of the transitions involved in the Thulium doped fiber. This thesis emphasizes on the 800 nm and 1552 nm pumping mechanism, thus certain energy levels have been omitted for simplicity, and only a three-level system is considered. The population density at $^3H_5$ level is neglected because of the high non-radiative decay rates ($\gg 10^5 s^{-1}$) transition of $^3H_5 \rightarrow {}^3F_4$ (Peterka *et al.*, 2011). The rate equations for the ion populations, *N* at each level are expressed as follows:

$$\frac{dN_0}{dt} = -(W_{01} + W_{03})N_0 + (W_{10} + A_1^{nr} + A_{10})N_1 + A_{30}N_3 \quad (2\text{-}3)$$

$$\frac{dN_1}{dt} = W_{01}N_0 - (W_{10} + A_{10})N_1 + (W_{31} + A_3^{nr} + A_{31} + A_{32})N_3 \quad (2\text{-}4)$$

$$\frac{dN_3}{dt} = W_{03}N_0 - (W_{31} + A_3^{nr} + A_{30} + A_{31} + A_{32})N_3 \quad (2\text{-}5)$$

$$\sum_{i=0}^{3} N_i = N_t \quad (2\text{-}6)$$

where W_{ij} is the stimulated absorption and emission rate accounts for amplified spontaneous emission (ASE), A_{ij} and A_i^{nr} are the spontaneous decay rate for the

radiative and non-radiative decay rates from level i to j, and N_t is the total thulium dopant concentration.

Another special feature of Tm^{3+} is the cross relaxation (CR) between Tm^{3+} pairs. This process allows the two Tm^{3+} ions occupy $^3F_4$ level. When two Tm^{3+} are close enough to each other, with a separation distance lower than that of the emission wavelength, the CR energy transfer ($^3H_4$,$^3H_6 \rightarrow {}^3F_4$,$^3F_4$) will be triggered. Figure 2.7 shows the schematic diagram for the CR process between two Tm^{3+} ions. The Thulium ion (donor ion) in the ground state absorbs photon from the 790 nm pump thus elevated to $^3H_4$ level. When the ion in this level de-excites to $^3F_4$, instead of emitting at of 1.47 µm, the energy is transferred to a nearby Thulium ion (acceptor ion). The ion that resides in the ground state absorbs the transferred energy to occupy the upper laser level, $^3F_4$. Both ions then drop to the ground state and emit at 1.9 µm photons. With each absorbed pump photon at 790 nm, two 1.9 µm photons are produced. Therefore, higher quantum efficiency is attainable under the above condition for Thulium operating at the 2 µm emission region. The amount of CR can be calculated according to Taher et. al (Taher *et al.*, 2011).

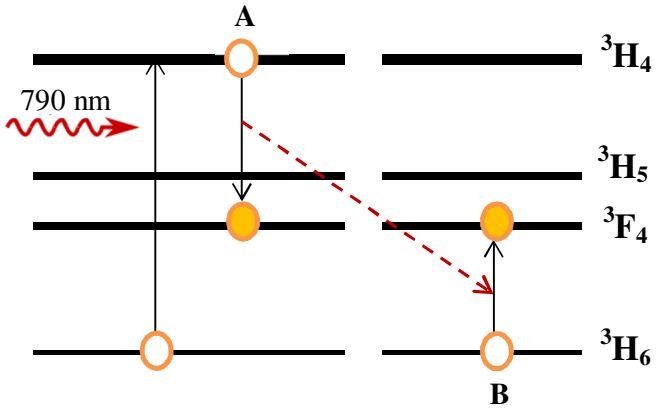

Figure 2.7: Process of cross relaxation between donor ion, A and acceptor ion, B.

2.3 Optical Fiber Lasers

LASER stands for light amplification by stimulated emission of radiation and is a device that allows the amplification of light in a coherent, monochromatic and unidirectional manner in the optical spectrum region. The common characteristic of all types of laser devices is the population inversion in the active gain medium in the laser cavity. In order to generate laser, three basic conditions must be satisfied. First, the laser should have an active gain medium. Secondly, the gain medium should be placed in between the reflective optical cavity to allow circulation of photons. Finally, the external pump source is needed to generate population inversion. All optical fiber lasers are built with these three basic elements. Several configurations of laser cavity will be discussed afterwards.

2.3.1 Laser cavity

The most common laser cavity used for optical fiber laser is a Fabry-Perot resonator as shown in Figure 2.8. It is typically constructed by placing an active gain medium in between two planar dielectric mirrors. The mirrors serve as an input and output coupler. Both ends of the fiber are either perpendicularly cleaved or polished flat. The pump power provided by the pump source is directly coupled into the fiber by splicing or by high transmittance mirror through the input coupler (mirror), which is transparent to the pump light and highly reflective to the generated light emission. The mirrors introduce optical feedback to the laser beam in the cavity, therefore causes a population inversion. The laser beam that propagates back and forth in the cavity enables amplification due to stimulated emission. The generated light leaves the laser cavity through the output coupler (mirror). To ensure that the laser can be realized, the population inversion which produces the gain within the cavity must be sufficient to compensate for the fraction of energy loss due to all causes. Several reflecting elements

such as fiber Bragg grating (FBG), selective wavelength filter and injection locking can also be used to replace the dielectric mirror.

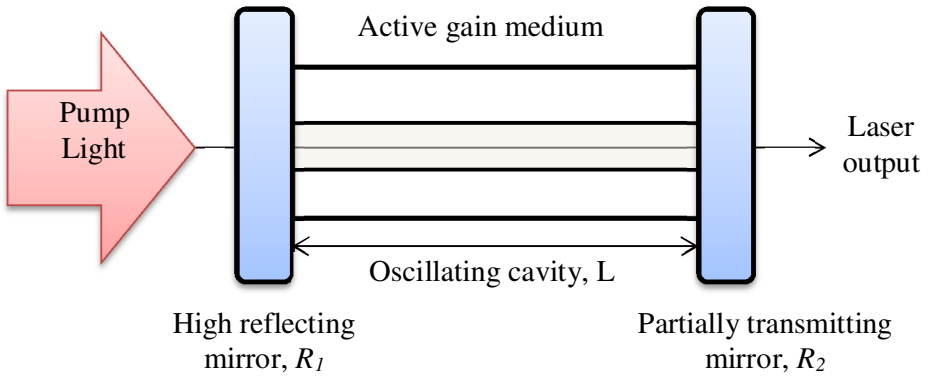

Figure 2.8: Schematic diagram of a Fabry-Perot fiber resonator.

The laser setup can also be configured in a ring cavity as shown in Figure 2.9. The cavity allows light to oscillate in both directions thus generates bidirectional output which limits the efficiency of the laser. The constructive interference between the counterpropagating signals produce a standing wave which induces the spatial hole burning. This effect allows the oscillation of several longitudinal modes in the laser cavity (Digonnet, 2002). The bidirectional signal light travelling in the cavity can be eliminated using an optical isolator by forcing the light travel in a unidirectional operation. However, the small amount of loss introduced by the isolator will increase the threshold of the laser. Another method to reduce the effect of spatial hole burning is to introduce the polarization controller (PC) that modifies the polarization state of light and allows continuous adjustment of the birefringence within the cavity to balance the gain and loss. The ring laser cavity offers the advantages of simplicity in design, low cost and low threshold operation. Ring cavities are commonly designed for pulse laser applications (Nelson *et al.*, 1997; Panasenko *et al.*, 2006).

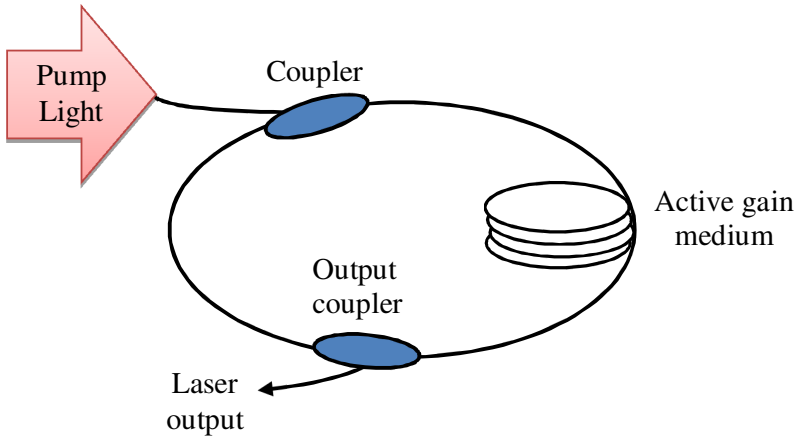

Figure 2.9: Schematic diagram of all-fiber ring laser resonator.

2.3.2 Important Laser parameters

Laser threshold, output power and efficiency are the important laser parameters. Laser threshold refers to the operation circumstance of a laser which laser emission just starts to occur. It is defined as the minimum amount of pump/input power or energy required to start the lasing action during which the gain coefficient becomes larger than the losses in the cavity. The output is considered to be a laser when the pump power is sufficiently high such that population inversion is achieved and therefore, the energy of the system has reached the lasing threshold. According to Figure 2.8, light beam will oscillate in the cavity length, L between two reflecting mirrors which are high reflecting, R_1 and partially transmitting, R_2 hence the reflection coefficient is less than one. The fraction of light that remains after a full round trip passage through the laser is denoted by (Reisfeld *et al.*, 1977):

$$e^{-2\gamma} = R_1 R_2 \tag{2-7}$$

where γ is the measured loss in a single passage and is positive, therefore:

$$\gamma = -\frac{1}{2}\ln R_1 R_2 \tag{2-8}$$

The intensity of the radiation increased as the laser oscillates in the cavity due to the continuous population inversion by a factor of $e^{\beta L}$ where β is amplification coefficient. β is given by $\beta = k\Delta N$, where k is the absorption coefficient of a pump wavelength and ΔN is the population inversion. By comparing the increased intensity of the radiation in a passage and the fraction of light remains in the cavity, the threshold of the laser oscillation is attained which satisfies the condition below (Reisfeld *et al.*, 1977)

$$\beta L > \gamma \tag{2-9}$$

The threshold power usually depends on the gain per unit pump power, the round trip cavity losses, and how strong the pump, signal and dopants are confined (Armitage, 1988).

The slope efficiency is one of the important parameters in characterizing a laser. The efficiency of the laser is given by the ratio of output power of the laser, P_{out}, over the absorbed pump power, P_{in}. According to (Digonnet, 2002), the output power, P_{out} is given by:

$$P_{out} = \frac{T_1}{\delta_0}\frac{h\nu_s}{h\nu_p}(P_{abs} - P_{th}) \tag{2-10}$$

where $h\nu_s$ and $h\nu_p$ is the signal photon energy and pump photon energy respectively. T_1 is the power transmission of the output coupler, δ_0 is the round-trip loss, P_{abs} is the total pump power absorbed by the dopant and P_{th} is the threshold power. The Eq. (2-10) states that the output power grows linearly with the absorbed pump power. Thus, the slope efficiency, defined as the output power divided by the absorbed pump power, $P_{in} = P_{abs} - P_{th}$ is (Digonnet, 2002):

$$\eta_s = \frac{T_1}{\delta_0}\frac{h\nu_s}{h\nu_p} \tag{2-11}$$

The efficiency depends on the slope of the graph. This is due to the active pump photon compared to the signal photon in order to excite ions to the higher level, and the energy difference between them is wasted usually in terms of phonons.

2.4 Cladding Pumping

The drastic improvement in fiber lasers performance has been realized with the enhancement in various approaches. One of the famous approaches is the novel design of double clad fibers and cladding pumping scheme (Mears *et al.*, 1985; Poole *et al.*, 1986). The conventional optical fiber, single mode fiber, has only one effective wave-guiding property which is the fiber core. Owing to this, the pump light from the source should be coupled into the small core area to achieve efficient laser operation. Therefore, the laser diode needs to be single mode with high intensity output. The use of high pump power which is coupled directly to the doped fiber core will damage the threshold of the semiconductor material. To overcome the limitation, E. Snitzer et. al. introduced a double-clad fiber which can be coupled to the high pump power provided by laser diode as mentioned earlier in Chapter 1.

(Snitzer *et al.*, 1988) use the available high-power multimode laser diodes of relative low brightness and with the newly designed double-cladding (or double-clad) fibers. This fiber uses a cladding-pumping scheme by injecting the pump light to the fiber's cladding as shown in Figure 2.10. Based on the figure, a second (outer) cladding is added with lower refractive index than that of the first (inner) cladding. This allows the injected pump light to be confined due to the TIR at the inner-outer cladding boundary. The large area of the inner cladding allows a larger fraction of the laser diode output power to be coupled to the fiber. The pump light travel in the first cladding overlaps with the doped core and gradually absorbed by it. The pump absorption is proportional to the ratio of the core area, A_{core} over the inner cladding area, A_{clad}

(Muendel, 1996), A_{core}/A_{clad}. Thus, the core/cladding area ratio is very crucial in designing the double-clad fiber. Confined within the core area, the generated output has relatively high brightness and power.

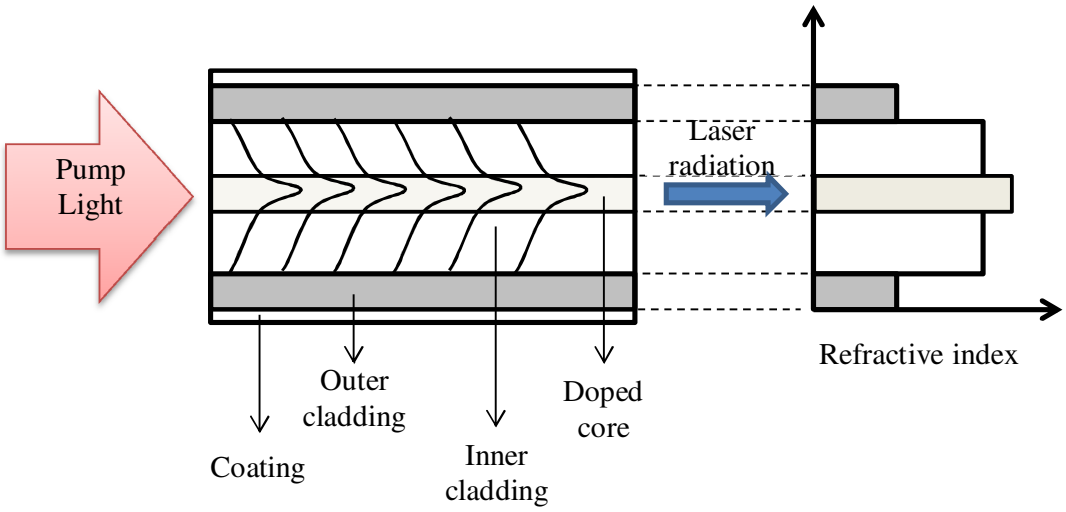

Figure 2.10: Schematic drawing of a double-cladding fiber.

Apart from that, the cladding-pumping laser scheme exhibit high thermal tolerance for high power CW laser operation provided that certain parameters are optimized (Brown *et al.*, 2001; Wang *et al.*, 2004). However, (Lapointe *et al.*, 2009) reported on the thermal degradation of double-clad optical fiber coatings which is known to be the major limiting factor for the operation of high power CW fiber lasers. Wang et. al proposed to overcome the limitation by decreasing the pump absorption and increasing the length of the fiber (Wang *et al.*, 2004), however the laser will suffer from low efficiency due to the needs of higher pump absorption. In conclusion, by optimizing the combination of pump powers, pump absorption and fiber lengths, an acceptable laser performance can be achieved.

Another work proposed by Muendel (Muendel, 1996) is to design various shapes of inner cladding to enhance the power transfer from the pump to the doped core (Li *et al.*, 2004; Liu *et al.*, 1996). The approaches taken were to offset the core of the

fiber and to alter the geometry of the inner cladding. Therefore, provides significant difference in the pump absorption efficiency of the double-clad fiber compared to the conventional circular shaped inner cladding. The designed were based on the ray propagation in the fiber. There are two types of rays propagating in the inner cladding which are the meridional rays and skew rays. Meridional rays are rays that pass through the axis of the optical fiber, while skew rays travel through an optical fiber without passing through its axis (Muddu, 2003). Most of the pump signal propagates as helical rays in the inner cladding, therefore most of the skew rays miss the core and only the meridional rays overlap with the doped core. This limitation can be overcome by offsetting the core from the center of the inner cladding (Liu *et al.*, 1996) as in Figure 2.11(a). According to Po et. al (Po *et al.*, 1989) the pump absorption increased by up to 23% with the adoption of this technique. The latter technique involves the alteration of the inner cladding shape. Rectangular, D-shaped and hexagonal shape have been proposed (Li *et al.*, 2004; Muendel, 1996). The designs shown in Figure 2.11(b, c, d) allow both meridional and skew rays to pass through the core and get absorbed more compared to the conventional circular shaped.

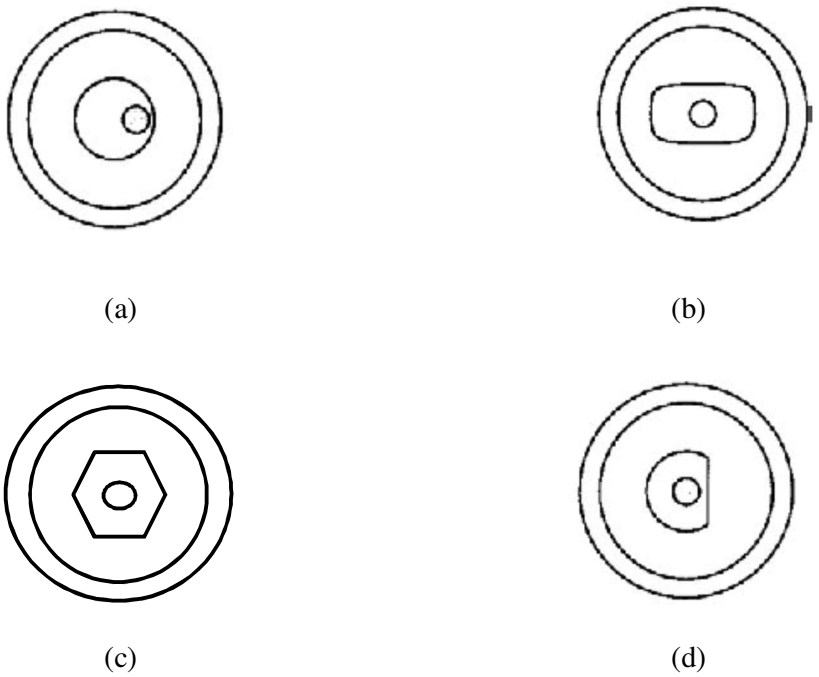

Figure 2.11: Various designs of inner cladding, double-clad fiber. (a) offset core (b) rectangular (c) hexagonal (d) D-shaped (Digonnet, 2002).

The tremendous growth of fiber lasers and their applications have sparked the interest of a lot of research groups to extend the wavelength availability of fiber lasers up to 2 μm. One of the earliest demonstrations of double-cladding Thulium doped fiber laser was reported in 1998 with 5.4 W output power at a slope efficiency of 31% with respect to the launched pump power (Jackson *et al.*, 1998). The gain medium was a double-clad thulium doped fiber with rectangular inner cladding. Two years later, (Hayward *et al.*, 2000) proposed a CW operation of a double-clad Tm-doped silica fiber laser at 2 μm, pumped by two beam-shaped diode bars which yielded an output power of 14 W using a 787 nm wavelength excitation. The slope efficiency with respect to the launched diode power was ~46%. The improved efficiency was reported because of the 'two-for-one' cross-relaxation effect. It is the first to be reported in silica. Before Hayward, this phenomenon was only observed in Tm-doped crystal lasers (Becker *et al.*, 1989). The CR effect happens in fibers with high thulium doping concentration;

however this may lead to ion clustering. Introducing aluminium in the glass doping will reduce clustering (Jackson, 2004; Jackson *et al.*, 2003). Owing to this, the output power and the efficiency of the Tm-doped fiber laser have risen steadily from tens to kilowatts (McComb *et al.*, 2010) level. The highest reported efficiency up to date is 68% utilizing a Tm-doped germanate glass (Wu *et al.*, 2007). Another alternative approach to generate fiber lasers at the 2 μm region was to co-doped the thulium with ytterbium which acts as a sensitizer and successfully generates 18 W output power with 35% efficiency (Jackson, 2003). In 2005, Jeong et.al reported on the generation of a 75 W output power with 32% efficiency (Jeong *et al.*, 2005). The reported works on high-power operation at the 2 μm region, mostly highlight on the high output power and thermal damage management, which makes cladding pump configuration an excellent candidate to replace conventional bulk solid-state lasers for many applications, such as remote sensing, LIDAR, medicine, material processing, and industrial machining.

2.5 Q-switched fiber lasers

Q-switching is a simple and well-known technique for achieving energetic and nanosecond pulses in a laser system. In 1962, Hellwarth together with Fred J. McClung, proved their laser theory and generated peak powers 100 times than that of ordinary ruby laser by using electrically switched Kerr cell shutters (McClung *et al.*, 1963). The invented pulse produces fast, intense and controllable 'giant' laser pulses by 'Q-modulation'. Nowadays, the generated pulse is called Q-switching. Generally, the fiber laser can be designed to operate either in CW or pulsed mode. Figure 2.12(a) shows the continuous output powers by CW lasers while Figure 2.12(b) shows the pulsed laser which generates the output power with constant time. Usually the important parameters for Q-switched laser are pulse width, repetition rate, output power and pulse energy. In

this section, a general overview of Q-switching is given in order to understand the results presented in chapter 5.

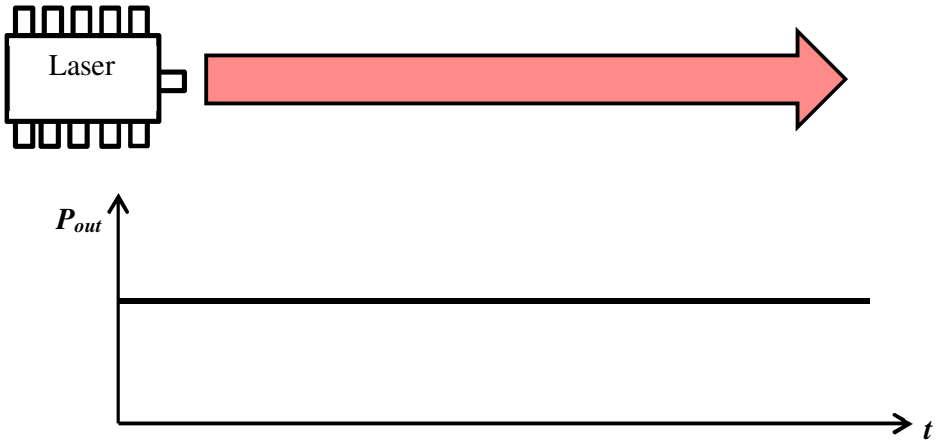

(a) Continuous wave laser

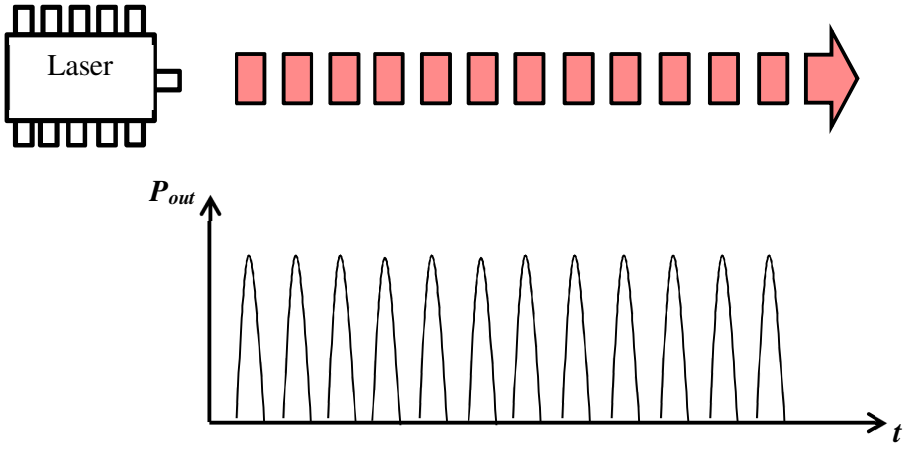

(b) Pulsed laser

Figure 2.12: The operation of CW and pulsed lasers.

2.5.1 Pulse formation in Q-switched lasers

Q-switching laser involves the technique of modulating the losses of the laser resonator by any method. The term Q represents the quality of the laser resonator which contains information regarding the cavity losses. The quality factor (Q-factor) portrays the ability of a laser cavity to preserve its energy. A higher Q indicates a lower intracavity loss. The Q-switching phrase describes the idea of switching the laser configuration from a low to high Q to create short pulse duration. Originally, the Q-factor is kept at low level (i.e. high losses), preventing any potential for lasing. The gain medium provides an accumulation of spontaneous emission in the cavity by constant pumping; thus energy is stored. At the moment that the Q-factor is suddenly switched to a high level and the desired amount of energy is stored, spontaneous emission grows into lasing and a laser pulse starts to build up in the laser cavity. The pulse grows stronger until the gain equals the losses. When the pulse peak power is reached and depletes the gain completely, the laser is no longer able to oscillate. The Q-switched is open again (low Q), and the process starts from the beginning to build up more inversion for the next consecutive pulse. It is useful to have a long upper state lifetime of a gain medium in order to store gain, therefore it does not disappear as fluorescence emission before the Q-switched is opened (Digonnet, 2002).

A Q-switched laser can be realized using active and passive means. The common devices of active Q-switching are electro-optic and acousto-optic modulators. Additionally, the rotating mirror or a prism can also be used. In active Q-switching, the repetition rate can be controlled and exhibit low timing jitter due to the exemption of movable parts in the cavity (Hjelme *et al.*, 1992; Zayhowski *et al.*, 1995). Basically, timing jitter cannot be avoided due to the oscillating photon originating from spontaneous emission from the gain medium. Typically, the pulse width in active Q-switching reduces and the pulse energy rises with the increase in pump power (Eichhorn

et al., 2007). The pulse width depends on the two factors which are the gain and the cavity round trip time whereas the pulse energy depends on the repetition rate (Zayhowski *et al.*, 1991). Since the repetition rate in the active Q-switched can be controlled by driving the modulator with different seed signal, increasing the pulse energy to a certain limit can be done by reducing the repetition rate. As the repetition rate reduces, the gain will be divided by fewer pulses, thus individual pulses will receive more gain.

On the other hand, passive Q-switching offers a simpler method in providing a compact setup and is more cost-effective. It does not need external modulation incorporated in the setup, thus the saturable absorber has been used to self-modulate the cavity losses and the gain. Saturable absorbers are made up of materials and methods such as semiconductor compounds (Spühler *et al.*, 1999) and crystal doped (Chen *et al.*, 2000; Tsai *et al.*, 2000). Other reported works focused on the generation of Q-switching using doped fiber (Jackson, 2007; Kurkov, 2011). The transmission and reflection of the saturable absorber are based on the light intensity. It absorbs the light up to a certain limit which is determined by the absorber saturation fluence (Keller, 2003). When the energy reaches the limit, pulse is released.

In this thesis, passively Q-switched fiber laser has been demonstrated in conjunction with a graphene and multi-walled carbon nanotubes (MWCNTs) based saturable absorber (SA). Graphene and carbon nanotubes are allotropes of carbon with a cylindrical nanostructure, which has been observed by previous scientists in 1991 (CNTs) and 2004 (graphene). The tremendous growth of these materials was due to their unique structure and physical properties (Hasan *et al.*, 2009; Sun *et al.*, 2010b). The carbon nanotubes and graphene saturable absorber characteristic will be discussed in section 2.6.1 and 2.6.2, respectively.

2.5.2 Passive Q-switching parameters

Figure 2.13 shows the formation of the Q-switched fiber laser of one pulse cycle (Spühler *et al.*, 1999). The saturable absorber with bleach, '0', unbleached conditions 'q_0' and a saturable absorber loss coefficient $q(t)$, have been considered and the total cavity loss within one cavity round trip is l. As can be seen in the figure, the pulse starts to emerge when the gain, $g(t)$ reaches the total cavity loss condition (low Q) at the saturable absorber unbleached conditions. At this point, the power increases until the gain is capable to bleach the absorber. Next, when the induced power causes the absorber to totally bleach, the gain is at the high Q until the gain starts to deplete. The maximum pulse occurs when the gain is equal to the total cavity loss at the bleach condition. Then, the gain depletion continues and reaches the negative value, therefore the intracavity power decreases. Finally, the absorber restores its unbleached state due to the shorter absorber's recovery time as compared to the gain. The continuous pumping of the gain medium will provide sufficient gain to attain the threshold level to start over for the next consecutive pulse.

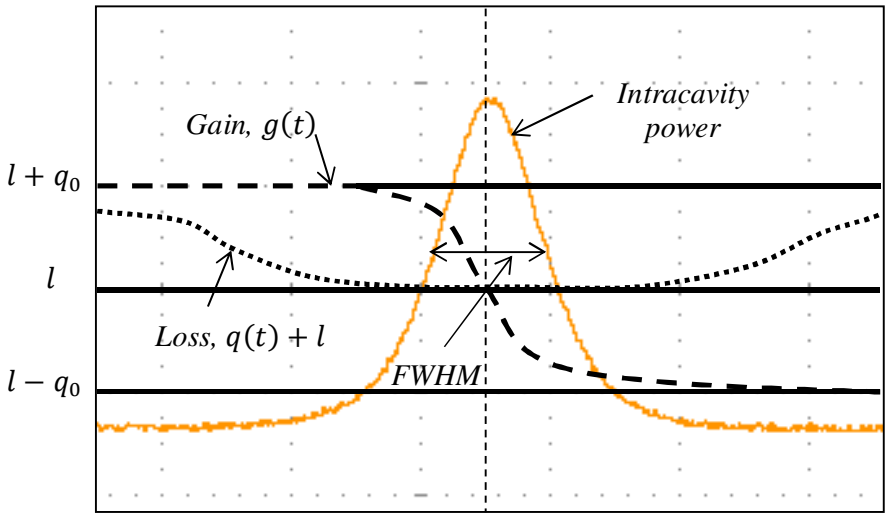

Figure 2.13: The formation of Q-switched fiber laser.

In passive Q-switching, pulse width and pulse energy are independent of the pump power (Spühler *et al.*, 1999). However, the pulse width usually decreased as the pump power increased as explained by (Herda *et al.*, 2008). The pulse width (which is sometimes called pulse duration) of the Q-switching can also be observed in Figure 2.13. The FWHM of the pulse determines the pulse width. According to (Zayhowski *et al.*, 1994) and based on the figure, the pulse width can be expressed as:

$$\tau_p = \frac{S_p T_r}{q_0}\left[\frac{\delta(1+\delta)\eta}{\delta - ln(1+\delta)}\right] \tag{2-12}$$

where S_p is the pulse shape factor, T_r is the cavity round-trip time, η is the energy extraction efficiency of a light pulse and δ is the ratio between saturable and unsaturable cavity loss. It can be seen that the pulse width is proportional to the cavity round-trip time and inversely proportional to the saturable losses of the cavity.

The repetition rate is defined as a number of emitted pulses per second or the inverse of adjacent pulse. It can be measured directly from the oscilloscope by observing the duration between the output pulse trains. The repetition rate is commonly observed to be linearly dependent on the pump power and normally in the range of 1–100 kHz. This has also been confirmed by various experiments using fiber lasers (Jackson, 2007).

The average power of the Q-switched laser is measured directly from the power meter. Since average power is measured while the laser is Q-switching, the repetition rate at which the measurement was taken should be considered to calculate the pulse energy. An equation for the pulse energy is determined by dividing the average power, P_{avg} by the repetition rate, f_{rep}:

$$E_p = \frac{P_{avg}}{f_{rep}} \tag{2-13}$$

According to (Spühler *et al.*, 1999), the pulse energy depends on the amount of energy stored in the gain medium. Therefore, the lifetime of the gain medium and the absorber saturation loss are crucial. This is due to their relation as shown in Figure 2.13. Nevertheless, passive Q-switching suffers from the timing jitter (Huang *et al.*, 1999). This is due to the fluctuations in pump power, temperature, losses and many more. In a fiber laser, the large amount of intracavity spontaneous emission is significant to produce jitter in a pulse.

2.6 Saturable absorber materials

The emerging of carbon materials in industrial applications has started since 60s (Savage, 1993). The evolving of carbon material namely carbon nanotubes and graphene provide greater benefits owing to their extraordinary properties. These carbon nanostructures are significant for current technological and scientific revolution; nanotechnology. A graphite is one of the allotropes of carbon materials instead of the famous diamond. Figure 2.14 shows the atomic structure of graphitic materials which consists of (a) 0D Fullerene, (b) 1D Carbon nanotubes (CNTs), and (c) single layer graphene (2D graphene). The terms graphene comes from the single atomic layer of graphite (Geim *et al.*, 2007).

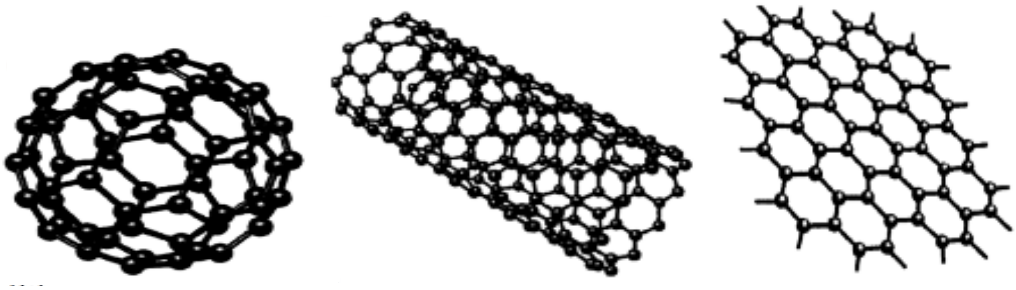

(a) (b) (c)

Figure 2.14: The atomic structure of graphitic materials which consists of (a) 0D Fullerene, (b) 1D Carbon nanotubes (CNTs), and (c) 2D graphene. (Geim *et al.*, 2007)

2.6.1 Carbon nanotubes (CNTs)

The CNTs was observed in 1991 by Iijima in the carbon soot of graphite electrodes during the arc discharge method (Ando *et al.*, 1993). CNTs can be formed by rolling the graphene sheet into a cylindrical nanostructure at specific discrete (chiral) angles (Figure 2.14(b)). The combination of the rolling angle and radius of the CNTs decide the nanotube properties. In CNTs, the bandgap is controlled by the diameter, which in turn defines the operating wavelength of the CNTs. According to the number of walls that form the nanotube, CNTs can be categorized as single-walled nanotubes (SWCNTs) or multi-walled nanotubes (MWCNTs). In the case of a MWCNT, concentric graphene sheets are stacked one on top of the other which then form the large diameter of the outer tubes of MWCNTs. Iijima reveals the structure of these tubes using transmission electron microscopy (TEM) (Iijima, 1991). Another important feature of MWCNTs is the rolled up diameter which are in the range of tens of nanometers and in some cases even more than 100 nm (Darabont *et al.*, 2005) as compared to SWCNTs which have a diameter of only up to 2 nm.

Many research works have been carried out for CNTs fabrication using various techniques such as arc discharge method and laser ablation method (Guo *et al.*, 1995). Nowadays, the fabrication of CNTs can be realize in a mass production and are commercially available. Most commercially available CNTs are produced at large scale by various Chemical Vapour Deposition (CVD) methods, for example high pressure carbon monoxide (HiPCO) (Bronikowski *et al.*, 2001) and Cobalt-Molybdenum catalyst (CoMoCAT) methods from carbon monoxide (Alvarez *et al.*, 2002), and Alcohol catalytic CVD (ACCVD) method from alcohol (Maruyama *et al.*, 2002). The available CNTs are supplied in the powder form or as the dispersed solution. Various methods have been implemented to integrate the SAs in the laser devices, for example free space arrangement, optical deposition in fiber ends and inside fiber, evanescent field using tapered fiber and sandwiching the SAs polymer composite between two fiber connectors (Sun *et al.*, 2012). The latter is the most famous technique used so far. Apart from that, host polymer is another important material to incorporate in the fabrication of CNTs. The characteristic of the host polymer is usually stable against humidity or other environmental factors and laser irradiation (Booth, 1989). The wide range of host polymer used include polivinyl alcohol (PVA), poly-carbonate (PC), polyimide (PI), polymethyl methacrylate (PMMA), carboxymethyl cellulose (CMC) and many more (Hasan *et al.*, 2009). Since the first demonstration of SWCNTs as SA in 2003, the performance of ultrafast laser has improved significantly.

2.6.2 Graphene

Single layer graphene (Figure 2.14(c)) was discovered by Geim and Novoselov in 2004, when it is understood that the material does not exist in free-state. A few-layer graphene and single layer graphene have been produced using scotch-tape method from graphite (Geim *et al.*, 2007). The method is called mechanical exfoliation of graphite.

The large-scale graphene production is called liquid-phase exfoliation (LPE) method, in which graphite flakes are dispersed in solvent, followed by ultrasonification and centrifugation to obtain dispersed solution of small flakes of few-layer and single-layer graphene (Hernandez *et al.*, 2008). However, the most promising method for graphene fabrication is a CVD method (Obraztsov *et al.*, 2007).

Graphene rapidly become a rising star due to its unique and valuable electronic properties (Geim *et al.*, 2007). A few layer or single layer graphene can be determined by Raman spectroscopy measurement (Graf *et al.*, 2007). Single layer graphene exhibits optical transmittance as high as 97.7% with linear Dirac electron dispersion which enables broadband application (Bonaccorso *et al.*, 2010). Graphene has been used in many fields and its nonlinear optical absorption properties enable graphene to be used in photonic applications (Hasan *et al.*, 2009). When a laser source is applied to the graphene, the electrons in the lower energy state (valence band) absorb the photon, hence higher electron energy state (conduction band) is occupied until further absorption is blocked, which is known as a Pauli blocking effect. This results in saturable absorption of graphene (Sun *et al.*, 2010a). Due to the ultrafast saturable absorption of graphene, it has been demonstrated to be a promising material as a saturable absorber in mode-locking to generate ultrashort laser pulses. The first reported mode-locked laser was in 2009 which incorporate graphene as a saturable absorber (Sun *et al.*, 2010a). Since then, graphene became a new SA material with ultrafast recovery time and operational wavelength independence.

CHAPTER 3

DEVELOPMENT OF THULIUM-YTTERBIUM FIBER LASERS

3.1 Introduction

Recently, the development of Thulium doped optical fiber lasers (TDFLs) operating at near 2000 nm has become an interesting topic for many researchers (Gumenyuk *et al.*, 2011; Wu *et al.*, 2007; Zhang *et al.*, 2011c). This is attributed to the possibility of achieving laser of high efficiency, high output power, and retina safe in addition to specific applications plausible for this wavelength, such as for remote sensing and biomedical applications (Slobodtchikov *et al.*, 2007). However, there are still many issues to be addressed such as low quantum efficiency of generated laser in high-phonon energy glass host matrix such as silica-based glass fibers. Thulium doped fibers (TDFs) normally employ low phonon energy glass hosts, for instance fluoride glass, in which the up-conversion intensity is reported to be quite high in ultraviolet region (Cao *et al.*, 2008). Nevertheless, since the fluoride host is a rather soft type of glass, it is very hard to draw optical fiber from the preform due to its lower melting temperature. Recently, the interest has shifted back to silica based host TDFs as the phonon energy of silica glass can be reduced by incorporating silica network modifiers like Aluminum (Al) and Germanium (Ge). Thus TDFs with modified silica host have emerged as a promising gain medium for achieving an efficient TDFL (Jander *et al.*, 2004).

Thulium presents three major absorption bands in the infrared region from the ground state absorption (GSA) which are $^3H_6$ to $^3F_4$ (~1670 nm), $^3H_5$ (~1210 nm) and

$^3H_4$ (~790 nm) (Moulton *et al.*, 2009). One of the advantages of thulium is the enormous bandwidth emission from $^3F_4 \rightarrow {}^3H_6$ transition which is close to 130 nm. Pumping with ~790 nm pump wavelength allows cross relaxation between Tm^{3+} ions provided that high power ~790 nm pump wavelength and significant amount of Tm^{3+} ions concentrations are applicable in the setup. Unfortunately, the availability of high power laser diode at ~790 nm pump wavelength is very costly as well as hard to find. Another problem associated with thulium ions is the lack of pumping source at their high absorption band of 1200 nm wavelength. Thus, an alternative approach has been taken in which the Yb^{3+} ion is co-dope to the Tm^{3+} ions. Ytterbium-thulium doped fiber (YTDF) relies on the indirect pumping from the Yb^{3+} usually over the wavelength region from 910 nm to 980 nm. The emission of Ytterbium at a wavelength of 1.0 µm to 1.2 µm allows the energy transfer between the $Yb^{3+} \rightarrow Tm^{3+}$ (Jackson, 2003). In this case, Yb^{3+} ions act as a sensitizer to the Tm^{3+} ions, as in the case of Ytterbium Erbium doped fiber (Simondi-Teisseire *et al.*, 1996).

In this chapter, a thorough study of newly fabricated double-clad Tm^{3+}/Yb^{3+} co-doped yttria alumina silicate fibers (YTDFs) is carried out. The performance of 1.9 µm fiber lasers are investigated based on cladding pumping technique using the YTDF as the gain medium. The new YTDF is drawn from a D-shape preform which is fabricated using modified chemical vapour deposition (MCVD) in conjunction with solution doping technique. In addition to the discussion on the fabrication process of YTDF, a thorough analysis on the performance of fiber laser has been investigated experimentally. Effect on the use of different pumping wavelength has also been investigated in terms of their ability to generate higher lasing efficiency as well as lower threshold power. For the efficient fiber laser, the effect on the various lengths and doping concentration on the lasing efficiency and threshold power are demonstrated.

3.2 Fabrication of Double Clad Ytterbium-Sensitized-Thulium-Doped fiber

Various types of YTDF with different Ytterbium host composition have been fabricated by the team from Central Glass and Ceramic Research Institute (CGCRI) in Kolkata, India, using a Modified Chemical Vapor Deposition (MCVD) technique and solution doping technique (Townsend *et al.*, 1987). The core of the preform was a combination of alumino-silicate and yttrium aluminosilicate fabricated through the deposition of multiple porous phosphosilicate layers at several deposition temperatures and various pre-sintering temperatures. In the MCVD process, a pure silica glass tube of outer/inner diameter 20/17 mm was used for the deposition of 3–8 multiple porous unsintered phospho-silicate (SiO_2-P_2O_5) soot layers to make a preform while maintaining a suitable deposition temperature at around 1400–1450 °C (Figure 3.1). Figure 3.2 shows the scanning electron microscopic (SEM) image of the multiple unsintered soot layer (before solution soaking) when it is scanned along the vertical direction. The deposited silica tube was then cut so that a suitable strength of dopant precursors can be doped in the glass using the solution doping technique (Figure 3.3).

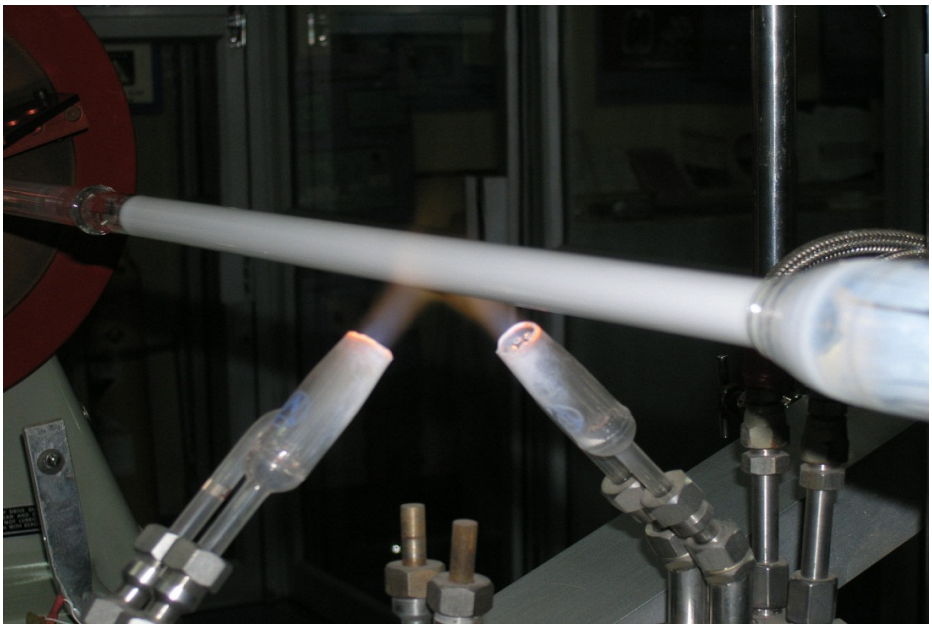

Figure 3.1: Deposition of multiple porous layer of composition SiO_2-P_2O_5 along forward direction by the MCVD process.

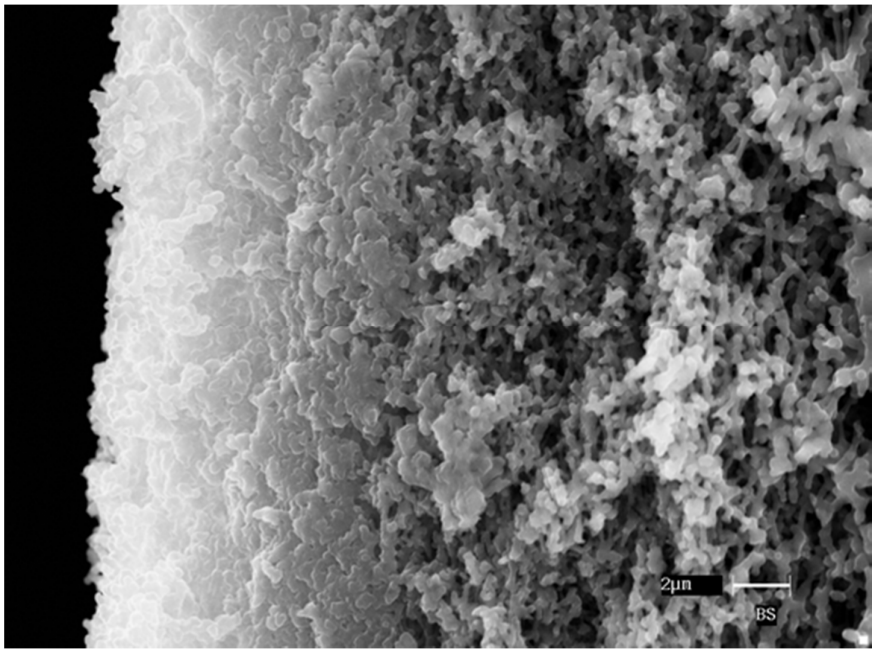

Figure 3.2: SEM image of multiple un-sintered soot layers which is obtained before solution soaking and scanned along the vertical direction.

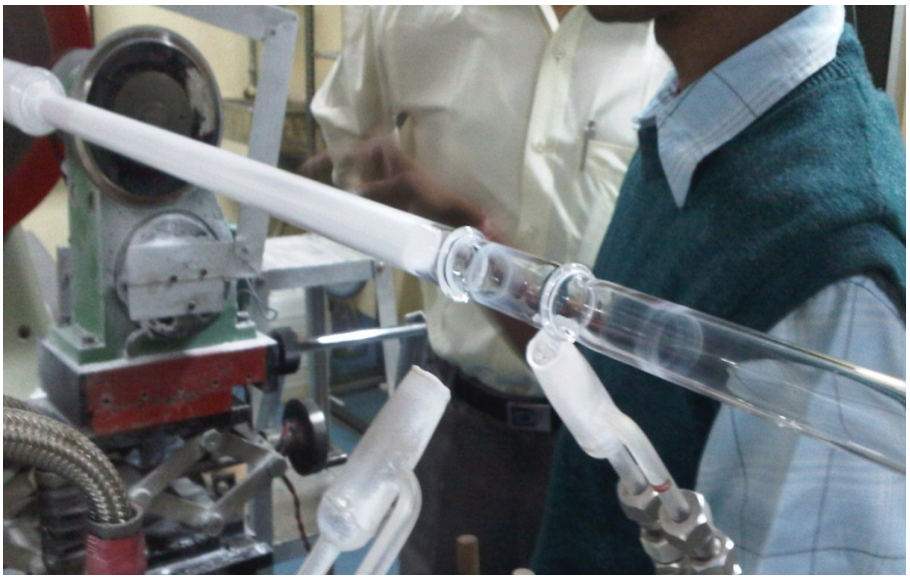

Figure 3.3: Process of cutting the deposited silica tube.

During the solution doping technique, the deposited multiple un-sintered SiO_2–P_2O_5 core layers are soaked with an alcoholic solution of suitable strength of $YbCl_3$ $6H_2O$, $TmCl_3$ $6H_2O$, $AlCl_3$ $6H_2O$ and YCl_3 $6H_2O$ for a certain period of time (30–45 min). Enough soaking duration was determined by the conductivity test for observing soaking kinetic path. The measurement was conducted by dipping the conductivity cell of the Radiometer analytical model-CDM 210 conductivity meter into the tube during solution soaking at a constant time interval. Figure 3.5 shows the plot of conductivity versus time according to the following equation.

$$\frac{d(C_t - C_\alpha)}{dt} = k(C_0 - C_t)^n \qquad (3\text{-}1)$$

where, C_t is the conductance of the solution at time t during soaking, C_α is the conductance of the solution after infinitely long soaking time (taken after 3 hours from the starting), C_0 is the conductance of the solution at the starting time of soaking (within 1 min after pouring the solution into the tube), k is the rate constant and n is the order of soaking kinetic path. This plot suggests that the optimum soaking period is around 30 to 45 min to achieve efficient doping.

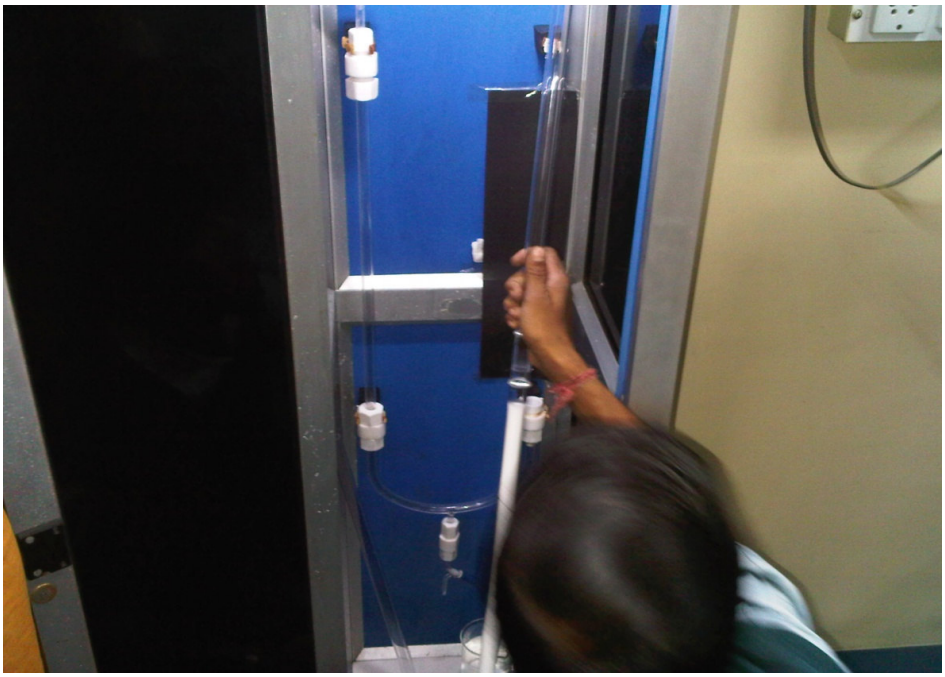

Figure 3.4: Image of the solution doping process.

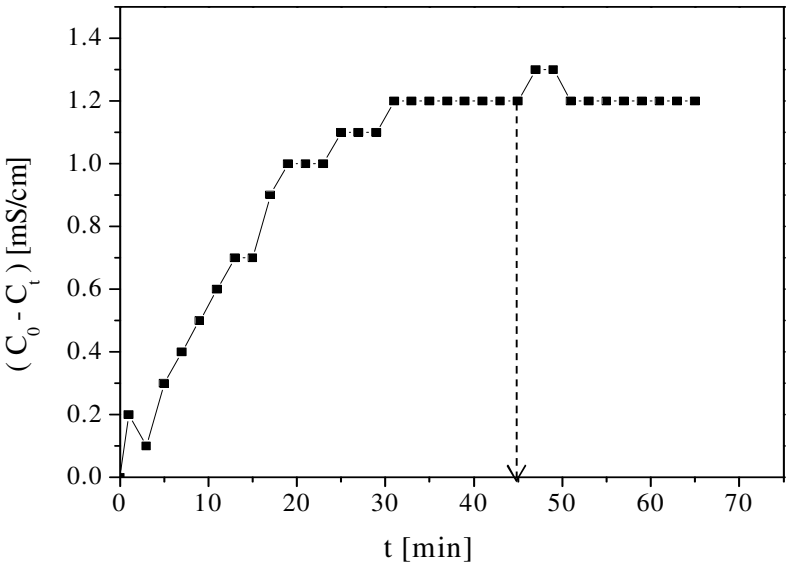

Figure 3.5: A plot of conductivity $(C_0 - C_t)$ versus time (t) during the solution soaking process.

Then, dehydration and oxidation were performed at the temperature of around 900–1000 °C. Sintering of the un-sintered layers were also done by slowly increasing the temperature from 1500 to 2000 °C. Upon the completion of sintering and oxidation, the tube was slowly collapsed to transform it into optical preform. During the collapsing process, the core glass is phase separated into silica rich and silica deficient areas so that it forms a glass matrix with a combination of Tm_2O_3 and Yb_2O_3 doped yttria alumino rich and deficient phase-separated silica glass matrix. It is done by increasing the temperature of the flame and decreasing the speed of the torch (burner) moving along the rotating tube.

The fabricated preform was then drawn into a double-clad D-shaped fiber with an outer cladding diameter of 125 μm. In the drawing process, the preform is vertically installed in the fiber drawing tower (Figure 3.6) before it is transferred into a high temperature furnace for heating and drawing process. The preform is heated and drawn at the temperature of 2050 °C. The D-shaped geometry of the cladding improves the pump absorption. The double-clad fiber allows the injected light to propagate into the cladding in contrast to the single mode fiber. The fabricated fiber is coated with a polymer resin with low refractive index of 1.379. In this thesis, we have selected only four fibers; LTY2, LTY3, LTY6 and LTY8 having Y/Al ratio of 0.84, 0.29, 0.95 and 3.00, respectively.

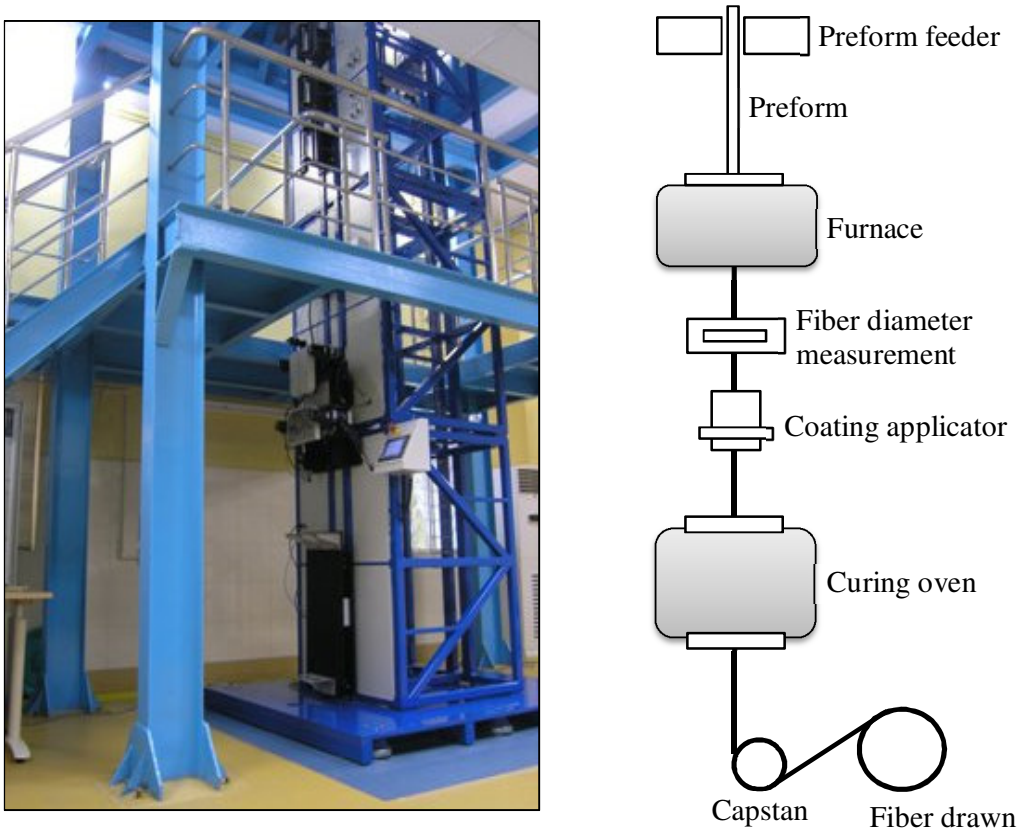

Figure 3.6: Schematic diagram of the drawing process. The left picture is the drawing tower used in the process.

3.3 Optical characteristic of the preform and YTDF samples

The distribution of the dopants along the whole diameter of the fabricated YTDF preform sample is analysed using an electron probe micro-analyser (EPMA) with the maximum spatial resolution of 30 μm. In the experiment, the polished preform sample with a thickness of 2.1 mm, is analysed after applying thin graphite coating layer for elemental distribution along the diameter of the central core. Figure 3.7 shows the cross sectional dopant distribution measured using the EPMA from one of our samples (LTY8). As seen in the figure, all the dopants are concentrated and homogeneously distributed at the core of optical perform. The core compositions of the preform is $1.0Al_2O_3 – 3.0Y_2O_3 – 0.5Tm_2O_3 – 2.0Yb_2O_3$ in terms of weight percentage (wt. %). The

preform profile was also analyzed by a preform analyzer (PKL 2600, Photon Kinetics, USA) to generate refractive index (RI) profiles as shown in Figure 3.8. From the profile plot, the difference in RI between the core and cladding is obtained. Using this value, the numerical aperture (NA) was calculated.

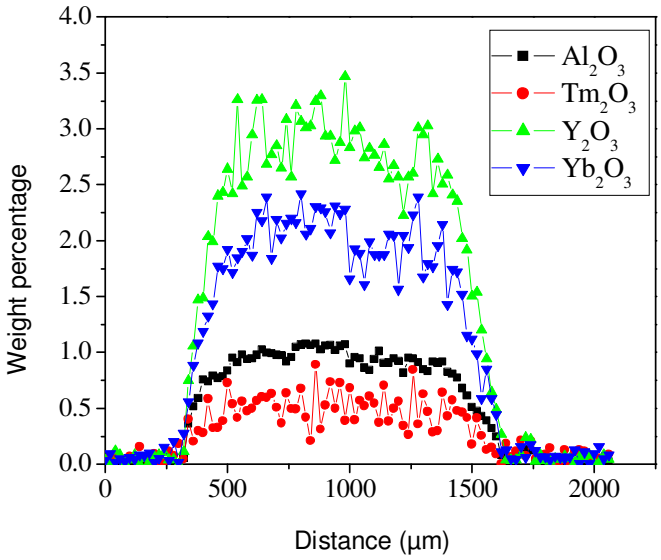

Figure 3.7: EPMA plot of weight percentage versus cross sectional distance (μm) of LTY8 preform.

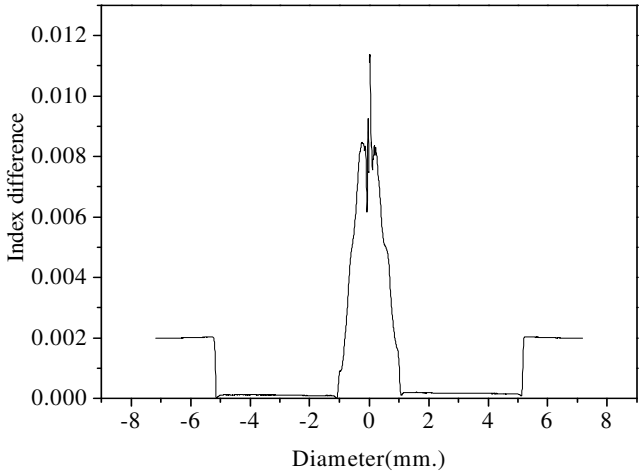

Figure 3.8: RI profile of one the preform showing the index difference between core and cladding.

For inspecting the microstructure of the core glass, a SEM analysis of those preforms is performed. Samples with a thickness of around 3-4 mm were cut out from the preforms. Both sides of these samples were grinded and polished to obtain a thickness of around 1-1.5 mm which is suitable for micro-structural analysis with the maximum spatial resolution of 1 μm after applying thin graphite coating layer. Figure 3.9 shows the SEM image of the core preform samples which indicates that there is no phase separated zone in the core formed during fabrication. As such, the light transference property of the core glass is very good. The presence of Y_2O_3 helps decrease the phonon energy of alumino-silica glass. The decreasing of phonon energy for both Al_2O_3 and Y_2O_3 assists in distributing ytterbium (Yb) and thulium (Tm) ions homogeneously into the core glass matrix which also increases the probability of radiative emission.

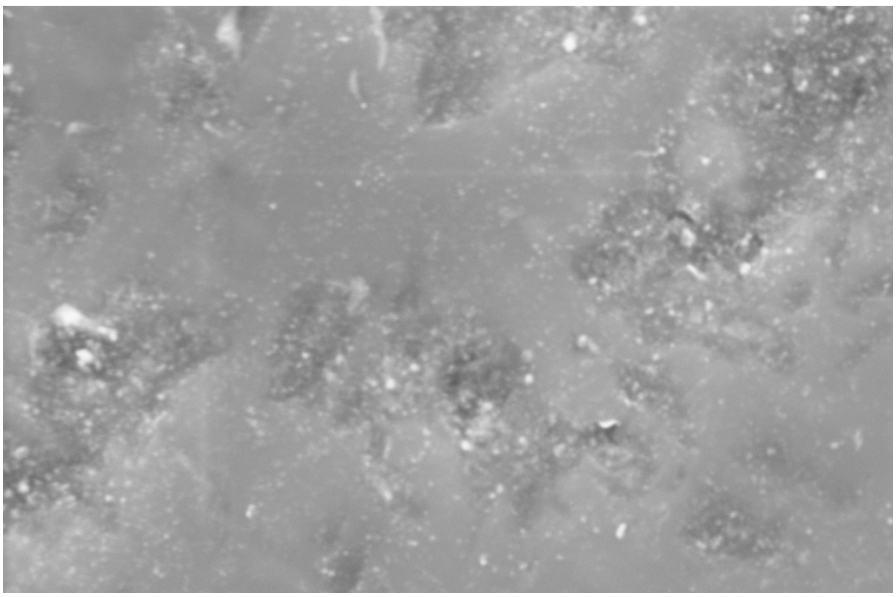

Figure 3.9: SEM image of the core of LTY8 preform, which is obtained after the fabrication process.

A geometry measurement of the YTDF was also carried out. Figure 3.10 shows the microscopic image of the fiber taken by Olympus BX51 microscope attached to a charge-coupled devices (CCD) camera. As shown in the figure, the fiber has a D-shaped geometry, which functions to improve the pump absorption. The characteristics of the fabricated double-clad D-shaped YTDF samples are summarized in Table 3.1.

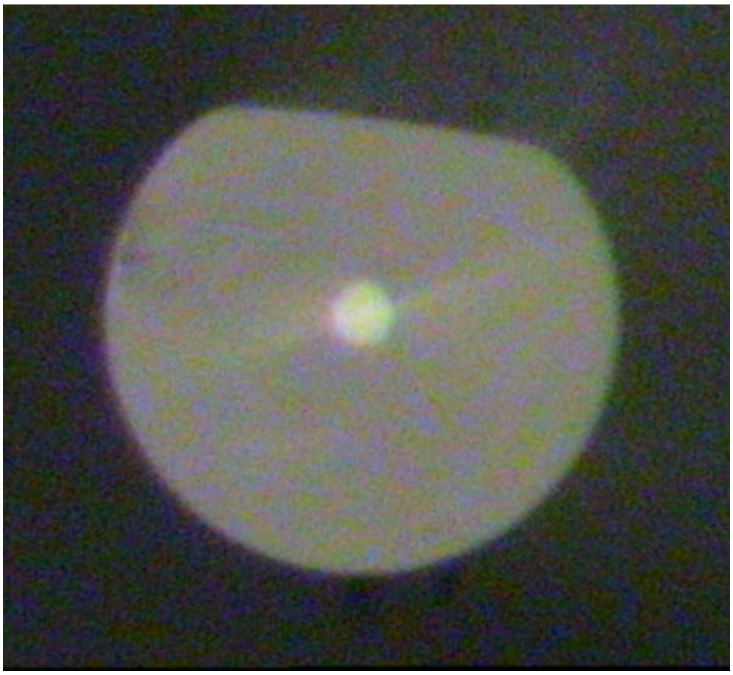

Figure 3.10: Cross section view of LTY8 optical fiber showing the D-shaped cladding structure.

Table 3.1: The characteristic of the double-clad YTDF samples.

Sample	Concentration of dopants into preforms (wt%)	Yb and Tm Ratio (Yb:Tm)	Core diameter of D-shaped fiber	N.A.
LTY2	0.78 Yb_2O_3, 0.68 Tm_2O_3, 0.95 Al_2O_3 and 0.80 Y_2O_3	1.15:1	23.87 µm	0.16
LTY3	0.60 Yb_2O_3, 0.45 Tm_2O_3, 2.0 Al_2O_3 and 0.57 Y_2O_3	1.33:1	27.84 µm	0.25
LTY6	1.98 Yb_2O_3, 0.8 Tm_2O_3, 2.0 Al_2O_3 and 1.90 Y_2O_3	2.5:1	15.87 µm	0.22
LTY8	2.00 Yb_2O_3, 0.5 Tm_2O_3, 1.0 Al_2O_3 and 3.00 Y_2O_3	4.0:1	14.21 µm	0.26

The absorption spectrum of the 40 cm long LYT8 fiber sample is investigated using the Benthom loss measurement technique within the 350-1100 nm range. Then using Lambert-Beer's law, absorbance is calculated for that length. Figure 3.11 shows the obtained absorbance converted into per centimeter length of fiber. From the figure, absorption peaks of Yb^{3+} are obtained at 975 nm and 920 nm due to electronic transitions from $^2F_{7/2}$ to $^2F_{5/2}$. Meanwhile, for Tm^{3+} ions there are three electronic transitions involved; $^3H_6 \rightarrow {}^3H_4$, $^3H_6 \rightarrow {}^3F_{2,3}$, $^3H_6 \rightarrow {}^1G_4$, which correspond to absorption wavelengths of 789 nm, 678 nm and 465 nm respectively (Watekar *et al.*, 2005; Zhou *et al.*, 2010a). The attenuation spectrum of the fiber was also measured using a cutback method at room temperature. In the experiments, a piece of 3 m and 0.5 m fibers used to represent the long and short length respectively, are taken for measuring the attenuation spectrum using a white light source. Figure 3.12 shows the attenuation spectrum of LTY8 optical fiber, which indicates that the measured absorption peaks of Yb^{3+} and Tm^{3+} ions are almost similar to that of Figure 3.11. The absorption peak of Tm^{3+} ion is also observed at 1205 nm, which represents the electronic transition from $^3H_6$ to $^3H_5$.

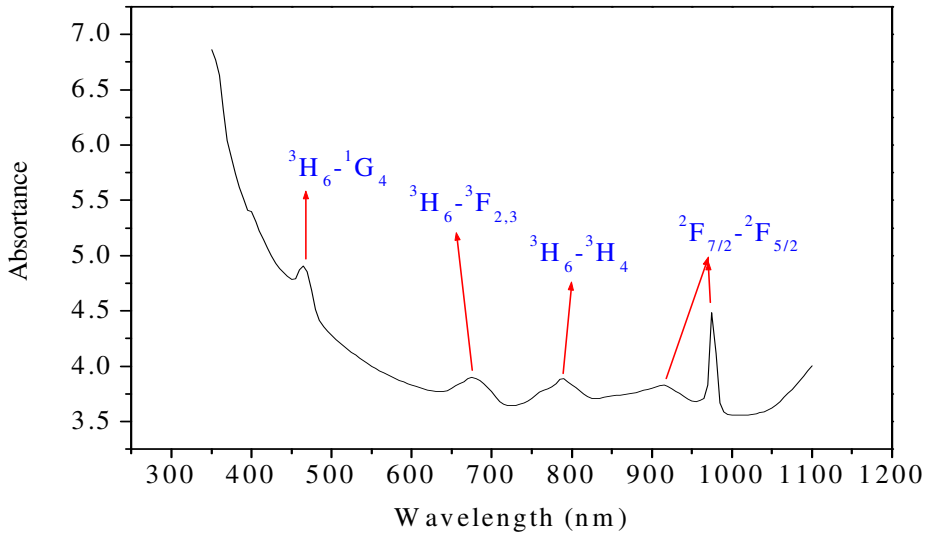

Figure 3.11: Absorption spectrum of LTY8 fiber per centimeter length.

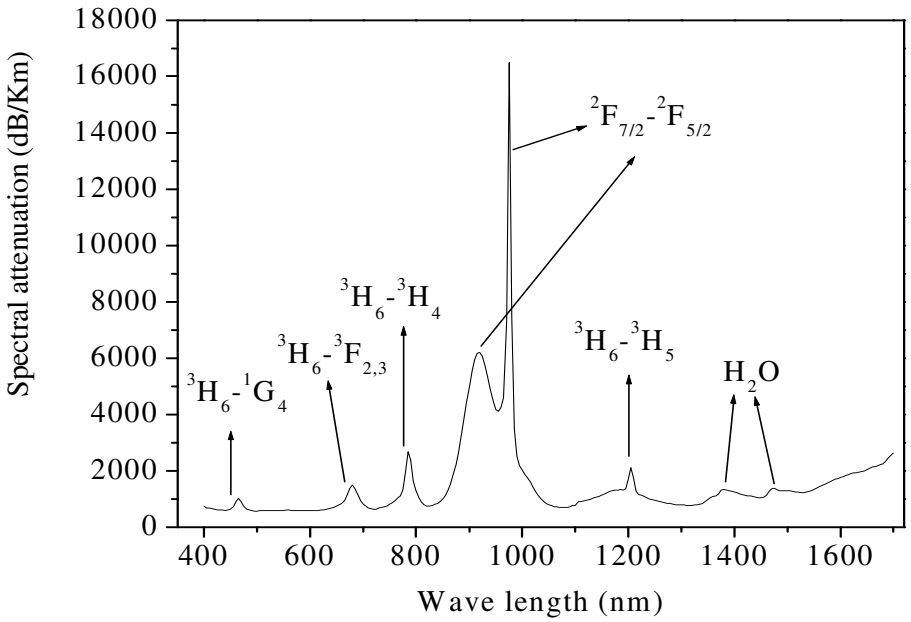

Figure 3.12: Attenuation spectrum of LTY8 fiber.

3.3.1 Up-conversion (UC) luminescence characteristic

The optically active materials in the core of the fiber are Yb and Tm ions. As shown in Figs. 3.11 and 3.12, Yb^{3+} ions have a wide absorption region ranging from 910 nm to 1100 nm and thus the fiber can be easily excited by commercially available laser diode. Then, the excited Yb^{3+} ions act as a good sensitizer by transferring maximum energy to Tm^{3+} ions and produce a strong blue and red UC luminescence that can be seen by the naked eye as it scatters out from the fabricated fibers' surface (Figure 3.13). In the experiment, the emission spectra of the UC luminescence for all YTDF samples were investigated by pumping 1 m long of this fiber with 931 nm laser diode pump at room temperature. The emission light was collected by a large core multimode fiber which was connected to a spectrometer.

Figure 3.14 exhibits the UC luminescence of visible emission peaking at 483 nm, 650 nm and 815 nm for Tm^{3+} and one peak at 1030 nm for Yb^{3+} at 931 nm pump power of 0.7 W. These luminescence peaks of 483 nm, 650 nm and 815 nm are attributed to the electronic transitions from the $^1G_4 \rightarrow {}^3H_6$, $^1G_4 \rightarrow {}^3F_4$, and ($^1G_4 \rightarrow {}^3H_5$ and $^3H_4 \rightarrow {}^3H_6$) manifolds, respectively. As shown in the figure, the intensity of the UC increased with the increased in Yb^{3+} concentration. This observation confirms the occurrence of energy transfer between the Yb^{3+} to Tm^{3+} ions since the luminescence is not observed in the singly doped thulium under the same excitation. It is also observed that the LTY8 and LTY6 pumping with 931 nm pump excitation shows the highest UC intensities for the three UC wavelengths (483, 650, and 815 nm) compared to LTY2 and LTY3. This is due to the higher amount of Yb^{3+} and Tm^{3+} ions in these fibers. The high Yb^{3+} ions indicate that more incident photons occurred between Yb^{3+} ions and the excitation pump, thus allows more photons to be absorbed and high energy transfer to the neighbouring Tm^{3+} ions. To understand the effect of Yb^{3+} concentration on UC luminescence, the spectra of LTY6 and LTY8 is observed under the same pumping excitation and pump power of 0.7 W. It is clearly observed that the Yb^{3+} luminescence intensity (1030 nm) gradually decreases as the Yb^{3+} concentration increased. The result indicates that the efficiency of the energy transfer from Yb^{3+} to Tm^{3+} is increased with the increase of Yb^{3+} concentration with respect to the Tm^{3+} ions. Higher luminescence emission at 483 nm and 650 nm wavelength was observed in LTY8 compared to LTY6. This is attributed to the more Yb^{3+} ions concentration to absorb the incident pump photons and transfer to the Tm^{3+} ions. However, at 815 nm emissions LTY6 shows the highest intensity. The fluorescence band at 815 nm is related to the two transitions which are $^3H_4 \rightarrow {}^3H_6$ and $^1G_4 \rightarrow {}^3H_5$ manifold. $^3H_4 \rightarrow {}^3H_6$ and $^1G_4 \rightarrow {}^3H_5$ transitions are dominant at low and high pump powers, respectively. This shows that the $^3H_4 \rightarrow {}^3H_6$ transition is dominant in the YTDF because the 815 nm emission is higher in LTY6

compared to that of LTY8 as shown in Figure 3.14. A high Yb^{3+} concentration may reduce the quenching effect in Tm^{3+} ions, however it causes the $^3F_{5/2}$ level lifetime of Yb^{3+} ions to drop resulting in decreasing the energy transfer to the Tm^{3+} ions. Therefore, less ions population at $^3H_4$ and $^1G_4$ lowers the luminescence intensity for LTY8 at 815 nm. Figure 3.15 shows the up-conversion spectra from LTY8 fiber at different input pump power. As shown in the figure, the intensity of up-conversion luminescence emission increases with pump power which indicates that the efficiency of the ET increases as well.

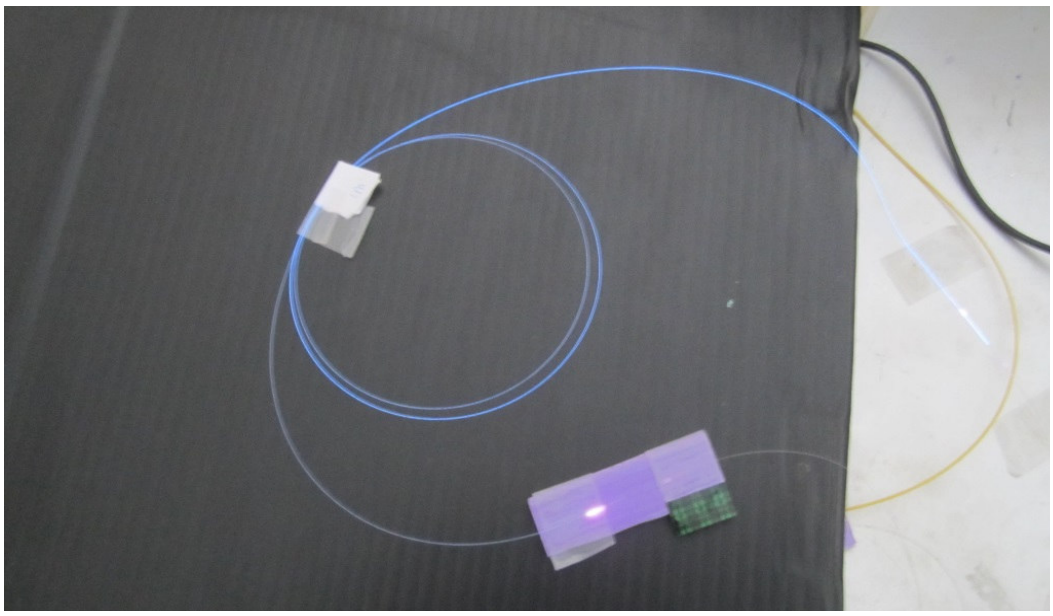

Figure 3.13: UC luminescence from the YTDF observed by a naked eye.

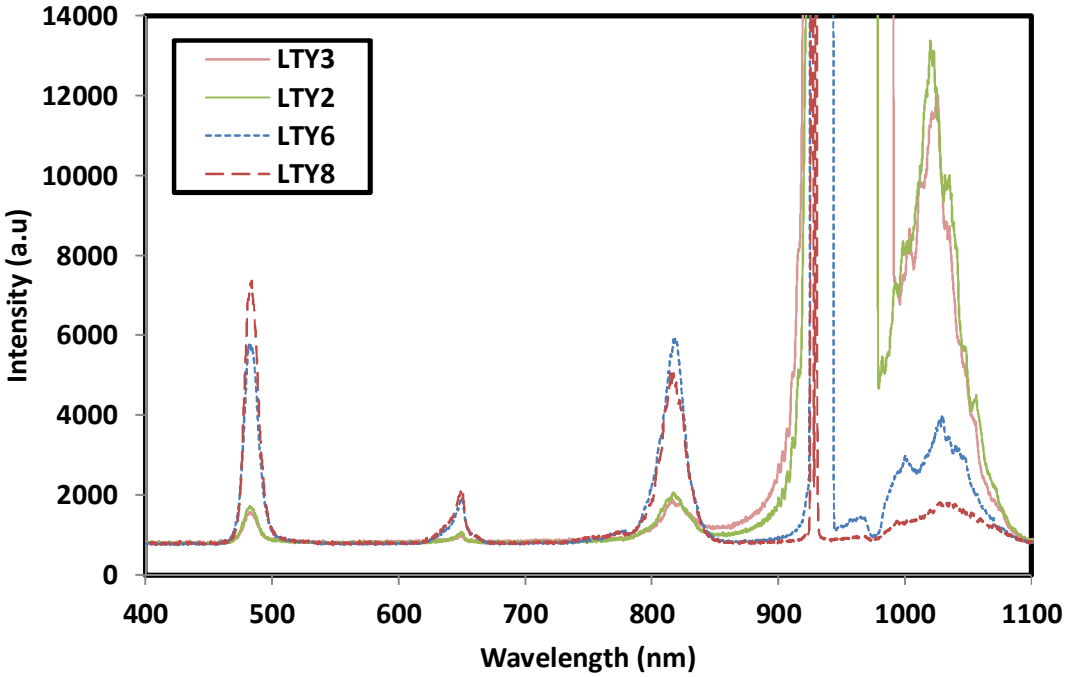

Figure 3.14: Emission spectra of all fibers at 931 nm pump power of 0.7 W.

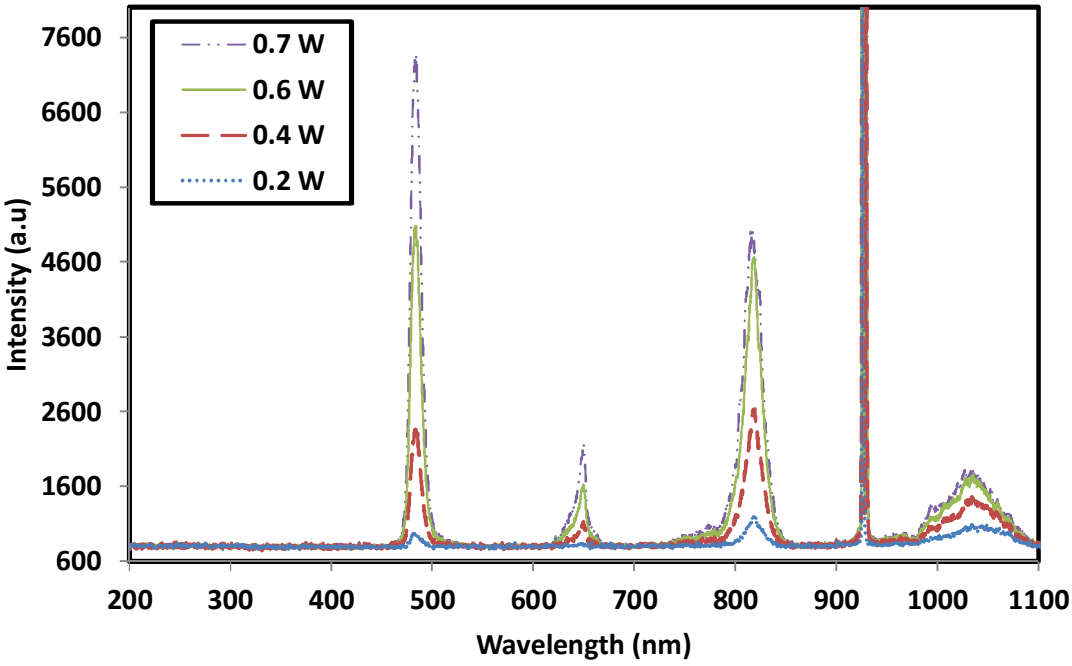

Figure 3.15: Up-conversion luminescence spectra of LTY8 fiber at various 931 nm pump powers.

Figure 3.16 shows a plot of UC peak intensity against pump power. It is observed the curve of intensity increment displays an exponential function of pump power for all UC wavelengths. As shown in Figure 3.16, at high pump power, main emission was dominated by 483 nm, while 815 nm photons dominates the overall UC emission at low pump power. At lower pump power, less amount of pump power absorbed by the sensitizer thus decreasing the number of photons transferred to the Tm^{3+} ions. Therefore, only two photons absorption needed to trigger the $^3H_4 \rightarrow {}^3H_6$ transition compared to the number of Tm^{3+} ions to populate $^1G_4$ level which needs three photons absorption. Since the 815 nm UC emission involves $^3H_4 \rightarrow {}^3H_6$ transition, thus UC emission at this wavelength is dominant. At higher pump power, the amount of Tm^{3+} ions that populate $^1G_4$ level increased significantly, thus the dominant transition for 815 nm UC emission is originating from $^1G_4 \rightarrow {}^3H_5$ transition. However, due to the high branching ratio of silica host for 483 nm (Walsh *et al.*, 2004), the luminescence switching occurred in which the 483 nm UC emission dominates. It can be seen from Figure 3.16, that the blue luminescence (483 nm) is much higher in intensity as compared to the red luminescence (650 nm).

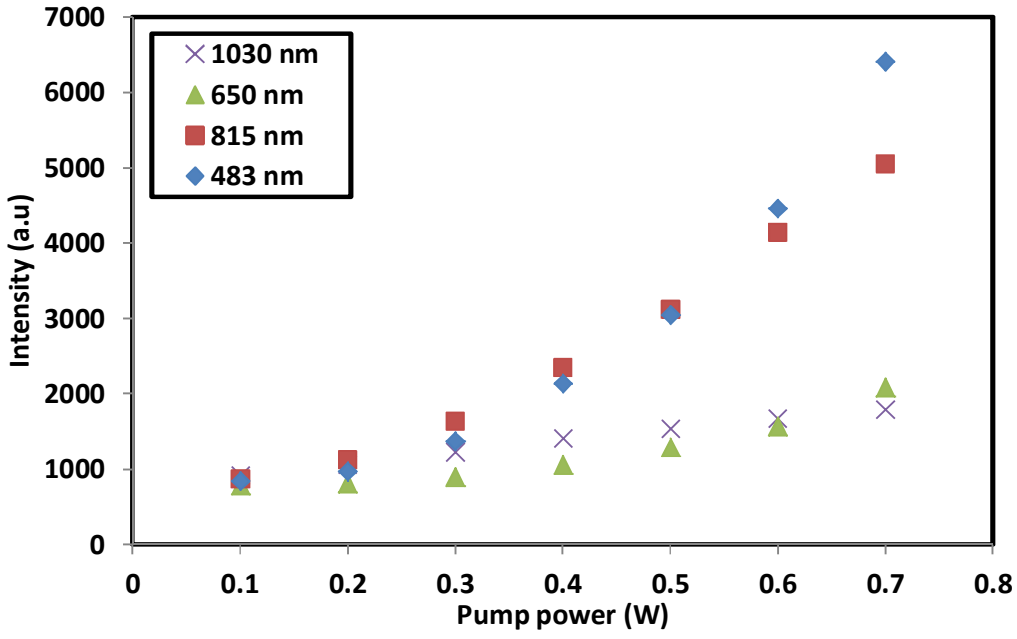

Figure 3.16: UC peak intensity against pump power for LTY8.

The UC process can be explained using Figure 3.17. The Yb^{3+} ions will experience population inversion at $^2F_{5/2}$ level due to the photon absorption from the 931 nm pumped. The excited ion will emits the similar amount of energy while decaying to the $^2F_{7/2}$ level thus transferred some of their energy to the neighbouring Tm^{3+} ions which indicate the 1st ET while the other portion will emits at 1030 nm wavelength (Yb^{3+} luminescence). The UC process in YTDF involves three ET steps. The 1st ET will populate the Tm^{3+} ions from the ground state level, $^3H_6$ to $^3H_5$ level. Due to the narrow gap between $^3H_5$ to $^3F_4$, the ions is then relaxes to the metastable state of $^3F_4$ which has a longer lifetime. Upon relaxation, the Tm^{3+} ions absorb the second photon emission from Yb^{3+} ions thus promoting it to the higher level of $^3F_{2,3}$ to indicate the 2nd ET. Again, the Tm^{3+} ions will relax at the metastable state of $^3H_4$ due to the non-radiative multi-phonon emission. At this level, some of the ions will emit light at 815 nm to the ground state level; $^3H_6$ while some of it will absorb the continuous photons emission from Yb^{3+} indicating the 3rd ET from Yb^{3+} to Tm^{3+}. This absorption will excite Tm^{3+} ions to the $^1G_4$ level. At this level, excited ions will produce the three UC luminescence lines of 483 nm, 650 nm and 815 nm due to the electronic transition from $^1G_4 \rightarrow {}^3H_6$, $^1G_4 \rightarrow {}^3F_4$ and ($^1G_4 \rightarrow {}^3H_5$ and $^3H_4 \rightarrow {}^3H_6$) respectively.

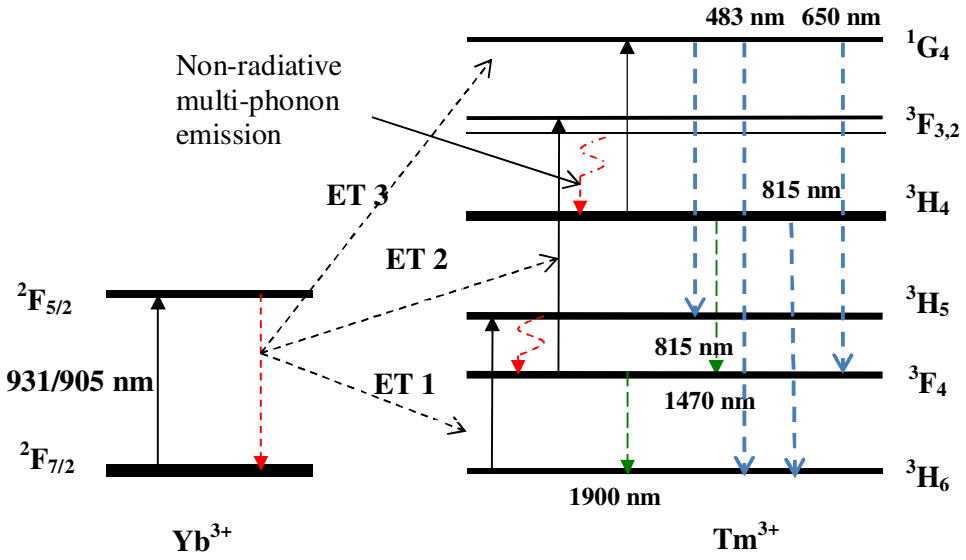

Figure 3.17: The proposed mechanism for UC processed occurred in YTDF via three steps energy transfer UC process.

To explain the above experimental results, the following equations are proposed for the up-conversion emissions under excitation at 931 nm:

$$Yb(^2F_{7/2}) + hv_{931nm} \rightarrow Yb(^2F_{5/2}) \quad (3\text{-}2)$$

$$Yb(^2F_{5/2}) \rightarrow hv_{1030nm} + ET \quad (3\text{-}3)$$

$$Tm(^3H_6) + ET \rightarrow Tm(^3H_5) \rightarrow Tm(^3F_4) + \Delta \quad (3\text{-}4)$$

$$Tm(^3F_4) + ET \rightarrow Tm(^3F_{2,3}) \rightarrow Tm(^3H_4) + \Delta \quad (3\text{-}5)$$

$$Tm(^3H_4) + ET \rightarrow Tm(^1G_4) + hv_{815nm} \quad (3\text{-}6)$$

$$Tm(^1G_4) \rightarrow hv_{650nm} + hv_{483nm} \quad (3\text{-}7)$$

where hv is the energy of absorbing and emitting photons during transitions, ET represent a resonant energy transfer and Δ indicate the heating effect due to the non-radiative emission.

In order to provide better understanding of the ET process from Yb^{3+} to Tm^{3+}, double logarithmic plot of intensity of Tm luminescence for 483 nm versus the intensity of Yb luminescence at 1030 nm is obtained. Figure 3.18 shows the plot for LTY6 and LTY8 samples, in which the spectral intensities are higher. As shown in the figure, the linear slope values are obtained at 2.60 and 2.98 for LTY6 and LTY8, respectively. This indicates that the 483 nm luminescence occurs due to the transition from the $^1G_4$ to $^3H_6$ state after undergoing a three-step ET process.

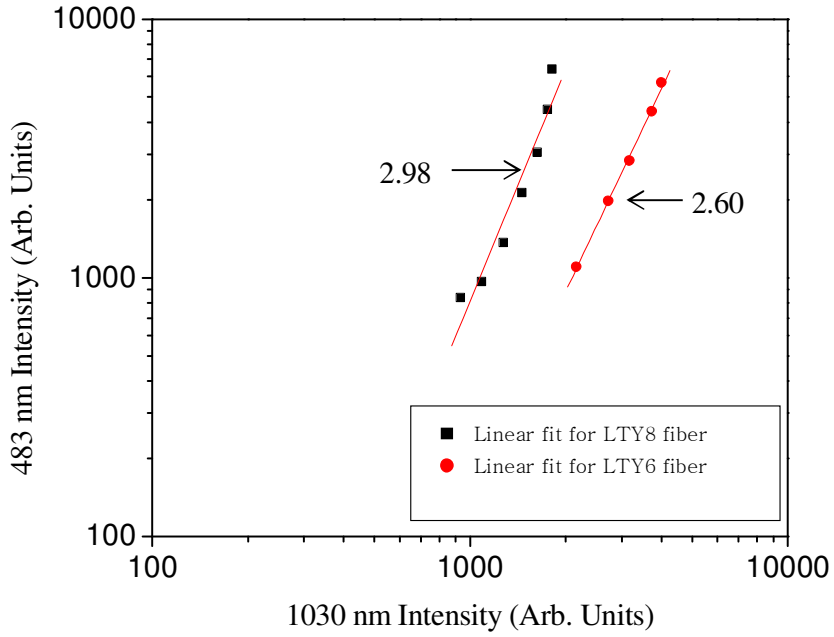

Figure 3.18: Double logarithmic plot for 483 nm versus 1030 nm luminescence for LTY6 and LTY8 fiber samples.

3.4 Amplified spontaneous emission (ASE)

In this section, the ASE characteristic of the YTDF (LTY6) is investigated for 4 different pumping wavelengths; 800 nm, 905 nm, 931 nm and 1552 nm. The 905 nm and 931 nm pumps are multimode whereas the 800 nm and 1552 nm are single mode. The experimental setup is shown in Figure 3.19 where the multimode pump is launched

into the YTDF via a multimode coupler (MMC). The MMC has a multimode input fiber with core/cladding diameter of 105/125 µm while the output fiber is a double-clad fiber with a core/inner cladding/outer cladding diameters of 8/105/125 µm. The generated ASE from YTDF was detected using an Optical Spectrum Analyzer (OSA) operating in a range of 1200 nm - 2400 nm wavelength with a resolution of 0.1 nm. The experiment is repeated with the single-mode pumping scheme by replacing the MMC with a wavelength division multiplexer (WDM).

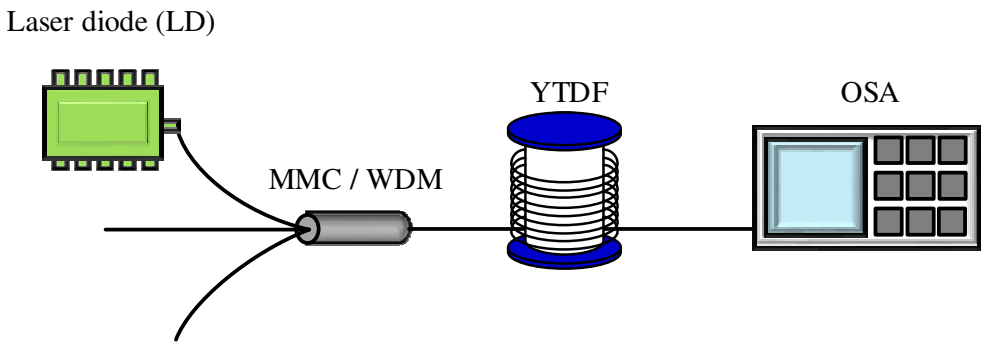

Figure 3.19: Experimental setup for ASE spectrum measurement.

Figure 3.20 shows the ASE spectra of the YTDF at different pumping wavelengths. In the experiment, the LTY6 length is fixed at 1.5 m while all the pump powers are fixed at 1 W except for 800 nm pumping, which has the maximum output power of 200 mW. As shown in the figure, the ASE spectra peak at 1910 nm due to the transition of thulium ion from $^3F_4$ to $^3H_6$. It is observed that both cladding pump wavelengths provide a higher ASE power compared to that of core pumping scheme. In this YTDF fiber, the ytterbium ions were used as a sensitizer to the thulium ions, thus 905 nm and 931 nm pumping excitation were used to excite the ytterbium ions. YTDF will experience the UC process in which the excited ytterbium ions will excite neighbouring thulium ions to the Tm^{3+} excited state in the 3-step electronic transitions process as mentioned in section 3.3.1. Based on Figs. 3.11 and 3.12, the absorption

cross sections at 905 and 931 nm are higher than that of 800 nm and 1552 nm. This also contributes to the higher ASE power.

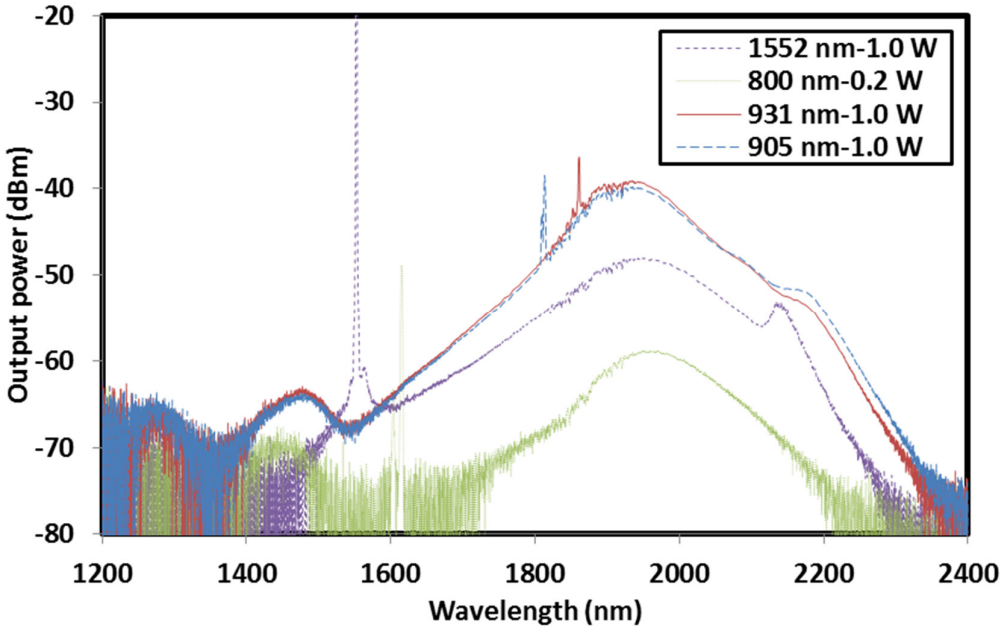

Figure 3.20: The ASE spectrum for LTY6 at 1.5 m using different pumping wavelength.

For single-mode pumping with 800 nm and 1552 nm, the pump light is directly launched into the core of the doped fiber and thus prevents the UC process. This is due to the absence of energy transfer from Yb^{3+} ions to Tm^{3+} ions. Therefore the ASE output power for the core-pumping is significantly lower than the cladding pumping scheme as depicted in Figure 3.20. Pumping with 800 nm pump allows the Tm^{3+} ions to excite to the $^3H_4$ level and experience non-radiative decay to the $^3F_4$ level before emits at 1910 nm wavelength whilst it drop to ground state. Another process that may happen is '2 to 1' cross relaxation. As explained in Chapter 2 (literature), when a significant amount of Tm^{3+} ions occupy the ground state, instead of experiencing multi-phonon emission, an energy transfer to a nearby Tm^{3+} ions happens. This process allows two thulium ions to occupy the $^3F_4$ upper laser level with only one pump photon. Both ions then descend to the ground state emitting the 1910 nm emission. Therefore, the 800 nm

pumping is expected to produce a higher ASE power than 1552 nm when the YTDF is pumped with the same amount of pump power. Aside from pumping with 800 nm, pumping using 1552 nm source only allows ground state absorption. The pumping process only involves thulium ion in the ground state absorbs 1552 nm laser light and excites to the upper laser level, $^3F_4$ before drops back to the ground state which emits at 1910 nm emission.

The emission at 1470 nm was also observed with 800 nm, 905 nm and 931 nm pumping due to the population inversion of thulium ion at $^3H_4$ level. Emission from energy transition from $^3H_4$ to $^3F_4$ creates the emission at 1470 nm region as shown in Figure 3.20 (Peterka et al., 2007). However, the S-band emission cannot be seen when 1552 nm pumping excitation was used to pump the YTDF. This is due to the direct excitation to the $^3F_4$ level without any emission at $^3H_4$ to $^3F_4$. Figure 3.21 shows the possible energy transfer from Yb^{3+} to Tm^{3+} associated to the ASE emission pumping by 931/905 nm, 800 nm and 1552 nm pumping excitation. Eq. (3-8) to (3-10) and (3-11) to (3-13) shows the electronic transition associated with the emission at 1470 nm and 1910 nm respectively.

$$Yb(^2F_{5/2}) + Tm(^3F_4) \rightarrow Yb(^2F_{7/2}) + Tm(^3F_{2,3}) \quad (3\text{-}8)$$

$$Tm(^3F_{2,3}) \rightarrow Tm(^3H_4) + \Delta \quad (3\text{-}9)$$

$$Tm(^3H_4) \rightarrow hv_{1470nm} + Tm(^3F_4) \quad (3\text{-}10)$$

$$Yb(^2F_{5/2}) + Tm(^3H_6) \rightarrow Yb(^2F_{7/2}) + Tm(^3H_5) \quad (3\text{-}11)$$

$$Tm(^3H_5) \rightarrow Tm(^3F_4) + \Delta \quad (3\text{-}12)$$

$$Tm(^3F_4) \rightarrow hv_{1910nm} + Tm(^3H_6) \quad (3\text{-}13)$$

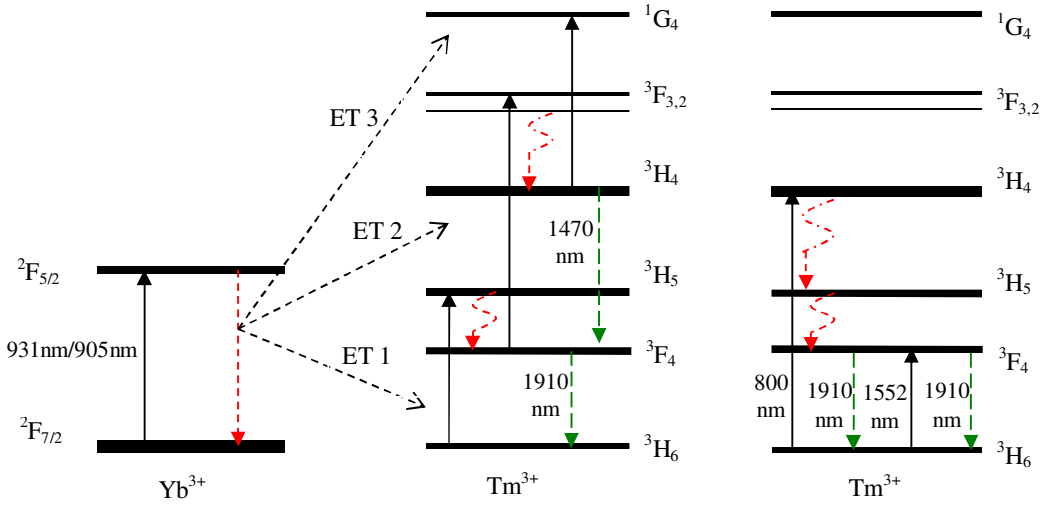

Figure 3.21: The possible energy transfer from Yb^{3+} to Tm^{3+} ions for the fabricated YTDF and the originating of ASE emission.

Figure 3.22 exhibits the ASE spectra of the LTY6 at different 905 nm pump powers. It is obvious that the peak power and the ASE bandwidth increase with the increment in pump power. At the maximum power of 1.0 W, a broadband ASE spectrum with a 10 dB bandwidth of more than 330 nm, which covers the wavelength range from 1770 nm to 2100 nm, is observed. A ripple and peaking at around the 1880 nm region is due to the spurious reflection inside the gain medium.

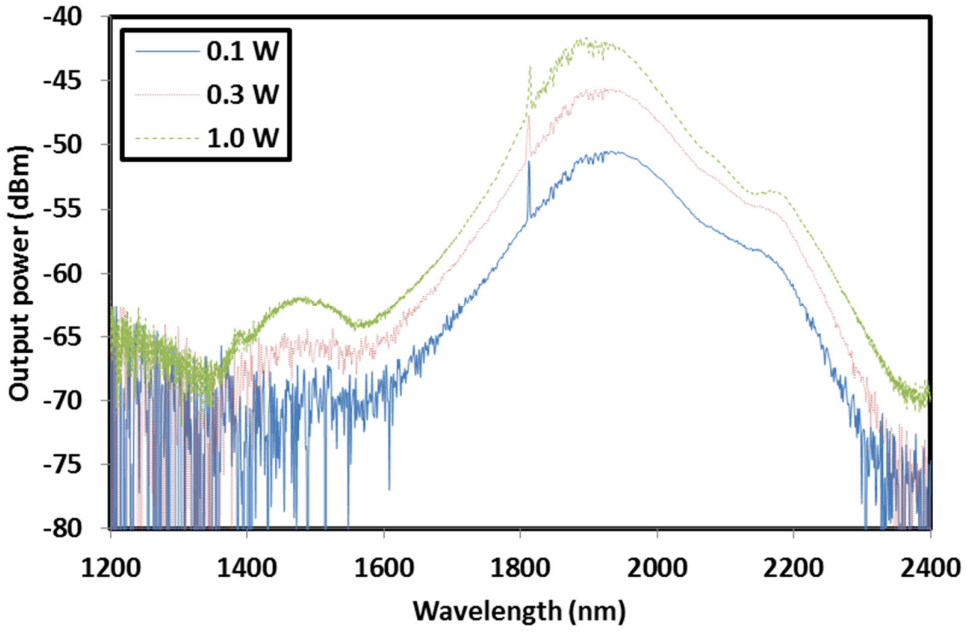

Figure 3.22: ASE spectrum at various pump power using 905 nm pump.

3.5 Fiber laser at 2 micron region using the double-clad YTDF

As discussed earlier, 2 micron laser sources are of interest for many applications in the scientific, defense and medical fields (Digonnet, 2002; Kurkov *et al.*, 2010). The 2 µm radiation has a strong absorption characteristic in water and biological tissues and thus these lasers have a number of potential applications in the medical field. Incisions in porcine tissue and chicken breast have been recently demonstrated with a 1.98 µm continuous wave Tm-doped fiber laser (TDFL) (Pierce *et al.*, 1999; Pierce *et al.*, 2001). Also, the penetration depth of 2 µm laser radiation matches with the subcutaneous depth of the pain nerve receptors in the skin such that the 2 µm laser makes an near-ideal source for experimental pain research as the damage on the skin surface can be minimized (Opsommer *et al.*, 2001). Recently, tissue interactions with a Q-switched TDFL have been reported (El-Sherif *et al.*, 2003a). The 2 µm laser normally uses TDF as a gain medium, which exhibits a significant advantage over other rare earth ions whereby the slope efficiency can exceed the Stokes limit (Hayward *et al.*, 2000; Tao *et*

al., 2013). As explained earlier, 2 micron lasing is achieved due to thulium ions transition from $^3F_4 \rightarrow {}^3H_6$. The ideal pumping wavelength is ~790 nm because of the cross-relaxation energy transfer between thulium ions, where two ground-level thulium ions can be excited to the upper lasing level of the $^3F_4$ by absorbing only one pump photon (Jackson, 2004). Nevertheless, high-power laser diode at this pump wavelength is very limited and costly in commercial market. Pumping thulium at other absorption wavelength of ~1200 nm or ~1600 nm needs intermediate laser source owing to the lack of high-power laser diodes at this wavelengths.

Due to the mentioned difficulties in pumping thulium at high-power level, Tm ion is doped with Yb ion and pump using 910 – 980 nm. The (quasi-) resonant of Tm^{3+} $^3H_5$ level with the excited Yb^{3+} level of $^2F_{5/2}$ allowing for the possibility of sensitization of Tm^{3+} with Yb^{3+}, similar to the case of Ytterbium Erbium doped fiber (Simondi-Teisseire *et al.*, 1996). In this section, a Ytterbium Thulium co-doped fiber laser (YTDFL) is demonstrated by using a newly developed double-clad YTDF as a gain medium. The experimental setup of the proposed YTDFL is depicted in Figure 3.23. It consists of a piece of the fabricated YTDF (LTY8) as a gain medium, a multimode combiner and a 10 dB output coupled to the OSA. The LTY8 length is fixed at 1 m, which optimized with the pump power. A 905 nm laser diode pump is coupled into the YTDF via the multimode combiner. The output of the YTDFL is tapped out using a 10 dB output coupler, which allows 90% of the light to oscillate in the cavity laser and characterized by the OSA. The experiment is repeated using another pump wavelength of 931 nm and 980 nm for comparison purpose. This laser device contains no adjustable parts and can only be controlled externally by the amount of pump power that is injected.

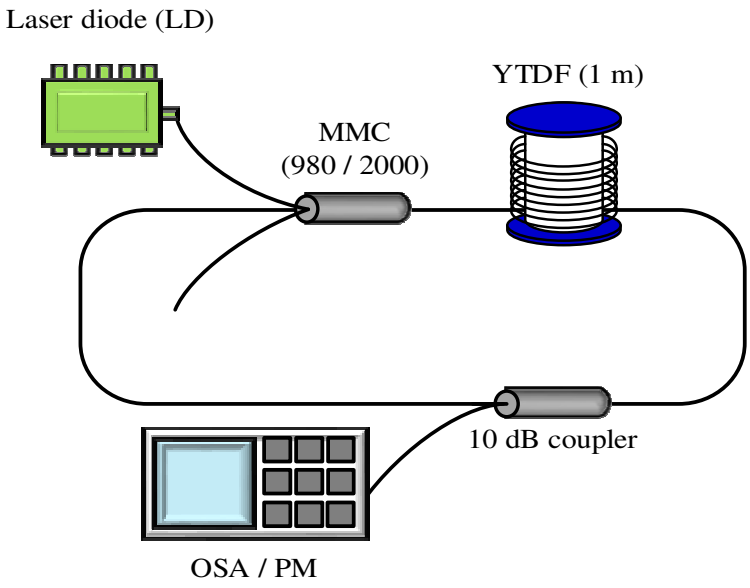

Figure 3.23: Experimental setup for the ring YTDFL operating at 2 µm region.

Figure 3.24 shows the output power of the proposed YTDFL against the launched pump power for two different pump wavelengths of 905 and 931 nm. As shown in the figure, lasing starts at a different threshold power depending on the YTDF lengths and the laser output is observed to linearly increase with the launched pump power. The threshold pump powers are obtained at 0.6 and 1.0 W with 905 and 931 nm pumping, respectively. A maximum output power of 10.5 mW was achieved with the 905 nm pumping at the maximum pump power of 1.5 W. The laser output showed no evidence of roll-over even at the highest output power, which was limited only by available pump power. There was no evidence of any power limitation due to nonlinear scattering, nor was any stimulated Raman scattering observed. Figure 3.25 shows the output spectrum of the attenuated laser with 980 nm pumping at pump power of 1.3 W. However, there is no lasing occurred as shown in the figure. The slope efficiency of 1.14% is obtained with 905 nm pumping, which is much higher than that of 931 nm pumping. The slope efficiency is only 0.42% with 931 nm pumping. This shows that the absorption and emission cross sections of the fabricated TYDF is higher in 905 nm

compared to that of two other wavelengths. The low output power mainly due to the cladding pump that provides insufficient absorption of a pump light.

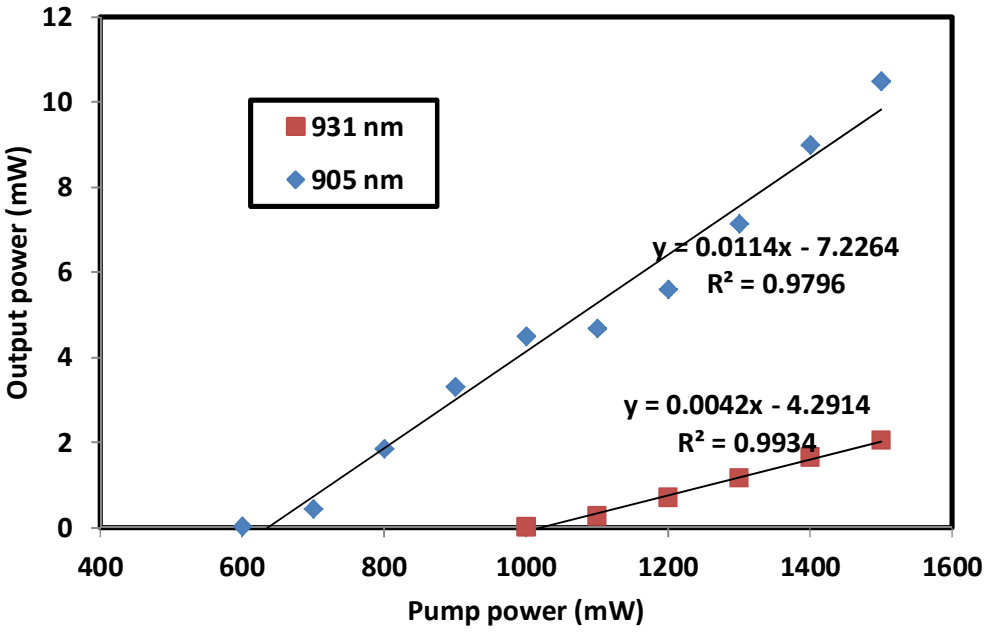

Figure 3.24: Output power against the pump power at two different pumping wavelengths of 905 nm and 931 nm.

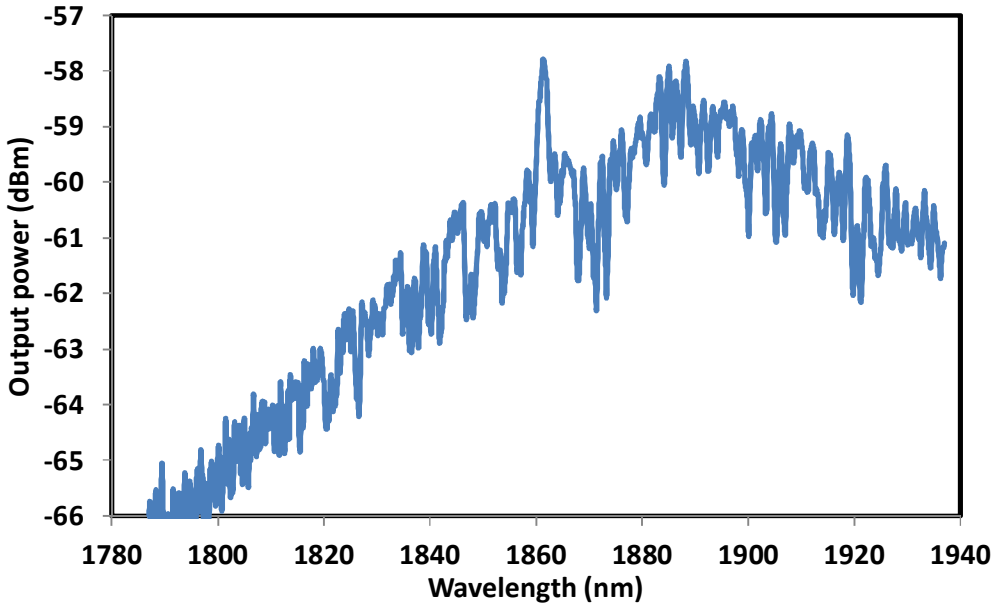

Figure 3.25: The attenuated output spectrum of the YTDFL with 980 nm pumping of 1.3 W.

Figure 3.26 shows the output spectrum of the YTDFL at different pump wavelengths with the input pump power of 1.1 W. As shown in the figure, the YTDFL operates at 1948.4 and 1947.2 nm with 905 and 931 nm pumping, respectively. The peak power of the laser is also observed to be higher with 905 nm pumping compared to that of the 931 nm pumping due to the same reason as explained earlier. The peak signal to noise ratios are obtained at 50 and 40 dB with 905 and 931 nm pumping, respectively. This is attributed to the population inversion which is more efficient with 905 nm pumping compared to 931 nm pumping. These results show that the 905 nm is the best pumping wavelength for the proposed ring YTDFL. The use of ring configuration usually exhibit low pump power threshold since laser action depends on the gain per unit pump power. Nevertheless, the proposed ring laser suffers from mode competition, thus degrade the performance of the slope efficiency. The efficiency of the proposed YTDFL can be further improved by using a linear configuration with fiber Bragg gratings (FBGs) to reduce the cavity loss.

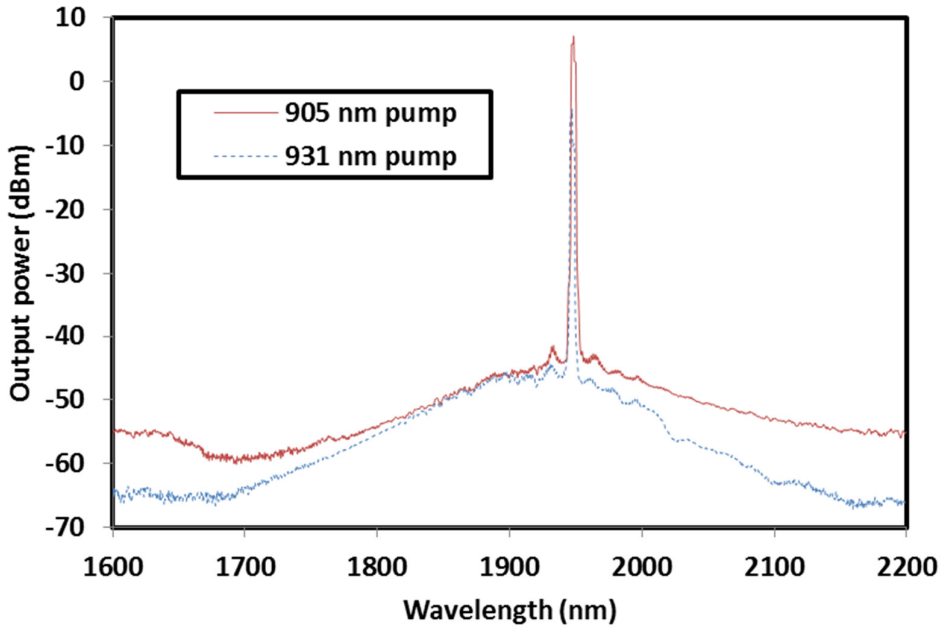

Figure 3.26: Output laser spectrum for different pumping wavelengths.

3.6 YTDFL with linear configuration

To achieve stable and efficient fiber lasers, fiber Bragg grating (FBG) was incorporated in the cavity design. Unlike free running laser, the oscillating light beam in the cavity will generate a population inversion in the selected wavelength of FBG. Therefore, the generated fiber laser output will have a significantly narrow linewidth and able to achieve single-frequency operation via suppression of the mode competition (Ball *et al.*, 1992). Figure 3.27 shows the experimental setup for the proposed YTDFL using the fabricated double-clad YTDF as a gain medium in conjunction with a cladding pumping approach. In this approach, the double-clad fiber is forward pumped by a multimode pump via a multimode combiner (MMC). In double clad fiber, the pump light travels down the fiber in the first cladding and get absorbed by the dopants, in this case the Yb ions when it overlaps with the core. The D-shape geometry of the cladding improves the pump absorption and furthermore, it is cheaper to be fabricated compared to other geometries such as hexagonal and rectangular. The FBGs with a reflectivity of 99.6% and 50% are fusion spliced to signal port of MMC and the active fiber respectively to establish a Fabry–Perot laser cavity.

The forward pumped YTDF generates an ASE centered at ~1910 nm region, which oscillates in the cavity to lase at the peak wavelength of the overlapping spectrum between the two FBGs. Figure 3.28 shows the transmission spectra of the FBGs used in the experiment. Both FBGs operate at the center wavelength of 1901.6 nm and 3 dB spectral bandwidths are measured to be around 1.5 nm and 0.6 nm for the reflectivity of 99.6% and 50% respectively. The spectrum and power of the output laser are obtained from the output port of the 50% FBG and measured using an OSA and power meter, respectively. The Y/Al ratio is a very important parameter in determining the performances of the fabricated YTDF. From fabrication point of view, when the ratio becomes greater than 3 the core glass becomes opaque in nature and loss of the

fabricated fiber is also increased. For this reason we have selected only two fibers, LTY6 and LTY8 having Y/Al ratio of 1.0 and 3.0 respectively for the experiment. The experiment is carried out using two different multimode pumps operating at wavelength around 931 nm.

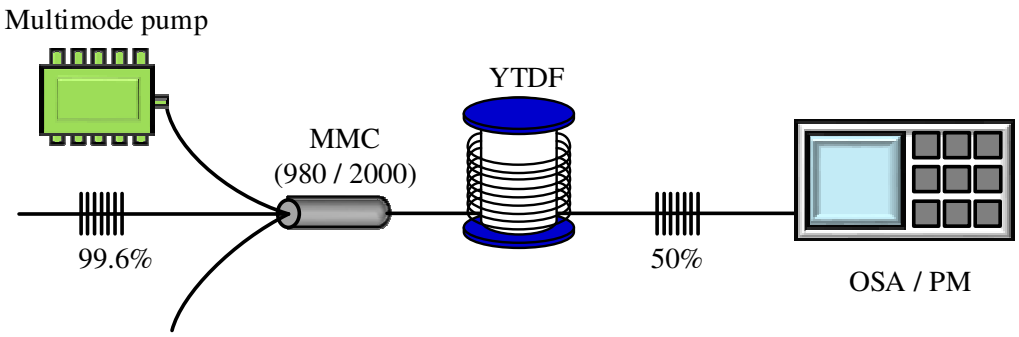

Figure 3.27: The experimental setup for the proposed YTDFL with linear configuration.

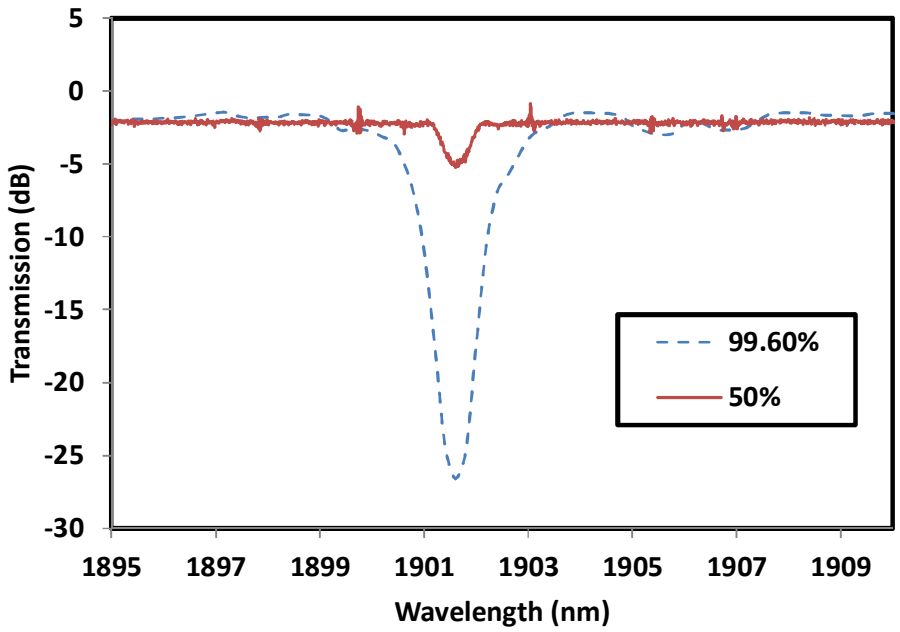

Figure 3.28: Transmission spectra of both FBGs used in the laser cavity.

This experiment is firstly conducted to find the optimal length to operate the proposed YTDFL for both fiber samples using 931 nm pumping. Figs. 3.29 and 3.30 show the laser output power against multimode pump power for YTDF samples LTY6 and LTY8 respectively at various fiber lengths. Both YTDFLs configured with LTY6 and LTY8 show the best lasing action operation at 2 m length where they exhibit the highest efficiencies of 2.23% and 2.47% respectively with the lowest lasing threshold. By pumping the doped fiber using 931 nm pump, the Yb^{3+} ions are excited to $^2F_{5/2}$ state with multiphonon assisted anti-Stokes excitation process. From $^2F_{5/2}$, the Yb^{3+} ions relax to the ground state and transfer their energy to the neighbouring Tm^{3+} ions non-resonantly. The Tm^{3+} ions absorb the incident infrared photon from the Yb^{3+} ions and thus promoting them from $^3H_6$ to $^3H_5$ level. The narrow gap between the $^3H_5$ and $^3F_4$ levels indicates a short ion lifetime at the $^3H_5$ level. Due to multi-phonon decay, ions at this level relax to the metastable level of $^3F_4$ which offers longer lifetime. The population inversion between the level generates an ASE light centered at 1910 nm region, which oscillates in the Fabry–Perot cavity to realize a laser at 1901.6 nm. However, the slope efficiency of the proposed laser is relatively low due to three possible reasons. The first reason is the size of the fabricated fiber core diameter, which is very large compared to that of the FBG fiber (around 7–8 μm). Therefore, when both fibers are spliced together, it generates a higher splicing loss of around 1 dB as a large portion of the pump power leaks out. The second reason is because we used 931 nm multimode pump source for which the absorption cross-section coefficient of Yb^{3+} peaks at around 975 nm. It is expected the proposed laser can produce a higher efficiency if the optimum pump wavelength is used. The third reason is that the higher possibility of multi-step energy transfer, which leads to upconversion and blue emission degrades the fiber laser efficiency.

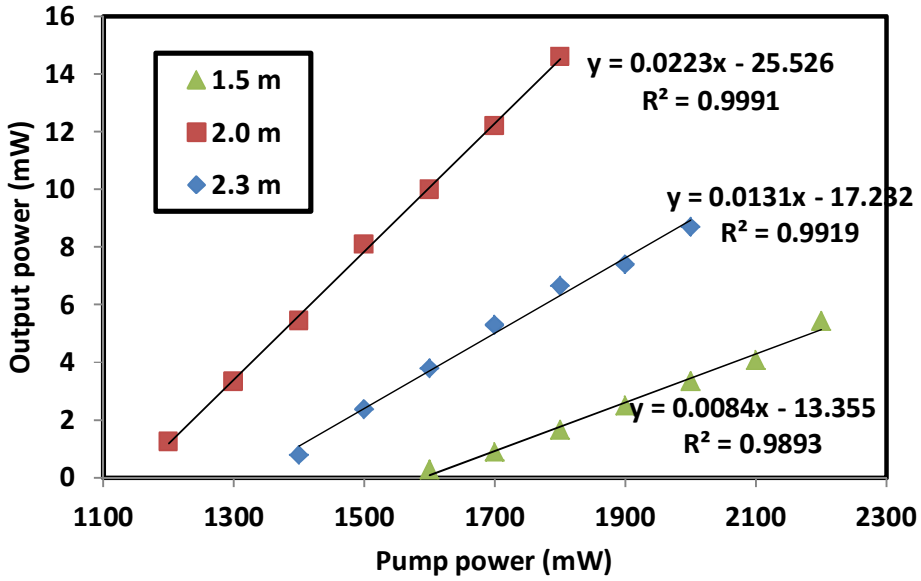

Figure 3.29: Output power of the proposed YTDFL against the pump power at different YTDF lengths using LTY6 samples as the gain medium.

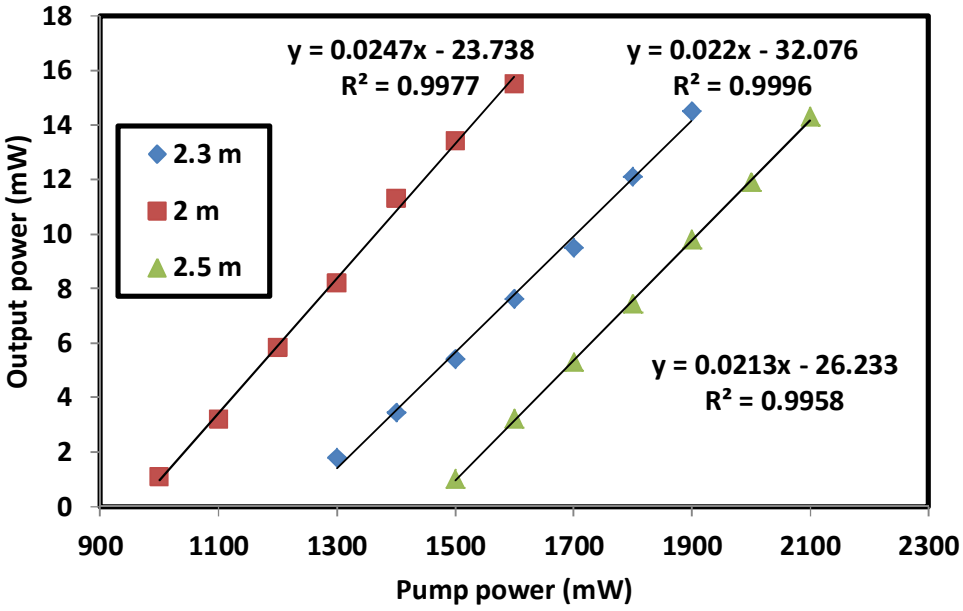

Figure 3.30: Output power of the proposed YTDFL against the pump power at different YTDF lengths using LTY8 samples as the gain medium.

Figure 3.31 shows the output spectrum of the YTDFL with 931 nm pumping and LTY8 recorded by an OSA. It operates at 1901.6 nm, which coincides with the center wavelength of both FBGs with a signal to noise ratio of more than 40 dB. The 3 dB bandwidth is measured to be less than 0.05 nm limited by the OSA resolution. High thulium doping concentration for both YTDF samples lead to efficient stepwise energy transfer such that the optimum length for lasing is comparatively short. To avoid clustering from high concentration of rare earth ions doping, yttria and aluminium are added as host modifiers. The presence of Al and Y_2O decreases phonon energy in the fiber and assists in distributing Yb and Tm ions homogeneously into the core glass matrix which also increases the probability of radiative emission and improves lasing efficiency. Several advantages of using short gain medium when generating laser are minimum reabsorption of pump power that results in high threshold and low efficiency laser, an increase in the stimulated scattering process threshold which prevents roll-off in output power, less total propagation loss in the setup and less use of fiber materials.

In the present work, yttria-alumino rich Tm_2O_3 and Yb_2O_3 doped silica glass based optical fibers was fabricated because of the highest known vibrational energy in yttria-alumino-silicate (Y_2O_3–Al_2O_3-SiO_2) glass, is about 950 cm^{-1} (Jander *et al.*, 2004), which is less than the maximum vibrational energy, around 1100 cm^{-1}, in silica glass (Sigel *et al.*, 1978). Consequently, we have chosen to combine the SiO_2 matrix with Al_2O_3 and Y_2O to increase the optical efficiency of the rare-earth dopants and avoid clustering effects. Moreover, Al^{3+} and Y^{3+} have the same electronic valence as rare earth ions, as well as similar lattice structures of Al_2O_3, Y_2O_3 and Yb_2O_3 oxides. In the fabricated fiber, we have also deposited SiO_2-P_2O_5 porous un-sintered multiple layers where the doping level of P_2O_5 content is very low, around 0.10–0.20 mol%, in order to provide good adhesion between layers (Ray, 1974). Otherwise, there will be disturbances of soot layer either during solution soaking process or thermal drying

process. Such low content of P_2O_5 does not increase the phonon energy of the glass host very much.

On the other hand the transition temperature of an oxide glass is normally related to a combination of several factors such as the density of covalent cross-linking, the number and strength of the coordinate links formed between oxygen and the cation, and the oxygen density of the network (Lahoz *et al.*, 2011). With increasing Y-content, more coordinate links are formed between oxygen and yttrium. More open structure needed to accommodate larger yttrium ions and depolymerization in the network with decreasing silica content or increasing the Y/Al ratio. The fabricated YTDFs were characterized by non-exponential decays. It is found that the Yb^{3+} decay time was shorter than the decay comprised of the fluorescence contributions from both Yb^{3+} and Tm^{3+} ions. The time constant of the Yb^{3+} decay amounted to 540 μs as compared to approximately 650 μs of the decay of the gathered fluorescence from Yb^{3+} and Tm^{3+}. In fact, the quantum yield of the Yb^{3+} to Tm^{3+} energy transfer process of such kind of Tm_2O_3-Yb_2O co-doped glass preform is estimated to be about 0.98, whereas it reduces to about 0.02 in the rare-earths poor phase (Paul *et al.*, 2010). This means that about every Yb^{3+} ion that is excited in the rare-earths rich phase transfers its energy to Tm^{3+} ions.

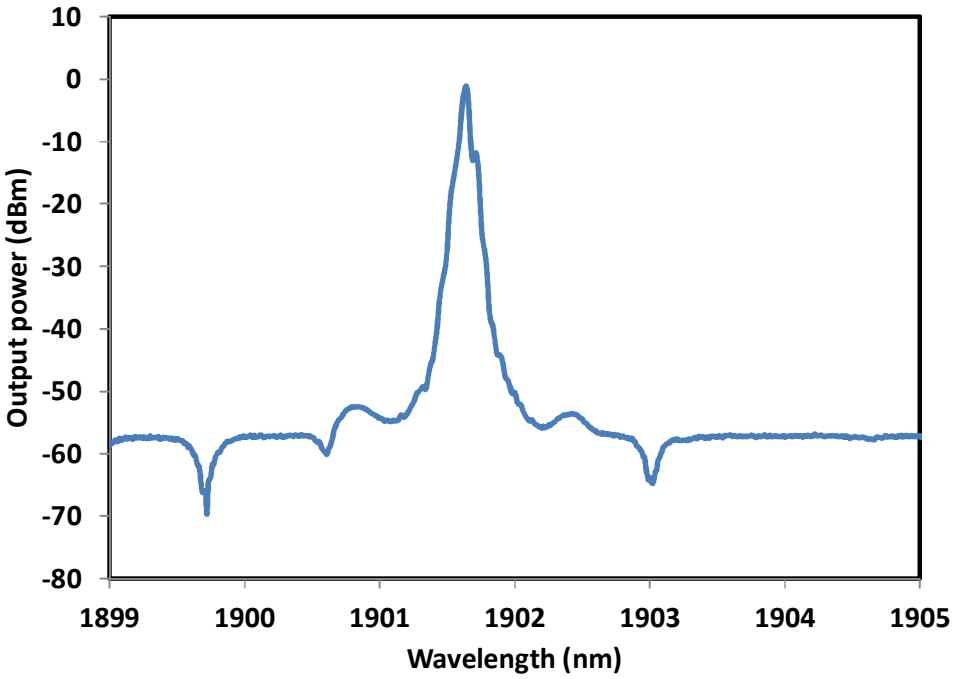

Figure 3.31: Output spectrum of LTY8 at 1.0 W pump power using 931 nm pump excitation.

From Figures 3.29 and 3.30, it can be seen that the YTDFL configured with LTY8 produces a better efficiency compared to that of LTY6. Referring to Table 3.1, LTY8 has a higher ytterbium to thulium doping concentration ratio, higher NA and also smaller core radius compared to that of LTY6. Higher NA allows the fiber to maintain the launched pump brightness in spite of smaller core radius. According to (Muendel, 1996), the pump absorption is proportional to the ratio of the core area over the inner cladding area, thus as the core radius reduces, the ratio of doped core area to cladding area increases, hence improving the overlapping between the pump light and the active core area. This enhances the pump light absorption and consequently the lasing action performance of the fiber. Apart from that, optical fibers with larger NA can collect more light especially in multimode structure thereby allowing them to generate higher efficiency fiber laser. Since LTY8 has a higher ytterbium ion concentration, the rate of cross relaxation between these ions is higher resulting in more energy transfer to

thulium which lowers the threshold of the generated laser. Furthermore, higher ytterbium to thulium concentration ratio contributes to more efficient energy transfer between the sensitizer and acceptor ions in LTY8. However, with the use of a unidirectional auxiliary pump at approximately 1600 nm in conjunction with a 980 nm primary pump, it was reported that an increase in Tm concentration along with Yb:Tm ratio of ~1 leads to the best laser performance (Pal *et al.*, 2010). The laser results in this work are clearly better than those obtained in (Pal *et al.*, 2010), which are most probably due to the pump wavelength used and the improved dopants compositions.

By using a 2 m long LTY8 as the gain medium, the proposed YTDFL performs the best with a threshold pump power of 961 mW with a slope efficiency of 2.47%. The performance of YTDFL is also investigated for two different pump sources, which have almost identical operating wavelength at around 931 nm. They have a slightly different spectrum as shown in Figure 3.32 and thus they are expected to perform differently. Aside from demonstrating laser with the highest power at wavelength of 931 nm (pump A), pump A has another peak with considerable power at 926 nm whereas pump B does not. Figure 3.33 compares the performance of the proposed YTDFL between two different pump sources. It is observed that the laser efficiency generated by pump A is better compared to that of pump B. This is attributed to the fiber's pump absorption, which peaks at around 920 nm and 975 nm and thus the fiber has more absorption at 926 nm compared to the wavelength longer than 931 nm. This results in an improvement of both laser's threshold and efficiency of the YTDFL as shown in Figure 3.33. With pump B, the laser threshold and efficiency are obtained at 1300 mW and 1.89% respectively, which are slightly inferior to that of pump A. The maximum power produced by pump A is 15.5 mW at the pump power of 1600 mW. It is obvious that higher output is expected with the use of higher pump power. Since the absorption cross-sectional area of Yb^{3+} is higher at 973 nm wavelength, the experiment is repeated

using this pump source in order to achieve higher efficiency. The laser threshold is obtained at the higher pump power of around 2600 mW and the laser output power is obtained at 17 mW with pump power of 2700 mW. However, the laser is unstable and diminishes as the pump power is further increased. The proposed YTDFL is theoretically less efficient than the conventional Tm system with 780 nm pumping, but the cost of high power 931 nm laser diodes is so much lower than that of 780 nm laser diode. Another benefit of the proposed 2 µm laser system is its operation in eye-safer wavelengths, where permissible free space transmission levels can be several orders of magnitude greater than 1 µm.

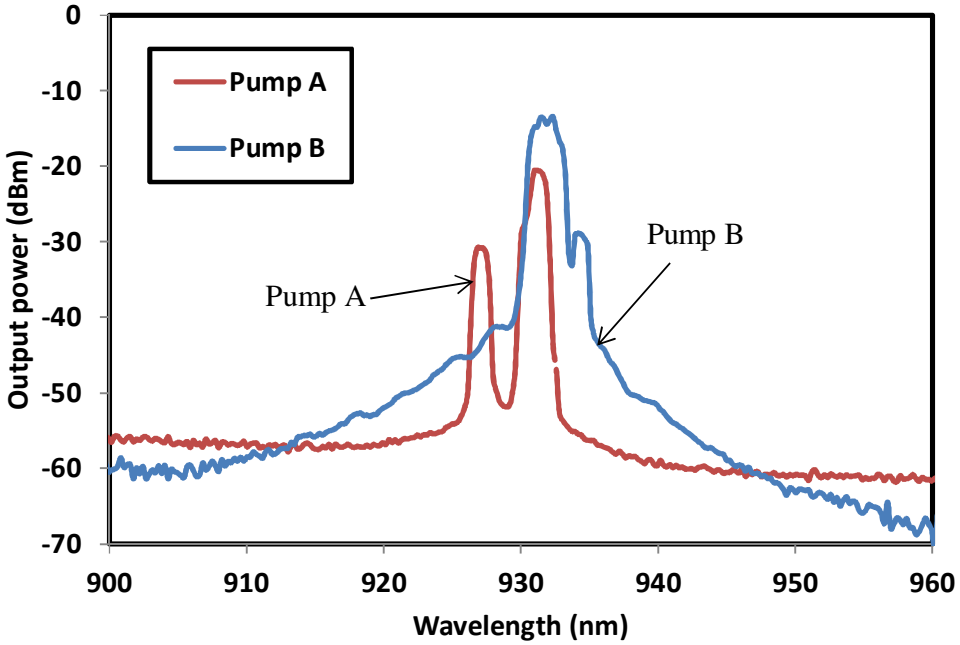

Figure 3.32: Output spectra of two different 931 nm pump sources used in the experiment.

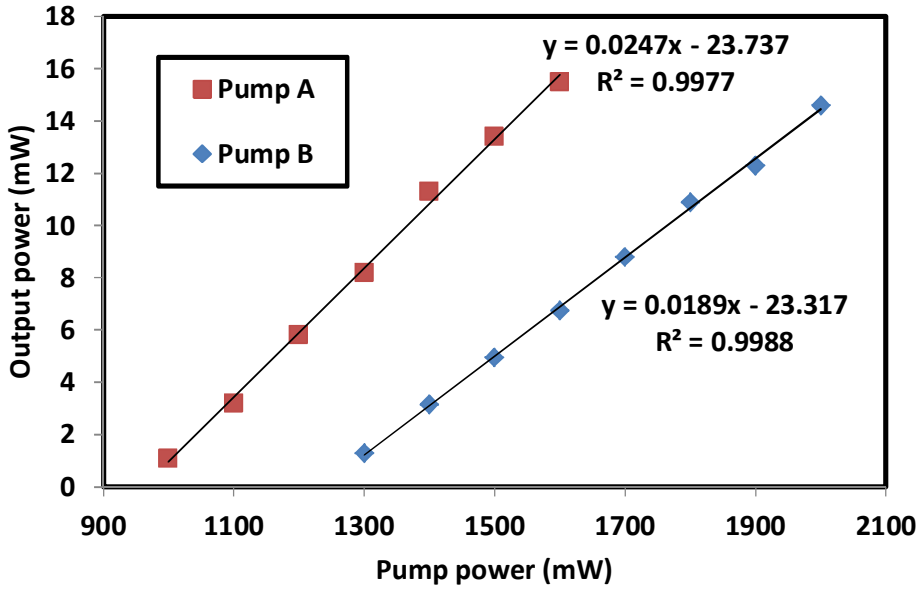

Figure 3.33: Output power against pump power characteristics for the proposed YTDFL with two different pump sources.

3.7 Enhancement of YTDFL efficiency using the dual-pumping method

Higher output power can be achieved either by adding doping concentration or applying dual pumping method (Kasamatsu *et al.*, 1999; Ng *et al.*, 2002). A very high doping concentration may induce clustering effect among the ions that prevents ion excitation. Adding host modifiers such as Al ions may reduce the effect, but it may also compromise the fiber's mechanical property. Dual-pumping approach has been proposed and demonstrated for gain enhancement of Thulium-doped fiber amplifiers (TDFAs) in a number of research works, (Martins-Filho *et al.*, 2003; Peterka *et al.*, 2004). However, the focus of these works is on the enhancement of S-band gain wherein the emphasis is more on the emission of $^3H_4$ level of the thulium ions. In this section, a dual-pumping scheme is utilized to improve the efficiency of the proposed YTDFL, which the configuration is based on a newly fabricated double-clad YTDF as the gain medium and a pair of FBG that form a linear cavity resonator. To our

knowledge, this is the only experimental laser demonstration of the thulium transition $^3F_4 \rightarrow {}^3H_6$ in a silica fiber which employs the dual pumping scheme.

The experimental setup of the double-clad YTDFL based on dual-pumping scheme is shown in Figure 3.34. The setup is almost similar to Figure 3.28, which uses the same MMC and FBGs. The YTDF is fusion spliced to an output port of a MMC. An FBG with a reflectivity of 99% was spliced to the input signal port of the MMC while another FBG with a reflectivity of 50% was fusion spliced to the output end of the YTDF (LTY8) to create a cavity. Figures 3.34(a) and (b) shows the proposed configurations with a multimode main pump and another multimode or single mode pump as an auxiliary pump respectively. The experiments were carried out using various combinations of pump wavelengths. In this experiment, the length of the YTDF was fixed at 2 m for optimum laser performance. In the setup of Figure 3.34(a), 905 nm and 931 nm (which is used as pump A in the previous experiment) are used alternately as the main and auxiliary pump. Both pumps are injected into the inner cladding of the YTDF via a multimode combiner to create a population inversion and then ASE which oscillates in the linear cavity to generate laser at the Bragg wavelength of 1901.6 nm. In Figure 3.34(b), a single mode pump of 800 nm or 1552 nm is used as the auxiliary pump while a multimode pump of 905 nm or 931 nm is used as the main pump. The output of the laser is tapped out from the cavity via the output port of the second FBG with 50% reflectivity. The output spectrum and power are measured by the OSA and power meter (PM), respectively.

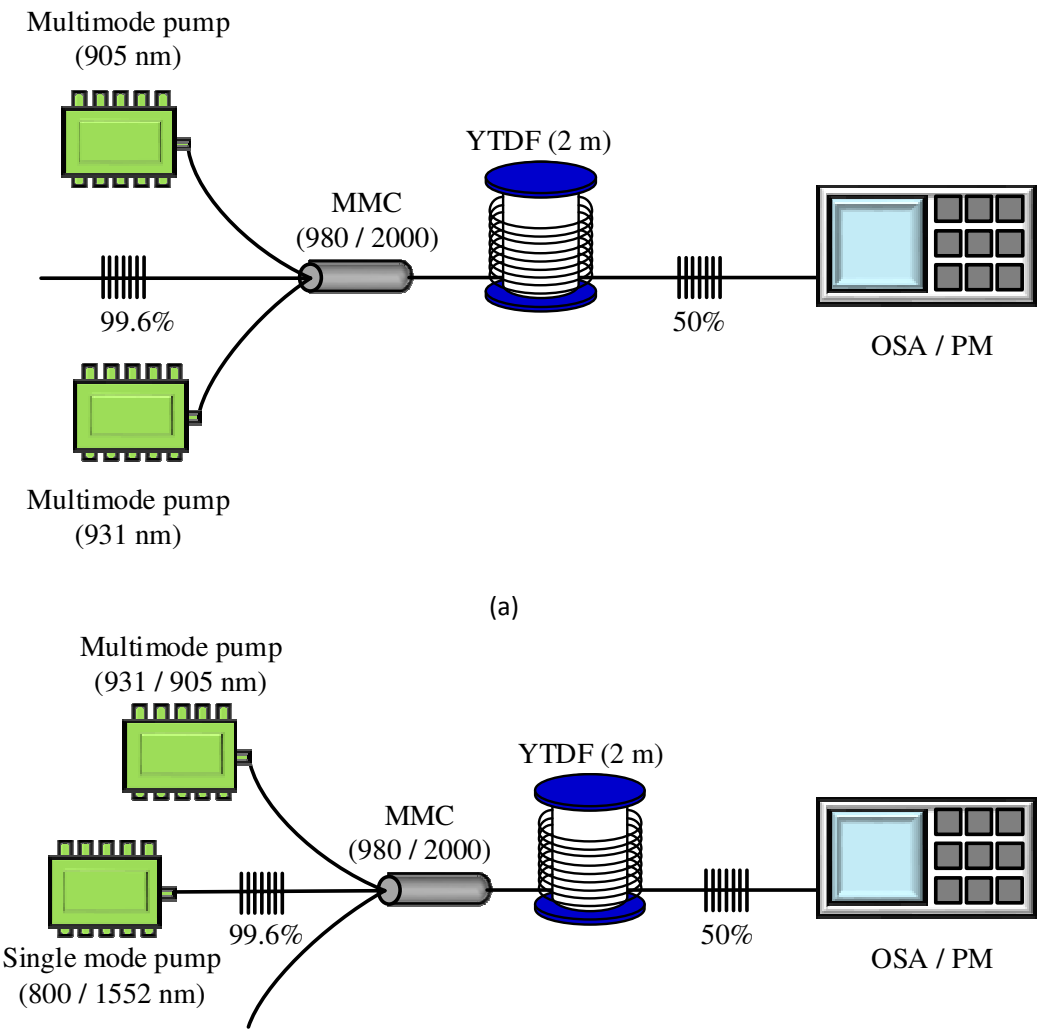

Figure 3.34: Configurations of the proposed YTDFL with dual pumping scheme when the auxiliary pump is (a) multimode (b) single mode.

The performance of the proposed YTDFL is firstly investigated with and without the auxiliary pump using two different multimode pumps of 931 nm and 905 nm according to the setup of Figure 3.34 (a). Figure 3.35 shows the experimental result where the unshaded legends indicate the results of the lasers without the auxiliary pump. With 931 nm pumping, the YTDFL has an efficiency of 1.24% with threshold pump power of 1200 mW. However, using 905 nm pumping, the efficiency drops to 0.99% and the threshold pump power increases to 1500 mW. This is most probably due

to two main reasons; the first reason is the absorption/emission cross-section of the YTDF is slightly higher at 931 nm compared to the one at 905 nm. The second reason is the cavity loss is slightly lower at longer wavelength and thus the operation of the laser is more efficient with the use of 931 nm pump. To measure the effects of dual pumping on the efficiency and output power of the laser, a main pump is used to initiate lasing before launching of an auxiliary pump which helps to increase the output power. First, 905 nm pump is used as the main pump alone and its power is increased from 1500 mW to the maximum level of 2100 mW. Then the auxiliary 931 nm pump is launched and its power is increased every 100 mW to record six new readings until it maximum output at the total power of 2700 mW. From the graph, the efficiency is seen to improve by 1.91% to 2.90% with the incorporation of the auxiliary pump. As the 905 nm photons are inefficiently absorbed, the amount of excited ytterbium ions is limited. When the 931 nm light is launched into the gain medium, more ytterbium ions occupy the excited state thereby increasing the energy transfer process. Therefore, the population of thulium ions at the upper state level also increases, and hence the laser efficiency improves. On the other hand, by adding 905 nm pump as an auxiliary pump for 931 nm pumped YTDF, the efficiency of the laser slightly reduces from 1.24% to 0.60%. This is most probably due to the early saturation of the Yb^{3+} ions when 931 nm main pump is used, thus reduces the energy transfer to the Tm^{3+} ions as the 905 nm pump power increases.

However, instead of having the highest efficiency of 2.90%, this combination of multimode pumps allows massive energy transfer from Yb^{3+} ions and UC occurred in the gain media. The ESA process introduces multistep excitations in a form of non-radiative decay which leads to the unwanted heat. Therefore, the core temperature will increase and the fiber may suffer from thermal effects such as heating, quenching and lensing affecting the efficiency of fiber laser (Jeong *et al.*, 2005).

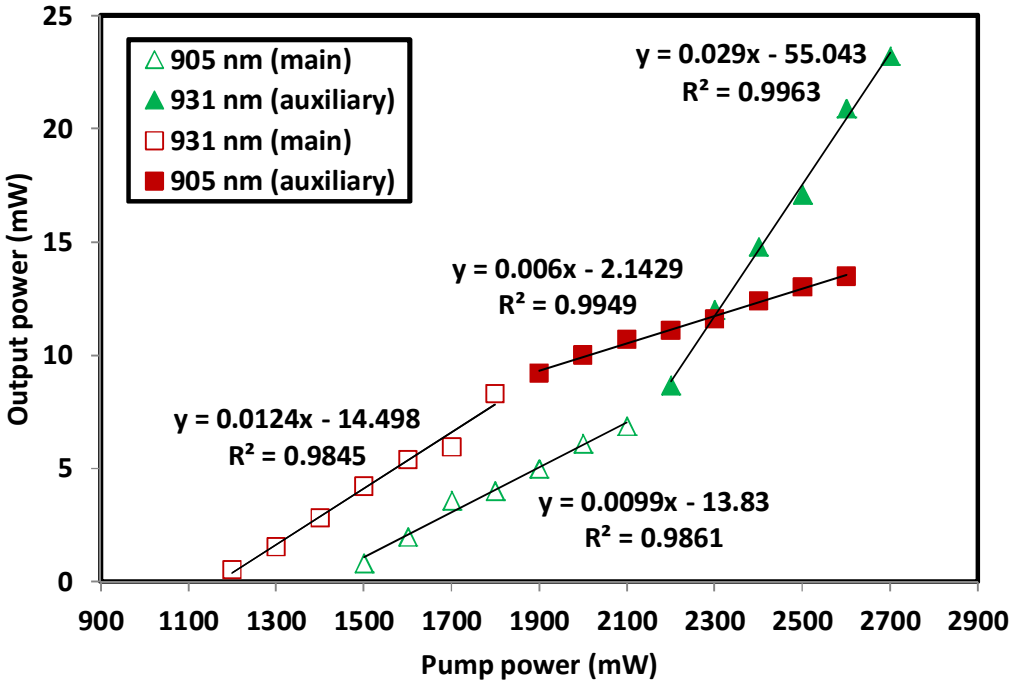

Figure 3.35: The performance of the YTDFL as another multimode pump is added as an auxiliary pump.

Figure 3.36 shows the experimental results obtained by the proposed YTDFL of Figure 3.34(b) where another dual pumping scheme combining a multimode and single mode pump is implemented. In order to increase the output power and efficiency total input power needed is high. Due to the high UC process which also reduces the efficiency of the laser when multimode pump is combined, we propose the use of 1552 nm and 800 nm laser diode as auxiliary pump. Both pumps only generate ground state absorption (GSA) in the fiber, thus high output power may be achieved with lower total input power. Firstly, the performance of the YTDFL is investigated when a single-mode 1552 nm is added in the cladding-pumped fiber laser. For this experiment, a fixed 1552 nm pump power of 32 mW is launched into the system before we start increasing the power of the multimode pump. As shown by the blue shaded triangle legend in Figure 3.36, when the 1552 nm pump is coupled with the 931 nm source, the laser is generated

at 1.9 μm at the threshold pump power of 1332 mW with an efficiency of 2.65%. The efficiency was improved by 1.41% as compared to the result of using 931 nm laser diode alone as a pump source. By combining 1552 nm single mode pump with 905 nm multimode pump, the efficiency of the laser increases by 0.41% from 0.99% to 1.40% with laser threshold at 1400 mW as shown by the unshaded triangle legend in Figure 3.36. It is found that the combination of single mode 1552 nm and multimode 931 nm pumps provides a better lasing operation compared to than the combination of 1552 nm and 905 nm pumps. In addition to the photon absorption donated by ytterbium ions, 1552 nm incident pump increases the GSA of thulium ions caused by higher population inversion in the upper laser level.

In another experiment, 800 nm single mode pump is used as the auxiliary pump instead of 1552 nm pump. Similar to the previous experiment, a fixed 800 nm pump power of 200 mW is launched into the system before we start increasing the power of the multimode pump. As compared to the previous 1552 nm pumping, the efficiency of this laser was higher and the threshold was lower. By combining 905 nm and 800 nm pumps, the lasing efficiency was improved by 1.78% and the threshold was reduced to 1400 mW. As indicated by the shaded square legend in the figure, combining 931 nm and 800 nm pumps produces an even better lasing output with relatively higher efficiency up to 2.58% and a lower threshold pump power of 1200 mW. This is due to the 2:1 cross relaxation that occurs in the fiber which allows a large number of thulium ions to occupy the upper laser level of $^3F_4$ thus improving the laser efficiency.

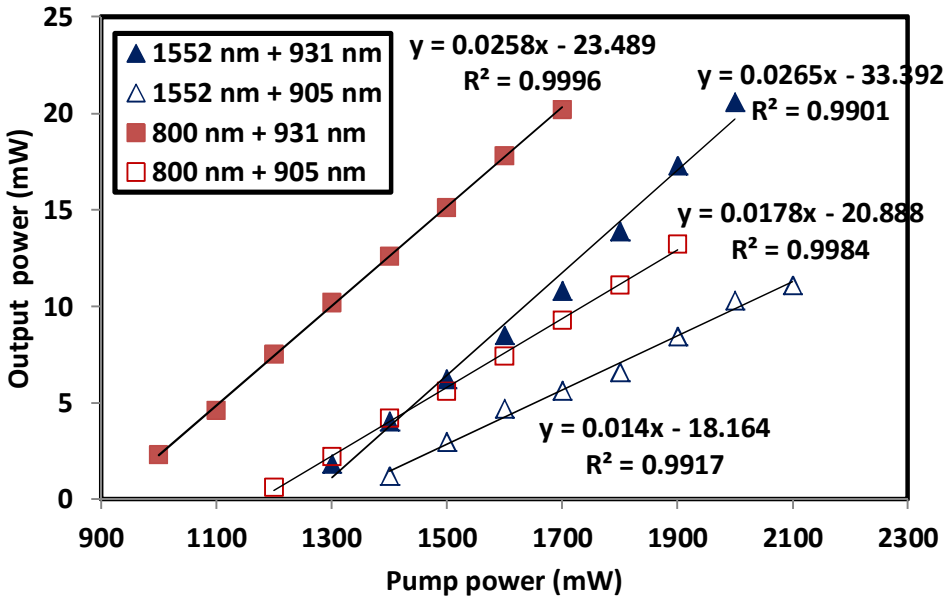

Figure 3.36: The performance of the YTDFL as another single mode pump is added as an auxiliary pump.

Figure 3.37 shows the attenuated optical spectrum recorded by an OSA for the proposed laser. It operates at 1901.6 nm, which coincides with the center wavelength of both FBGs with a signal to noise ratio of more than 40 dB. The 3 dB bandwidth is measured to be less than 0.05 nm and is limited by the OSA resolution. It is found that the best efficiency of 2.9% is obtained by combining 905/931 nm pump with the highest output power of 23 mW at 2700 mW input pump power. However, in order to generate the same amount of output power, combining 1552/931 nm source require 2128 mW total input power. The best combination of pumps would be 800/931 nm where only a total pump power of 1802 mW is required to generate 23 mW of 1.9 μm laser output.

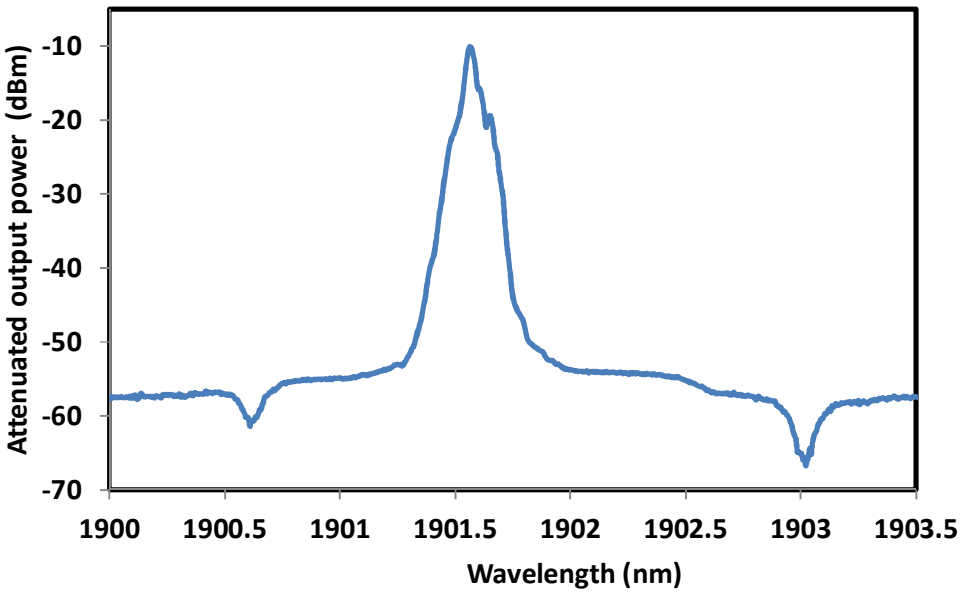

Figure 3.37: The attenuated output spectrum of the proposed laser.

3.8 Summary

A lasing action from newly fabricated double-clad YTDFs has been successfully demonstrated. A single-mode laser operating in the 1900 nm region is demonstrated using the fiber in conjunction with multimode pumping through the transition of thulium ion from $^3F_4$ to $^3H_6$ with the assistance of ytterbium to thulium ion energy transfer. The YTDF used was drawn from a D-shaped preform, which was fabricated using the MCVD and solution-doping technique. With a ring configuration, the fiber laser operates at a wavelength of 1948.4 and 1947.2 nm with pump power thresholds of 0.6 and 1.0 W for 905 and 931 nm pumping respectively. The maximum output power of 10.5 mW was achieved with the 905 nm pumping at the maximum pump power of 1.5 W. It was found that the laser is more efficient with a 905 nm pumping compared to the 931 nm pumping. In another experiment, a Fabry–Perot cavity configuration with two FBGs has been used to perform laser. The results exhibit that more efficient energy transfer occurred between the Yb^{3+} and Tm^{3+} ions in YTDF when higher ytterbium to

thulium concentration ratio is used. The 2 m long YTDF (LTY8) generate laser at a threshold power of 1.0 W at 1901.6 nm with an efficiency of 2.47%. The lowest threshold pump power of the proposed YTDFL is around 961 mW. The effect of multimode pumping wavelength of slightly lower than 931 nm is also observed. Lastly, the enhancement on lasing efficiency has been demonstrated using the dual-pumping method. Single-mode pumped as an auxiliary pump allows only GSA transitions compared to combination of multimode pump, thus exhibit better lasing performance. The combinations avoid unwanted heat increased in the core fiber consequently reduces the possibility of fiber burnt at the high output power. The best combination of pumps is 200 mW of 800 nm pump with 931 nm pump which needs total input power of 1802 mW in order to generate 23 mW of 1.9 μm laser output.

CHAPTER 4

THULIUM-BISMUTH CO-DOPED FIBER LASERS

4.1 Introduction

Co-doping Thulium with other elements such as Erbium, Ytterbium, Terbium and Bismuth has been demonstrated to improve the S-band amplification and 2 μm lasing of Thulium doped fiber (TDF). For instance, co-doping Thulium-Terbium in germanate glass was performed by Librantz et al (Librantz *et al.*, 2008) to improve amplification in the 1450 nm region i.e. S-band by depopulating $^3F_4$ via an energy transfer process from Thulium to Terbium. Meanwhile, Braud et al (Braud *et al.*, 2000) capitalized the energy transfer from Ytterbium to Thulium to decrease the effective lifetime of $^3F_4$ level to generate the 1500 nm laser emission. In our earlier work, a newly fabricated double-clad D-shaped Yb/Tm co-doped fiber laser (YTDFL) has been proposed for generating laser at 1900 nm region. Owing to the limitation occurred in the YTDFL, a core-pumping fiber laser operating at 2 μm region is proposed in this work.

Previously, many works have been reported on high power Thulium doped fiber laser (TDFL) and the Thulium-Holmium doped fiber laser utilizing double-clad fiber to achieve efficiency of around 47% - 68% (Jackson *et al.*, 2007; Wu *et al.*, 2007). However, there is still a lack of research works on core-pumping TDFL. In an earlier work, Geng et. al. (Geng *et al.*, 2007) demonstrated highly efficient diode-pumped fiber laser with 35% slope efficiency and 50 mW output power operating near 2 μm, generated from a 2 cm long piece of highly Tm-doped germanate glass fiber pumped at 805 nm. In this chapter, an efficient core-pumping fiber laser is proposed using a newly developed single-mode Thulium-Bismuth co-doped lithium-alumino-germano-silicate (LAGS) fiber (TBF) as the gain medium. The TBF provides effective energy transfer

from active bismuth to thulium ions that improves amplification efficiency at 1.9 μm region besides cross relaxation process. Higher dopant concentration of thulium ions can also be achieved in the co-doped fibers since clustering effect is suppressed by the presence of the co-doping ions. The TBF is obtained from optical preform, which was made using the conventional modified chemical vapour deposition (MCVD) process in conjunction with solution doping (SD) technique. The performance of the proposed TBF laser (TBFL) is also investigated and then compared with the one obtained using a commercial TDF. The advantage of the proposed TBFL is that it operates in the eye-safe wavelength region with significantly lower pump power threshold compared to commercial TDF. The novelty of this work lies on the use of core pumping silica fiber to produce a single mode laser output with high efficiency and low threshold by using a relatively short gain medium.

4.2 Fabrication and characterisation of Tm-Bi co-doped optical fiber

The TBF was fabricated from a lithium-alumino-germano-silicate (LAGS) core glass optical preform co-doped with Tm and Bi ions using fiber drawing tower. The optical preform is fabricated through the conventional MCVD process, followed by optimised SD technique. In the MCVD process, at first a pure silica glass tube with inner/outer diameter of 17/20 mm is mounted at lathe. Then the tube was collapsed by applying a high temperature of 2180 ^{o}C until its outer diameter reduces to ~15 mm. After that a single porous un-sintered SiO_2-GeO_2 soot layer is deposited inside a silica glass tube. The deposition process was carried out at a temperature around 1420-1475 ^{o}C. Then the un-sintered layer inside the tube was immersed into an alcoholic solution of $TmCl_3$, $Bi(NO_3)_3$, $Al(NO_3)_3$, $LiNO_3$ and ~5% HNO_3 using a 'U' tube SD set up and kept for about 45 minutes to achieve uniform soaking. After the SD, the glass undergoes dehydration and oxidation processes at temperature around 900-1000 ^{o}C. The next

process is sintering of the un-sintered layers by gradually increasing the temperature from 1500 to 2000 ^{o}C. After the oxidation and sintering processes, the tube is slowly collapsed to transform it into a transparent optical preform. A spool of bare TBF sample coated with normal poly-acrylate resin for protection is obtained by drawing of the preform at 2050 ^{o}C at the fiber drawing tower.

Three TBF samples (TB1, TB2 and TB3) are fabricated for demonstration of TBFL operating at 1.9 μm region. Electron probe microscopic analysis (EPMA) is carried out for all samples to determine the dopant concentrations into the core glass. Figure 4.1 shows the dopant concentration distribution plot obtained from the EPMA of one of the samples (TB2). As shown in Figure 4.1, the composition of the core-glass consists of Bi_2O_3, Tm_2O_3, Al_2O_3 and GeO_2. The dopant concentrations (in wt. %) are 0.35 Bi_2O_3, 0.9 Tm_2O_3, 3.0 Al_2O_3 and 4.0 GeO_2, which correspond to Bi and Tm ratio (Bi:Tm) of 1:2.5. The contribution of Li_2O can't be obtained by EPMA as it lies beyond the lower element limit of EPMA. Aluminium is used to increase the refractive index of the core compared to the cladding and to improve the solubility of the dopant material (Digonnet, 2002). The profile of the fabricated preform was also analysed by a preform analyzer (model PKL2600, Photon Kinetics) and the generated refractive index profile is shown in Figure 4.2. From the profile plot, the refractive index (RI) difference between the core and cladding can be obtained to calculate the numerical aperture (NA) of the fabricated fiber. A dip at the center of the RI profile can be observed, which is believed to have affected the laser's performance. The single mode pump has the highest intensity in the middle of the core. If the RI profile of the fiber does not have the dip, the Tm^{3+} ions at the center of the core may interact with higher pump intensity producing higher intensity laser (Emami *et al.*, 2011). However, the imperfection leaves the Tm^{3+} ions populating outer regions of the core interacting with lower-intensity

pump. Therefore, it may have cost us the laser efficiency. The details of the three samples are summarized in Table 4.1.

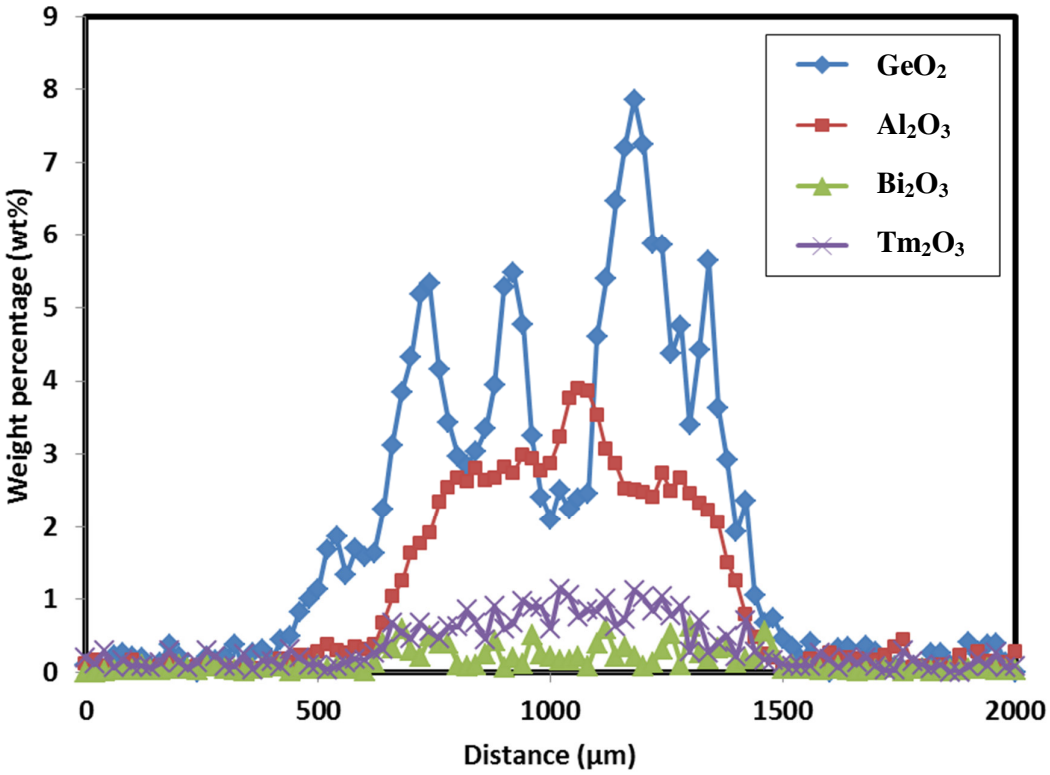

Figure 4.1: EPMA plot of dopants showing a distribution of Bi_2O_3, Tm_2O_3, Al_2O_3 and GeO_2 for TB2 sample.

Table 4.1: The composition of three optical preform samples of TBF.

Sample	Concentration of dopants into preforms (wt.%)	Bi and Tm Ratio (Bi:Tm)	Core diameter	NA.
TB1	0.15 Bi_2O_3, 0.3 Tm_2O_3, 1.0 Al_2O_3 and 12.0 GeO_2	1:2	6.9 µm	0.21
TB2	0.35 Bi_2O_3, 0.9 Tm_2O_3, 3.0 Al_2O_3 and 4.0 GeO_2	1:2.57	7.2 µm	0.23
TB3	0.2 Bi_2O_3, 0.06 Tm_2O_3, 0.05 Al_2O_3 and 0.3 GeO_2	1:0.3	9.0 µm	0.14

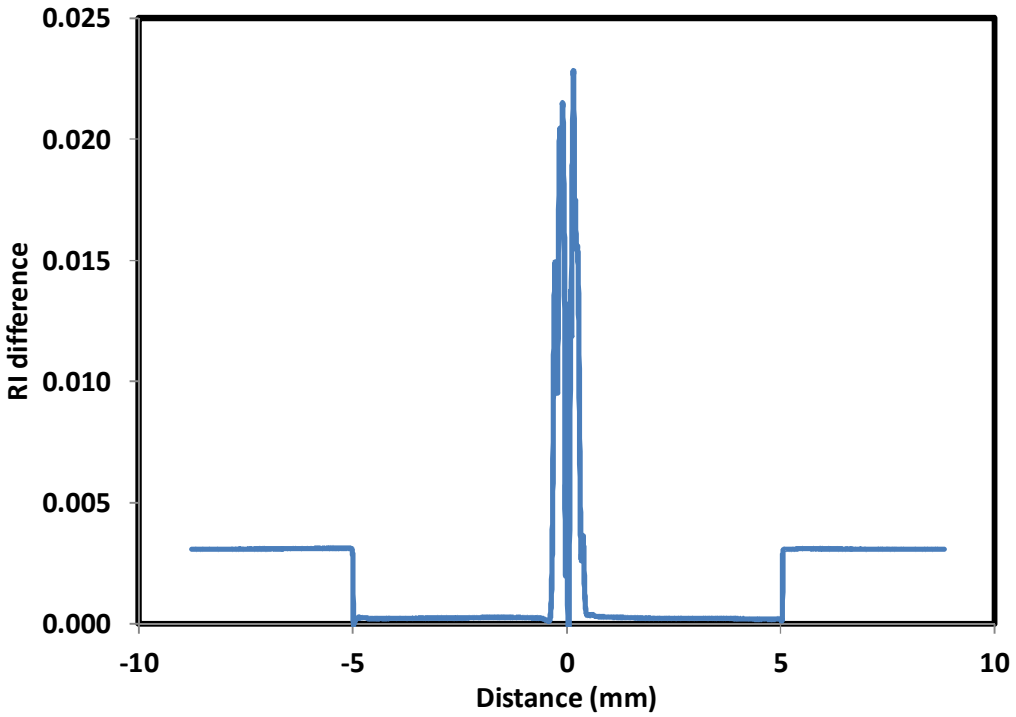

Figure 4.2: A plot of RI profile for the TB2, Tm-Bi co-doped preform, which is used to fabricate TBF (TB2).

The absorption spectrum of TB2 is also investigated using cut-back method and the result is shown in Figure 4.3. As shown in the figure, the absorption bands of the TBF are obtained at 465 nm, 680 nm, 785 nm, 1205 nm, and 1650 nm. It has a peak attenuation of 239 dB/m at 785 nm, which is much higher than that of a commercial TDF. Inset of Figure 4.3 shows the absorption spectrum of the commercial fiber (Nufern), which was obtained using the same method. It has a peak absorption of 27 dB/m at 793 nm, NA of 0.15, core diameter of 9 μm and thulium ion concentration of 0.25 wt.%. Since 785 nm pump laser is not commercially available, in this work, the 800 nm pump wavelength was used instead as it is the closest that we can get to 785 nm.

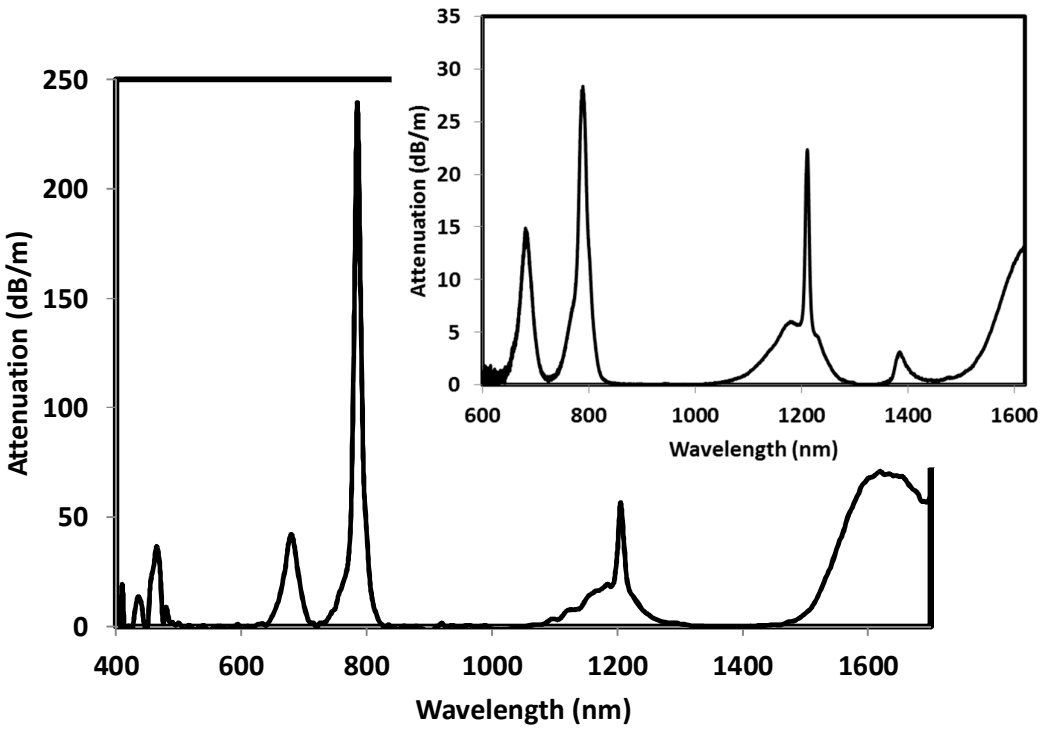

Figure 4.3: An absorption spectrum of the TBF (TB2). Inset shows the absorption spectrum for the commercial TDF.

4.3 Energy transfer of Tm-Bi and energy level analysis for the TBF

The energy level diagram of the TBF is shown in Figure 4.4 to explain three possible energy transitions in the fiber under 800 nm pumping (Zhou *et al.*, 2011). Figures 4.4 (a), (b) and (c) show the energy transition involving only Tm^{3+}, cross relaxation between Tm^{3+}, and energy transfer from Tm^{3+} to active bismuth, respectively. By pumping the TBF using 800 nm pump beam, both thulium and active bismuth ions are excited to the upper level. As shown in Figure 4.4(a), thulium ion will be excited to $^3H_4$ level as it absorbs the pump photon. Then it decays non-radiatively twice so that it can occupy the $^3F_4$ level that has a longer lifetime. From the $^3F_4$ level, it will drop to the ground state ($^3H_6$) while emitting at 1.9 μm. Since the thulium ion doping concentration in this fiber is relatively high, Tm-Tm cross relaxation may occur (Figure 4.4(b)).

Thulium ion in the ground state absorbs 800 nm photons such that it is elevated to $^3H_4$ level. When the ion in this level de-excites to $^3F_4$, instead of emitting at 1.47 µm, the energy is transferred to nearby thulium ion. The ion that resides in the ground state absorbs the donated photon to occupy the upper level laser, $^3F_4$. Both ions then drop to the ground state while emitting the 1.9 µm photons. With each absorbed pump photon, two 1.9 µm photons are produced, as shown in Figure 4.4(b). On the other hand, active bismuth ion absorbs the pump photon in order to occupy the excited state of $^1S_0$. The active bismuth ions then decays non-radiatively while dropping to $^3P_1$ level. From the $^3P_1$ level, the ion will descend to ground state and emits at 1.47 µm.

Figure 4.4(c) demonstrates three possible energy transfer mechanism that may occur in the TBF with 800 nm pumping. As the active bismuth ion drops to the ground state from $^3P_1$ state, it donates its energy to a nearby thulium ion. The thulium ion got elevated from the ground state to $^3F_4$ level before it emits at 1.9 µm. The second possible transition is, the thulium ion is excited from $^3H_6$ to $^3H_5$ level instead, only then it will relax non-radiatively to $^3F_4$ level. The ion will de-excite to ground state emitting at 1.9 µm. The final possible electronic transition is for the nearby thulium ion from $^3F_4$ to $^3H_4$. The ion then drops to $^3F_4$ level while emitting at 1.47 µm. Two out of three energy transfer process help to increase the $^3F_4$ population and thus improves the laser efficiency compared to the conventional TDF.

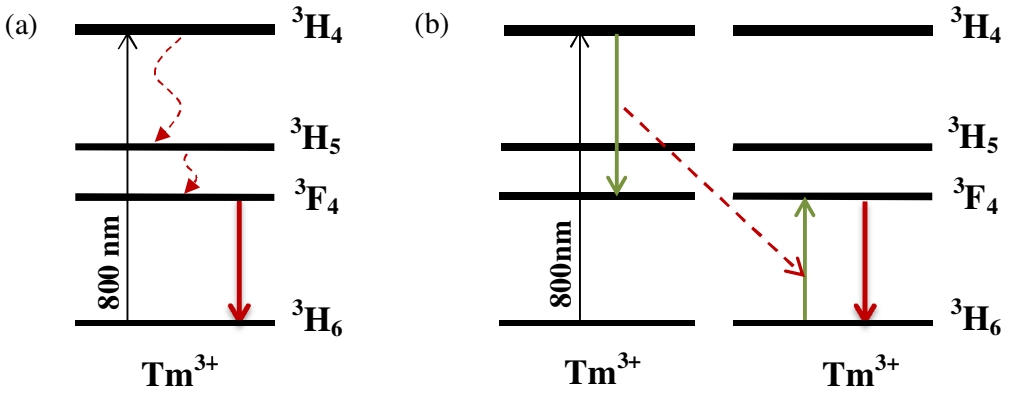

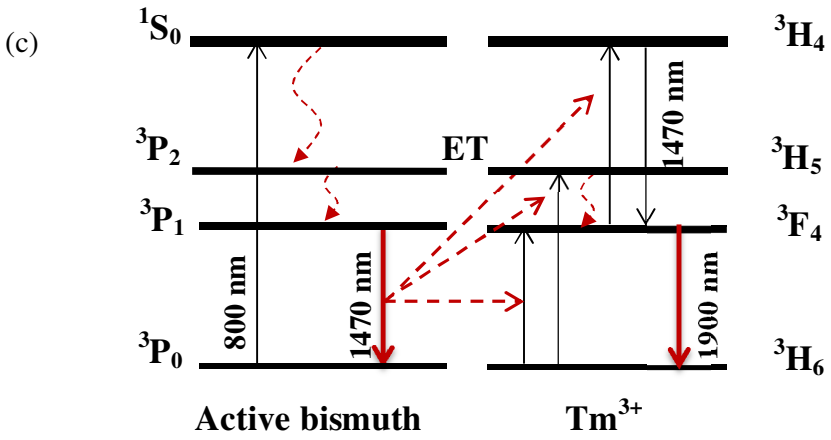

Figure 4.4: Energy level diagrams for various transitions in TBF with 800 nm pumping involving (a) Tm^{3+} (b) cross relaxation between Tm^{3+} (c) energy transfers from active bismuth to Tm^{3+}.

4.4 Broadband Amplified Spontaneous Emission (ASE) generation at 1.9 µm

Fiber ASE light has a broadband spectrum and can thus be used as a broadband light source. It is developed using the emission characteristics, which depends on the energy structure of dopant ions in the glass host and pumping wavelength. The pump laser energizes the dopant ion hence spontaneously emitted light from the ion propagates along the fiber. It is then amplified by the gain properties of the fiber and emitted as the ASE. Light is emitted in both forward and backward directions, and thus either one can be selected as the source output. Unlike lasers, ASE sources do not rely on optical feedback, and thus, the full-width half-maximum (FWHM) bandwidth of the ASE is generally very broad, typically greater than 10 nm. The most common fiber ASE source comprises a single-mode pump that energizes a length of Er-doped single-mode silica fiber, typically in tens of meter, to emit at 1550 nm (Cheng *et al.*, 2010; Lin *et al.*, 2004). Recently, ASE sources operating around the mid infrared spectral region (1.9 µm) have gained tremendous interest for possible applications in spectroscopy, gas

sensing, low-coherence interferometer, and medical imaging via optical coherence tomography. Currently, commercial light-emitting diodes (LEDs) and semiconductor lasers operating in mid-infrared region are normally used for these applications. However, the main drawbacks of these sources are its stability, which is strongly dependent on temperature, high coupling loss when connected to the standard single mode fibers and fabrication cost. In this section, ASE generation in the 1900 nm waveband is demonstrated using the fabricated TBF as a gain medium.

The proposed ASE source consists of a piece of 1.0 m long TBF sample, which is forward pumped by a 800 nm laser diode with 200 mW pump power as shown in Figure 4.5. In the experiment, 800 nm pump laser was used because it operates at one of the most efficient Tm^{3+} and active bismuth absorption wavelength. Furthermore, it is easily available and cheap. The 800/2000 nm wavelength division multiplexer (WDM) was used to launch the 800 nm pump into the gain medium. The generated ASE was detected using an optical spectrum analyser (OSA) operating in a range of 1200 nm - 2400 nm wavelength with a resolution of 0.1 nm. The ASE emission was firstly investigated for three different fabricated samples, as shown in Figure 4.6. In the experiment, the pump power is fixed at 27.5 mW to avoid the excess pump power from TB3 sample. As seen in the figure, all three fibers emit broadband ASE at 1880 nm region. This is attributed to the 800 nm pumping, which excites both Tm^{3+} and active bismuth ion from the ground state to the higher energy levels of $^3H_4$ and $^1S_0$, respectively (Figure 4.4(c)). Then, the Tm^{3+} ions decay to $^3F_4$ to create a population inversion between $^3F_4$ and $^3H_6$ levels of the Tm^{3+}, which generates spontaneous emission at around 1900 nm region. After a fast decay into $^3P_2$ then to $^3P_1$ level, the active Bi ions transfer their energy to the Tm^{3+} ions via multipolar interactions. Immediately after this energy transfer, the Tm^{3+} ions move from $^3H_5$ to $^3F_4$ energy level through rapid multi-phonon relaxations. This improves the amplification and ASE

generation at around 1900 nm region. Another peak observed at 2050 nm region is associated with the characteristics of the 800 nm pump source that exists even without the use of the gain medium. As shown in Figure 4.6, TB2 exhibits the ASE power with the highest peak output of -51.4 dBm centered at 1880 nm region. The peak ASE powers of TB1 and TB3 are obtained at -53.4 dBm and -58.4 dBm, respectively. This is attributed to the TB2, which has the highest Tm^{3+} and active bismuth ion concentrations compared with other samples while TB3 sample has the lowest Tm^{3+} ions concentrations, thus exhibit the lowest ASE spectrum. Using TB2, the 3 dB bandwidth of the ASE spectrum covers from 1820 nm to 1975 nm, while 10 dB bandwidth covers from 1735 nm to 2077 nm.

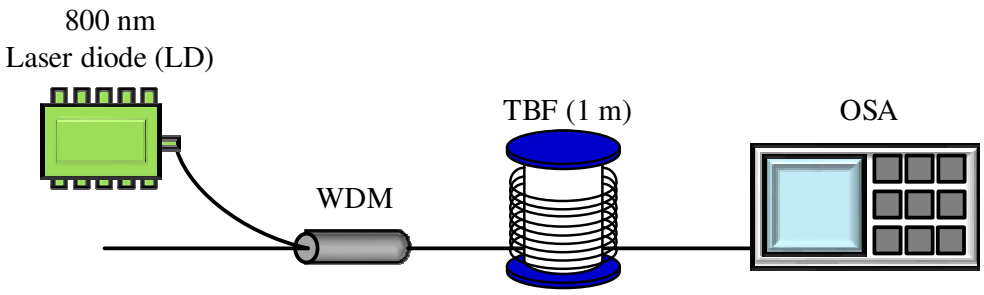

Figure 4.5: Configuration of the proposed 1.9 µm broadband source.

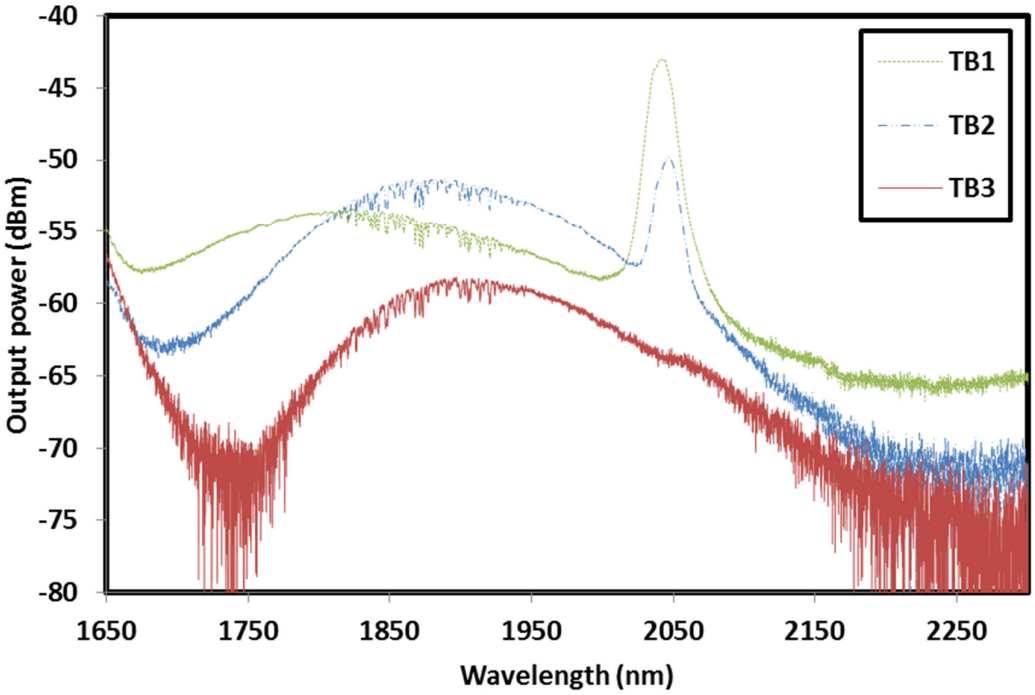

Figure 4.6: ASE spectra of different TBF samples with TBF length of 1 m and a fixed pump power of 27.5 mW.

Figure 4.7 shows the ASE spectra of the different lengths of TB2 under 800 nm wavelength excitation when the pump power is fixed at 200 mW. As seen in the figure, the power of the broadband ASE spectrum rises drastically as the TB2 length increases from 0.5 m to the optimum length of 1.0 m. This is attributed to the additional Tm^{3+} and active bismuth ions from the longer length, which can absorb more pump power and emit stronger ASE light. However, the ASE power drops as the gain medium length is further increased due to saturation effects. The unused Tm^{3+} and active bismuth ions will absorb the 1880 nm ASE and reduces the output power of the ASE spectrum. It is also observed that the ASE's peak wavelength is shifted to a longer wavelength as the fiber length increases from 0.5 m to 2.5 m. This is attributed to the shorter wavelength ASE being absorbed by the unused Tm^{3+} and active bismuth ions and emitted at a longer wavelength and thus shifts the peak wavelength to a longer wavelength. Figure 4.8 compares the ASE spectrum obtained at two different pumping power of 100 mW

and 200 mW when TB2 is fixed at 1.0 m. It is observed that the ASE power increases with the pump power. Further increase of pump power is expected to further raise the attainable power of the ASE spectrum owing to the increment of population inversion in the active bismuth ions and Tm^{3+} ions and thus enhances the ASE.

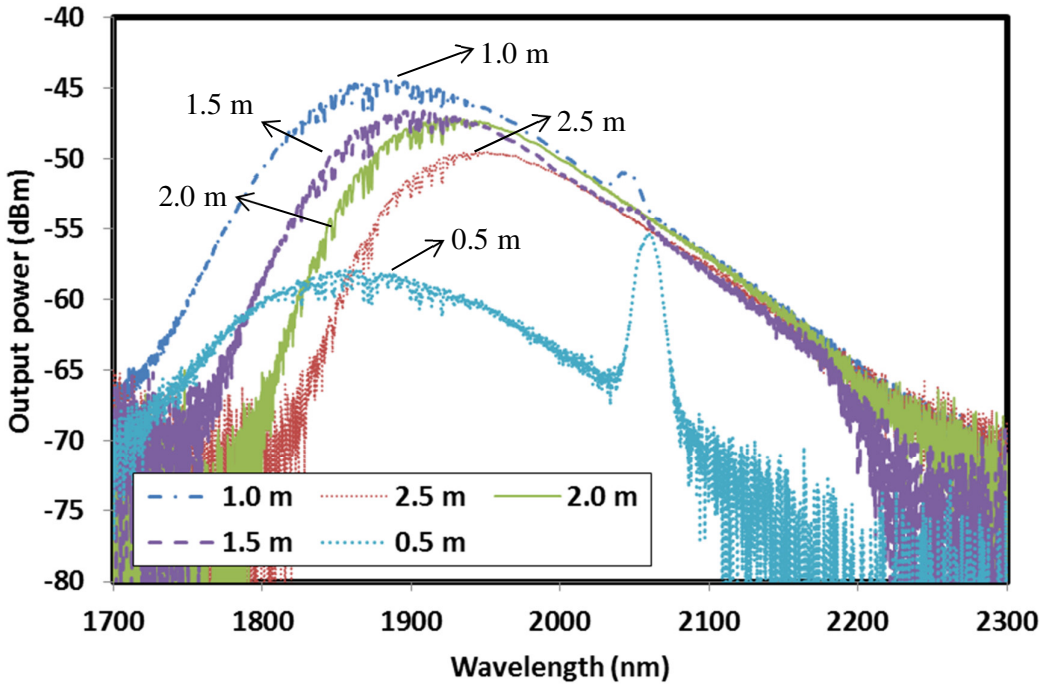

Figure 4.7: ASE spectra at different TB2 lengths at the fixed 800 nm pump power of 200 mW.

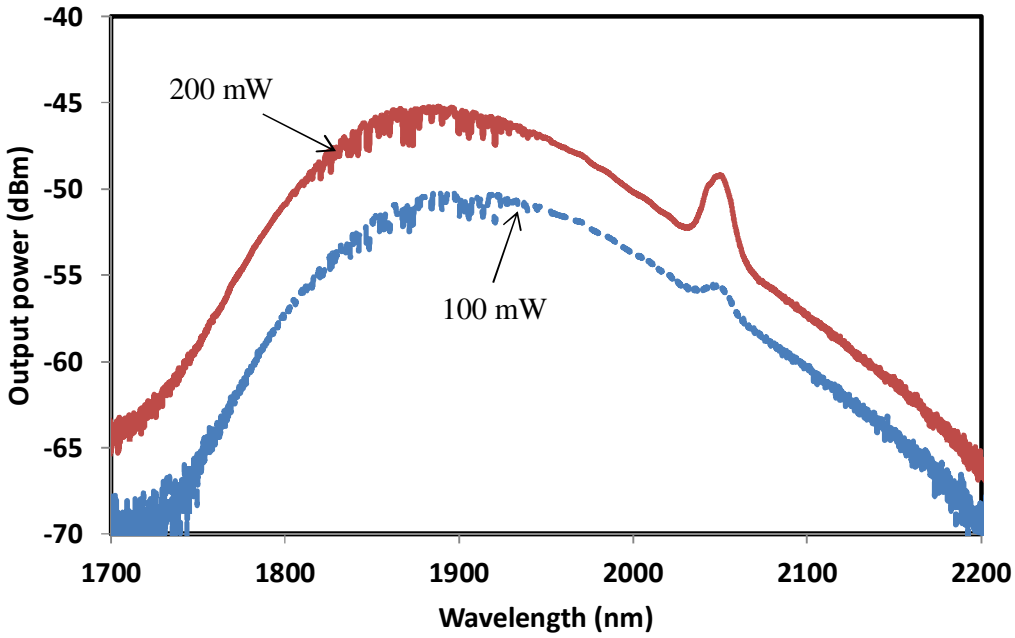

Figure 4.8: The ASE spectrum of TB2 (1.0 m) at two different pumping powers.

The effect of a secondary pump of 1552 nm on the performance of the ASE spectrum was also investigated. Figure 4.9 shows the ASE spectrum of the TB2 with and without a secondary pump of 1552 nm when the primary pump of 800 nm is fixed at 100 mW. As seen in the figure, the ASE power is increased by more than 10 dB at 1850 nm region as the 500 mW secondary pump is injected into the gain medium. This is due to the Tm^{3+} excitation to $^3F_4$ level, which enhances the population inversion and thus increases the output intensity of the ASE via $^3F_4 \rightarrow {}^3H_6$ transition, particularly at 1850 nm region.

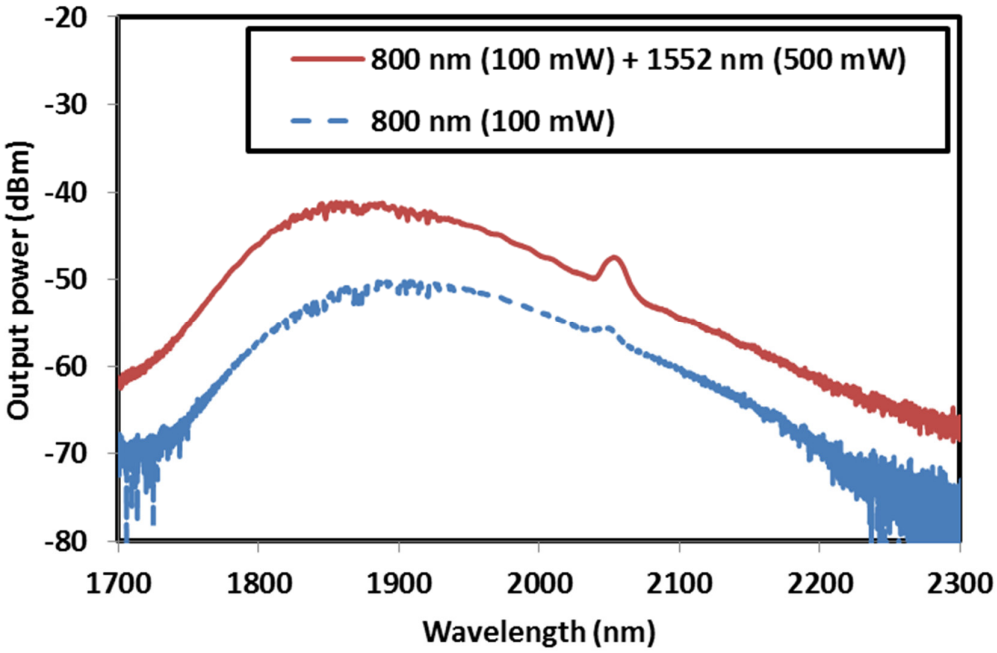

Figure 4.9: ASE spectrum with and without 500 mW of 1552 nm pumping when the primary pump of 800 nm is fixed at 100 mW using 1.0 m TB2.

The performance of the proposed TBF ASE source is also compared with the commercial TDF under 800 nm excitation as shown in Figure 4.10. In the experiment, the ASE spectrum of TB2 is compared with the TDF when the fiber length and pump power are fixed at 1 m and 27.5 mW, respectively. As shown in Figure 4.10, both fibers generate an almost similar ASE spectrum centred at 1880 nm. With TBF, the ASE spectrum is higher by 5 dB compared to that of the commercial TDF. This is attributed to the thulium ion concentration, which is higher in TB2 (0.9 wt.%) compared to the TDF, which has a thulium ion concentration of around 0.25 wt.%.

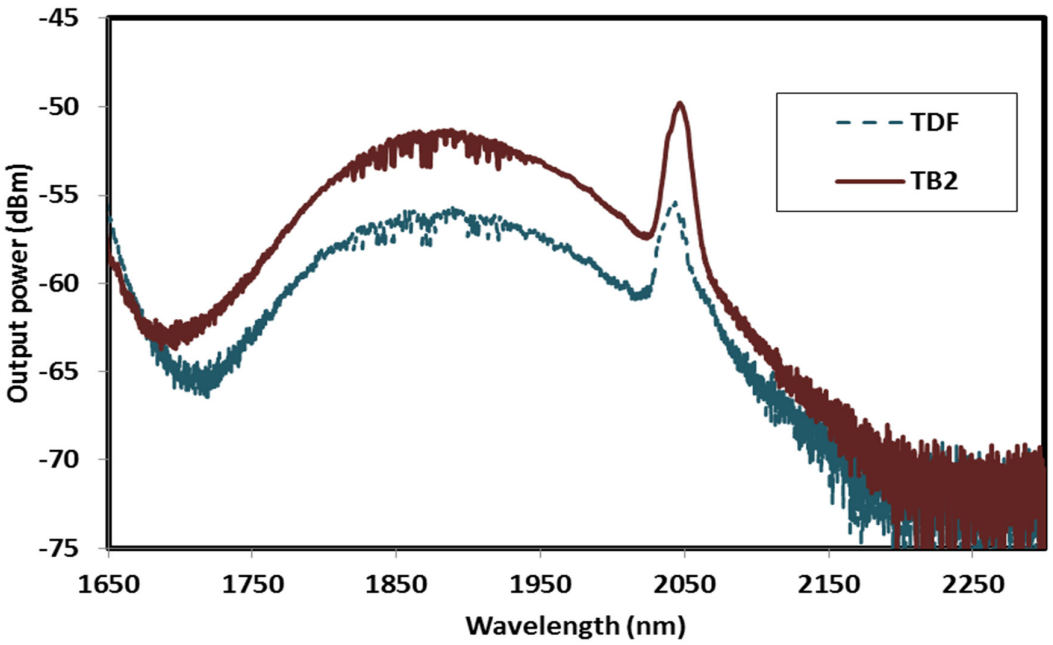

Figure 4.10: Comparison of the ASE emission between TBF sample (TB2) and the commercial TDF when it is pumped by 27.5 mW 800 nm pump.

4.5 Thulium Bismuth co-doped fiber lasers at 1.9 μm by 800 nm pumping

Lasers with emission in the two-micron spectral region are of great interest for a variety of applications including material processing, remote sensing, as well as biomedicine (Scholle *et al.*, 2010). Due to the strong absorption of water and biological tissue at 1.9 micron makes the laser transitions at this region possible for medical applications. As such, two primary categories of applications; those that seek to minimize atmospheric absorption, such as directed energy and free space optical communication (Koch *et al.*, 2004), or those such as LIDAR that rely upon narrow molecular vibration absorption resonances to sense atmospheric constituents such as water vapour and CO_2 (Koch *et al.*, 2008). Thulium and Thulium-Holmium doped fibers have been demonstrated to be promising gain medium candidates for the two-micron fiber laser (Gumenyuk *et al.*, 2011; Zhang *et al.*, 2011c). As discussed in the earlier section, thulium fiber has a broad and efficient emission within a wavelength

range between 1600 nm to 2100 nm from $^3F_4 \rightarrow {}^3H_6$ transitions and is suitable for lasing at 2 μm regions.

In this section, an efficient Thulium Bismuth co-doped fiber laser (TBFL) operating at 1.9 μm region is experimentally demonstrated using a newly developed TBF as the gain medium. The lasing performance is compared with a commercial TDF. The configuration of the proposed 1.9 μm laser with the fabricated TBF as the gain medium is shown in Figure 4.11. It employs two FBGs operating at the center wavelength of 1901.6 nm to establish linear laser cavity (refer Figure 3.29 in the previous chapter). They have a reflectivity of 99.6% and 50% with the corresponding 3 dB spectral width of 1.5 nm and 0.6 nm respectively. The TBF is pumped using an 800 nm laser diode at the 99.6% FBG port and the output laser is taken out from the 50% FBG port. The output spectrum and intensity of the laser are monitored by using an optical spectrum analyzer (OSA) and power meter (PM) respectively. The performance of the 1.9 μm fiber laser is also investigated by replacing the TBF with a commercial TDF for comparison. The core diameter of the commercially available TDF is 9 μm while its NA and thulium ion concentration are 0.15 and 0.25 wt.% accordingly. The lasing experiments were carried out for all TBF samples (TB1, TB2 and TB3) and the commercial TDF.

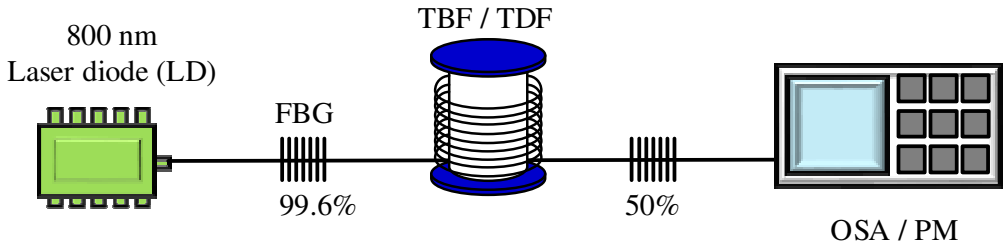

Figure 4.11: Experimental setup for the proposed 1.9 μm TBFL.

It is observed that the 1.9 μm lasing was achieved for all fibers except for TB3. The optimized fiber lengths for TB1, TB2 and TDF are 3.0 m, 0.4 m and 2.0 m, respectively for maximum efficiency of the laser generation. The experiment has been carried out using several other TDF lengths pumped by 800 nm wavelength excitation with the maximum input power of 200 mW, however no lasing has been observed due to insufficient pump to reach the threshold power. Figure 4.12 shows the relationship of the output power against the pump power at the optimized fiber lengths for three different gain media (TB1, TB2 and TDF). As seen in the figures, the slope efficiencies of 31.0, 42.2 and 9.0% are obtained for the laser of TB1, TB2 and TDF, respectively. Compared to the TDF, both TBFs produce laser with a higher efficiency at a significantly lower threshold pump power. The threshold pump power for both TBFLs are observed to be around 75.0 – 80.1 mW, which is much lower than the threshold pump power of the TDFL (177.5 mW). The optimum length is much shorter for TB2 compared to that of TB1 since the thulium ion concentration in TB2 is 3 times as high. High thulium doping concentration in TB2 increases the efficiency of stepwise energy transfer such that the optimum length for lasing is comparatively shorter. To avoid clustering from the high concentration of rare earth ion, aluminium is added as host modifiers (Blanc *et al.*, 2008). It also helps reduce phonon energy of the core glass in the fiber, thus increases the probability of radiative emission and improves lasing efficiency.

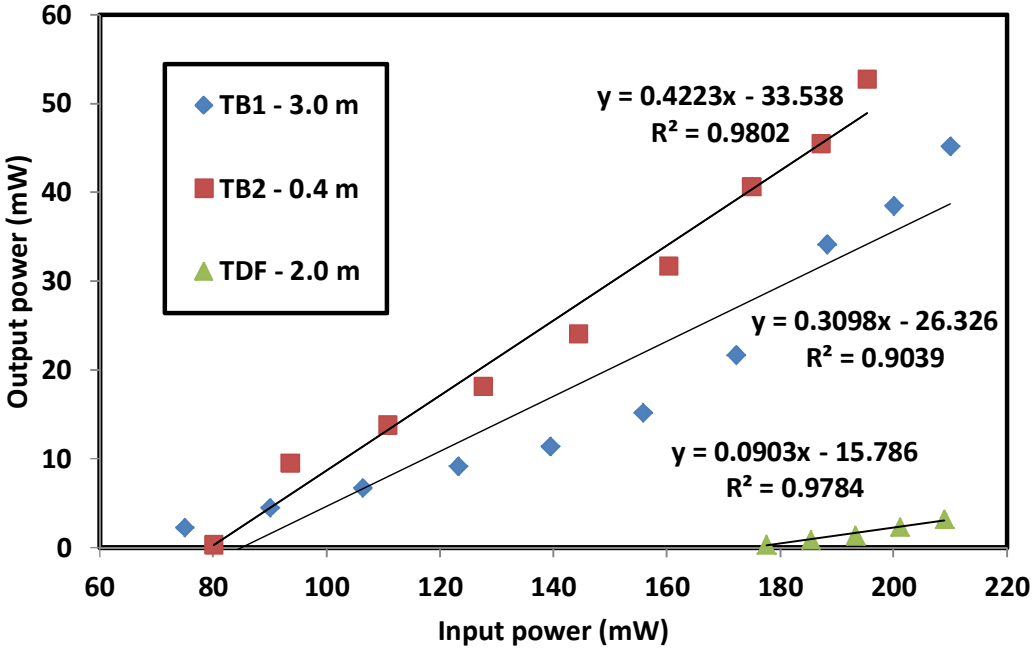

Figure 4.12: Performance comparison for three different gain media of TB1, TB2 and TDF.

Figure 4.13 shows the relationship of the output power against the pump power at different TBF lengths. The figure shows that the efficiency of the laser increases from 13.7 % to 42.2 % as the length of the gain medium is reduced from 1.5 m to 0.4 m. At the optimal length of 0.4 m a maximum output power of 52.7 mW is achieved at the pump power of 195 mW. The proposed laser performance is higher by 7% in efficiency and 2.7 mW higher in output power in comparison to the work of Geng et. al. (Geng *et al.*, 2007). Figure 4.14 shows the attenuated output spectrum of the TBFL at the optimum length of 0.4 m when the 800 nm pump is fixed at 195 mW. The laser operates at 1901.6 nm, which corresponds to the center wavelength of both FBGs. Its signal to noise ratio (SNR) is more than 50 dB while its 3 dB bandwidth is less than 0.05 nm (limited by the OSA resolution). It is also observed that the peak power of the residual pump (800 nm) is about 3.05 dBm and the peak power of the lasing wavelength (1901.6 nm) is 5.30 dBm. This indicates that the output power measured by a power meter is

mainly contributed by the lasing wavelength. The efficiency of the laser is observed to drastically decrease as the TBF length reduces below 0.4 m. In addition, the ratio of residue pump/output power is approximately 0.58 at 0.4 m. As the fiber length becomes shorter, it is observed that the residual pump power is higher than the peak laser power.

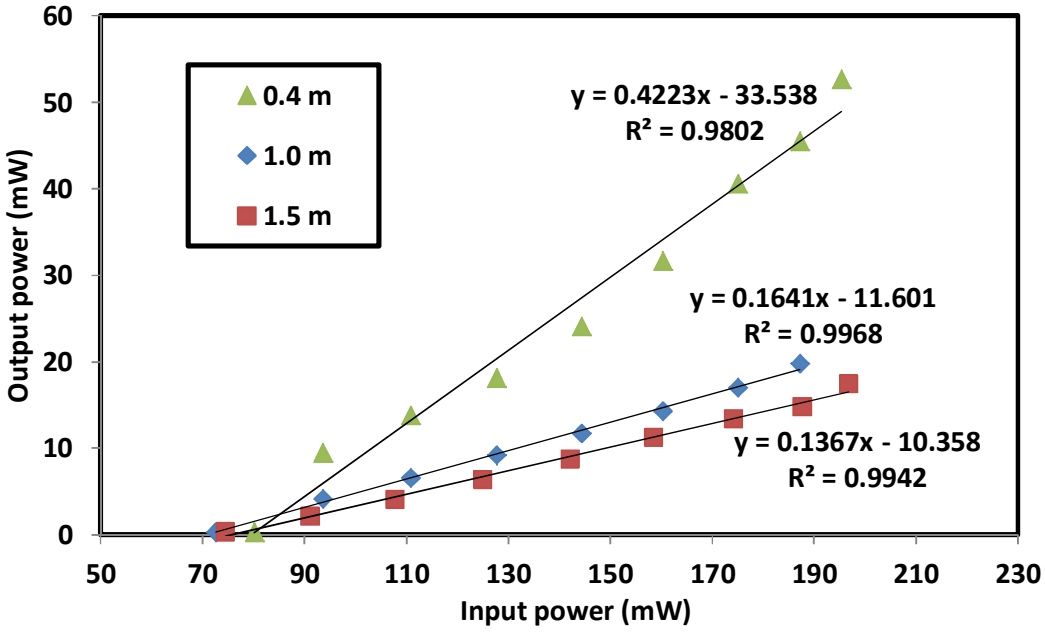

Figure 4.13: Output power of the proposed TBFL against the pump power at different TBF (TB2) lengths.

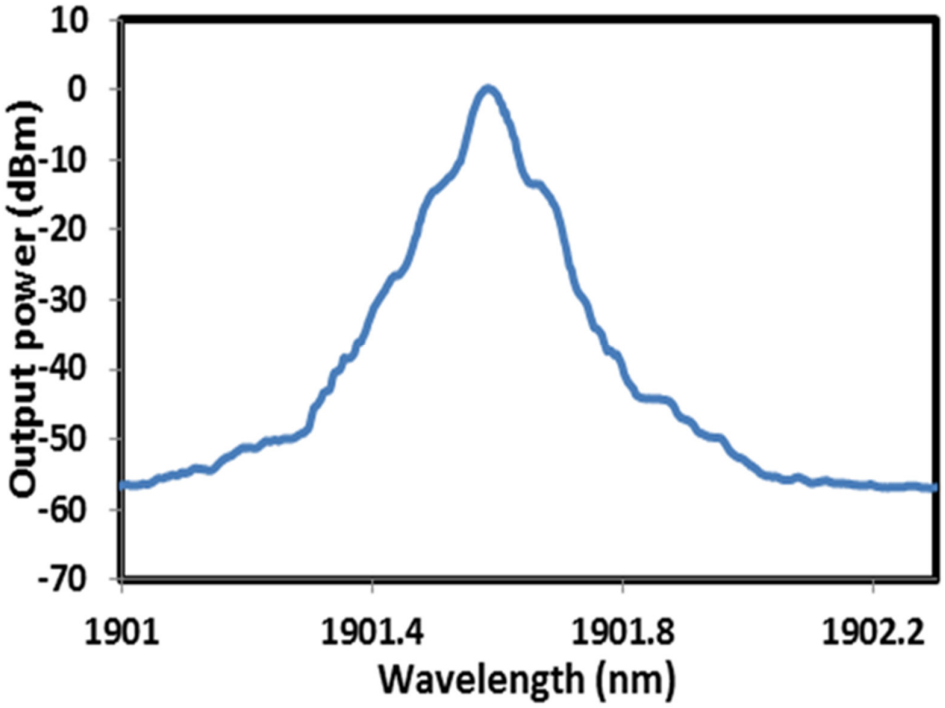

Figure 4.14: The attenuated output spectrum of the laser at the maximum pump power.

By pumping the TBF with 800 nm pump, both thulium and active bismuth ions are excited to the upper level to create a population inversion for lasing at 1.9 µm region. The improved threshold and efficiency was due to the incorporation of active bismuth in the gain medium, which enables energy transfer processes between active bismuth ion to Tm^{3+} ions as explained earlier in Figure 4.4 (c). Compared to the TDFL, the proposed TBFL has shown a significantly higher efficiency due to various factors such as doping concentration and the assistance from cross relaxation and energy transfer process. The thulium ion concentration is higher in the TBF (0.90 wt.% in TB2) than the TDF, which has a thulium ion concentration of around 0.25 wt.%. The higher dopant density is possible due to the incorporation of active bismuth ions in the fiber. The Bi ions also help to increase the $^3F_4$ population and thus improve the efficiency of the laser through energy transfer processes. As also shown in Figure 4.13, the pump

power threshold for the proposed laser is around 72.5, 74.5 and 80.1 mW for 1.0, 1.5, and 0.4 m TB2, respectively. As the longer length is used (1.0 m and 1.5 m), the comparatively lower threshold is obtained. This is due to the higher population inversion at low pump power for the longer TBF. In general, these thresholds are significantly lower than that of the TDFL, which is around 177.5 mW. The presence of active bismuth ions improves the population inversion by the energy transfer process. Other TDF lengths failed to exhibit any laser radiation. Failure to generate any laser at the other TDF lengths was due to the insufficient input pump power to excite enough Tm^{3+} ions to the upper state level, resulted in limited population inversion to compensate all the losses in the cavity. The performance of both TBFL and TDFL in terms of threshold and efficiency is expected to improve significantly if the pump operated at the optimum wavelength of 785 nm is used. The proposed TBFL could be scaled up in power if higher input pump power in 785 nm is available and better heat management is taken into account.

4.6 TBFLs with 1552 nm pumping

In this section, lasing at 1901.6 nm is experimentally demonstrated using the fabricated TBF in conjunction with 1552 nm pumping. The configuration of the proposed TBFL is similar to Figure 4.11 except for the pump laser. It uses a cladding pumped Erbium-Ytterbium fiber laser operating at 1552 nm as a pump source instead of the 800 nm laser diode. The fabricated TBF has thulium ions absorption bands at 785 nm ($^3H_6 \rightarrow {}^3H_4$), 1205 nm ($^3H_6 \rightarrow {}^3H_5$) and 1650 nm ($^3H_6 \rightarrow {}^3F_4$) regions. A 1552 nm wavelength excitation falls within the thulium absorption band centred at 1650 nm. Figure 4.15 shows the attenuated output spectrum of the TBFL recorded by an OSA when the TBF (TB1) length and 1552 nm pump are fixed at 2 m and 100 mW, respectively. Inset of the figure shows an enlarged figure of the output spectrum at 1900

nm region. As seen in the inset figure, the TBFL operates at 1901.6 nm, which coincides with the center wavelength of both FBGs with a SNR of more than 60 dB. The 3 dB bandwidth is measured to be less than 0.05 nm limited by the OSA resolution. It is also shown in Figure 4.15 that the peak wavelength of the residual pump at 1552 nm is about 5 dB lower than the peak power of the lasing wavelength. This shows that the output power measured by a power meter is mainly contributed by the lasing wavelength of 1901.6 nm. As the TBF is pumped by 1552 nm pump, a broad ASE is generated at 1900 nm region that oscillates in the Fabry-Perot cavity for the laser generation. Thulium ions will be excited to $^3F_4$ level as it absorbs the pump photon to create a population inversion between $^3H_6$ and this energy level. Then it drops to the ground state ($^3H_6$) while emitting at 1.9 µm.

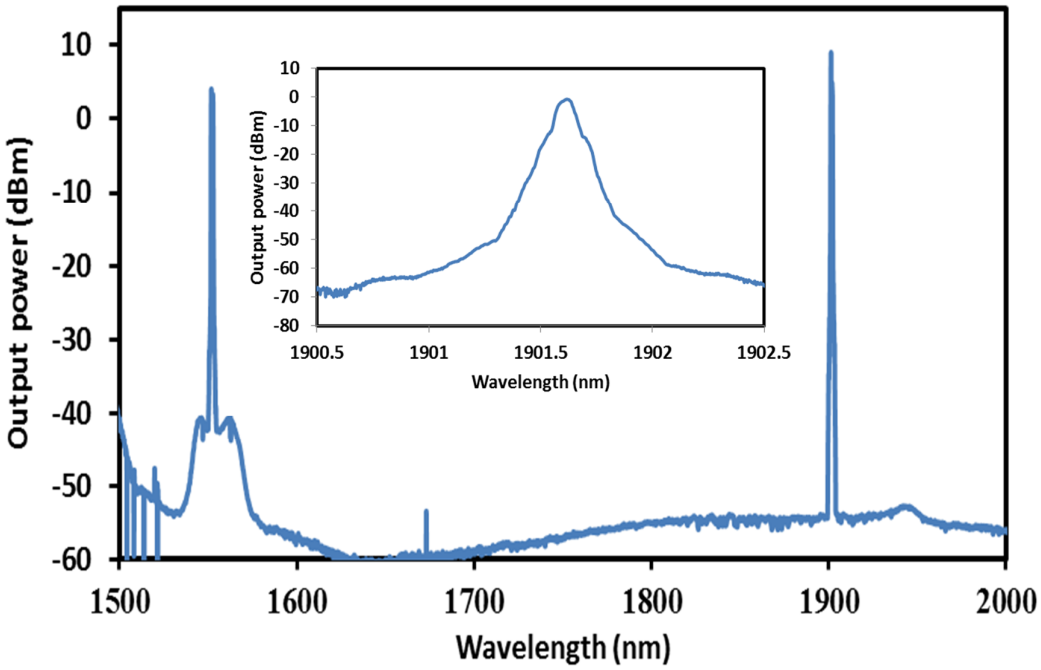

Figure 4.15: Attenuated output spectrum of the TBFL. Inset shows the enlarged output spectrum within the 1900 nm region.

Figure 4.16 shows the laser output power against 1552 nm pump power at various gain media at the optimized length. As shown in the figure, all TBF samples produce 1901.6 nm laser, in which the output powers linearly increase with the pump power. The highest efficiency of 32.5% was generated from 2.0 m long TB1 sample as the gain medium. The TBFL configured with TB2 (1.0 m) and TB3 (3.0 m) has an efficiency of 32.2% and 16.1%, respectively. Since the Tm ions dopant in TB2 is the highest (0.90 wt.%), it uses only half of the TB1 length to produce a comparable efficiency with the TB1. On the other hand, the threshold pump powers are 52.2 mW, 62.3 mW and 323.0 mW for the TBFL configured with TB1, TB2 and TB3, respectively. The highest output power of about 211 mW was produced by TB1 and the comparative output power produced by TB2 is around 208 mW at the pump power of 700 mW. For TB3 sample, the low output power of 108.2 mW and high threshold pump power of 323 mW as compared to TB1 and TB2 are resulted from the low thulium ion concentration of only 0.06 wt.%.

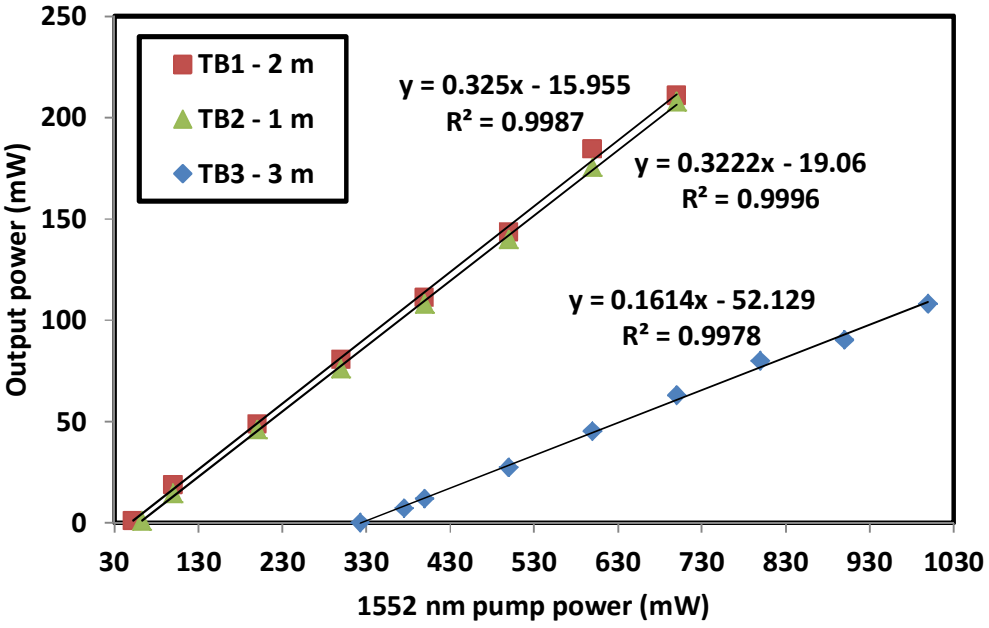

Figure 4.16: Output power characteristic against pump power for the proposed TBFL with different TBFs under 1552 nm pump excitation.

Figure 4.17 shows the laser output power against 1552 nm pump power at various fiber lengths for TB1 gain medium. As shown in the figure, the efficiency of the proposed TBFL increases as the TBF length is reduced from 5 m to 2 m. The maximum efficiency of 32.5 % is obtained at the TBF length of 2 m. The maximum output power of 211 mW is achieved at the pump power of 700 mW with the optimum length of 2 m. A further decrease of the TBF length is expected to improve the total efficiency of the laser, but the residual pump will also increase. The pump power thresholds for the proposed laser slightly reduces from 77.9 mW to 52.2 mW as the TBF length reduces from 5 m to 2 m. This is attributed to the population inversion, which is more efficient at a shorter TBF length and thus a slightly smaller pump power is required to initiate lasing. The optimum length for lasing is comparatively short due to the high thulium doping concentration in the developed TBF. To avoid clustering from high concentration of rare earth ion doping, aluminium is added as host modifiers to reduce phonon energy in the fiber. This in turn increases the probability of radiative emission and improves lasing efficiency. The incorporation of Bi ions has not significantly affected the efficiency of laser since the active bismuth ion absorption is very low at 1550 nm region. However, doping of suitable amounts of Al_2O_3, GeO_2, and Bi_2O_3 will be responsible to increase the intensity of the luminescent center of active bismuth through the formation of Al–O–Bi complexes with changing the covalency character of oxygen atom linked to active bismuth. Due to a large ionic radius it is difficult for Bi to substitute for Si in SiO_4 tetrahedron. Stabilization of the Bi ion inside the SiO_4-tetrahedra rings is done through an oxidation by $[AlO_{4/2}]$ – complexes (Firstov *et al.*, 2011). Here Al will form such complexes in silica glass and tend to oxidize network modifier cations. In this glass, +1 oxidation state of Bi ions will be more probable than +5. So, in such silica glass the formation of $\{[AlO_{4/2}]-, Bi+\}$ complexes (Firstov *et al.*, 2011) embedded in the glass network may change the surrounding environment of Tm

ions drastically compared to the normal alumino-germano silica glass based Tm doped optical fibers. It may take part indirectly to increase the lasing efficiency under pumping at 1552 nm wavelength.

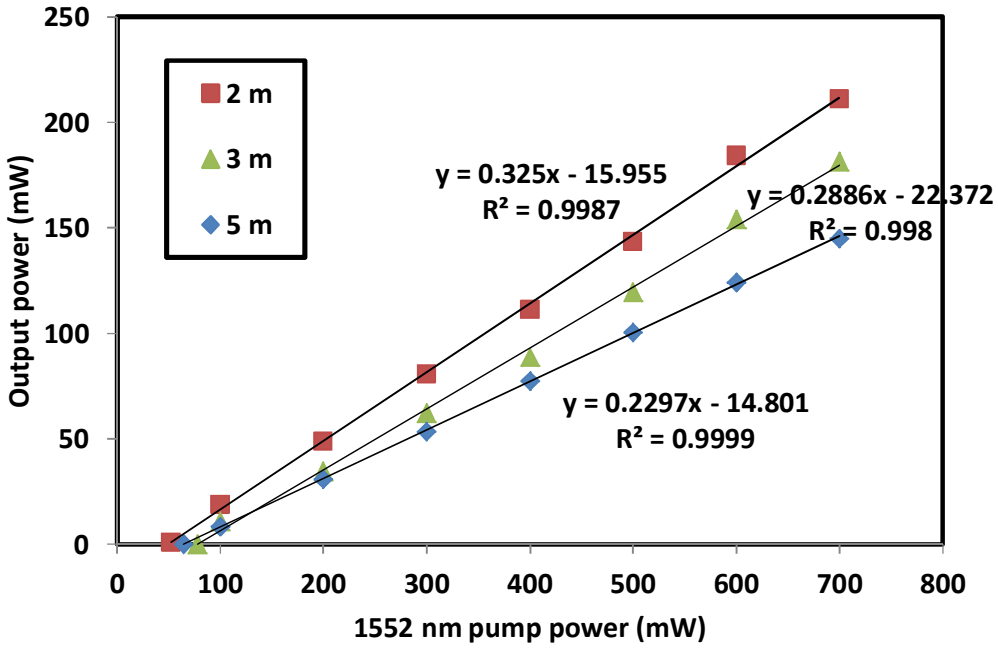

Figure 4.17: Output power of the proposed TBFL against the pump power at different TB1 lengths under 1552 nm pump excitation.

4.7 TBFLs with dual pumping scheme

Doping thulium with active bismuth may enhance the luminescence properties and exhibit broad emission spectrum usually ranging from ~1000 nm to ~1800 nm (Zhou *et al.*, 2011). In the attempt to enhance the efficiency of TBFL, dual-pumping method has been utilized in several earlier works (Battiato *et al.*, 1997). As discussed in section 4.4, the TBF ASE can be enhanced by incorporating an additional 1552 nm pumping excitation to the main pump (800 nm). The result shows that the increment in ASE power of almost 10 dB can be achieved with the assistance of 1552 nm excitation. In this section, we propose a dual pumping method to improve the efficiency of 1901.6

nm TBFL. An additional pumping at 1552 nm is added into the laser cavity to complement the 800 nm pumping.

Figure 4.18 shows the configuration of the proposed 1.9 μm laser using the fabricated TB2 sample as the gain medium. The proposed TBFL employs two FBG operating at the same wavelength of 1901.6 nm to establish laser cavity. The FBGs have different reflectivity of 99.6% and 50% with a 3 dB spectral width of 1.5 nm and 0.6 nm, respectively. The TB2 sample is pumped by 800 nm and 1552 nm laser diodes via a WDM while the output laser is tapped out from the 50% FBG port. The output spectrum and the power of the laser are measured by using an OSA and PM, respectively. The experiment is repeated for three different TB2 lengths of 1, 1.5 and 5 m.

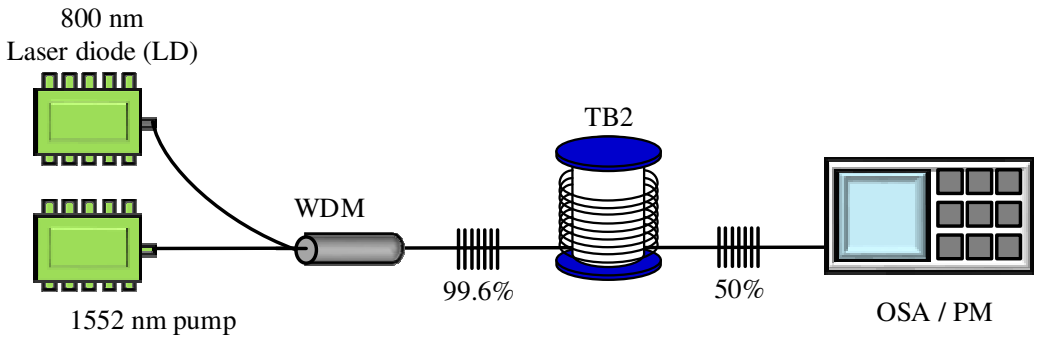

Figure 4.18: Configuration of the proposed TBFL with dual pumping scheme.

Figure 4.19 shows the attenuated output spectrum of the TBFL recorded by an OSA. The TBFL operated at 1901.6 nm with a SNR of more than 30 dB. The 3 dB bandwidth was measured to be less than 0.05 nm. The accuracy was limited by the OSA resolution. The inset of Figure 4.19 shows a similar attenuated output spectrum in another wavelength region between 700 nm to 1700 nm. It is shown that the power of the peak wavelength of the residual pump at 800 nm and 1552 nm is about 10 dB lower than the peak power of the lasing wavelength.

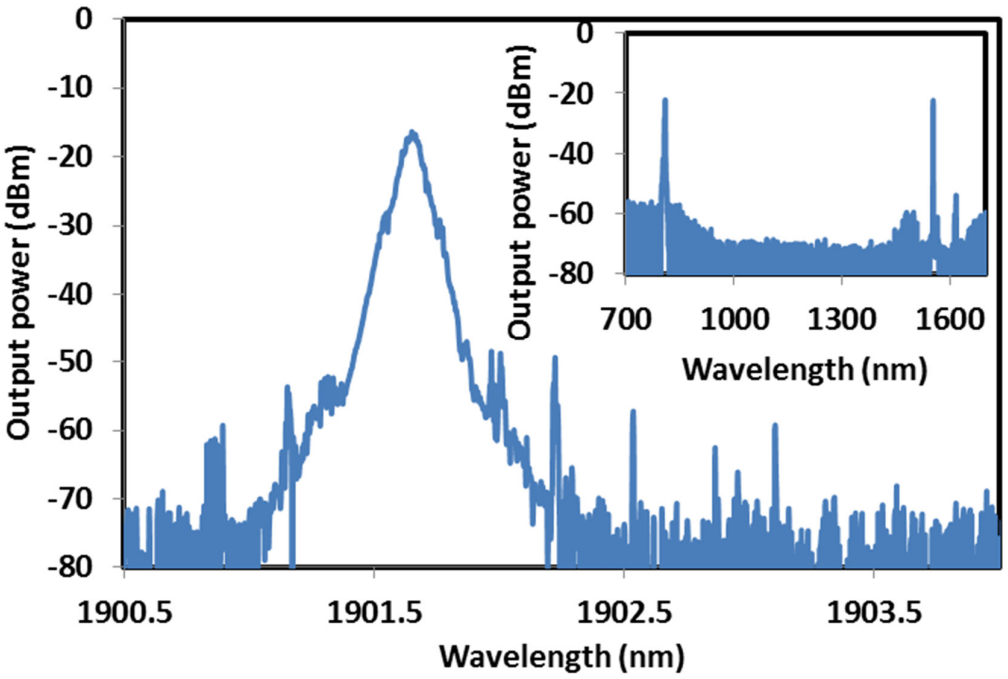

Figure 4.19: Attenuated optical spectrum of the TBFL with dual pumping. Inset shows the attenuated spectrum in a wider span ranging from 700 nm to 1700 nm.

Figure 4.20 shows the laser output power against the total pump power at various TB2 lengths. In the experiment, the 800 nm pump is fixed at 120 mW and the 1552 nm pump is varied in order to increase the total pump power. As shown in the figure, the efficiency of the proposed TBFL increases as the TB2 length reduces from 5 m to 1 m. The maximum efficiency of 35.06% is obtained at the TB2 length of 1 m. As compared to single pumping by 1552 nm excitation, an increment as much as 2.84% was observed. The maximum output power of 256 mW is achieved at the pump power of 820 mW with the optimum length of 1 m. As the length of TB2 is reduced, the residual pump will increase. For instance, the remaining of 1552 nm pump is observed to be higher than that of the lasing peak power at TB2 for less than 1 m length. At other TB2 lengths of 1.5 m and 5 m, the laser efficiency improved about 1.6% and 1.63% respectively as compared to the previous results with only 1552 nm single pumping. It is also observed that the pump power thresholds for the proposed laser are reduced from

220 mW to 120 mW as the TBF length decreases from 5 m to 1 m. The result shows that the use of a shorter TB2 length yields better performance due to the high thulium doping concentration in the gain medium, which requires a smaller pump power to initiate lasing.

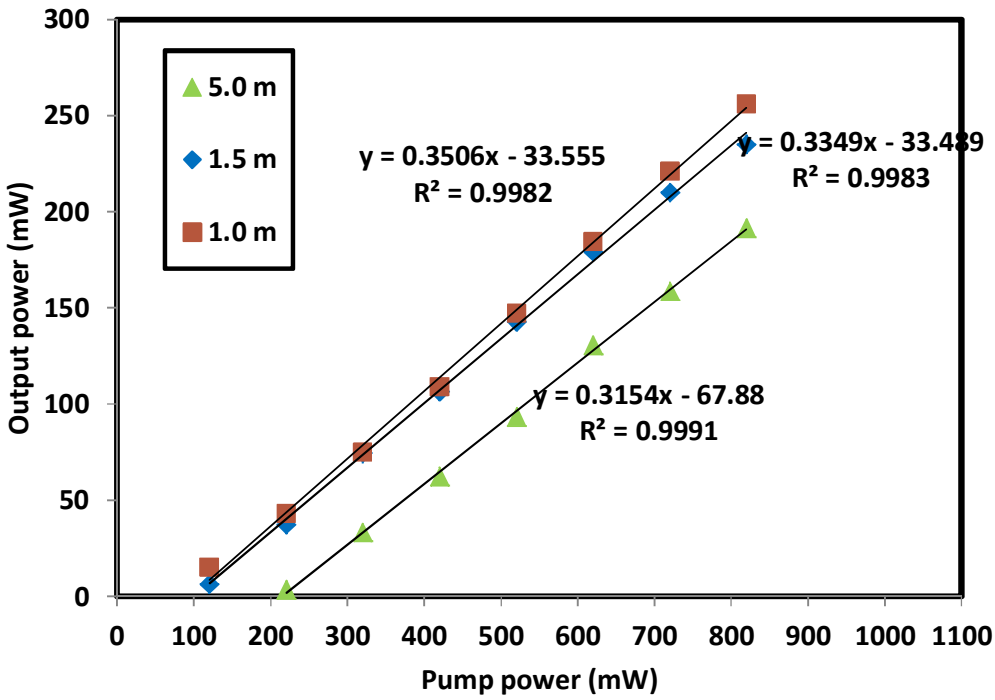

Figure 4.20: Output power of the TBFL as a function of the launched pump power at different fiber lengths using the dual-pumping method.

The 1552 nm pumping allows only ground state absorption to contribute to the stimulated emission and lasing. In this process, Tm^{3+} ions absorb pump photons and are excited to upper laser level $^3F_4$, which causes a population inversion between $^3H_6$ and $^3F_4$ level. As the Tm^{3+} ions drop back to the ground state they emit photons in the 1900 nm region. On the other hand, 800 nm pumping creates excitation of photons for both active bismuth and Tm^{3+} ions. Thulium ions at the $^3H_6$ level absorb pump photons and are excited to the upper laser level of $^3H_4$. The excited ions are then transferred non-

radiatively to the $^3H_5$ level before they relax at the $^3F_4$ level to emit photons in the 1900 nm region. The high thulium doping concentration may increase the possibility of Tm cross relaxation to occur, by pumping Tm ions with 800 nm pump, the 'two for one' cross relaxation process may contribute to the population inversion at $^3F_4$ level. As sufficient numbers of Tm^{3+} ions occupy the ground state, some of the neighbouring ions will absorb the emitted photons, which are the result of other Tm^{3+} ions going through the transition from $^3H_4$ to $^3F_4$ level. Consequently, two ions can be excited to $^3F_4$ level using only one pump photon and this enhances the emission in the 1900 nm region. Moreover, active bismuth ions can also be excited from the ground level of $^3P_0$ to the $^1S_0$ level by the 800 nm pumping (Zhang *et al.*, 2012). The excited ions then decay non-radiatively twice to level $^3P_1$ before emitting photons in the 1450 nm region as they relax to the ground state level. This emission will be absorbed by the nearby Tm^{3+} ions to improve population inversion between $^3F_4$ and $^3H_6$ and hence enhances the 1900 nm emission (Ruan *et al.*, 2009). In brief, the dual-pumping method assists the process of energy transfer from active Bi to Tm ions and improves the efficiency of the laser in comparison to the single wavelength pumping.

4.8 TBFLs with ring configuration

In the previous sections, we use the linear setup, which are made such that the light bounces back and forth between two FBGs, to achieve an efficient lasing. Besides linear configuration, a laser can also be designed based on a ring resonator, where an optical component within a resonator is hit by the light once per round trip instead of twice per round trip in a linear setup. In the ring resonator, the injected light will experience various effects such as birefringence, spatial hole burning effect, diffraction and sometimes involve optical nonlinearities. In some cases, addition of polarization controller, isolator or saturable absorber will change the spatial distribution of light.

Therefore, most of the Q-switched and mode-locked fiber lasers are generated based on a ring cavity to facilitate dispersion manipulation (Madsen *et al.*, 1998). In this section, we investigate the performance of the TBFL using TB2 with a ring configuration pumped by 800 nm and 1552 nm pump source for the use in the later chapter.

Figure 4.21 shows the proposed ring TBFL, which comprises of the TB2 as a gain medium, an 800/2000 nm WDM and a 10 dB output coupler. The TBF is forward pumped by an 800 nm laser diode to generate ASE in the 1.9 micron region, which then oscillates in the ring resonator to create a laser. A 10 dB coupler is used to split the oscillating light and allows 10 % of the light to couple out as an output. The laser output spectrum and power is characterized by an OSA and power meter, respectively. The performance of the ring TDFL is also observed which was obtained by replacing the TBF with a TDF. The ring resonator performance is also investigated using 1552 nm pumping scheme. In this case, a 1550/1900 nm WDM is used instead of an 800/2000 nm.

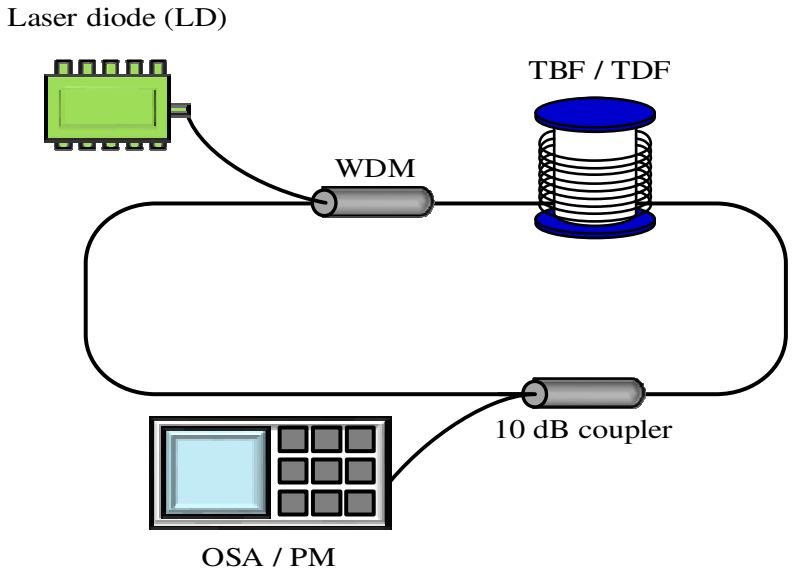

Figure 4.21: The proposed experimental setup for the ring resonator.

The effect of gain medium length on the performance of the ring TBFL was first investigated. Figure 4.22 depicts the output spectrum of the laser at three different TBF

(TB2) lengths when the pump power is fixed at its threshold. As shown in the figure, the operating wavelength of the laser shifts from 1867.9 nm to 1930.8 nm as the TB2 length increases from 0.4 to 1.5 m. This is due to the population inversion of the laser, which increases with an increment of the amount of thulium ion in the gain medium. Thus, the operating wavelength of the laser shifts towards the longer wavelength. Figure 4.23 shows the output power of the laser against the pump power at various TB2 lengths. The lasing performance of the conventional TDFL is also included in the figure for comparison. As shown in the figure, the TBFL starts to lase at threshold pump powers of 76.4, 64.1 and 146.7 mW for TB2 lengths of 0.4, 1.0 and 1.5 m, respectively. It is observed that the threshold pump power is drastically increased from 64.1 mW to 146.7 mW as the gain medium length increases from 1.0 to 1.5 m. This is attributed to the operating wavelength of the laser, which shifts to 1930.8 nm and thus it encounters a higher cavity loss since our components produces a higher loss at a longer wavelength. The lasing efficiencies of the laser are obtained at 1.7 %, 3.0 % and 2.2 % with TB2 lengths of 0.4, 1.0 and 1.5 m, respectively while the TDFL has an efficiency of 3.8 %. The TBFL exhibits a significantly lower threshold pump power compared to the TDFL except for the use of 1.5 m TB2 length. The TBFL starts to lase at pump power as low as 64.1 mW compared to that of TDFL which only starts to lase at 100.5 mW pump power at its optimum length of 2.0 m. This proves that the incorporation of active bismuth ion in the gain medium produces an energy transfer to the thulium ion, which resulted in an efficient population inversion and thus reduces the threshold pump power with the use of shorter gain medium.

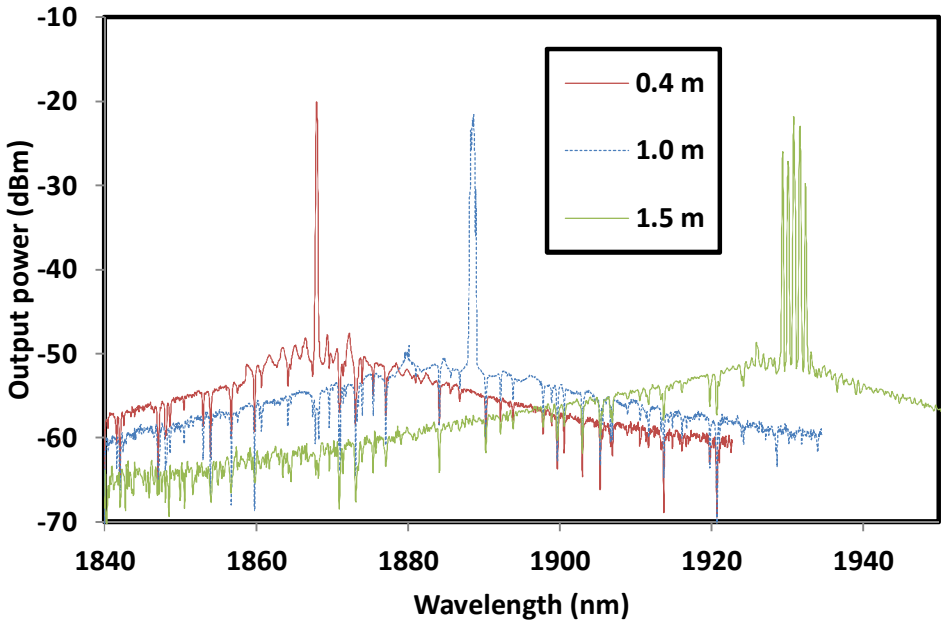

Figure 4.22: Output spectrum of the TBFL at different TB2 lengths.

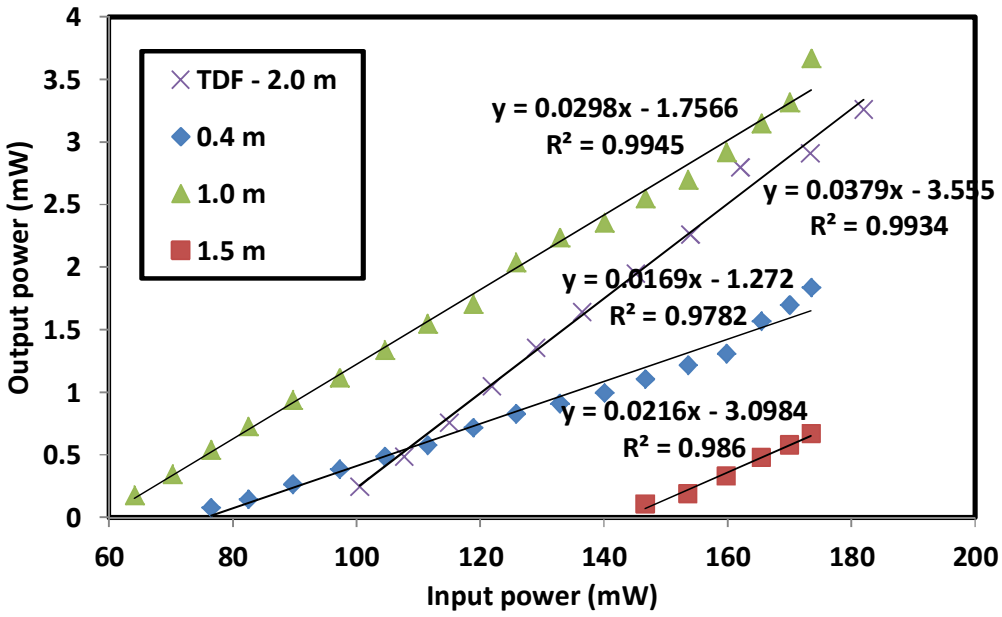

Figure 4.23: Output power against the input pump power for three different TB2 lengths and conventional TDF.

The lasing performance of the TBFL is also investigated with 1552 nm pumping scheme. Figure 4.24 shows the result at 1.5 and 5.0 m TB2 lengths and 4.0 m TDF. A large different in TB2 fiber length is chosen to compare the threshold pump power and efficiency of both longer and shorter lengths. The 4.0 m TDF is the optimum length for TDF compared to the other TDF length. The threshold pump powers of the ring laser are obtained at 178 mW, 450 mW and 416 mW with the utilization of 1.5, 5.0 m TB2 and 4.0 m TDF, respectively as the gain medium. Compared to the TDFL, it is observed that the 1.5 m TB2 operates at a lower threshold pump power. This is attributed to the Tm ion concentration, which is relatively higher in the TB2 compared to the conventional TDF. The longer TB2 length exhibit reabsorption of the Tm ions thus degrades the performance of the laser. On the other hand, the TDFL produces a higher lasing efficiency up to 6.7 % compared to TBFL, which can only produce the maximum efficiency of 1.6 % with the use of TB2 as the gain medium. The efficiencies of the ring laser are obtained at 1.6 %, 1.3 %, and 6.7 % with the use of 1.5, 5.0 m TB2 and 4.0 m TDF, respectively. The direct excitation process of $^3H_6 \rightarrow {}^3F_4$ fully utilizes the Tm^{3+} ions in the TDF which enhances the output power at 1900 nm region. In both ring TBFL and TDFL experiments, it is observed that the residual pump from 1552 nm will dominates the lasing emission as the length of gain medium was further decreased. The absence of energy transfer as in 800 nm pumping scheme contributes to the higher threshold and lower efficiency of TBFL when 1552 nm pump excitation was used.

Compared to the previously demonstrated linear cavity laser, the efficiency of the ring TBFLs and TDFL are significantly lower due to the high insertion loss of the optical components such as WDM and an output coupler used. The mode competition, which arises due to the absence of FBG in the cavity, also contributes to the deterioration of the laser efficiency.

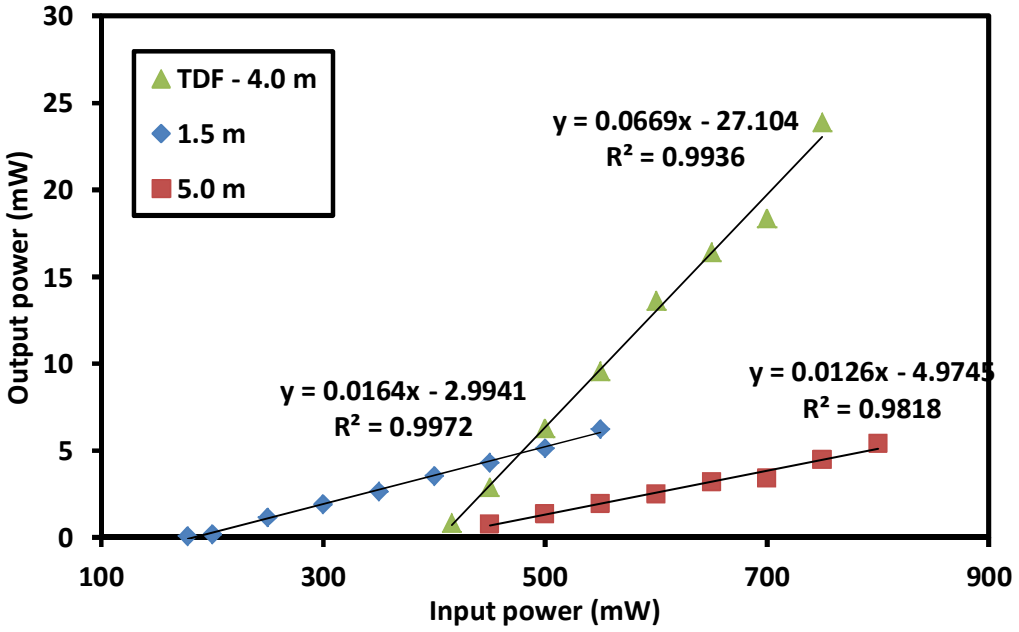

Figure 4.24: Lasing performance of the ring TBFLs and TDFL using 1552 nm pump excitation.

4.9 Dual-wavelengths Thulium Bismuth co-doped fiber laser

All-fiber dual-wavelength fiber lasers have also gained a tremendous interest in recent years due to their potential applications in various areas such as microwave photonics, fiber sensing systems, optical instrument testing, and optical signal processing (Ahmad *et al.*, 2009; Jeon *et al.*, 2010). To date, various methods have been proposed and demonstrated to achieve a dual-wavelength lasing such as by using a dual-cavity configuration and twin-peak reflection grating. In this section, a room temperature all-fiber dual-wavelength TBFL operating in the 1900 nm region is demonstrated based on single FBG in a ring configuration. The proposed laser uses a 1552 nm pumping scheme to generate ASE in the 1900 nm region, which then oscillates in the ring cavity to produce a dual-wavelength output as the state of polarization in the cavity is optimized.

The schematic of the dual-wavelength TBFL is shown in Figure 4.25. The fiber laser is constructed using a simple ring cavity, in which a 5 m long TB1 sample is used for the active gain medium. The TBF is pumped by a 1552 nm Erbium–Ytterbium co-doped fiber laser via a 1550/1900 nm WDM. The operating wavelength of the proposed TBFL is determined by the FBG, which is connected to port 2 of the circulator so that the reflection from the FBG can be routed back into the laser cavity via port 3. The circulator is used to allow the reflected light from the FBG to oscillate in the ring cavity as well as to ensure a unidirectional operation of the laser. A polarization controller (PC) is used to control the state of polarization of the oscillating light.

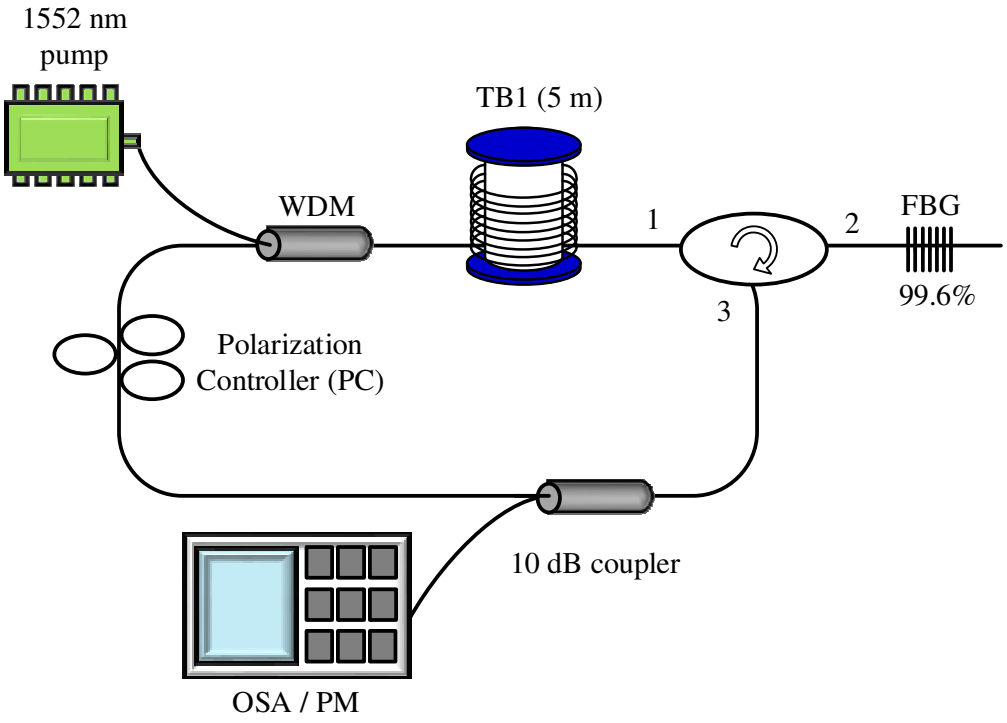

Figure 4.25: Experiment setup for dual-wavelength fiber ring laser.

Figure 4.26 shows the transmission and reflection spectra of the FBG. As shown in the figure, it has a center wavelength of 1901.6 nm with a 3 dB bandwidth of 1.5 nm and a transmission dip of about 23 dB, which translates to the reflectivity of 99.6%. As

the TB1 is pumped by a 1552 nm light, a broad ASE is generated at 1900 nm region via spontaneous and stimulated emission process. Thulium ions are excited to $^3F_4$ level as they absorb the pump photon to create a population inversion between $^3H_6$ and this energy level. Then, they drop to the ground state ($^3H_6$) while emitting at 1.9 μm. The ASE oscillates in the ring cavity to generate laser that operates within the reflection bandwidth of the FBG. As the FBG has a wide bandwidth and flat top characteristic, the generation of dual-wavelength laser output was realized by adjusting the PC. The output of the dual-wavelength laser is tapped from a 10 dB output coupler while allowing 90% of the light to remain in the cavity. The output spectrum of the laser is measured by using an OSA.

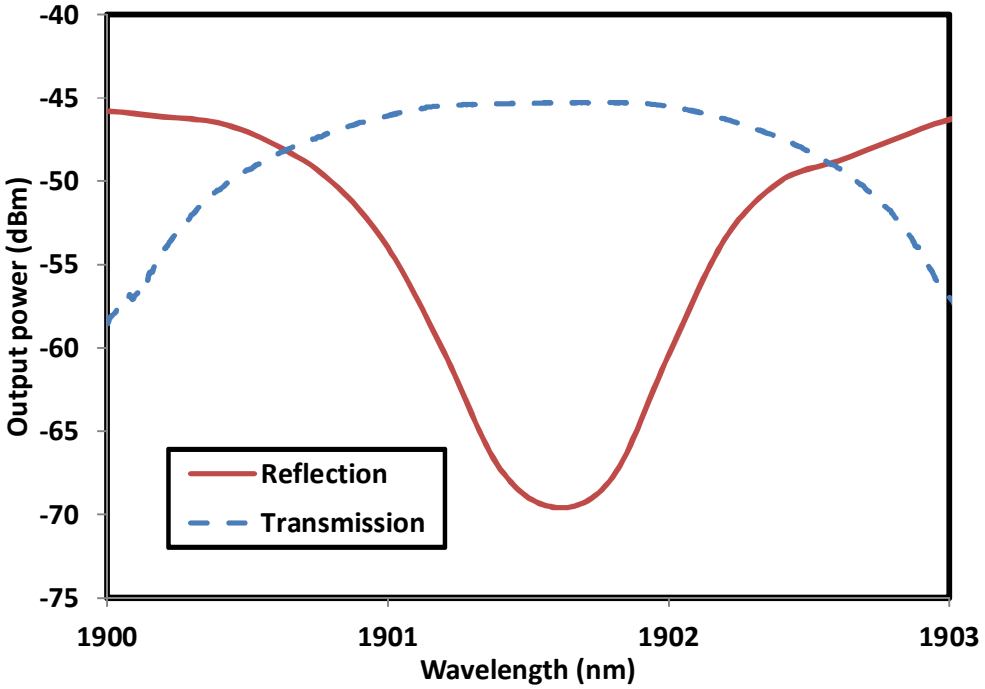

Figure 4.26: The transmission and reflection spectra of the grating.

As the TBF is pumped, an ASE is generated at 1900 nm region that oscillates in the ring cavity to generate laser within the reflection bandwidth of the FBG. Due to the reflectivity characteristic of the grating, it is possible to have the oscillation of two wavelengths in the cavity if the difference of cavity loss between them can be reduced.

By adjusting the PC, the cavity loss of the two wavelengths can be tuned to seek dual-wavelength oscillation with the help of the fabricated TB1, whose gain broadening behaves inhomogeneously. The addition of active bismuth ions co-dopant in the fiber, further enhances the inhomogeneous broadening effect in the fiber. Figure 4.27 shows the output spectrum of the TBFL recorded by an OSA when the 1552 nm pump is fixed at 930 mW at various PC orientations. As seen in the figure, a dual-wavelength output lines are obtained at 1901.09 and 1901.98 nm with a spacing of 0.89 nm and SNR of more than 45 dB as the PC orientation is adjusted to balance the loss between the two wavelengths. Both lasers peak at around 1 dBm.

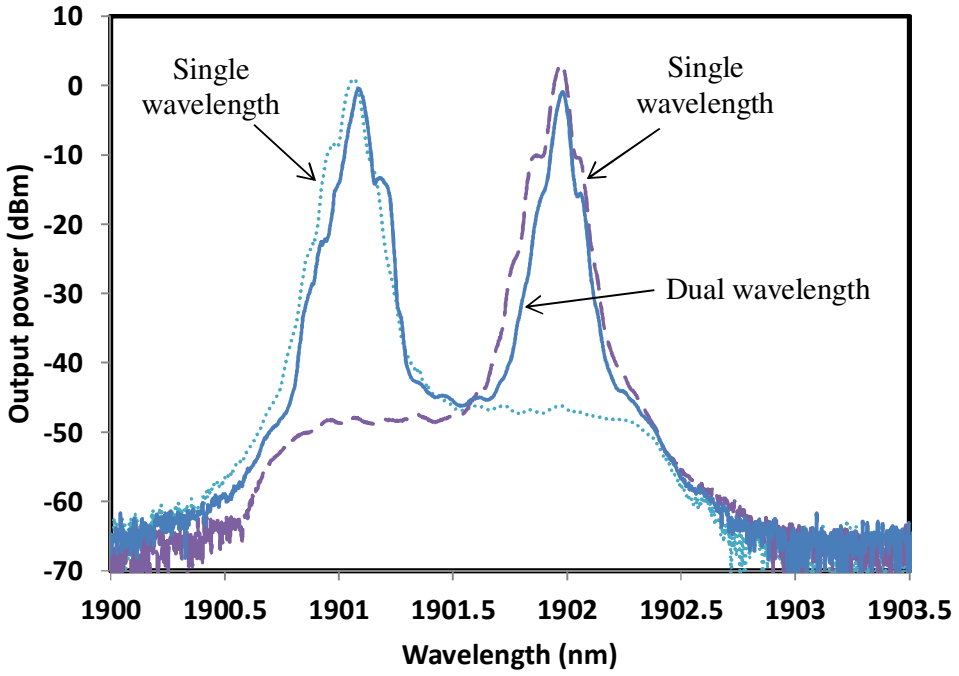

Figure 4.27: Output spectra for the TBFL at both dual-wavelength and single-wavelength operations.

The dual-wavelength laser can also be switched to operate in single-wavelength at either 1901.07 or 1901.98 nm by altering the intra-cavity polarization using the PC. As shown in Figure 4.27, both single-wavelength lines have a 3 dB bandwidth of 0.05

nm with SNR of more than 45 dB. The narrow reflection band of the FBG assures that the wavelength outside the reflection band of FBG will not oscillate. The peak power of the laser is obtained at slightly more than 1 dBm. Figure 4.28 shows the output optical spectrum of the dual-wavelength laser with a scanning time interval of 10 minutes. In our experiment, the dual-wavelength operation can be stable for more than 2 hours if the temperature variation and mechanical vibration are reasonably small (i.e., in a laboratory). As seen in the inset of Figure 4.28, the difference in each laser wavelength is less than 2 dB, which indicates the stability of the output. No other lasing modes are observed in the thulium gain band. As the laser wavelength is only determined by the FBG, the operating wavelength could be tuned by stretching the FBG or other mechanism.

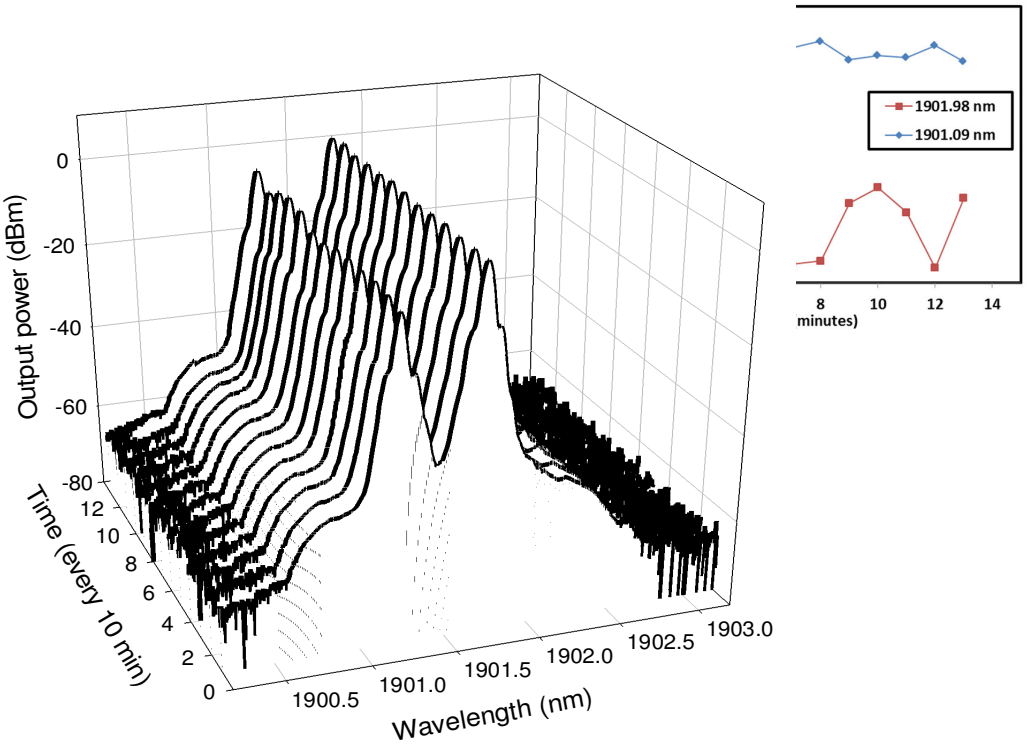

Figure 4.28: The stability graph with 10 minutes period of each interval. Inset shows the peak power fluctuation for dual-wavelength at 1901.09 nm and 1901.98 nm for 13 readings over 13 minutes.

4.10 Summary

An efficient fiber laser operating at 1901.6 nm using a newly fabricated TBF under both 800 nm and 1552 nm pumping schemes have been demonstrated. The TBF was fabricated using MCVD process associated with optimized SD techniques. With 800 nm pumping, the TBFLs at 1901.6 nm are obtained at a noticeably low threshold pump power of 75-92 mW using two fiber Bragg gratings (FBGs) in a Fabry-Perot cavity. The highest efficiency of 42.2% is achieved using a 0.4 m long TB2 fiber with a core dopant concentration (in wt%) of 0.35 Bi_2O_3, 0.9 Tm_2O_3, 3.0 Al_2O_3 and 4.0 GeO_2. Compared to the laser from a commercially available TDF, the proposed laser has a significantly higher efficiency and lower threshold pump power due to the presence of active bismuth ions in the gain medium. The maximum output power of 52.7 mW is achieved at the pump power of 195 mW. With 1552 nm pumping, the TBFL generates 1901.6 nm laser with an efficiency of 32.5% and pump power threshold of 49 mW using 2 m long TB1 in a Fabry-Perot cavity with two FBGs. The maximum output power of 210 mW is achieved at the pump power of 700 mW with the optimum length of 2 m. We also demonstrate an efficient TBFL with dual pumping at 800 nm and 1552 nm. The TBFL operates at 1901.6 nm with a lasing efficiency of 35.06% and pump power threshold of 120 mW using a 1-m-long TB2 in a linear cavity setup. The high efficiency is attributed to the use of additional 1552 nm pump to complement 800 nm pumping. The maximum output power of 256 mW is achieved at the pump power of 820 mW with the optimum length of 1 m. An all-fiber dual-wavelength TBFL operating in the 1900 nm region in the room temperature is also demonstrated using a single FBG in a ring configuration. The addition of active bismuth ions as co-dopant in the gain medium enhances the inhomogeneous broadening effect in the fiber, therefore allows a dual-wavelength oscillation with the assistance of the FBG that has a flat top reflection spectrum. By pumping the gain medium with 1552 nm laser, a dual-wavelength output

lines are obtained at 1901.09 and 1901.98 nm with a spacing of 0.89 nm and an optical SNR of more than 45 dB as the PC orientation is adjusted. The dual wavelength laser can be switched to operate in single-wavelength at either 1901.09 or 1901.98 nm by altering the intracavity polarization using the PC. The benefit of the proposed 1.9 μm laser system is that it operates in the eye-safer wavelengths, where permissible free space transmission levels can be several orders of magnitude greater than 1 μm.

CHAPTER 5

1.9 μm Q-SWITCHED FIBER LASER

5.1 Introduction

Pulsed fiber-based laser systems operating in the 1.9 μm wavelength region is promising for applications such as light detection and ranging (lidar), medicine, and as pumps for mid-IR generation. In the past several years, many studies on passively mode-locked or Q-switched thulium-doped pulse fiber lasers have been reported based on either active or passive methods (El-Sherif *et al.*, 2003b; Jiang *et al.*, 2013; Wang *et al.*, 2011). Compared to the ones derived via active techniques, passively Q-switched fiber lasers possess attractive advantages of compactness, simplicity, and flexibility in design. Furthermore, passively Q-switched fiber laser features flexibility of configuration and do not require additional switching electronics. These lasers have been extensively investigated using different kinds of saturable absorbers (SAs), for instance the well-known technique using semiconductor saturable absorber mirrors (SESAMs) (Kivistö *et al.*, 2008), however, SESAMs are still expensive and complex to be fabricated and consequently only one or two companies can supply 2 μm SESAMs.

More recently, novel nano-materials such as graphene and carbon nanotubes (CNTs) have caught much attention as it was reportedly used in broadband functional SAs (Hasan *et al.*, 2009; Sun *et al.*, 2010a). Both graphene and CNTs has their unique characteristic that brings advantages to the user as SAs. Graphene is a two-dimensional crystal of carbon atoms arranged in a honeycomb lattice. Isolated graphene nanosheets were firstly produced by mechanical exfoliation from bulk graphite in 2004 (Novoselov *et al.*, 2004). Graphene has outstanding linear and nonlinear optical properties, such as low threshold level of saturable absorption (~0.7 MW cm^{-2}), ultrafast recovery time

(200 fs) and an ultrabroad wavelength independent saturable absorption range, which covers the wavelength range from the visible to mid infrared (Bao *et al.*, 2009; Cunning *et al.*, 2011). This is due to the gapless linear dispersion of Dirac electron in graphene which allows a broadband operation.

Apart from that, the utilization of CNTs in high performance electronic and photonic devices due to their excellent electrical and optical properties have gathered tremendous attention in recent years (Cao *et al.*, 2008; Halder *et al.*, 2012). Their successful implementation in a wide range of photonic devices, such as saturable absorbers (Hasan *et al.*, 2009), ultra-fast optical switches (Song *et al.*, 2006), and wavelength converters (Chow *et al.*, 2010) are particularly due to their unique nonlinear optical properties.

In this chapter, Q-switched fiber lasers operating in the 1900 nm region are demonstrated using a simple and low cost graphene and multi-walled carbon nanotubes (MWCNTs) as saturable absorber. Both graphene and MWCNTs are embedded in polymer composite film before it is integrated into a ring laser cavity by sandwiching it between two fiber connectors. The novelty of this work lies in the use of a new type of SAs preparation method in conjunction with an all-fiber ring cavity configuration due to the compatibility of silica host with standard optical components. Compared to the other 2 μm Q-switched fiber laser, the proposed laser configuration is simpler and more compact.

5.2 Q-switched Thulium-doped fiber laser (TDFL) using a graphene based SA

This section discusses about the generation of Q-switched fiber laser using a commercial Thulium-doped fiber (TDF) as a gain medium. As explained in the previous chapter, the TDF used has a core and cladding diameters of 9 µm and 125 µm respectively, with a loss of less than 0.2 dB/km at 1900 nm. The Tm ion absorptions are 27 dB/m at 793 nm. The performance of the Q-switched TDFL is investigated for two different pumping schemes; 800 nm and 1552 nm.

5.2.1 Fabrication and characterization of graphene film

In constructing a graphene based SA, the first step is to produce graphene flakes using electrochemical exfoliation process**.** In this process, a constant voltage difference of 20 V was applied to two graphite rod electrodes, which are placed 1 cm apart in an electrolysis cell filled with electrolyte (1% Sodium dodecyl sulfate (SDS) in deionized water) as shown in Figure 5.1. Hydroxyl and oxygen radicals are generated due to electrolysis of the water at the electrode during the electrochemical process. Then oxygen radicals started to corrode the graphite anode. This was followed by the intercalation of anionic surfactant and finally graphene sheets are created in the solution. In our work, black sediments (graphene) started to peel off from the anode after several minutes. The exfoliation process was continued for 2 hours to obtain a stable graphene suspension in the SDS solution. The stable graphene suspension was centrifuged at 3000 rpm for 30 minutes to remove large agglomerates. Then, the supernatant portion of the suspension was decanted. The concentration of the centrifuged graphene was estimated from the weight of the suspension used. To fabricate the composite, 1 g of polyethylene oxide (PEO) (Mw = 1 000 000 $gmol^{-1}$) was dissolved in 120 ml of deionized water. The graphene solution obtained from the electrochemical exfoliation was then mixed with a PEO solution at ratios of 5:5 of

graphene:PEO in ml respectively. The solution was dried in petri dishes at 56^{o}C to obtain free standing films with 50 µm thickness.

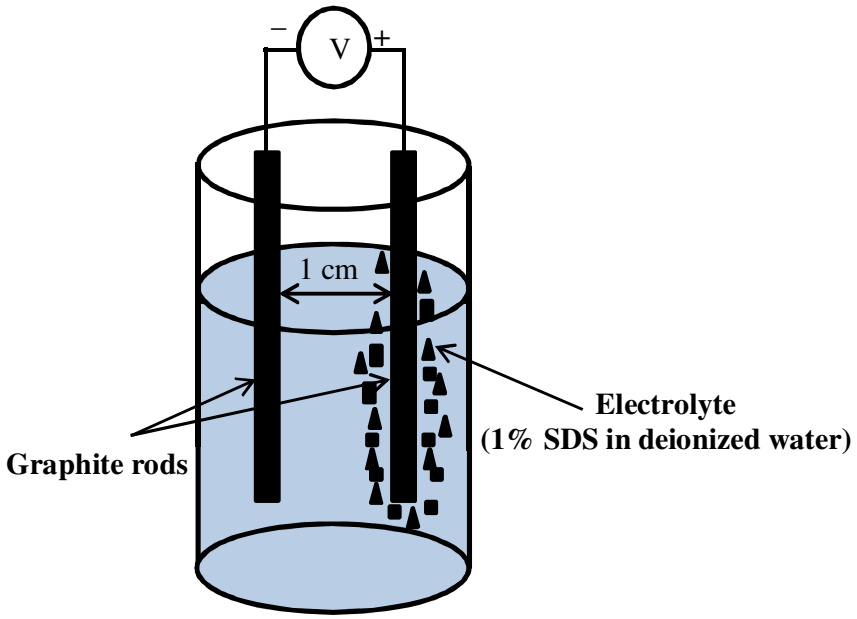

Figure 5.1: Electrochemical exfoliation of the graphene.

Raman spectroscopy was performed to confirm the presence of graphene layer in the fabricated thin film using laser excitation at 532 nm (2.33 eV) with an exposure time of 10 seconds. The detector was a charge-coupled device (CCD) camera. Figure 5.2 illustrates the measured Raman spectrum from the graphene film. It shows three prominent peaks, which are located at approximately 1351 cm^{-1}, 1617 cm^{-1} and 2911 cm^{-1}, generally known as the D, G and 2D band, respectively. G-band contributes to an E_{2g} mode of graphite and is related to the in-plane vibration of sp^2-bonded carbon atoms, while D-band is associated with the vibrations of carbon atoms with sp^3 electronic configuration of disordered graphite. The intensity ratio of the D and G-band of the graphene sheet is about 1.2, indicating defects in the graphene samples. However, the amount of structural defects is not large since the D-peak is not very broad (Sun *et al.*, 2010a). The intensity ratio between G and 2-D peak can be used to determine the

graphene layer. It was reported that single-layer graphene has a low intensity ratio, usually lower than 0.5 while multi-layer graphene shows higher intensity ratio (≥1) (Reina *et al.*, 2008). The shape of the 2-D peak can also be used to estimate the number of graphene layers. As the graphene layer increases, the full-width half maximum (FWHM) of the 2-D peak follows (Ferrari *et al.*, 2006). The Raman spectroscopy reveals a broad 2-D peak, which indicates the graphene has a multi-layer structure. As shown in Figure 5.2, the FWHM for G and 2-D peaks are obtained at 39 and 67 cm^{-1}, respectively. From the intensity ratio of G and 2-D peaks and their FWHM, it can be inferred that the number of graphene layers is more than four (Graf *et al.*, 2007). Figure 5.3 shows the loss spectrum of the graphene saturable absorber (GSA) at 1900 nm region. The insertion loss of the SA is estimated to be around 2 dB at 1900 nm. The weak 2-D peak is due to the multi-layered graphene, which significantly decreases the relative intensity (Ferrari *et al.*, 2006).

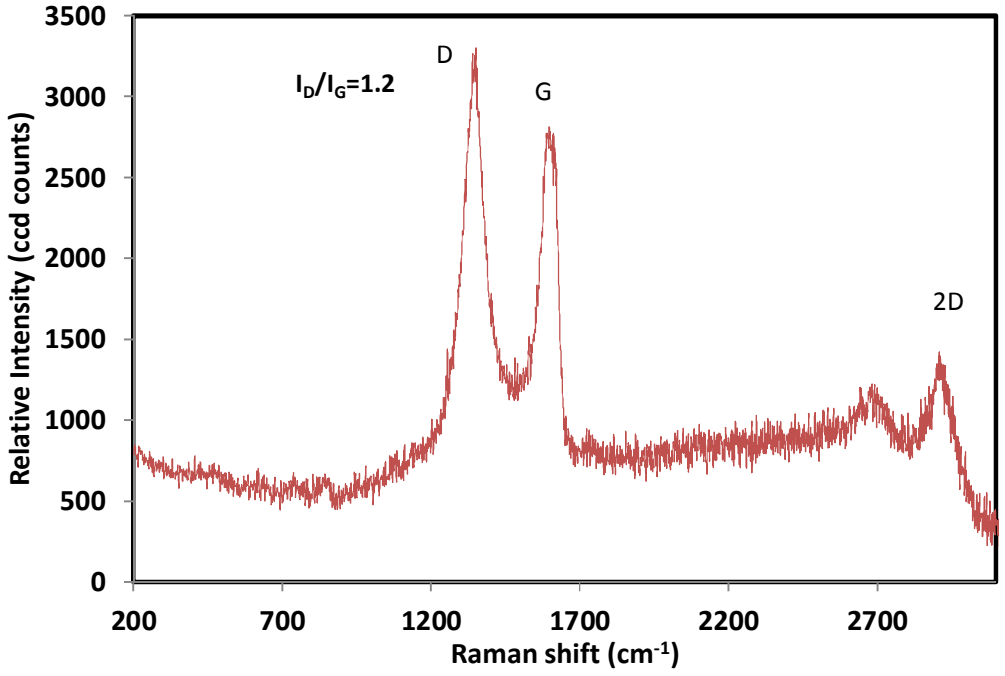

Figure 5.2: Raman spectrum of the graphene film.

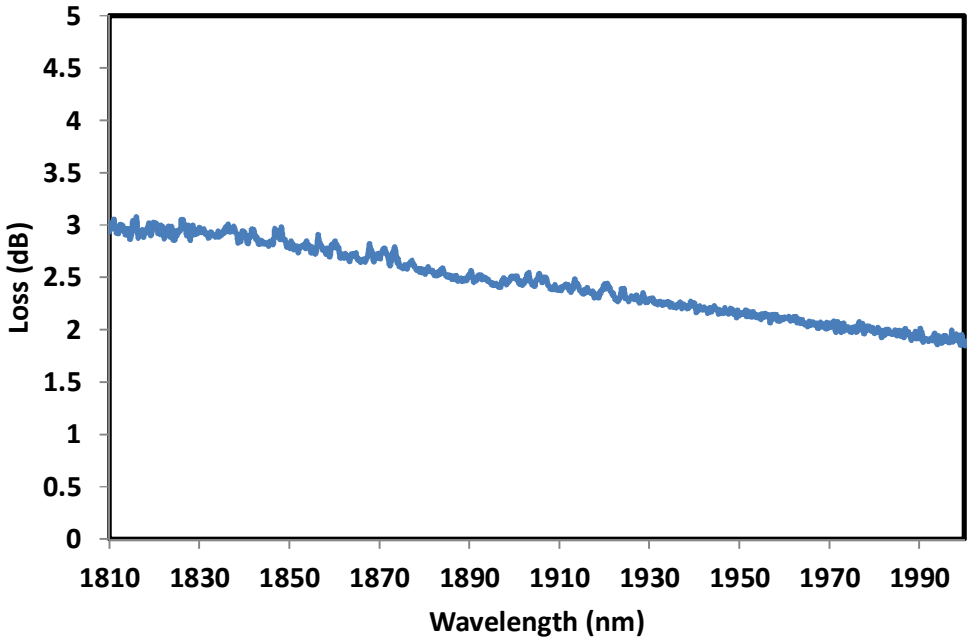

Figure 5.3: The loss spectrum of the graphene saturable absorber at 1900 nm region.

5.2.2 Laser configuration

The experimental setup of the proposed Q-switched TDFL is shown in Figure 5.4, which consists of a 2 m long TDF, a 800/2000 nm wavelength division multiplexer (WDM), a graphene film based SA, and 10 dB output coupler in a ring configuration. The SA is fabricated by cutting a small part of the prepared film (2×2 mm^2) and sandwiching it between two FC/PC fiber connectors, after depositing index-matching gel onto the fiber ends. The TDF is pumped by an 800 nm laser diode via the WDM. The output of the laser is tapped from the cavity through a 10 % port of the 10 dB coupler. The optical spectrum analyser (OSA, Yokogawa, AQ6375) is used for the spectral analysis of the Q-switched TDFL with a spectral resolution of 0.05 nm whereas the oscilloscope (OSC, Tektronix, TDS 3052C) is used to observe the output pulse train of the Q-switched operation via a photo-detector (EOT, ET-5010-F). The total cavity length of the ring resonator is measured to be around 8.7 m.

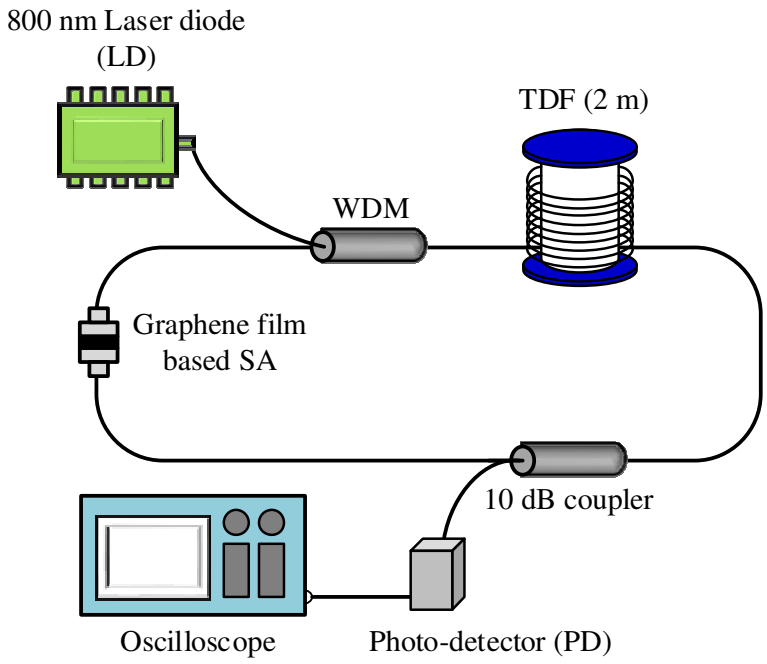

Figure 5.4: Schematic configuration of the Q-switched TDFL.

5.2.3 Performance of the graphene based Q-switched TDFL

Stable and self-starting Q-switching operation is obtained just by adjusting the pump power over the threshold of 186 mW. There is no lasing below the threshold pump power. Figure 5.5 shows the output spectrum of the Q-switched laser at the pump power of 186 mW. As seen, the laser operates at a wavelength of 1900 nm with FWHM of around 2.6 nm and optical signal to noise ratio (OSNR) of more than 30 dB. The optical spectrum of Figure 5.5 is noisy due to the OSA measurement which uses the high resolution setting. Without the SA, the TDFL generates a continuous wave (CW) laser as the pump power is set above the threshold power of 100.5 mW. Figure 5.6 shows the output spectrum of the CW laser at the pump power of 100.5 mW, which operates at 1929 nm. The spectrum contains other subsidiary peak due to the spurious back reflection in the cavity. The operating wavelength shifts to a shorter wavelength by the incorporation of SA due to the insertion loss of the SA, which increases the cavity loss. Therefore, the oscillating laser shifts toward the peak absorption wavelength of the

thulium fiber, which is near to 1900 nm to acquire more gain so that it can compensate the additional cavity loss. Spectral broadening is also observed with the graphene-based SA due to self-phase modulation (SPM) and cross-phase modulation (XPM) effects in the ring cavity.

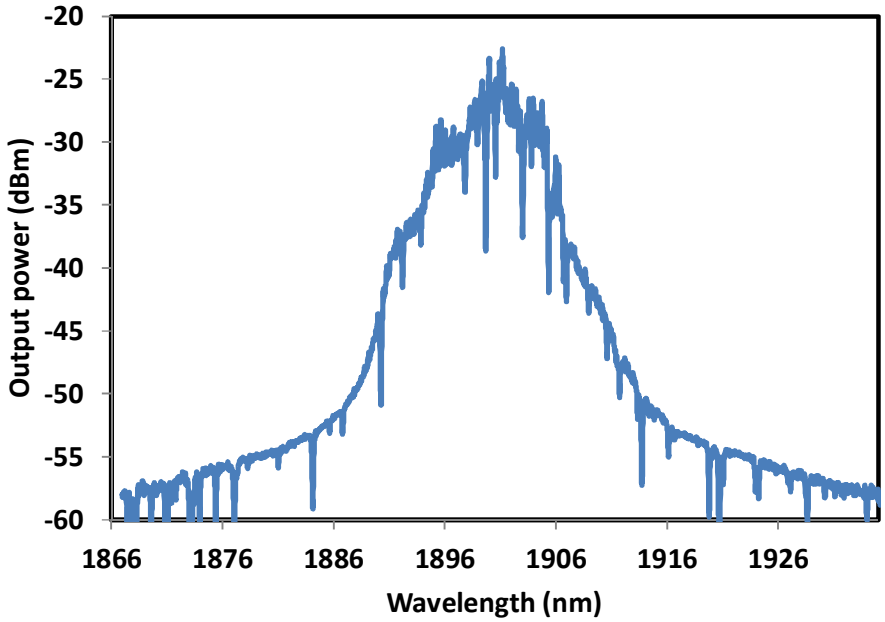

Figure 5.5: Output spectrum from the Q-switched TDFL at pump power of 186 mW.

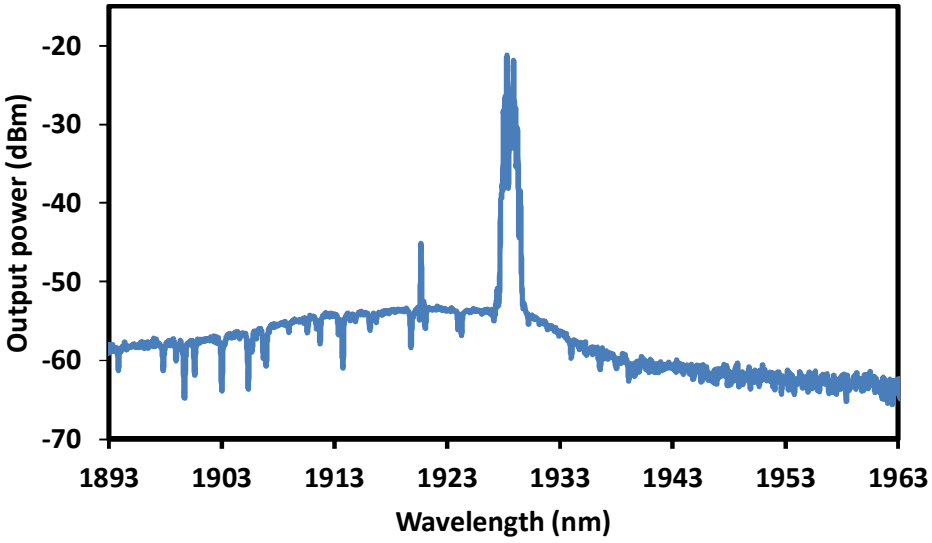

Figure 5.6: The output spectrum of the CW TDFL, which is obtained without the SA at pump power of 100.5 mW.

Figure 5.7 shows the oscilloscope traces of the Q-switched pulse train at pump power of 202 mW. There is no distinct amplitude modulation in each Q-switched envelop spectrum, which indicates that the self-mode locking effect on the Q-switching is weak (Zhou *et al.*, 2010b). At 186 mW pump power, a stable passively Q-switching operation starts to occur with an average output power of 0.5 mW and a repetition rate of 7.5 kHz. The pulse energy is calculated to be around 66.6 nJ at this pump power. The pulse energy could be improved by reducing the insertion loss of the GSA and optimizing the laser cavity. Figure 5.8 shows the typical oscilloscope trace of the pulse envelop at the pump power of 202 mW. As seen in the figure, the FWHM or pulse width is approximately 17.7 μs.

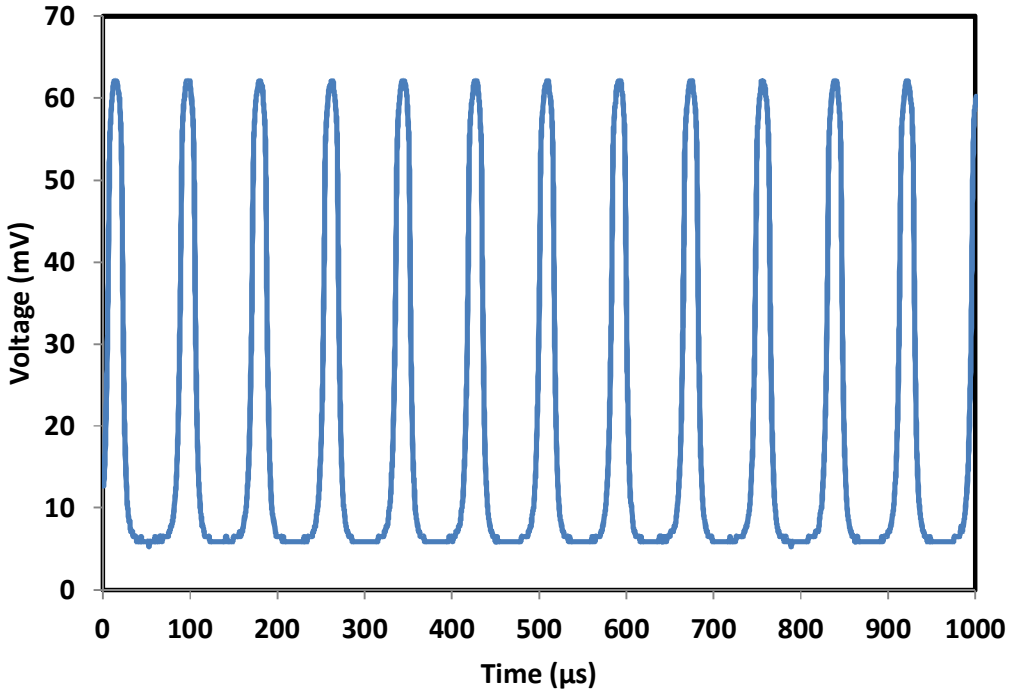

Figure 5.7: The pulse train for the proposed TDFL with graphene based SA at 202 mW pump power with the repetition rate of 12.1 kHz.

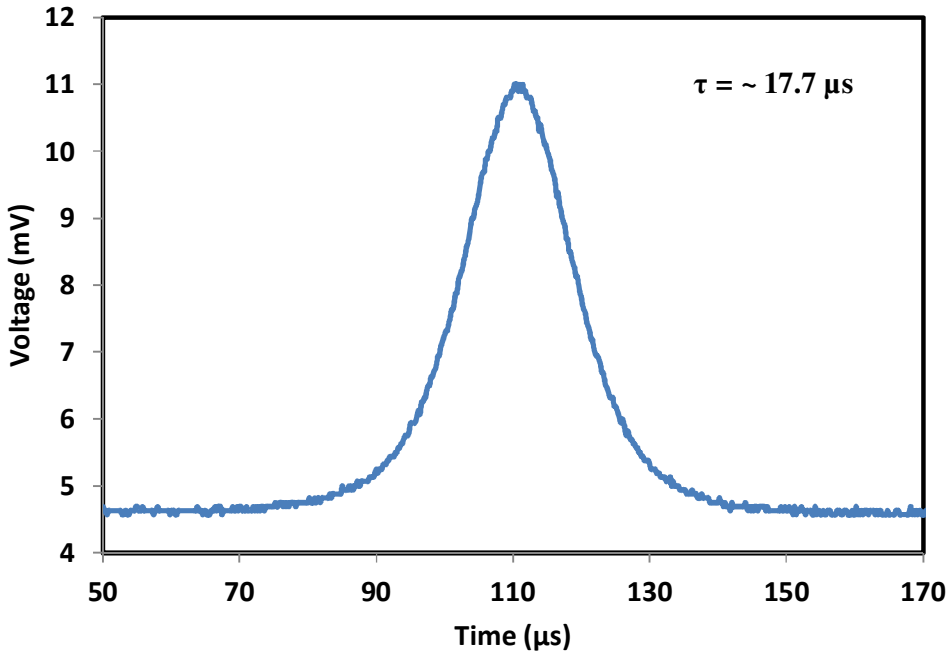

Figure 5.8: Enlarge pulse width spectrum.

Figure 5.9 shows the repetition rate and the pulse width versus the pump power. The repetition rate of the graphene based Q-switched TDFL has a monotonically increasing, near-linear relationship with the pump power level, which is consistent with the result of EDFL for 1552 nm operation (Popa *et al.*, 2011). When the pump power is tuned from 186 to 207 mW, the pulse train repetition rate varies from 7.5 to 13.1 kHz. On the other hand, the pulse width drops from 19.7 µs to 16.9 µs as the pump power increases from 186 to 194 mW. As the pump power is further increased, the pulse width starts to increase instead of reducing as shown in Figure 5.9. The V-shape trend of the resulting pulse width is similar to the one reported by (Jiang *et al.*, 2013; Lu *et al.*, 2013; Wang *et al.*, 2012c), where ~793 nm laser diode was used to pump the TDF. However, the trend was not observed by (Wang *et al.*, 2012a), where a 1560 nm laser diode was used as the pump instead. When a TDF was pumped by 800 nm source, the Tm^{3+} ions were excited to the $^3H_4$ level. When the ions occupy the upper lasing level, $^3F_4$, they experience a non-radiative transition where phonon is emitted. The phonon

generates heat in the fiber system. As the pump power increases, more Tm^{3+} ions occupy the $^3H_4$ level and increase the non-radiative decay rate of the Tm^{3+} ions. Hence, more heat is introduced in the cavity where the GSA ends up absorbing the accumulated heat. This will energize some electrons in the graphene's valence band to move up to the conduction band from the strong internal thermal motion. As less electrons in the valence band are available for photon absorption, the initial transmittance of the GSA becomes greater as the pump power or absorbed heat increases (Jiang *et al.*, 2013). Thus graphene's efficiency as a saturable absorber is greatly reduced such that the pulse width begins to increase again after the saturation of the GSA. The use of metal connector for the construction of the GSA further increases the heat accumulation since metal contact limits thermal dissipation from the graphene (Koh *et al.*, 2010).

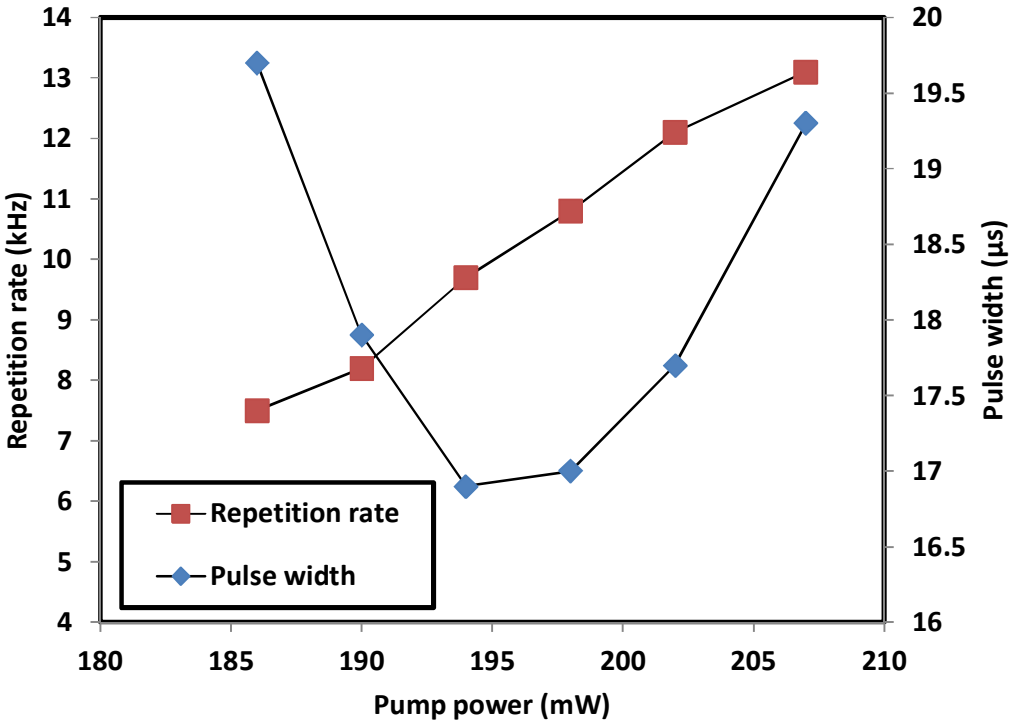

Figure 5.9: Repetition rate and pulse width as a function of pump power.

Figure 5.10 shows the average output power and pulse energy of the Q-switched TDFL as a function of pump power. Inset of Figure 5.10 shows the CW laser efficiency

of the TDFL. Both output power and pulse energy increase as the pump power increases. The output power efficiency was 2.44%, which is a bit low compared to the efficiency of the CW laser which is 3.77%. The lower efficiency is attributed to the introduction of the SA inside the cavity which incurs a loss. Another possible reason for the low efficiency is probably due to the pump source that operates at slightly off the peak absorption wavelength of 793 nm. The operating pump emission spectrum was observed at 800 nm instead of 793 nm, thus the TDF fiber's absorption was only around 13 dB/m at 800 nm instead of 27 dB/m at 793 nm. The performance of the laser in terms of threshold and efficiency is expected to improve significantly if the pump operated at the optimum wavelength of 793 nm. The highest pulse energy obtained is 77.2 nJ at pump power of 207 mW. Figure 5.10 shows the Q-switched laser output in frequency domain, which was obtained by using the Radio Frequency (RF) Spectrum Analyzer. The measured RF spectrum shows a repetition rate of 10.8 kHz. The peak-to-background ratio, which is obtained from the intensity ratio of the fundamental peak to the pedestal extinction, is around 31 dB, which indicates the stability of the laser.

In the next section, the use of a 1552 nm pump source will be examined since the photon will only excite to the $^3F_4$ laser level. Therefore, the system will not experience non-radiative decay and lattice vibration. The performance of the Q-switched laser is expected to improve as less accumulated heat will be absorbed by the GSA as compared to the condition with ~800 nm pump wavelength.

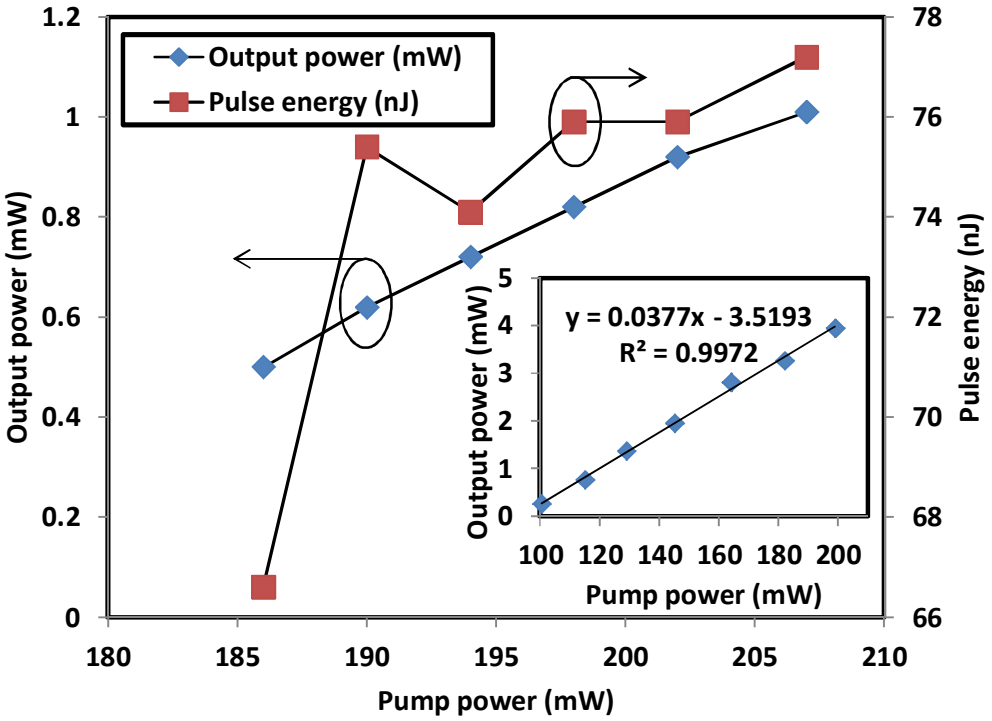

Figure 5.10: Output power and pulse energy versus pump power. Inset shows the efficiency of the CW TDFL.

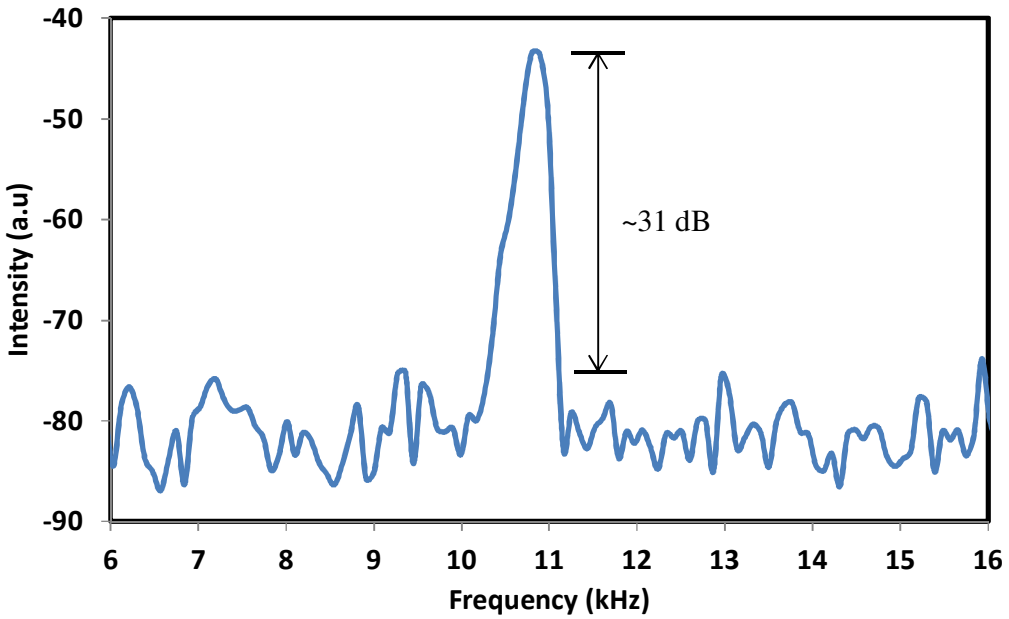

Figure 5.11: RF spectrum of the Q-switched TDFL at 10.8 kHz repetition rate.

5.3 Graphene based Q-switched TDFL using a 1552 nm pumping

Figure 5.12 shows the experimental setup of the proposed Q-switched TDFL using 1552 nm pumping excitation. The same GSA is used as a passive Q-switcher. The experiment setup comprises of a 4 m long TDF, which was pumped by a 1552 nm laser via a 1550/1900 nm WDM, an isolator, the graphene film based SA, and 10 dB output coupler in a ring configuration. An isolator is used to ensure a unidirectional operation of the laser. The laser output is obtained via a 10 dB optical coupler located after the SA, which channels out about 10% of the oscillating light from the ring cavity. The total cavity length of the ring resonator is measured to be around 13.6 m.

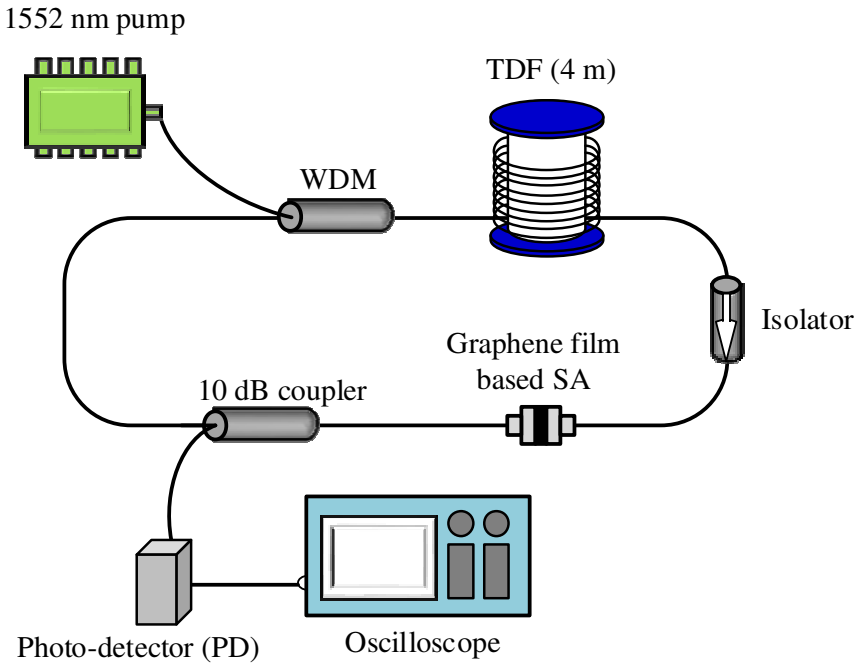

Figure 5.12: Experimental setup of the graphene based Q-switched TDFL using a 1552 nm pumping scheme.

Figure 5.13 shows the output spectrum of the Q-switched laser analyzed by an OSA with a resolution of 0.05 nm. Inset of Figure 5.13 shows the CW laser spectrum at the threshold pump power of 416 mW, which operates at 1849.5 nm. Once the SA is inserted into the laser cavity, the laser starts to operate in a passive Q-switching operation as the pump power is adjusted to 513 mW. As seen in Figure 5.13, the Q-switched laser operates at a wavelength of 1844.1 nm with the FWHM of 0.24 nm and signal to noise ratio of about 29 dB. As in 800 nm pumping, the threshold value is slightly higher and the operating wavelength shifts to a shorter wavelength by the incorporation of the SA.

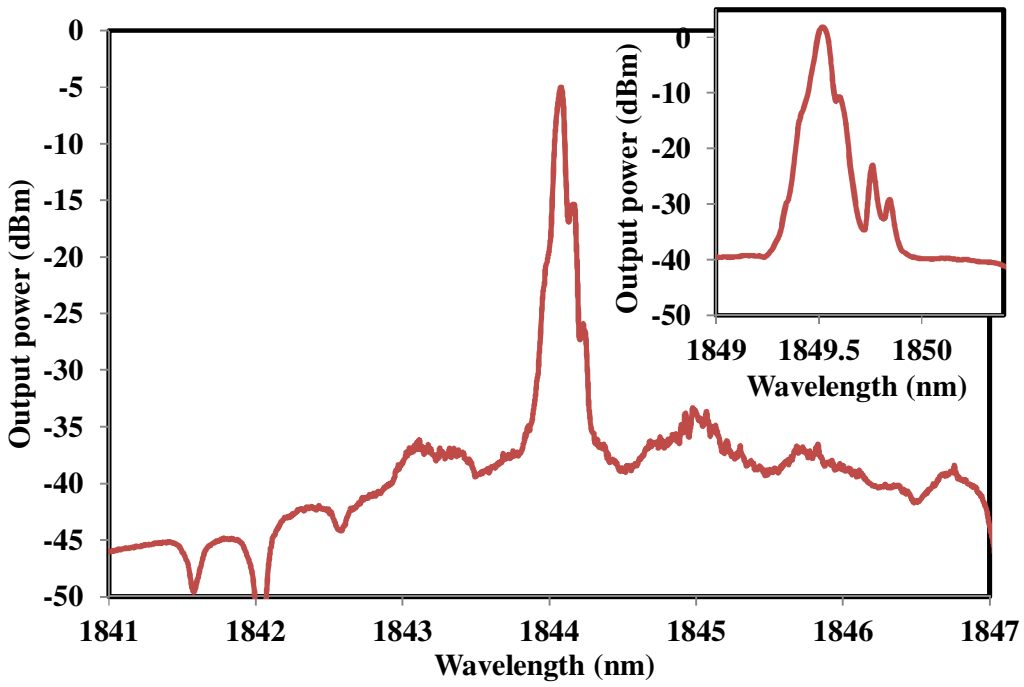

Figure 5.13: Output spectrum of the generated Q-switched TDFL. Inset shows the output spectrum of the CW laser.

Figure 5.14 exhibits the Q-switched pulse train when the pump power is fixed at the threshold value of 513 mW. A stable passive Q-switching operation starts to occur with an average output power of 0.61 mW and repetition rate of 6.73 kHz. The pulse energy is calculated to be around 90.64 nJ at this pump power. Figure 5.15 shows the enlarged oscilloscope trace of the pulse train at the pump power of 513 mW with 11.41 μs pulse width.

Figure 5.16 shows the repetition rate and pulse width versus the pump power. Contrary to a mode-locked fiber laser, where the repetition rate is dependent on cavity length, the repetition rate in Q-switched fiber laser varies with pump power (Liu *et al.*, 2013). As the pump power increases, more gain is provided to saturate the SA. Since pulse generation relies on saturation, the repetition rate increases with the pump power (Spühler *et al.*, 1999) as shown in Figure 5.16. When the pump power is tuned from 513 to 539 mW, the pulse train repetition rate varies from 6.73 to 24.16 kHz. The pulse width reduces from 11.41 to 8.17 μs within the same pump power range. Further reduction in pulse width is expected when the pump power increases to the point allowable by the damage threshold of the GSA. The V-shape trend of the pulse width is not observed in this experiment where 1552 nm laser diode was used to pump the TDF. The use of 1552 nm as a pump source allows the photon to excite into the $^3F_4$ laser level instead of $^3H_4$. The performance of the Q-switched laser has improved as expected since less accumulated heat will be absorbed by the graphene based SA compared to the condition observed with the 800 nm pump wavelength.

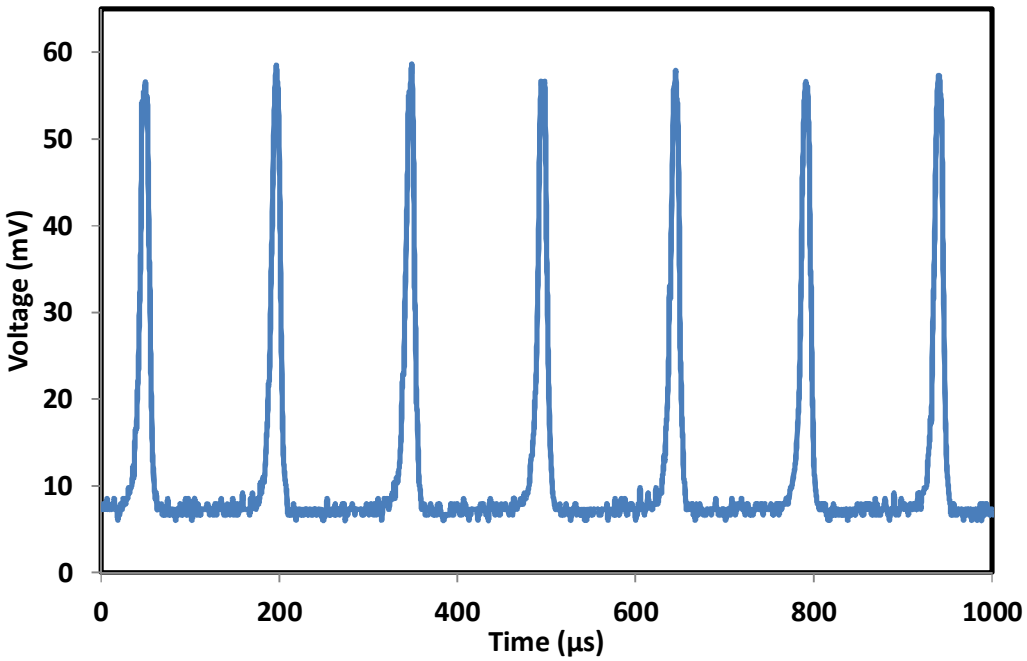

Figure 5.14: The pulse train for the proposed TDFL with multi-layer graphene film based SA at threshold with the repetition rate of 6.73 kHz.

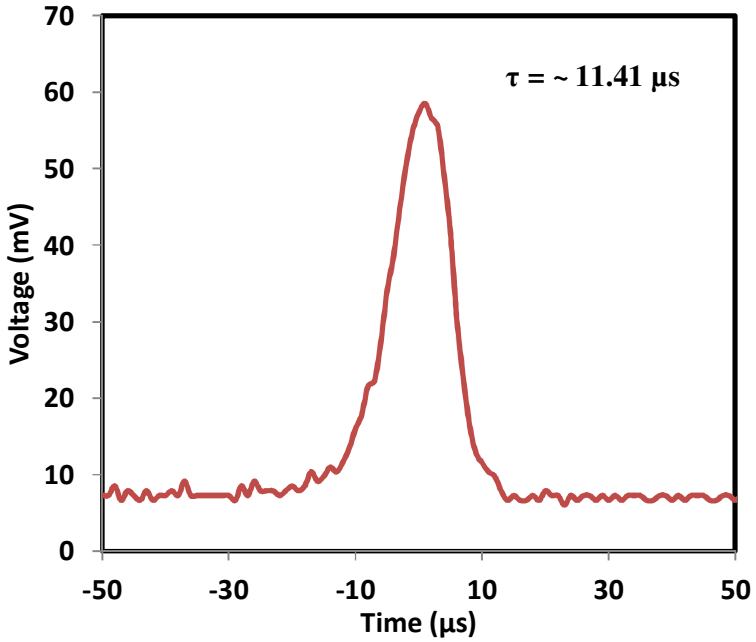

Figure 5.15: Enlarged pulse envelop with pulse width of 11.41 µs.

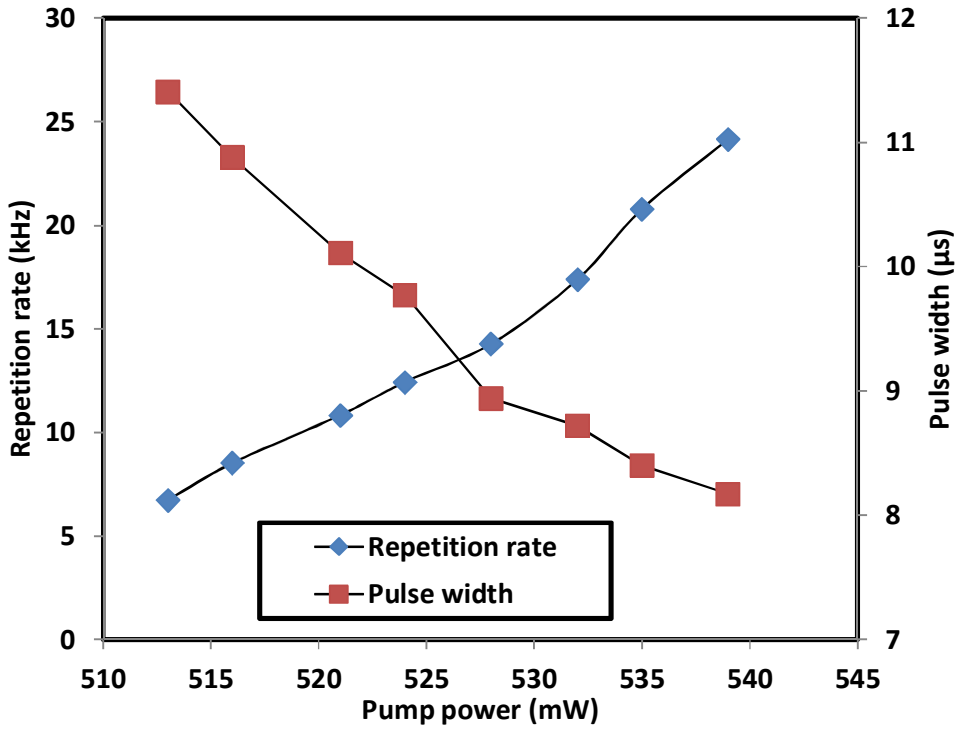

Figure 5.16: Repetition rate and pulse energy as a function of pump power.

Figure 5.17 shows the average output power and pulse energy of the Q-switched TDFL as a function of pump power. The output power increases from 0.61 to 1.01 mW and the pulse energy reduces from 90.64 to 41.8 nJ as the pump power is increased from 513 mW to 539 mW. These results indicate that GSA has a big potential for superior Q-switching compared to conventional light absorbing components when carefully employed in an appropriate laser system. The fabrication of the GSA is also simple and thus the cost of the laser should be low. The simple and low cost laser is suitable for various applications.

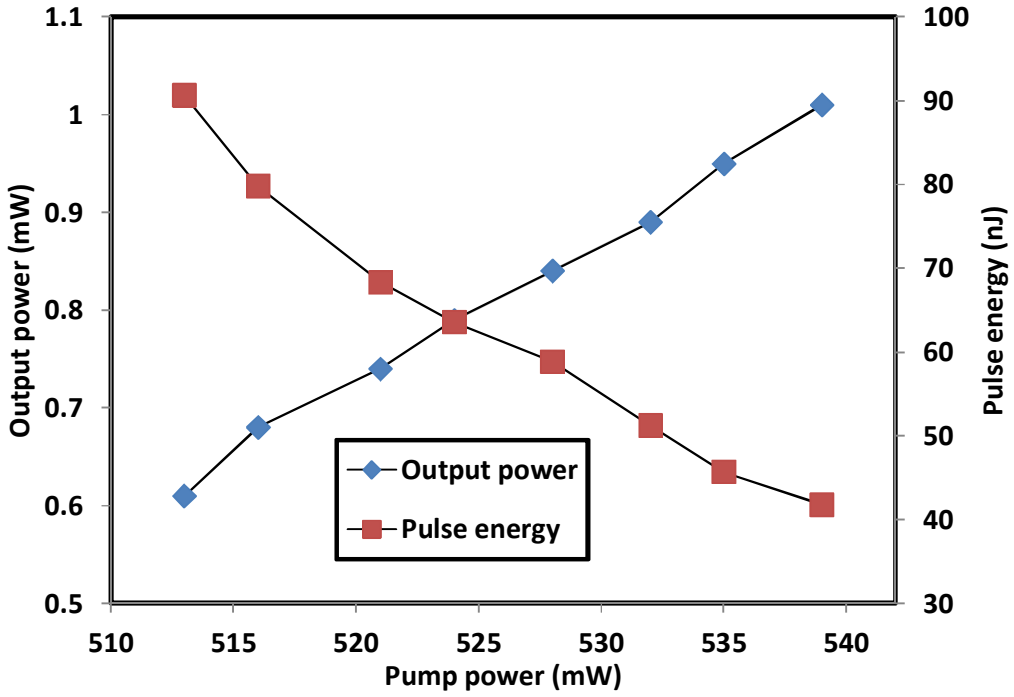

Figure 5.17: Output power and pulse energy versus pump power.

5.4 Multi-walled carbon nanotubes (MWCNTs) based SA for Q-switching in the 2 micron region

Carbon nanotubes (CNTs) have gained great attention due to their excellent electrical and optical properties, which enable them to be used in various electronic and photonic devices (El-Sherif *et al.*, 2003b). To date, many works have been reported on the use of CNT-based saturable absorbers for the generation of Q-switched or mode-locked lasers. Most of these works focus on 1550 nm and 1060 nm applications using an erbium or ytterbium doped fiber gain medium, respectively (Hasan *et al.*, 2009; Kieu *et al.*, 2009).

Recently, a new member of the carbon nanotubes family, multi-walled carbon nanotubes (MWCNTs) (Costa *et al.*, 2008; Dresselhaus *et al.*, 2005) have also attracted many attentions for nonlinear optics applications. Compared with SWCNTs, the MWCNTs have a higher mechanical strength, better thermal stability as well as the

ability to absorb more photons per nanotube due to its higher mass density of the multi-walls (Banhart, 1999; Ramadurai *et al.*, 2008). To date, there are only a few reported works on applications of MWCNTs material as a saturable absorber. Recently, (Lin *et al.*, 2013) employs MWCNTs based saturable absorber for mode locking of a Nd:YVO_4 laser.

In this section, an all-fiber Q-switched TDFL is demonstrated using a simple and low cost newly developed MWCNTs based SA as the Q-switcher. The saturable absorber employs MWCNTs which is embedded in polyvinyl alcohol (PVA) film. A stable Q-switched TDFL is generated using an 800 nm pump power. The performance of the TDFL is also investigated with 1552 nm pumping.

5.4.1 Fabrication and Raman Characterisation of MWCNT-PVA Film

The SA was fabricated using MWCNTs powder with a diameter of 10-20 nm and the length distribution of 1-2 μm as a raw material. The MWCNTs was functionalized so that it can be dissolved in water. The functionalizer solution was prepared by disolving 4 g of sodium dodecyl sulphate (SDS) in 400 ml deionized water. 250 mg MWCNT was added to the solution and the homogenous dispersion of MWCNTs was achieved after the mixed solution was sonicated for 60 minutes at 50 W. The solution was then centrifuged at 1000 rpm to remove large particles of undispersed MWCNTs to obtain dispersed suspension that is stable for weeks. MWCNTs-PVA composite was prepared by adding the dispersed MWCNTs suspension into a PVA solution by three to two ratio. The PVA solution was prepared by dissolving 1 g of PVA ($M_w = 89\times10^3$ g/mol) in 120 ml of deionized water. The homogeneous MWCNTs-PVA composite was obtained by sonification process for more than one hour. The MWCNT-PVA composite was casted onto a glass petri dish and left to dry at room temperature for about one week to produce a thin film with thickness around 50 μm.

Figure 5.18 shows the Raman spectrum which was performed on the MWCNTs-PVA film. The Raman spectrum bears a lot of similarity to the one for graphene, which is not too surprising as it is simply a rolled up sheet of graphene. We can see well defined G (1580 cm^{-1}) and D (1350 cm^{-1}) bands in Figure 5.18 as normally observed in the spectra of graphene and graphite. The G-band originates from in-plane tangential stretching of the carbon-carbon bonds in graphene sheet. The existence of a prominent D band in the Raman spectrum indicates that the carbon nanotubes are a multi-walled type, which has multi-layer configuration and disordered structure. The D-band originates from a hybridized vibrational mode associated with CNT edges and it indicates the presence of some disorder to its structure. The D'-band which is a weak shoulder of the G-band is also observed at 1613 cm^{-1} due to the double resonance feature induced by disorder and defect. The absence of Radial Breathing Mode (RBM) at ~250 cm^{-1} band in the Raman spectrum confirms the multi-walled type of CNT used in our experiment (Dresselhaus *et al.*, 2005). This is due to the diameter of the wrapped CNT which consist of too many walls or the inner wall diameter is too big (Zdrojek *et al.*, 2004). In addition, other distinguishable features like a G' (2705 cm^{-1}) band which is attributed to the overtone (second-order) of the D-band, D+G band (2920 cm^{-1}), a small peak at 854 cm^{-1} and Si were also observed. Figure 5.19 shows the transmission spectrum of the fabricated MWCNTs-PVA film. As shown in the figure, the transmission is featureless in the near infra-red region, showing the broadband property of our saturable absorber. The transmittance is observed to be about 50.8% at 1900 nm region.

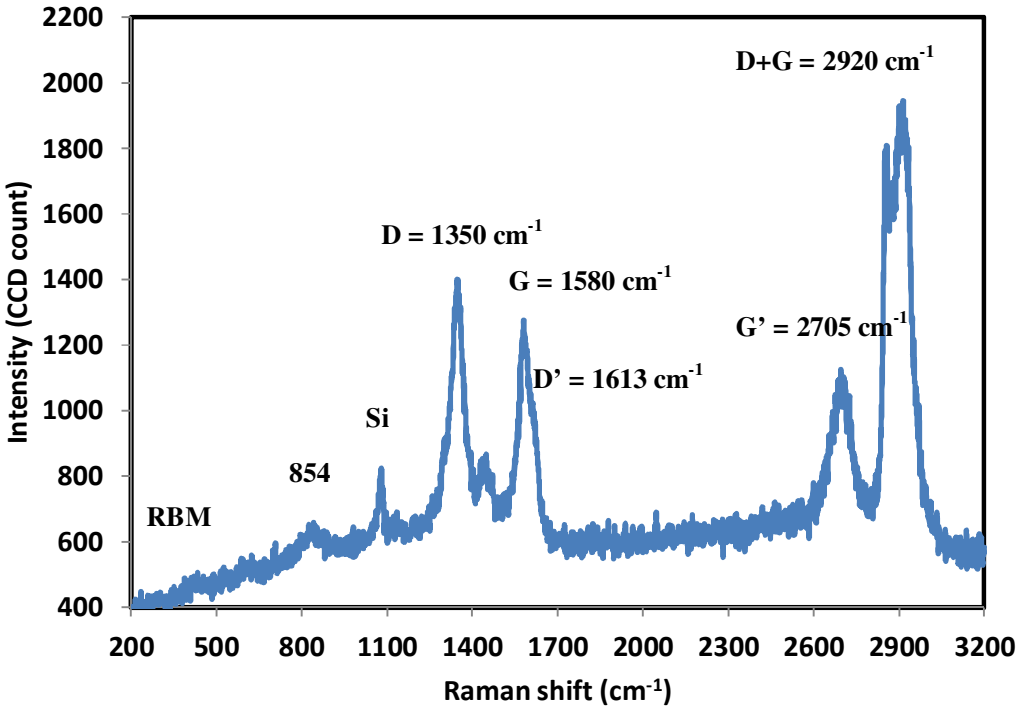

Figure 5.18: Raman spectrum obtained from the MWCNTs-PVA film.

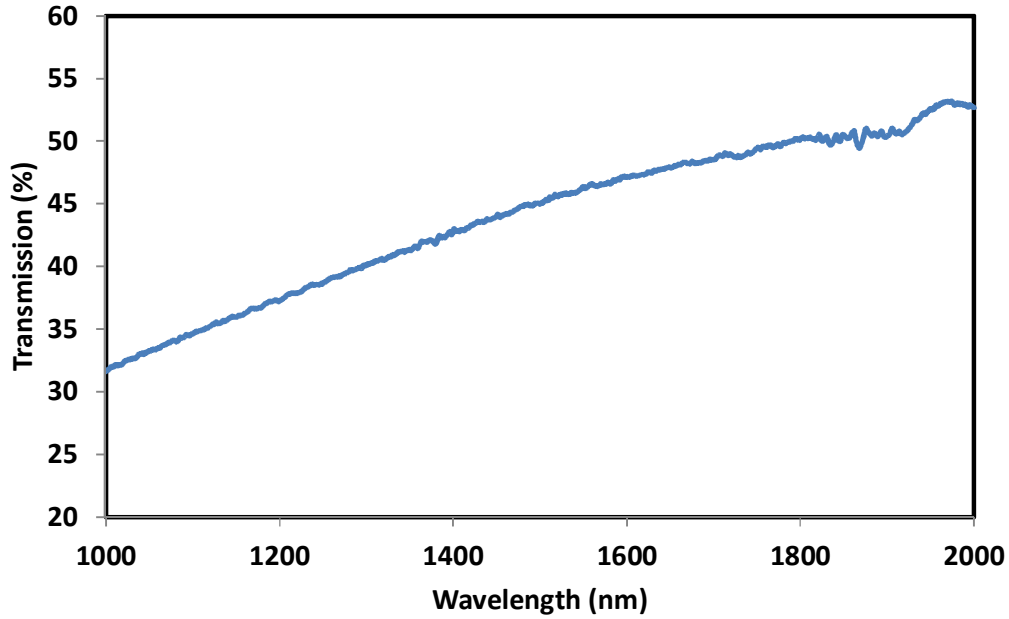

Figure 5.19: Transmission spectrum of the MWCNTs-PVA film.

5.4.2 Configuration of the laser

The schematic of the proposed Q-switched TDFL is shown in Figure 5.20. It was constructed using a simple ring cavity, in which a 2 m long TDF was used for the active gain medium and the fabricated MWCNT-based SA was used as a Q-switcher. Figures 5.21 (a) and (b) show the image of the film attached onto a fiber ferrule and the constructed SA, respectively. The insertion loss of the SA is measured to be around 3.3 dB at 1900 nm. The TDF was pumped by an 800 nm laser diode via an 800/2000 nm WDM. The temporal characteristics of the laser output were monitored using a combination of a photo-detector and a real time oscilloscope. The optical spectrum was measured using an OSA. The cavity length is approximately 7.6 m. The performance of the Q-switched TDFL is also investigated for 1552 nm pumping. In the experiment, 800 nm laser diode and an 800/2000 nm WDM are replaced with 1552 nm pump and 1550/1900 nm WDM while the TDF length is increased to 5 m for optimum laser performance.

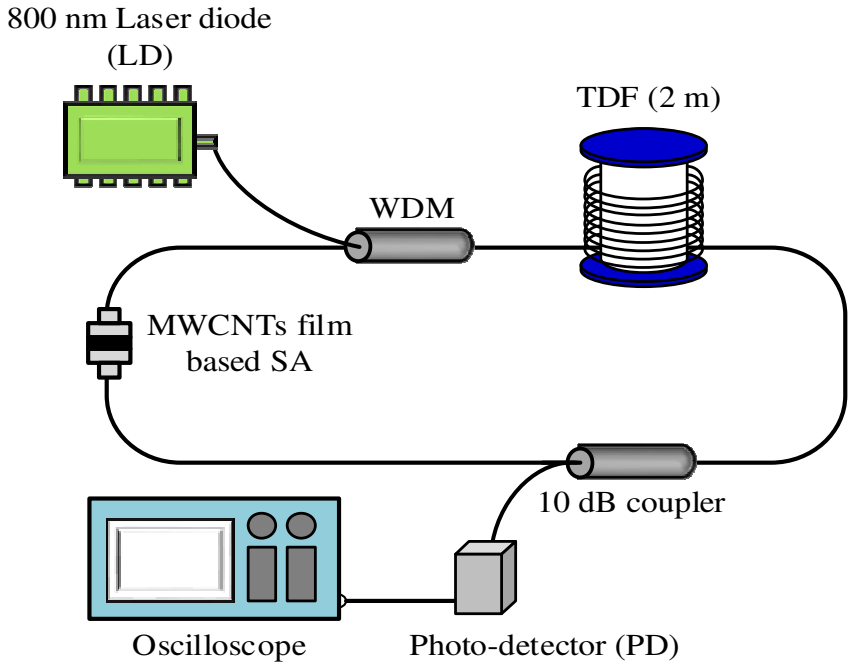

Figure 5.20: Schematic configuration of the Q-switched TDFL with 800 nm pumping.

Figure 5.21: MWCNTs-PVA film based saturable absorber (a) the attachment of the film on the fiber ferrule (b) integration of MWCNTs composite film in the laser cavity.

5.4.3 Q-switching performance with 800 nm pumping

Figure 5.22 shows the output power of both Q-switched and CW lasers against the input pump power, which are obtained with and without the SA, respectively. A CW laser operates with an efficiency of 3.77% and threshold pump power of 133.1 mW. The efficiency is relatively low since the components used have a considerably high insertion loss at 1900 nm region. As the SA is inserted into the ring cavity, a stable and self-starting Q-switching operation is obtained by adjusting the pump power over a threshold of 187.3 mW. However, the efficiency of the laser is slightly reduced to 2.68% due to the increased cavity loss. Figure 5.23 shows the output spectrum of the TDFL with and without SA at the pump power threshold of 187.3 mW. As can be seen from the figure, the Q-switched laser operates at a wavelength of 1892.4 nm, which is closer to the peak absorption of the TDF at around 1900 nm to compensate for the loss as compared to the CW laser (without SA). The OSNR is more than 30 dB. The spectrum bandwidth is also broadened in the Q-switched laser due to the self-phase modulation effect in the ring cavity.

Figure 5.22: Output power characteristic against the pump power with and without the SA.

Figure 5.23: The output spectrum of the ring TDFL with and without the SA.

Figure 5.24 shows the Q-switched pulse train trace by the oscilloscope at the pump power of 191.7 mW. At this pump power, the proposed TDFL generates a stable Q-switching pulse with an average output power of 0.5 mW and repetition rate of 4.5 kHz. The pulse energy is calculated to be around 111.1 nJ at this pump power. Figure 5.25 exhibits the single spectrum of the pulse width taken from the oscilloscope at the pump power of 191.7 mW. As seen in the figure, the FWHM or pulse width was obtained at 18.4 μs.

Figure 5.24: Q-switching pulse train at the pump power of 191.7 mW.

Figure 5.25: The pulse envelop of the Q-switched laser at the pump power of 191.7 mW.

Figure 5.26 shows the repetition rate and the pulse width of the proposed Q-switched TDFL versus the pump power. The repetition rate has a monotonically increasing, near-linear relationship with the pump power level, which is consistent with other reported results of the SWCNTs based fiber lasers (Ahmad *et al.*, 2013). When the pump power is tuned from 187.3 to 194.2 mW, the pulse train repetition rate varies from 3.8 to 4.6 kHz. However, the pulse width is inversely proportional to the tuned pump power, where the pulse width becomes shorter as the pump power increases. The shortest pulse width of 18.3 μs is achieved at the maximum pump power of 194.2 mW. The pulse width is expected to decrease further if the pump power can be augmented beyond 194.2 mW as long as it is still kept below the damage threshold of the MWCNT-PVA based SA. Shortening the total cavity length of the fiber laser is another alternative to get a shorter pulse (Luo *et al.*, 2010). Figure 5.27 shows the output power and pulse energy as a function of pump power. It is found that both output pump power and pulse energy increase with the pump power. At the maximum pump power of 194.2 mW, the average pump power and pulse energy of the Q-switched laser are obtained at 0.58 mW and 126.1 nJ, respectively.

Figure 5.26: Repetition rate and pulse width as a function of pump power.

Figure 5.27: Average output power and pulse energy as a function of pump power.

5.4.4 Q-switching performance with 1552 nm pumping

Aside from 800 nm pumping, the TDFL can also be pumped by 1552 nm light to create a population inversion between $^3F_4$ and $^3H_6$ energy levels and generates laser at the 1900 nm region. Here, the performance of the Q-switched TDFL is investigated using a 1552 nm pump as the pump source based on the similar setup of Figure 5.20. The total cavity length is measured to be around 11.6 m due to the increment of both TDF (4 m) and WDM fiber length. The TDFL starts to operate in CW mode at threshold pump power of 256 mW. As the SA is incorporated into the cavity, a stable self-started Q-switching pulse train is obtained at the slightly higher pump power of 302.2 mW than the CW operation. Figure 5.28 compares the optical spectrum of the Q-switched TDFL with the CW. The Q-switched TDFL operates at a wavelength of 1910.8 nm, which is slightly shorter than the CW laser owing to the insertion loss produced by the SA. It has

a broad FWHM of 3.0 nm due to the SPM effect in the ring cavity and signal to noise ratio (SNR) of approximately 30 dB.

Figure 5.28: Optical spectra of the TDFL with CW and Q-switching modes of operation.

Figure 5.29 shows the oscilloscope trace of the typical Q-switched pulse train at 1552 nm pump power of 382.1 mW. It is observed that the Q-switching operation is stable for the TDFL where neither amplitude variation nor timing jitter was noticeable in the pulse train. This indicates that the self-mode locking effect on the Q-switching is suppressed (Zhou *et al.*, 2010b). The spacing between two pulses in Figure 5.29 is measured to be around 46.0 μs, which can be translated to repetition rate of 21.7 kHz. At this pump power, the pulse width and an average output power were measured to be 7.9 μs and 2.2 mW, respectively and thus the pulse energy is calculated to be 103.4 nJ. Figure 5.30 shows the relation of repetition rate and pulse width with the pump power for the TDFL. In the Q-switched laser, the dependence of the pulse repetition rate can be seen to increase, while the pulse width decreases almost linearly with the pump power. This agrees well with the previous result on a 800 nm pumping. By varying the

pump power from 302.2 mW to 382.1 mW, the pulse repetition rate of the Q-switched TDFL configured with 1552 nm pumping can be tuned from 13.1 kHz to 21.7 kHz while the corresponding pulse width reduces from 11.5 to 7.9 μs.

Figure 5.29: The typical pulse train for the proposed TDFL at 1552 nm pump power of 382.1 mW.

Figure 5.30: Repetition rate and pulse width as a function of a 1552 nm pump power.

Figure 5.31 shows the average output power and pulse energy of the proposed Q-switched TDFL as a function of a 1552 nm pump power. It is observed that both output power and pulse energy increase with the increment of the pump power from 302.2 to 382.1 mW. Further increasing the pump power leads to randomizing the pulses and the pulse train of the passively Q-switched laser became unstable and strong amplitude variation appeared. It is predicted that the fluctuation is caused by the lower damage threshold of the MWCNT under higher pump power, considering the fact that the laser will completely stop lasing if the pump power is further increased. It is also

observed that the Q-switching operation of the laser can be resumed back as the pump power is reduced within 302.2 to 382.1 mW. These results indicate that both 800 and 1552 nm pumping schemes can be used for generating Q-switching pulse train in the TDFL. The fabrication of the SA is also simple. Furthermore, the material cost of MWCNTs is cheaper compared to the graphene and single-walled CNT; hence the MWCNTs based Q-switched laser is preferable.

Figure 5.31: Average output power and pulse energy as a function of a 1552 nm pump power.

5.5 2 µm Q-switched TBFL

A significant research interest has emerged in the field of 2 micron Q-switched lasers due to their usefulness in various applications. Most of the Q-switched lasers use graphene saturable absorbers (GSAs), which are considered as a broadband SA. For instance, Wang et. al. (Wang *et al.*, 2012b) reported a Q-switched TDFL with a maximum pulse energy of 69 nJ and repetition rate of 26 kHz using the GSA. In another work, Jiang et. al. (Jiang *et al.*, 2013) demonstrated a Q-switched laser with pulse duration and repetition rate of 760 ns and 202 kHz, respectively, using GSA transferred to a high reflective mirror as saturable absorber. In Chapter 4, a newly developed Thulium Bismuth co-doped fiber (TBF) is demonstrated to generate an efficient laser operating in the 1900 nm wavelength region. In this section, a Q-switched Thulium Bismuth co-doped fiber laser (TBFL) is demonstrated for the first time using a similar TBF in conjunction with a simple and low cost MWCNTs based SA. The performance of the proposed Q-switched TBFL is then compared with a previously demonstrated Q-switched TDFL, which was obtained by using a commercial TDF and the same MWCNTs-PVA film based SA.

5.5.1 Experimental arrangement

The TBF was obtained by drawing a preform, which was fabricated using a deposition of porous layer by modified chemical vapor deposition (MCVD) process in conjunction with a solution doping technique as discussed in the section 4.2, in the previous chapter. The fabricated TBF sample used as a gain medium in this chapter is TB2 which has a circular cladding with the core and cladding diameters of 7.2 μm and 125 μm, respectively. The EPMA result shows its core has dopant concentrations (in wt%) of 0.35 Bi_2O_3, 0.9 Tm_2O_3, 3.0 Al_2O_3 and 4.0 GeO_2, which correspond to Bi and Tm ratio (Bi:Tm) of 1:2.57. The NA of the fiber is measured to be around 0.23.

Figure 5.32 shows the configuration of the proposed Q-switched TBFL using the fabricated TBF as the gain medium in conjunction with the homemade MWCNTs-PVA film SA. The fabrication of the SA has explained in detail in the section 5.4.1. The TBFL employs 0.4 m long TBF, which is pumped by an 800 nm laser diode via an 800/2000 nm WDM. The output laser is sent to the 10 dB coupler in which 10% of it was measured by an OSA with a spectral resolution of 0.05 nm and an oscilloscope is used to observe the output pulse train of the Q-switched operation via a photo-detector. Another 90% of the light is kept oscillating in the ring cavity. The overall length of the laser cavity was ~6.0 m. The performance of the Q-switched TBFL operating at 1.9 μm is also compared with a previously demonstrated Q-switched TDFL. The TDF has a length of 2 m, NA of 0.15, core diameter of 9 μm and thulium ion concentration of 0.25wt. %.

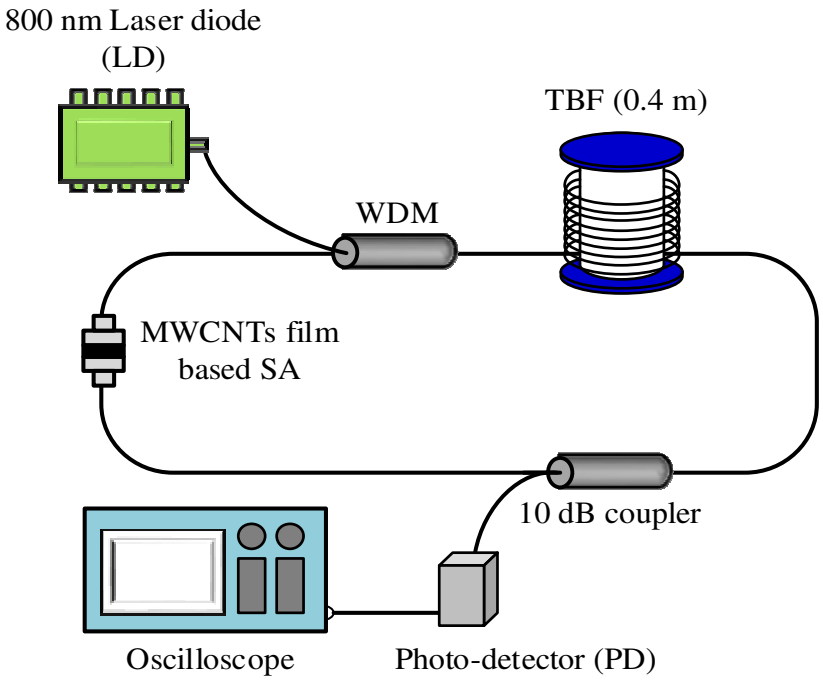

Figure 5.32: Schematic configuration of the proposed Q-switched TBFL with MWCNTs-PVA SA.

5.5.2 Q-switching performance

Figure 5.33 shows the output power characteristics of both the Q-switched TBFL and TDFL against the input pump power. There is no Q-switching pulse observed below the threshold pump power for both lasers. The threshold pump power of the Q-switched TBFL is obtained at 106.6 mW, which is much lower than that of the conventional TDFL. Stable Q-switching pulse can only be generated within a pump power range from 187.3 to 194.2 mW for the TDFL. At the threshold pump power, the output power of TBFL and TDFL are obtained at 0.37 mW and 0.40 mW, respectively. This shows that the efficiency of the TBFL is significantly higher than the conventional TDFL. The improved threshold and efficiency characteristics are due to the use of highly concentrated TBF as the gain medium, which reduces the cavity length of the laser. In addition, the presence of active bismuth ions in the gain medium improves the population inversion via the energy transfer process. However, the efficiency of both

TBFL and TDFL are comparatively low due to the insertion loss of the WDM, the output coupler and a saturable absorber.

Figure 5.33: The lasing characteristic of the Q-switched laser with two different gain media.

The output spectra of both Q-switched lasers were also monitored by an OSA, whose resolution is limited at 0.05 nm. Figure 5.34 shows the optical spectra of the TBFL and TDFL at the pump power threshold of 106.6 mW and 187.3 mW respectively. The TBFL operates at the center wavelength of 1857.8 nm, which is shorter than TDFL operating at 1892.4 nm due to the energy transfer from active bismuth, which provides a higher gain at shorter wavelength. The FWHM of the output spectra are obtained at ~0.18 nm and ~10.9 nm for TBFL and TDFL, respectively. The absence of spectral broadening in the Q-switched TBFL is due to the gain medium length used which is just around 0.4 m and thus prevents the non-linear effect to take place in the cavity. It is worth noting that the operating wavelength shifts to a shorter wavelength with the incorporation of the MWCNT-SA for both experiments due to the

insertion loss of the SA as compared to CW laser's operating wavelength. As the cavity loss increases, the oscillating laser shifts toward the peak absorption wavelength of the gain medium as explained earlier.

Figure 5.34: The output spectra of the Q-switched TBFL and TDFL at the threshold pump power.

When the SA is inserted into the ring cavity, a stable and self-starting Q-switching operation is obtained within a pump power of 106.6 - 160.0 mW and 187.3 - 194.2 mW for TBFL and TDFL, respectively. Figure 5.35 shows the typical oscilloscope traces of those Q-switched pulse trains, which were measured at its threshold pump power by an oscilloscope via photo-detector. As shown in the figure, the pulse to pulse durations for the TBFL and TDFL are measured at 77.9 and 263.2 μs, which correspond to the repetition rates of 12.84 kHz and 3.8 kHz, respectively. The TBFL has a relatively higher repetition rate due to the gain medium length used which is reasonably shorter. The corresponding pulse widths are 9.6 μs and 22.1 μs for the

TBFL and TDFL, respectively. At the threshold pump powers of 106.6 and 187.3 mW, the average output power of the Q-switched TBFL and TDFL are 0.37 mW and 0.4 mW, respectively.

Figure 5.35: Q-switching pulse train observed from an oscilloscope for TBFL and TDFL.

Figure 5.36 shows how repetition rate and pulse width for both Q-switched lasers are related to the pump power. The pulse repetition rate can be seen to increase almost linearly with pump power, while the pulse width decreases in the same fashion for both lasers. The pulse repetition rate of the Q-switched TBFL can be widely tuned from 12.84 to 29.48 kHz by varying the pump power from 106.6 to 160.0 mW. This agrees well with the passive Q-switching theory with a saturable absorber (Spühler *et al.*, 1999). Meanwhile, its pulse width reduces from 9.6 to 6.1 μs. The tuning range of the repetition rate for TDFL is smaller than the one for TBFL due to the limited available pump power range. The lowest pulse width of the TDFL is 18.3 μs, which is

obtained at the maximum pump power of 194.2 mW. The repetition rate / pulse width of the TDFL is expected to increase / drop further by increasing the pump power, as long as the damage threshold of the SA is not exceeded. Compared to the TDFL, the pulse width of the Q-switched TBFL is significantly shorter due to the use of a higher doped fiber, which shortens the cavity length of the fiber laser.

Figure 5.36: Repetition rate and pulse width as a function of pump power.

Figure 5.37 shows the average output power and pulse energy characteristics for both Q-switched lasers against the injected pump power. It is found that the output power and pulse energy increase with the pump power for both lasers. For instance, the output power of the TBFL increases from 0.37 to 1.82 mW and the pulse energy also increases from 28.8 to 61.7 nJ as the pump power is varied from 106.6 mW to 160.0 mW. However, the highest pulse energy of 126.1 nJ is obtained by the TDFL at the maximum pump power of 194.2 mW. This is attributed to the repetition rate of the Q-switched TDFL, which is significantly lower than that of the TBFL. The new fabricated

TBF exhibits a better Q-switching laser performance compared to the conventional TDF. This is most probably due to the use of TBF, which has a suitable lifetime for enhancing Q-switching operation (Keller, 2003).

Figure 5.37: Average output power and pulse energy as a function of pump power.

5.6 Q-switched TBFL with 1552 nm pumping

In this section, a new Q-switched TBFL is demonstrated using a 1552 nm pumping. The proposed laser uses the same SA and gain medium as the previous Q-switched TBFL. Besides 800 nm pumping, the 1900 nm emission and lasing can be realized by pumping the TBF with a 1552 nm laser. Using a 1552 nm laser light, the Tm^{3+} is excited to excited state level to create a population inversion between $^3F_4$ and $^3H_6$ level. When the thulium ions dropped to the ground state, it emits photons at 1900 nm. Recently, a high power pump source at 1550 nm region can be easily realized using a double-clad Erbium-Ytterbium fiber as a gain medium and a 980 nm laser diode as a pumping source. The 980 nm laser diode is widely available and much cheaper than 800 nm laser diode. The configuration of the proposed new Q-switched TBFL is almost

similar to the previous setup of Figure 5.32 except for the pumping scheme used in this experiment which uses a 1552 nm pump and the WDM. The total length of the ring cavity is ~7.84 m. It employs 1.5 m long the fabricated TBF as the gain medium in conjunction with the homemade MWCNTs-PVA film SA. The light is split 90/10 by the 10 dB coupler. 90% of the light oscillating in the ring cavity and propagates through the 1550/2000 nm WDM to initiate laser oscillation. The output laser is measured by an OSA and the output pulse train of the Q-switched operation is observed using an oscilloscope via a photo-detector.

At first, the performance of the TBFL configured with and without SA is investigated by varying the 1552 nm pump power. Without the SA, the CW lasing was observed at the pump power threshold of 178 mW. A stable and self-starting Q-switching operation is then obtained at threshold pump power of 500 mW by incorporating the SA in the cavity. Figure 5.38 compares the output spectrum of the CW and Q-switched TBFL when the pump power is fixed at 178 mW and 500 mW, respectively. The CW and Q-switched lasers operate at the center wavelength of 1881.7 nm and 1843.0 nm, respectively. As mentioned earlier, the operating wavelength of Q-switched TBFL shifts to a shorter wavelength due to the increment in the total cavity loss. The spectral broadening is also observed due to self-phase modulation effect in the cavity of Q-switched TBFL. The 3-dB bandwidth and signal to noise ratio of the Q-switched fiber TBFL is measured to be ~10 nm and ~22 dB, respectively. A weak chirp is also observed for both lasers in the peak wavelength range of the output spectrum as shown in Figure 5.38 due to the multimode oscillations and cavity perturbations (Dong *et al.*, 2010). As the pump power is increased further, the chirp disappears due to the suppression of the mode-competition in the cavity.

Figure 5.38: The output spectrum of the TBFL with and without the SA.

Figure 5.39(a) shows the oscilloscope trace of the Q-switched pulse train at pump power of 500 mW. The spacing between two pulses is measured to be around 44.4 μs, which can be translated to repetition rate of 22.5 kHz. Figure 5.39(b) illustrates the enlarged pulse envelop of the pulse train with a pulse width of 5.6 μs at 500 mW. It is observed that the Q-switching operation is stable without any distinct amplitude modulation in each Q-switched envelop of the spectrum. In the absence of the SA in the cavity, no pulse generation is observed. Therefore, it is proven that the observed pulse originates from the MWCNTs-SA in the cavity and is not from the gain medium. At the threshold pump power of 500 mW, the average output power of the Q-switched pulse laser is measured to be 0.62 mW, which corresponds to pulse energy of 27.5 nJ.

(a) (b)

Figure 5.39: (a) The pulse train for the proposed TBFL with MWCNTs-SA at threshold with the repetition rate of 22.52 kHz. (b) Enlarged pulse width spectrum with a pulse width of 5.6 μs.

Figure 5.40 shows the relation between repetition rate and pulse width of the 1552 nm pump power. The pulse repetition rate is increased almost linearly with the pump power, while the pulse width reduces with the same trend which is similar to the previous Q-switching results for both TDFL and TBFL. The pulse repetition rate of the Q-switched TBFL can be widely tuned from 22.52 kHz to 61.99 kHz by varying the 1552 nm pump power from 500 mW to 800 mW. The tuning range is wider compared to that of 800 nm pumping. As can be seen, the pulse width reduces from 5.6 to 4.0 μs as the pump power increases from 500 to 800 mW. The pulse duration could be reduced

by using shorter highly doped gain medium and further shortening the fiber between the components of the laser cavity. Since the higher pump power will destroy the MWCNTs-PVA SA due to the thermal characteristics of the carbon nanotubes, the applied pump power was controlled below 800 mW. The Q-switching tuning range of the proposed laser is also found to be higher than that of the previous report on the Q-switching based on SWCNTs-SA (Dong *et al.*, 2010; Zhou *et al.*, 2010b). This is most probably due to the saturation fluence of the proposed MWCNTs-SA, which is higher than the SWCNTs-SA.

Figure 5.40: Repetition rate and pulse width as a function of pump power.

Figure 5.41 shows the average output power and pulse energy of the Q-switched TBFL versus the pump power. The average output power is found to increase with the increase in pump power. The slope efficiency is calculated to be 0.85%; the lower efficiency is attributed to the introduction of the SA inside the cavity and the employment of 1550 nm components which incurs a loss. The maximum output power of the TBFL is obtained at 3.35 mW when the pump power is 800 mW. On the other

hand, the pulse energy fluctuates with the pump power increment. The highest pulse energy of 54.1 nJ is achieved at the pump power of 650 mW. The Q-switched fiber laser shows a stable operation without significant degradation of the deposited MWCNTs with such output pulse energy level.

Figure 5.41: Average output power and pulse energy versus pump power.

5.7 Summary

In this chapter, a couple of new configurations and techniques for realizing an all-fiber Q-switched fiber lasers have been demonstrated. These lasers are based on commercial TDF and newly developed TBF as the gain medium in conjunction with 800 and 1552 nm pumping. Two passive saturable absorbers; graphene and MWCNTs are developed and fabricated in-house to realize the Q-switching. The graphene flakes are obtained via electrochemical exfoliation of graphite rod in the electrolyte at room temperature and then mixed with the polymer to form a free standing film with a thickness of 50 μm. On the other hand, the MWCNTs composite is prepared by mixing the MWCNTs homogeneous solution with a dilute polyvinyl alcohol (PVA) polymer solution before leaving it to dry at room temperature to produce a film. The fabricated SA is then attached to the end of fiber ferrule with the aid of index matching gel and connected with another clean fiber ferrule via FC/PC connector to construct the SA. The SA is incorporated in a ring TDFL and TBFL to generate Q-switching pulse train. The performance of the Q-switched lasers is summarized in Table 5.1. It is found that the MWCNTs-SA performs better than the GSA. This is due to the better thermal management and the saturation fluence of the MWCNTs. To the best of our knowledge, this is the first reported Q-switched laser at 2 μm region using MWCNTs based SA.

Table 5.1: Q-switched performance of the GSA and MWCNTs

Types of SA	Gain media	Pumping excitation (nm) / length of fiber (m)	Input range (mW)	Highest average output (mW)	Lowest pulse width (μs)	Highest Repetition rate (kHz)	Highest Pulse energy (nJ)
Graphene	TDF	800 / 2	186 – 207	1.01	19.3	13.1	77.2
		1552 / 4	513 – 539	1.01	8.17	24.16	90.64
MWCNTs	TDF	800 / 2	187.3 – 194.2	0.58	18.3	4.6	126.1
		1552 / 5	302.2 – 382.1	2.2	21.7	46.1	103.4
	TBF	800 / 0.4	106.6 – 160	1.82	6.1	29.48	61.7
		1552 / 1.5	500 – 800	3.35	4	61.99	54.1

The Q-switch TDFL was successfully demonstrated using a 2 m long TDF, which is pumped by an 800 nm laser diode and a GSA. At the maximum pump power of 207 mW, the laser produces the highest repetition rate of 13.1 kHz and the highest pulse energy of 77.2 nJ. The pulse width trend follows a V-shaped curve due to the effect of heat transfer to the GSA, which was initiated by the non-radiative emission from $^3H_4$ to $^3F_4$ level of thulium. The curved is eliminated by using 1552 nm ($^3H_6$ to $^3F_4$) pumped wavelength to excite the thulium ions. The attainable pulse energy can be increased to 90.64 nJ. We also demonstrated a Q-switched TBFL using a MWCNTs based SA in conjunction with 800 nm pumping. The performance of the TBFL is also compared to that of a TDFL. The TDFL generates an optical pulse train with a repetition rate from 3.8 to 4.6 kHz with a pulse width of 22.1 to 18.3 μs when the pump power is tuned from 187.3 to 194.2 mW. Meanwhile, the pulse train of the Q-switched TBFL has a repetition rate ranging from 12.84 to 29.48 kHz, pulse width of 9.6 to 6.1 μs with the pump power varied from 106.6 to 160 mW. The Q-switched laser is generated at the lowest threshold pump power of 106.6 mW. The Q-switched TBFL is also

demonstrated using 1552 nm pumping. It operates within a wide pump power range of 300 mW. The repetition rate increases from 22.52 to 61.99 kHz while the pulse width reduces from 5.6 to 4.0 μs by increasing the pump power from 500 to 800 mW. The proposed laser is expected to have various practical applications in fiber communications and sensors.

CHAPTER 6

CONCLUSIONS AND FUTURE WORKS

6.1 Conclusion

This research work is devoted to the construction of fiber lasers that emit longer wavelength beams (in the spectral region of around 1.9 μm) utilizing thulium doped and co-doped fiber laser for the improvement of lasing efficiency and threshold pump power. The approach taken involves employing two different co-doping elements which are Ytterbium-Thulium doped fiber (YTDF) and Thulium-Bismuth doped fiber (TBF) as the gain media. Both fibers are newly fabricated and their spectroscopic properties as well as energy transfer processes have been investigated. In the Q-switched laser, new implementation of saturable absorbers which are graphene and multi-walled carbon nanotubes (MWCNTs) have been proposed using commercial Thulium-doped fiber (TDF) and TBF as the gain media. The proposed pulse laser performances are comparable to the reported published works.

A spectroscopic study of YTDF exhibit possible degradation of the fiber laser performance in 2 μm region due to the upconversion (UC) processes which contribute to the effect of excited state absorption (ESA). A lasing action was successfully obtained using two YTDF samples with different Yb:Tm concentration (LTY6 and LTY8) based on a cladding pumping technique through the transition of thulium ions from $^3F_4$ to $^3H_6$ with the assistance of ytterbium to thulium ion energy transfer. With a ring configuration, the laser is more efficient when coupled with a 905 nm pumping source compared to the 931 nm pumping source. In the Fabry–Perot cavity with two FBGs configuration, the YTDF laser (YTDFL) operates at 1901.6 nm with an efficiency of 2.47% using an optimized 2 m long YTDF (LTY8). It is found that the higher

ytterbium to thulium concentration ratio of 4.0:1 contribute to more efficient energy transfer between the sensitizer and acceptor ions in YTDF, which in turn lowers the threshold of the laser. Higher NA and smaller core radius also contribute to the higher lasing efficiency. The use of multimode pump with slightly lower wavelength than 931 nm is shown to improve both the laser's threshold and efficiency of the YTDFL. Finally, a series of dual-pumping schemes are proposed to improve the lasing efficiency of YTDFL based on linear cavity configuration. However, the proposed YTDFL is experimentally less efficient than other reported works due to three possible reasons. The first reason is the size of the fabricated fiber core diameter, which is approximately two times larger compared to that of the FBG fiber (around 7–8 micron). When both fibers are spliced together, a higher splicing loss of around 1 dB is generated as a large portion of the pump power leaks out. The second reason is due to the poor thermal management of the YTDF. The YTDF cannot operate at pump powers higher than 3 W due to the fiber damage at the splicing point. The burnt fiber problem has been solved using a water bath, however the output power is still low. The third reason is due to the high possibility of multi-step energy transfer which leads to UC and blue emission.

In comparison with YTDF, the enhancement of lasing performance has been identified in TBF using three TBF samples with different thulium and active bismuth concentration (TB1, TB2, and TB3). The incorporation of active bismuth ions in the gain medium helps increase the $^3F_4$ population and thus improves the efficiency of the laser through energy transfer processes without any degradation from UC. The experimental results reveal that TB2 with a comparatively short length (0.4 m) of fiber can achieve higher efficiency as compared to the conventional TDF. This is attributed to the incorporation of Bi ions in the gain medium which help to increase the $^3F_4$ population through energy transfer processes. TB2 which has the highest amount of active bismuth and thulium concentrations exhibits the highest lasing efficiency. An

efficient TBFL with dual pumping at 800 nm and 1552 nm wavelength was also demonstrated. Higher efficiency than single pumping method is attributed to the use of an additional 1552 nm pump to complement the 800 nm pumping. Apart from that, the energy transfer processes can be optimized by modifying the dopants compositions thus increase the efficiency of stepwise energy transfer. By pumping the TBF with an 800 nm pumping excitation, 2 energy transfer processes may occur which are cross relaxation and energy transfer from active bismuth to Tm^{3+} ions. Due to the efficient energy transfer, a broadband Amplified Spontaneous Emission (ASE) from TBF was proposed. Finally, an all-fiber dual wavelength TBFL operating in the 1900 nm region is demonstrated using a single FBG in a ring configuration. A dual wavelength laser output is obtained as the polarization controller (PC) orientation is adjusted to balance the loss between the two wavelengths. By controlling the intracavity polarization, the dual wavelength laser can also be switched to operate in the single-wavelength.

In the final part of this research work, an all-fiber 1.9 μm Q-switched laser has been successfully produced using commercial TDF and TBF as the gain media in a ring cavity configuration. Reliable self-starting Q-switched based on graphene saturable absorber (GSA) and multi-walled carbon nanotube saturable absorber (MWCNT-SA) were observed. Both of the GSA and MWCNT-SA were fabricated in-house. The graphene flakes were fabricated using electrochemical exfoliation technique whereas MWCNT thin-film was used as received without extra purification process. Both of the SAs were fabricated by cutting a small part of the prepared film and sandwiching it between two FC/PC fiber connectors, after depositing an index-matching gel onto the fiber ends. By using the GSA, a Q-switched fiber laser has been demonstrated using a TDF pumped by an 800 nm pump wavelength and the experiment has been repeated using a 1552 nm pump wavelength. The V-shaped curve of the pulse duration is observed when an 800 nm pump is used which is attributed to the contribution of heat

transferred to the GSA initiated by the non-radiative emission from $^3H_4$ to $^3F_4$ level of thulium. This curve was not observed when the 1552 nm pump source was used to excite the Tm^{3+} ions due to the absence of non-radiative decay and lattice vibration in the system. Unlike the GSA, the MWCNT-SA successfully generated the Q-switching for both the TDF and TBF-based gain media. The Q-switched performance comparison between TDF and TBF has been made. It is found that the best Q-switched laser performance is exhibited by a TBF pumped by a 1552 nm laser in conjunction with the use of the MWCNTs-SA. It is proven that the pumping of the TDF using a 1552 nm laser excitation enables the possibility to eliminate the accumulated heat in the SA. The Q-switched TBFL has the lowest threshold pump power of 106.6 mW using an 800 nm pumping excitation. With a 1552 nm laser excitation, Q-switched TBFL based MWCNTs pulses have been observed within a wide pump power range of 500 to 800 mW. The corresponding pulse train has a repetition rate ranging from 22.52 to 61.99 kHz with a pulse width of 5.6 to 4.0 μs.

The primary focus on the development of CW and Q-switching fiber laser at 1.9 μm region has been achieved. Even though several results are not as expected, the discussion and analysis of the performances have been carried out. The laser performances on the effect of co-doping ytterbium and bismuth to the thulium ions have been investigated. The experimental results show that TBFL has better performance compared to the commercial TDFL and YTDFL. Although YTDFL has been expected to give better lasing performance, several limiting factors have been identified to be the reason of poor lasing performance. The successful construction of a passively Q-switched fiber laser at the 1.9 μm region using in-house fabricated GSA and MWCNTs-SA facilitates numerous applications in fiber communications and sensor. The findings in this work could be used in the future for the development of fiber based sources targeting new applications.

6.2 Future work

Up to this point, the objective of this thesis has been fulfilled. However, the discussion can be further enhanced by establishing the cross-relaxation, energy transfer upconversion (ETU) and excited state absorption (ESA) measurement of the YTDF and TBF. These important parameters should be thoroughly studied by means of their respective level lifetime of the Tm^{3+} and active bismuth ions. The understanding of these effects and knowledge of the parameters can accurately describe the performance of the CW laser. The performance of a fiber can be considerably impaired by undesired effects such as unsaturable absorption and ESA. Another important consideration which can be taken into account is the fabrication of the double-cladding YTDF. The YTDF cannot be pumped experimentally up to the kilowatt power level as usually reported in the literature, due to the fiber damage at the splicing point. The relatively high numerical aperture (NA) of the pump cladding can be further designed to meet the high power applications.

TBFL is suitable for compact multi-wavelength operation due to the use of the significantly shorter TB2 sample as well as its broad emission wavelength. The compact device such as Array Waveguide Grating (AWG) which is used as a wavelength slicing mechanism may contribute to the multi-wavelength fiber laser generation. Another related field of interest to explore is the demonstration of the nonlinear effect such as Brillouin fiber laser (BFL) at the 1.9 μm region. The proposed Brillouin pump can be seeded by the TBFL or YTDFL, provided that the laser can be tunable in several wavelength ranges which can be done by an external filter or a tunable bandpass filter. The realization of the fiber laser at 1.9 μm also enables some of the sensor-based experiments within the 1.9 μm region to be further studied. Since the 1.9 μm wavelength has strong absorption of water and biological tissue, the 1.9 μm fiber laser can be proposed as a source for the tissue samples in an experiment.

In an attempt to improve pulse laser, the average power and pulse energy of the nanosecond pulses can be further scaled up by using power amplifier stage. To realize this, a high pump power requirement which implies the use of a Master Oscillator/Power Amplifier (MOPA) can be designed. Apart from that, another method of implementing pulse laser such as nonlinear polarization rotation (NPR) method can be further explored and the performance can be compared with the GSA and MWCNTs based SA. Apart from that, upgrading the Q-switched laser to mode locked laser is crucial due to their femtosecond pulse laser generation which is widely used in most applications. The design of intracavity dispersion management of the laser needs to be comprehensively studied in order to achieve femtosecond pulse generation. The outcomes from this thesis may provide optimism in facing the future challenges.

REFERENCES

Agger, S. D., & Povlsen, J. H. (2006). Emission and absorption cross section of thulium doped silica fibers. *Optics Express, 14*(1), 50-57.

Ahmad, F., Harun, S., Nor, R., Zulkepely, N., Ahmad, H., & Shum, P. (2013). A Passively Mode-Locked Erbium-Doped Fiber Laser Based on a Single-Wall Carbon Nanotube Polymer. *Chinese Physics Letters, 30*(5), 054210.

Ahmad, H., Zulkifli, M., Latif, A., & Harun, S. (2009). Tunable dual wavelength fiber laser incorporating AWG and optical channel selector by controlling the cavity loss. *Optics Communications, 282*(24), 4771-4775.

Alcock, I., Ferguson, A., Hanna, D., & Tropper, A. (1986a). Mode-locking of a neodymium-doped monomode fibre laser. *Electronics Letters, 22*(5), 268-269.

Alcock, I., Tropper, A., Ferguson, A., & Hanna, D. (1986b). Q-switched operation of a neodymium-doped monomode fibre laser. *Electronics Letters, 22*(2), 84-85.

Allain, J., Monerie, M., & Poignant, H. (1989). Tunable CW lasing around 0.82, 1.48, 1.88 and 2.35 μm in thulium-doped fluorozirconate fibre. *Electronics Letters, 25*(24), 1660-1662.

Alvarez-Chavez, J., Offerhaus, H., Nilsson, J., Turner, P., Clarkson, W., & Richardson, D. (2000). High-energy, high-power ytterbium-doped Q-switched fiber laser. *Optics Letters, 25*(1), 37-39.

Alvarez, W., Pompeo, F., Herrera, J., Balzano, L., & Resasco, D. (2002). Characterization of single-walled carbon nanotubes (SWNTs) produced by CO disproportionation on Co-Mo catalysts. *Chemistry of materials, 14*(4), 1853-1858.

Ando, Y., & Iijima, S. (1993). Preparation of carbon nanotubes by arc-discharge evaporation. *JAPANESE JOURNAL OF APPLIED PHYSICS PART 2 LETTERS, 32*, L107-L107.

Armitage, J. R. (1988). Three-level fiber laser amplifier: a theoretical model. *Applied Optics, 27*(23), 4831-4836.

Ball, G. A., & Glenn, W. (1992). Design of a single-mode linear-cavity erbium fiber laser utilizing Bragg reflectors. *Lightwave Technology, Journal of, 10*(10), 1338-1343.

Banhart, F. (1999). Irradiation effects in carbon nanostructures. *Reports on Progress in Physics, 62*(8), 1181.

Bao, Q., Zhang, H., Wang, Y., Ni, Z., Yan, Y., Shen, Z. X., Loh, K. P., & Tang, D. Y. (2009). Atomic-Layer Graphene as a Saturable Absorber for Ultrafast Pulsed Lasers. *Advanced Functional Materials, 19*(19), 3077-3083.

Battiato, J. M., Morse, T., & Kostuk, R. K. (1997). Dual-wavelength common-cavity codoped fiber laser. *Photonics Technology Letters, IEEE, 9*(7), 913-915.

Becker, T., Clausen, R., Huber, G., Duczynski, E., & Mitzscherlich, P. (1989). *Spectroscopic and Laser Properties of Tm-doped YAG at 2 μm.* Paper presented at the Advanced Solid State Lasers (p. DD1). Optical Society of America.

Blanc, W., Sebastian, T. L., Dussardier, B., Michel, C., Faure, B., Ude, M., & Monnom, G. (2008). Thulium environment in a silica doped optical fibre. *Journal of non-crystalline solids, 354*(2), 435-439.

Bonaccorso, F., Sun, Z., Hasan, T., & Ferrari, A. (2010). Graphene photonics and optoelectronics. *Nature Photonics, 4*(9), 611-622.

Booth, B. L. (1989). Low loss channel waveguides in polymers. *Journal of Lightwave Technology, 7*(10), 1445-1453.

Braud, A., Girard, S., Doualan, J., Thuau, M., Moncorge, R., & Tkachuk, A. (2000). Energy-transfer processes in Yb: Tm-doped KY_ {3} F_ {10}, LiYF_ {4}, and BaY_ {2} F_ {8} single crystals for laser operation at 1.5 and 2.3 μm. *Physical Review B, 61*(8), 5280.

Bronikowski, M. J., Willis, P. A., Colbert, D. T., Smith, K., & Smalley, R. E. (2001). Gas-phase production of carbon single-walled nanotubes from carbon monoxide via the HiPco process: A parametric study. *Journal of Vacuum Science & Technology A, 19*(4), 1800-1805.

Brown, D. C., & Hoffman, H. J. (2001). Thermal, stress, and thermo-optic effects in high average power double-clad silica fiber lasers. *IEEE Journal of Quantum Electronics, 37*(2), 207-217.

Bünzli, J.-C. G., & Piguet, C. (2005). Taking advantage of luminescent lanthanide ions. *Chemical Society Reviews, 34*(12), 1048-1077.

Burrus, C. A., Stone, J., & Dentai, A. G. (1976). Room-temperature 1.3 μm c.w. operation of a glass-clad Nd:y.a.g. single-crystal fibre laser end pumped with a single l.e.d. *Electronics Letters, 12*(22), 600-602. doi: 10.1049/el:19760457

Cao, C., Qin, W., Zhang, J., Wang, Y., Zhu, P., Wang, G., Wei, G., Wang, L., & Jin, L. (2008). Enhanced ultraviolet up-conversion emissions of Tm< sup> 3+</sup>/Yb< sup> 3+</sup> codoped YF< sub> 3</sub> nanocrystals. *Journal of Fluorine Chemistry, 129*(3), 204-209.

Chen, Y.-F., Tsai, S., & Wang, S. (2000). High-power diode-pumped Q-switched and mode-locked Nd: YVO< sub> 4</sub> laser with a Cr< sup> 4+</sup>: YAG saturable absorber. *Optics Letters, 25*(19), 1442-1444.

Cheng, X., Ahmad, H., & Harun, S. (2010). Broadband ASE source using bismuth-based erbium-doped fibers in double-pass set-up. *Microwave and Optical Technology Letters, 52*(7), 1636-1638.

Chow, K., Yamashita, S., & Set, S. (2010). Four-wave-mixing-based wavelength conversion using a single-walled carbon-nanotube-deposited planar lightwave circuit waveguide. *Optics Letters, 35*(12), 2070-2072.

Costa, S., Borowiak-Palen, E., Kruszyńska, M., Bachmatiuk, A., & Kaleńzuk, R. (2008). Characterization of carbon nanotubes by Raman spectroscopy. *Materials Science (0137-1339), 26*(2).

Coté, G. L. (2001). Noninvasive and minimally-invasive optical monitoring technologies. *The Journal of nutrition, 131*(5), 1596S-1604S.

Cunning, B., Brown, C., & Kielpinski, D. (2011). Low-loss flake-graphene saturable absorber mirror for laser mode-locking at sub-200-fs pulse duration. *Applied Physics Letters, 99*(26), 261109-261109-261103.

Darabont, A., Nemes-Incze, P., Kertész, K., Tapasztó, L., Koós, A., Osváth, Z., Sárközi, Z., Vértesy, Z., Horváth, Z., & Biró, L. (2005). Synthesis of carbon nanotubes by spray pyrolysis and their investigation by electron microscopy. *Journal of Optoelectronics and Advanced Materials, 7*(2), 631-636.

Dieke, G. H., & Crosswhite, H. (1963). The spectra of the doubly and triply ionized rare earths. *Applied Optics, 2*(7), 675-686.

Digonnet, M. J. (2002). *Rare-Earth-Doped Fiber Lasers and Amplifiers, Revised and Expanded*: CRC press.

Dong, B., Hao, J., Hu, J., & Liaw, C.-Y. (2010). Wide Pulse-Repetition-Rate Range Tunable Nanotube-Switched Low Threshold Erbium-Doped Fiber Laser. *Photonics Technology Letters, IEEE, 22*(24), 1853-1855.

Dresselhaus, M. S., Dresselhaus, G., Saito, R., & Jorio, A. (2005). Raman spectroscopy of carbon nanotubes. *Physics Reports, 409*(2), 47-99.

Eichhorn, M., & Jackson, S. D. (2007). High-pulse-energy actively Q-switched Tm< sup> 3+</sup>-doped silica 2 μm fiber laser pumped at 792 nm. *Optics Letters, 32*(19), 2780-2782.

El-Sherif, A., & King, T. (2003a). Soft and hard tissue ablation with short-pulse high peak power and continuous thulium-silica fibre lasers. *Lasers in Medical Science, 18*(3), 139-147.

El-Sherif, A. F., & King, T. A. (2003b). High-energy, high-brightness Q-switched Tm< sup> 3+</sup>-doped fiber laser using an electro-optic modulator. *Optics Communications, 218*(4), 337-344.

Emami, S., Abdul-Rashid, H., Ahmad, H., Ahmadi, A., & Harun, S. (2011). Effect of transverse distribution profile of thulium on the performance of thulium-doped fibre amplifiers. *Ukr. J. Phys. Opt, 13*, 74-81.

Fang, Q., Shi, W., Petersen, E., Kieu, K., Chavez-Pirson, A., & Peyghambarian, N. (2012). Half-mJ All-Fiber-Based Single-Frequency Nanosecond Pulsed Fiber

Laser at 2-< formula formulatype=. *Photonics Technology Letters, IEEE, 24*(5), 353-355.

Ferrari, A., Meyer, J., Scardaci, V., Casiraghi, C., Lazzeri, M., Mauri, F., Piscanec, S., Jiang, D., Novoselov, K., & Roth, S. (2006). Raman spectrum of graphene and graphene layers. *Physical Review Letters, 97*(18), 187401.

Firstov, S., Khopin, V., Bufetov, I., Firstova, E., Guryanov, A., & Dianov, E. (2011). Combined excitation-emission spectroscopy of bismuth active centers in optical fibers. *Optics Express, 19*(20), 19551-19561.

Geim, A. K., & Novoselov, K. S. (2007). The rise of graphene. *Nature materials, 6*(3), 183-191.

Geng, J., Wu, J., Jiang, S., & Yu, J. (2007). Efficient operation of diode-pumped single-frequency thulium-doped fiber lasers near 2< i> μ</i> m. *Optics Letters, 32*(4), 355-357.

Gomes, A., de Araujo, C. B., Ainslie, B., & Craig-Ryan, S. (1990). Amplified spontaneous emission in Tm3+-doped monomode optical fibers in the visible region. *Applied Physics Letters, 57*(21), 2169-2171.

Gould, R. G. (1959). *The LASER, light amplification by stimulated emission of radiation.* Paper presented at the The Ann Arbor Conference on Optical Pumping, the University of Michigan.

Graf, D., Molitor, F., Ensslin, K., Stampfer, C., Jungen, A., Hierold, C., & Wirtz, L. (2007). Spatially resolved Raman spectroscopy of single-and few-layer graphene. *Nano Letters, 7*(2), 238-242.

Greinacher, E. (1980). History of rare earth applications, rare earth market today: overview. *Industrial Applications of Rare Earth Elements*, 3-17.

Gumenyuk, R., Vartiainen, I., Tuovinen, H., & Okhotnikov, O. G. (2011). Dissipative dispersion-managed soliton 2 μm thulium/holmium fiber laser. *Optics Letters, 36*(5), 609-611.

Guo, T., Nikolaev, P., Thess, A., Colbert, D., & Smalley, R. (1995). Catalytic growth of single-walled manotubes by laser vaporization. *Chemical Physics Letters, 243*(1), 49-54.

Halder, A., Paul, M. C., Damanhuri, S., Huri, N., Hamzah, A., Harun, S., Ahmad, H., Das, S., Pal, M., & Bhadra, S. K. (2012). Upconversion luminescence in Tm3+/Yb3+ co-doped double-clad silica fibers under 980 nm cladding pumping. *Journal of Modern Optics, 59*(6), 527-532.

Hanna, D., Percival, R., Perry, I., Smart, R., Suni, P., & Tropper, A. (1990a). An Ytterbium-doped Monomode Fibre Laser: Broadly Tunable Operation from 1· 010 μm to 1· 162 μm and Three-level Operation at 974 Nm. *Journal of Modern Optics, 37*(4), 517-525.

Hanna, D., Percival, R., Perry, I., Smart, R., Townsend, J., & Tropper, A. (1990b). Frequency upconversion in Tm-and Yb: Tm-doped silica fibers. *Optics Communications, 78*(2), 187-194.

Hanna, D., Perry, I., Lincoln, J., & Townsend, J. (1990c). A 1-Watt thulium-doped cw fibre laser operating at 2 μm. *Optics Communications, 80*(1), 52-56.

Hasan, T., Sun, Z., Wang, F., Bonaccorso, F., Tan, P. H., Rozhin, A. G., & Ferrari, A. C. (2009). Nanotube–polymer composites for ultrafast photonics. *Advanced Materials, 21*(38-39), 3874-3899.

Hayward, R., Clarkson, W., Turner, P., Nilsson, J., Grudinin, A., & Hanna, D. (2000). Efficient cladding-pumped Tm-doped silica fibre laser with high power singlemode output at 2/spl mu/m. *Electronics Letters, 36*(8), 711-712.

Hecht, J. (2004). *City of light: the story of fiber optics*: Oxford University Press.

Herda, R., Kivistö, S., & Okhotnikov, O. G. (2008). Dynamic gain induced pulse shortening in< i> Q</i>-switched lasers. *Optics Letters, 33*(9), 1011-1013.

Hernandez, Y., Nicolosi, V., Lotya, M., Blighe, F. M., Sun, Z., De, S., McGovern, I., Holland, B., Byrne, M., & Gun'Ko, Y. K. (2008). High-yield production of graphene by liquid-phase exfoliation of graphite. *Nature Nanotechnology, 3*(9), 563-568.

Hjelme, D. R., & Mickelson, A. R. (1992). Theory of timing jitter in actively mode-locked lasers. *Quantum Electronics, IEEE Journal of, 28*(6), 1594-1606.

Huang, S.-L., Tsui, T.-Y., Wang, C.-H., & Kao, F.-J. (1999). Timing jitter reduction of a passively Q-switched laser. *Japanese Journal of Applied Physics, 38*(3A), L239.

Iijima, S. (1991). Helical microtubules of graphitic carbon. *Nature, 354*(6348), 56-58.

Jackson, S. D. (2003). Power scaling method for 2-μm diode-cladding-pumped Tm< sup> 3+</sup>-doped silica fiber lasers that uses Yb< sup> 3+</sup> codoping. *Optics Letters, 28*(22), 2192-2194.

Jackson, S. D. (2004). Cross relaxation and energy transfer upconversion processes relevant to the functioning of 2 μm Tm< sup> 3+</sup>-doped silica fibre lasers. *Optics Communications, 230*(1), 197-203.

Jackson, S. D. (2007). Passively Q-switched Tm3+-doped silica fiber lasers. *Applied Optics, 46*(16), 3311-3317. doi: 10.1364/AO.46.003311

Jackson, S. D., & King, T. (1998). High-power diode-cladding-pumped Tm-doped silica fiber laser. *Optics Letters, 23*(18), 1462-1464.

Jackson, S. D., & Mossman, S. (2003). Efficiency Dependence on the Tm< sup> 3+</sup> and Al< sup> 3+</sup> Concentrations for Tm< sup> 3+</sup>-Doped Silica Double-Clad Fiber Lasers. *Applied Optics, 42*(15), 2702-2707.

Jackson, S. D., Sabella, A., & Lancaster, D. G. (2007). Application and development of high-power and highly efficient silica-based fiber lasers operating at 2 μm. *Selected Topics in Quantum Electronics, IEEE Journal of, 13*(3), 567-572.

James, C. (1911). THULIUM I. 1. *Journal of the American Chemical Society, 33*(8), 1332-1344.

Jander, P., & Brocklesby, W. S. (2004). Spectroscopy of yttria-alumina-silica glass doped with thulium and erbium. *Quantum Electronics, IEEE Journal of, 40*(5), 509-512.

Javan, A., Bennett Jr, W. R., & Herriott, D. R. (1961). Population inversion and continuous optical maser oscillation in a gas discharge containing a He-Ne mixture. *Physical Review Letters, 6*(3), 106.

Jeon, M. Y., Kim, N., Shin, J., Jeong, J. S., Han, S.-P., Lee, C. W., Leem, Y. A., Yee, D.-S., Chun, H. S., & Park, K. H. (2010). Widely tunable dual-wavelength Er< sup> 3+</sup>-doped fiber laser for tunable continuous-wave terahertz radiation. *Optics Express, 18*(12), 12291-12297.

Jeong, Y., Dupriez, P., Sahu, J. K., Nilsson, J., Shen, D., Clarkson, W., & Jackson, S. (2005). Power scaling of 2 μm ytterbium-sensitised thulium-doped silica fibre laser diode-pumped at 975 nm. *Electronics Letters, 41*(4), 173-174.

Jeong, Y., Yoo, S., Coderaard, C., Nilsson, J., Sahu, J. K., Payne, D. N., Horley, R., Turner, P., Hickey, L., & Harker, A. (2007). Erbium: ytterbium codoped large-core fiber laser with 297-W continuous-wave output power. *Selected Topics in Quantum Electronics, IEEE Journal of, 13*(3), 573-579.

Jeong, Y., Sahu, J. K., Payne, D. N., & Nilsson, J. (2004). Ytterbium-doped large-core fiber laser with 1.36 kW continuous-wave output power. *Optics Express, 12*(25), 6088-6092.

Jiang, M., Ma, H., Ren, Z., Chen, X., Long, J., Qi, M., Shen, D., Wang, Y., & Bai, J. (2013). A graphene Q-switched nanosecond Tm-doped fiber laser at 2 μm. *Laser Physics Letters, 10*(5), 055103.

Kafka, J., Hall, D., & Baer, T. (1989). Mode-locked erbium-doped fiber laser with soliton pulse shaping. *Optics Letters, 14*(22), 1269-1271.

Kapron, F., & Keck, D. (1971). Pulse transmission through a dielectric optical waveguide. *Applied Optics, 10*(7), 1519-1523.

Kasamatsu, T., Yano, Y., & Sekita, H. (1999). 1.50-μm-band gain-shifted thulium-doped fiber amplifier with 1.05-and 1.56-μm dual-wavelength pumping. *Optics Letters, 24*(23), 1684-1686.

Kato, T., Hirano, M., Onishi, M., & Nishimura, M. (1999). Ultra-low nonlinearity low-loss pure silica core fibre for long-haul WDM transmission. *Electronics Letters, 35*(19), 1615-1617. doi: 10.1049/el:19991094

Keller, U. (2003). Recent developments in compact ultrafast lasers. *Nature, 424*(6950), 831-838.

Kieu, K., & Wise, F. (2009). Soliton thulium-doped fiber laser with carbon nanotube saturable absorber. *Photonics Technology Letters, IEEE, 21*(3), 128-130.

Kivistö, S., Koskinen, R., Paajaste, J., Jackson, S. D., Guina, M., & Okhotnikov, O. G. (2008). Passively Q-switched Tm3+, Ho3+-doped silica fiber laser using a highly nonlinear saturable absorber and dynamic gain pulse compression. *Optics Express, 16*(26), 22058.

Koch, G. J., Barnes, B. W., Petros, M., Beyon, J. Y., Amzajerdian, F., Yu, J., Davis, R. E., Ismail, S., Vay, S., & Kavaya, M. J. (2004). Coherent Differential Absorption Lidar Measurements of CO< sub> 2</sub>. *Applied Optics, 43*(26), 5092-5099.

Koch, G. J., Beyon, J. Y., Gibert, F., Barnes, B. W., Ismail, S., Petros, M., Petzar, P. J., Yu, J., Modlin, E. A., & Davis, K. J. (2008). Side-line tunable laser transmitter for differential absorption lidar measurements of CO< sub> 2</sub>: design and application to atmospheric measurements. *Applied Optics, 47*(7), 944-956.

Koester, C. J., & Snitzer, E. (1964). Amplification in a fiber laser. *Applied Optics, 3*(10), 1182-1186.

Koh, Y. K., Bae, M.-H., Cahill, D. G., & Pop, E. (2010). Heat conduction across monolayer and few-layer graphenes. *Nano Letters, 10*(11), 4363-4368.

Kurkov, A. (2011). Q-switched all-fiber lasers with saturable absorbers. *Laser Physics Letters, 8*(5), 335.

Kurkov, A. S., Ya, E. S., Marakulin, A. V., & Sholokhov, E. M. (2010). All fiber Er-Tm Q-switched laser. *Laser Physics Letters, 7*(11), 795.

Lahoz, F., Pérez-Rodríguez, C., Halder, A., Das, S., Paul, M. C., Pal, M., Bhadra, S. K., & Vasconcelos, H. (2011). Complete energy transfer due to rare-earth phase segregation in optical fiber preform glasses. *Journal of applied physics, 110*(8), 083121-083121-083126.

Lapointe, M.-A., Chatigny, S., Piché, M., Cain-Skaff, M., & Maran, J.-N. (2009). *Thermal effects in high-power CW fiber lasers.* Paper presented at the SPIE LASE: Lasers and Applications in Science and Engineering (pp. 71951U-71951U). International Society for Optics and Photonics.

Layne, C. B., Lowdermilk, W. H., & Weber, M. J. (1975). Nonradiative relaxation of rare-earth ions in silicate laser glass. *IEEE Journal of Quantum Electronics, 11*, 798.

Layne, C. B., Lowdermilk, W. H., & Weber, M. J. (1977). Multiphonon relaxation of rare-earth ions in oxide glasses. *Physical Review B, 16*(1), 10.

Li, Y., Jackson, S. D., & Fleming, S. (2004). High absorption and low splice loss properties of hexagonal double-clad fiber. *Photonics Technology Letters, IEEE, 16*(11), 2502-2504.

Librantz, A., Gomes, L., Pairier, G., Ribeiro, S., & Messaddeq, Y. (2008). Tm and Tm–Tb-doped germanate glasses for S-band amplifiers. *Journal of Luminescence, 128*(1), 51-59.

Lin, H., & Chang, C.-H. (2004). High power C+ L-band Erbium ASE source using optical circulator with double-pass and bidirectional pumping configuration. *Optics Express, 12*(25), 6135-6140.

Lin, X. C., Zhang, L., Tsang, Y. H., Wang, Y. G., Yu, H. J., Yan, S. L., Sun, W., Yang, Y. Y., Han, Z., & Hou, W. (2013). Multi-walled carbon nanotube as a saturable absorber for a passively mode-locked Nd: YVO4 laser. *Laser Physics Letters, 10*(5), 055805.

Liu, A., & Ueda, K. (1996). The absorption characteristics of circular, offset, and rectangular double-clad fibers. *Optics Communications, 132*(5), 511-518.

Liu, H., Chow, K., Yamashita, S., & Set, S. (2013). Carbon-nanotube-based passively Q-switched fiber laser for high energy pulse generation. *Optics & Laser Technology, 45*, 713-716.

Lu, B., Chen, H., Jiang, M., Chen, X., Ren, Z., & Bai, J. (2013). Graphene-based passive Q-switching for a 2 μm thulium-doped fiber laser. *Laser Physics, 23*(4), 045111.

Luo, Z., Zhou, M., Weng, J., Huang, G., Xu, H., Ye, C., & Cai, Z. (2010). Graphene-based passively Q-switched dual-wavelength erbium-doped fiber laser. *Optics Letters, 35*(21), 3709-3711.

Madsen, C., & Lenz, G. (1998). Optical all-pass filters for phase response design with applications for dispersion compensation. *Photonics Technology Letters, IEEE, 10*(7), 994-996.

Maiman, T. H. (1960). Stimulated optical radiation in ruby.

Martins-Filho, J., Bastos-Filho, C., Carvalho, M., Sundheimer, M., & Gomes, A. (2003). Dual-wavelength (1050 nm+ 1550 nm) pumped thulium-doped fiber amplifier characterization by optical frequency-domain reflectometry. *Photonics Technology Letters, IEEE, 15*(1), 24-26.

Maruyama, S., Kojima, R., Miyauchi, Y., Chiashi, S., & Kohno, M. (2002). Low-temperature synthesis of high-purity single-walled carbon nanotubes from alcohol. *Chemical Physics Letters, 360*(3), 229-234.

McClung, F., & Hellwarth, R. (1963). Characteristics of giant optical pulsations from ruby. *Proceedings of the IEEE, 51*(1), 46-53.

McComb, T. S., Sims, R. A., Willis, C. C., Kadwani, P., Sudesh, V., Shah, L., & Richardson, M. (2010). High-power widely tunable thulium fiber lasers. *Applied Optics, 49*(32), 6236-6242.

Mears, R. J, Reekie, L., Jauncey, I., & Payne, D. N (1987). Low-noise erbium-doped fibre amplifier operating at 1.54μm. *Electronics Letters, 23*(19), 1026-1028.

Mears, R. J., Reekie, L., Poole, S. B., & Payne, D. N. (1985). Neodymium-doped silica single-mode fibre lasers. *Electronics Letters, 21*(17), 738-740. doi: 10.1049/el:19850521

Miya, T., Terunuma, Y., Hosaka, T., & Miyashita, T. (1979). Ultimate low-loss single-mode fibre at 1.55 μm. *Electronics Letters, 15*(4), 106-108.

Moulton, P. F., Rines, G. A., Slobodtchikov, E. V., Wall, K. F., Frith, G., Samson, B., & Carter, A. L. (2009). Tm-doped fiber lasers: fundamentals and power scaling. *Selected Topics in Quantum Electronics, IEEE Journal of, 15*(1), 85-92.

Muddu, P. S. (2003). A Study of Image Transmission Through a Fiber-Optic Conduit and its Enhancement Using Digital Image Processing Techniques.

Muendel, M. H. (1996). *Optimal inner cladding shapes for double-clad fiber lasers.* Paper presented at the Lasers and Electro-Optics, 1996. CLEO'96., Summaries of papers presented at the Conference on (p. 209). IEEE.

Nelson, L., Jones, D., Tamura, K., Haus, H., & Ippen, E. (1997). Ultrashort-pulse fiber ring lasers. *Applied Physics B: Lasers and Optics, 65*(2), 277-294.

Ng, L. N., Taylor, E., & Nilsson, J. (2002). 795 nm and 1064 nm dual pump thulium-doped tellurite fibre for S-band amplification. *Electronics Letters, 38*(21), 1246-1247.

Novoselov, K. S., Geim, A. K., Morozov, S., Jiang, D., Zhang, Y., Dubonos, S., Grigorieva, I., & Firsov, A. (2004). Electric field effect in atomically thin carbon films. *Science, 306*(5696), 666-669.

Obraztsov, A., Obraztsova, E., Tyurnina, A., & Zolotukhin, A. (2007). Chemical vapor deposition of thin graphite films of nanometer thickness. *Carbon, 45*(10), 2017-2021.

Opsommer, E., Weiss, T., Miltner, W., & Plaghki, L. (2001). Scalp topography of ultralate (C-fibres) evoked potentials following thulium YAG laser stimuli to tiny skin surface areas in humans. *Clinical Neurophysiology, 112*(10), 1868-1874.

Pal, A., Dhar, A., Das, S., Chen, S. Y., Sun, T., Sen, R., & Grattan, K. T. V. (2010). Ytterbium-sensitized Thulium-doped fiber laser in the near-IR with 980 nm pumping. *Optics Express, 18*(5), 5068-5074.

Panasenko, D., Polynkin, P., Polynkin, A., Moloney, J. V., Mansuripur, M., & Peyghambarian, N. (2006). Er-Yb femtosecond ring fiber oscillator with 1.1-W

average power and GHz repetition rates. *Photonics Technology Letters, IEEE, 18*(7), 853-855.

Paschotta, R., Häring, R., Gini, E., Melchior, H., Keller, U., Offerhaus, H., & Richardson, D. (1999). Passively< i> Q</i>-switched 0.1-mJ fiber laser system at 1.53 μm. *Optics Letters, 24*(6), 388-390.

Pask, H., Carman, R. J., Hanna, D. C., Tropper, A. C., Mackechnie, C. J., Barber, P. R., & Dawes, J. M. (1995). Ytterbium-doped silica fiber lasers: versatile sources for the 1-1.2 μm region. *Selected Topics in Quantum Electronics, IEEE Journal of, 1*(1), 2-13.

Paul, M., Upadhyaya, B., Das, S., Dhar, A., Pal, M., Kher, S., Dasgupta, K., Bhadra, S., & Sen, R. (2010). Study of the fabrication parameters of large core Yb< sub> 2</sub> O< sub> 3</sub> doped optical fibre through solution doping technique. *Optics Communications, 283*(6), 1039-1046.

Peterka, P., Faure, B., Blanc, W., Karasek, M., & Dussardier, B. (2004). Theoretical modelling of S-band thulium-doped silica fibre amplifiers. *Optical and Quantum Electronics, 36*(1-3), 201-212.

Peterka, P., Kašík, I., Dhar, A., Dussardier, B., & Blanc, W. (2011). Theoretical modeling of fiber laser at 810 nm based on thulium-doped silica fibers with enhanced 3H4 level lifetime. *Optics Express, 19*(3).

Pierce, M. C., Jackson, S. D., Dickinson, M. R., & King, T. A. (1999). Laser–tissue interaction with a high-power 2-μm fiber laser: Preliminary studies with soft tissue. *Lasers in Surgery and Medicine, 25*(5), 407-413.

Pierce, M. C., Jackson, S. D., Golding, P. S., Dickinson, B., Dickinson, M. R., King, T. A., & Sloan, P. (2001). *Development and application of fiber lasers for medical applications.* Paper presented at the Proc. SPIE. In BiOS 2001 The International Symposium on Biomedical Optics (pp. 144-154). International Society for Optics and Photonics.

Po, H., Snitzer, E., Tumminelli, R., Zenteno, L., Hakimi, F., Cho, N., & Haw, T. (1989). *Double clad high brightness Nd fiber laser pumped by GaAlAs phased array.* Paper presented at the Optical Fiber Communication Conference (p. PD7). Optical Society of America.

Poole, S. B., Payne, D. N., Mears, R. J., Fermann, M. E., & Laming, R. (1986). Fabrication and characterization of low-loss optical fibers containing rare-earth ions. *Lightwave Technology, Journal of, 4*(7), 870-876.

Popa, D., Sun, Z., Hasan, T., Torrisi, F., Wang, F., & Ferrari, A. (2011). Graphene Q-switched, tunable fiber laser. *Applied Physics Letters, 98*(7), 073106.

Ramadurai, K., Cromer, C. L., Lewis, L. A., Hurst, K. E., Dillon, A. C., Mahajan, R. L., & Lehman, J. H. (2008). High-performance carbon nanotube coatings for high-power laser radiometry. *Journal of applied physics, 103*(1), 013103.

Ray, N. (1974). Composition—property relationships in inorganic oxide glasses. *Journal of non-crystalline solids, 15*(3), 423-434.

Reina, A., Jia, X., Ho, J., Nezich, D., Son, H., Bulovic, V., Dresselhaus, M. S., & Kong, J. (2008). Large area, few-layer graphene films on arbitrary substrates by chemical vapor deposition. *Nano Letters, 9*(1), 30-35.

Reisfeld, R., & Jørgensen, C. K. (1977). *Lasers and excited states of rare earths*: Springer-Verlag Berlin.

Richards, B. D., Tsang, Y. H., Binks, D. J., Lousteau, J., & Jha, A. (2008). *CW and Q-switched 2.1 μm Tm3+/Ho3+/Yb3+-triply-doped tellurite fibre lasers.* Paper presented at the Remote Sensing. In SPIE Remote Sensing (pp. 711105-711105). International Society for Optics and Photonics.

Ruan, J., Dong, G., Liu, X., Zhang, Q., Chen, D., & Qiu, J. (2009). Enhanced broadband near-infrared emission and energy transfer in Bi-Tm-codoped germanate glasses for broadband optical amplification. *Optics Letters, 34*(16), 2486-2488.

Savage, G. (1993). *Applications of Carbon-carbon Composites*: Springer.

Schmidt, O., Rothhardt, J., Röser, F., Linke, S., Schreiber, T., Rademaker, K., Limpert, J., Ermeneux, S., Yvernault, P., & Salin, F. (2007). Millijoule pulse energy Q-switched short-length fiber laser. *Optics Letters, 32*(11), 1551-1553.

Scholle, K., Lamrini, S., Koopmann, P., & Fuhrberg, P. (2010). 2 µm laser sources and their possible applications.

Sigel, G., Tomozawa, M., Doremus, R., Tomozawa, M., & Doremus, R. (1978). Glass I: Interaction with Electromagnetic Radiation, 12Academic. *New York*, 5-89.

Simondi-Teisseire, B., Viana, B., Vivien, D., & Lejus, A. (1996). Yb< sup> 3+</sup> to Er< sup> 3+</sup> energy transfer and rate-equations formalism in the eye safe laser material Yb: Er: Ca< sub> 2</sub> Al< sub> 2</sub> SiO< sub> 7</sub>. *Optical Materials, 6*(4), 267-274.

Slobodtchikov, E., Moulton, P. F., & Frith, G. (2007). *Efficient, high-power, Tm-doped silica fiber laser.* Paper presented at the Advanced Solid-State Photonics.

Snitzer, E. (1961). Optical Maser Action of Nd^{+ 3} in a Barium Crown Glass. *Physical Review Letters, 7*(12), 444.

Snitzer, E., Po, H., Hakimi, F., Tumminelli, R., & McCollum, B. (1988). *Double clad, offset core Nd fiber laser.* Paper presented at the Optical Fiber Sensors. (p. PD5). Optical Society of America.

Song, Y. W., Set, S. Y., & Yamashita, S. (2006, May). Novel Kerr shutter using carbon nanotubes deposited onto a 5-cm D-shaped fiber. In *Conference on Lasers and Electro-Optics* (p. CMA4). Optical Society of America.

Spühler, G., Paschotta, R., Fluck, R., Braun, B., Moser, M., Zhang, G., Gini, E., & Keller, U. (1999). Experimentally confirmed design guidelines for passively Q-

switched microchip lasers using semiconductor saturable absorbers. *JOSA B, 16*(3), 376-388.

Stone, J., & Burrus, C. (1974). Neodymium-doped fiber lasers: room temperature cw operation with an injection laser pump. *Applied Optics, 13*(6), 1256-1258.

Stone, J., & Burrus, C. A. (1973). Neodymium‐doped silica lasers in end‐pumped fiber geometry. *Applied Physics Letters, 23*(7), 388-389. doi: 10.1063/1.1654929

Stone, J., Burrus, C. A., Dentai, A. G., & Miller, B. I. (1976). Nd:YAG single‐crystal fiber laser: Room‐temperature cw operation using a single LED as an end pump. *Applied Physics Letters, 29*(1), 37-39. doi: 10.1063/1.88863

Sun, Z., Hasan, T., & Ferrari, A. (2012). Ultrafast lasers mode-locked by nanotubes and graphene. *Physica E: Low-dimensional Systems and Nanostructures, 44*(6), 1082-1091.

Sun, Z., Hasan, T., Torrisi, F., Popa, D., Privitera, G., Wang, F., Bonaccorso, F., Basko, D. M., & Ferrari, A. C. (2010a). Graphene Mode-Locked Ultrafast Laser. *ACS Nano, 4*(2), 803-810. doi: 10.1021/nn901703e

Sun, Z., Popa, D., Hasan, T., Torrisi, F., Wang, F., Kelleher, E. J., Travers, J. C., Nicolosi, V., & Ferrari, A. C. (2010b). A stable, wideband tunable, near transform-limited, graphene-mode-locked, ultrafast laser. *Nano Research, 3*(9), 653-660.

Taher, M., Gebavi, H., Taccheo, S., Milanese, D., & Balda, R. (2011). Novel approach towards cross-relaxation energy transfer calculation applied on highly thulium doped tellurite glasses. *Optics Express, 19*(27), 26269-26274.

Tan, S., Harun, S., Ahmad, F., Nor, R., Zulkepely, N., & Ahmad, H. (2013). A Q-switched multi-wavelength Brillouin erbium fiber laser with a single-walled carbon nanotube saturable absorber. *Laser Physics, 23*(5), 055101.

Tao, M., Huang, Q., Yu, T., Yang, P., Chen, W., & Ye, X. (2013). A highly efficient 57 pm Tm-doped fiber laser with two multimode fiber Bragg gratings. *Laser Physics, 23*(7), 075111.

Townsend, J. E., Poole, S. B., & Payne, D. N. (1987). Solution-doping technique for fabrication of rare-earth-doped optical fibres. *Electronics Letters, 23*(7), 329-331. doi: 10.1049/el:19870244

Tsai, T.-Y., & Birnbaum, M. (2000). Co 2+: ZnS and Co 2+: ZnSe saturable absorber Q switches. *Journal of applied physics, 87*(1), 25-29.

Walsh, B., & Barnes, N. (2004). Comparison of Tm: ZBLAN and Tm: silica fiber lasers; spectroscopy and tunable pulsed laser operation around 1.9 μm. *Applied Physics B, 78*(3-4), 325-333.

Wang, F., Torrisi, F., Jiang, Z., Popa, D., Hasan, T., Sun, Z., Cho, W., & Ferrari, A. C. (2012a). *Graphene passively Q-switched two-micron fiber lasers.* Paper presented at the Quantum Electronics and Laser Science Conference (pp. JW2A-72). Optical Society of America

Wang, F., Torrisi, F., Jiang, Z., Popa, D., Hasan, T., Sun, Z., Cho, W. B., & Ferrari, A. C. (2012b, 6-11 May 2012). *Graphene passively Q-switched two-micron fiber lasers.* Paper presented at the Lasers and Electro-Optics (CLEO), 2012 Conference on (pp. JW2A-72). Optical Society of America.

Wang, Q., Geng, J., Jiang, Z., Luo, T., & Jiang, S. (2011). *Mode-locked Tm-Ho fiber laser with a Sb-based SESAM.* Paper presented at the CLEO: Science and Innovations. (p. CMK2). Optical Society of America.

Wang, Q., Teng, H., Zou, Y., Zhang, Z., Li, D., Wang, R., Gao, C., Lin, J., Guo, L., & Wei, Z. (2012c). Graphene on SiC as a Q-switcher for a 2 μm laser. *Optics Letters, 37*(3), 395-397.

Wang, Y., Xu, C.-Q., & Po, H. (2004). Thermal effects in kilowatt fiber lasers. *Photonics Technology Letters, IEEE, 16*(1), 63-65.

Watekar, P. R., Ju, S., Boo, S., & Han, W.-T. (2005). Linear and non-linear optical properties of Yb3+/Tm3+ co-doped alumino-silicate glass prepared by sol–gel method. *Journal of non-crystalline solids, 351*(30–32), 2446-2452. doi: http://dx.doi.org/10.1016/j.jnoncrysol.2005.06.036

Wu, J., Jiang, S., Qua, T., Kuwata-Gonokami, M., & Peyghambarian, N. (2005). 2 μm lasing from highly thulium doped tellurite glass microsphere. *Applied Physics Letters, 87*, 211118.

Wu, J., Yao, Z., Zong, J., & Jiang, S. (2007). Highly efficient high-power thulium-doped germanate glass fiber laser. *Optics Letters, 32*(6), 638-640.

Yang, L.-M., Walton, D., Nees, J., & Weber, W. H. (1996). Compact, high power, modelocked upconversion laser using a thulium-doped ZBLAN fibre. *Electronics Letters, 32*(7), 658-659.

Yu, Z., Song, Y., Tian, C., Li, J., Zhang, X., & Wang, Y. (2012). *Q-switched Yb-doped double cladding fiber laser with single wall carbon nanotube saturable absorber.* Paper presented at the Photonics Asia.

Zayhowski, J., & Dill, C. (1994). Diode-pumped passively Q-switched picosecond microchip lasers. *Optics Letters, 19*(18), 1427-1429.

Zayhowski, J., & Dill, C. (1995). Coupled-cavity electro-optically Q-switched Nd: YVO< sub> 4</sub> microchip lasers. *Optics Letters, 20*(7), 716-718.

Zayhowski, J. J., & Kelley, P. L. (1991). Optimization of <e1>Q</e1>-switched lasers. *Quantum Electronics, IEEE Journal of, 27*(9), 2220-2225. doi: 10.1109/3.135181

Zdrojek, M., Gebicki, W., Jastrzebski, C., Melin, T., & Huczko, A. (2004). Studies of multiwall carbon nanotubes using Raman spectroscopy and atomic force microscopy. *Solid State Phenomena, 99*, 265-268.

Zhang, L., Dong, G., Wu, J., Peng, M., & Qiu, J. (2012). Excitation wavelength-dependent near-infrared luminescence from Bi-doped silica glass. *Journal of Alloys and Compounds, 531*, 10-13.

Zhang, L., Wang, Y., Yu, H., Sun, L., Guo, L., Hou, W., Tang, J., Lin, X., & Li, J. (2011a). 880 nm LD pumped passive Q-switched and mode-locked Nd: YVO4 laser using a single-walled carbon nanotube saturable absorber. *Laser Physics, 21*(3), 454-458.

Zhang, L., Wang, Y., Yu, H., Sun, L., Hou, W., Lin, X., & Li, J. (2011b). Passive mode-locked Nd: YVO4 laser using a multi-walled carbon nanotube saturable absorber. *Laser Physics, 21*(8), 1382-1386.

Zhang, X., Hong, P., Bass, M., & Chai, B. (1995). Blue upconversion with excitation into Tm ions at 780 nm in Yb-and Tm-codoped fluoride crystals. *Physical Review B, 51*(14), 9298.

Zhang, Z., Boyland, A., Sahu, J. K., Clarkson, W., & Ibsen, M. (2011c). High-power single-frequency thulium-doped fiber DBR laser at 1943 nm. *Photonics Technology Letters, IEEE, 23*(7), 417-419.

Zhou, B., Lin, H., Chen, B., & Pun, E. Y.-B. (2011). Superbroadband near-infrared emission in Tm-Bi codoped sodium-germanium-gallate glasses. *Optics Express, 19*(7), 6514-6523.

Zhou, B., Lin, H., & Pun, E. Y.-B. (2010a). Tm3+-doped tellurite glasses for fiber amplifiers in broadband optical communication at 1.20 μm wavelength region. *Optics Express, 18*(18), 18805-18810. doi: 10.1364/OE.18.018805

Zhou, D.-P., Wei, L., Dong, B., & Liu, W.-K. (2010b). Tunable passively-switched erbium-doped fiber laser with carbon nanotubes as a saturable absorber. *Photonics Technology Letters, IEEE, 22*(1), 9-11.

Zyskind, J., Mizrahi, V., DiGiovanni, D., & Sulhoff, J. (1992). Short single frequency erbium-doped fibre laser. *Electronics Letters, 28*(15), 1385-1387.

LIST OF PUBLICATIONS

Journal Publications

1. Harun, S., Saidin, N., Damanhuri, S., Ahmad, H., Halder, A., Paul, M. C., Das, S., Pal, M., & Bhadra, S. K. (2012). Fiber laser at 2 micron region using double-clad thulium/ytterbium co-doped yttria-alumino-silicate fiber. *Laser Physics Letters, 9*(1), 50.

2. Damanhuri, S. S. A., Halder, A., Paul, M. C., Ali, S. M. M., Saidin, N., Harun, S. W., Ahmad, H., Das, S., Pal, M., & Bhadra, S. (2013). Effects of Yb/Tm concentration and pump wavelength on the performance of Ytterbium-sensitized Thulium-doped fiber laser. *Quantum Electronics, IEEE Journal of* , vol.49, no.1, pp.95-99, Jan. 2013

3. Halder, A., Paul, M. C., Harun, S., Ali, S., Saidin, N., Damanhuri, S., Ahmad, H., Das, S., Pal, M., & Bhadra, S. K. (2012). 1880-nm Broadband ASE Generation With Bismuth–Thulium Codoped Fiber. *Photonics Journal, IEEE, 4*(6), 2176-2181.

4. Halder, A., Saidin, N., Zen, D. I. M., Damanhuri, S. S. A., Harun, S. W., Ahmad, H., Dimyati, K., Paul, M. C., Das, S., & Bhadra, S. K. (2014). Thulium Bismuth Co-Doped Fiber Lasers at 1901 nm by 802 nm Pumping. *Selected Topics in Quantum Electronics, IEEE Journal of, 20*(5), 1-6. doi: 10.1109/JSTQE.2014.2304420

5. Saidin, N., Harun, S., Damanhuri, S., Ali, S., Ahmad, H., Halder, A., Paul, M., Das, S., Pal, M., & Bhadra, S. (2013). A Tm-Bi Co-Doped Fiber Laser with Dual Pumping Operation. *Chinese Physics Letters, 30*(3), 034204.

6. Saidin, N., Zen, D., Damanhuri, S., Harun, S., Ahmad, H., Dimyati, K., Halder, A., Paul, M., Pal, M., & Bhadra, S. (2013). All-Fiber Dual-Wavelength Thulium–Bismuth Codoped Fiber Laser. *Microwave and Optical Technology Letters, 55*(10), 2324-2326.

7. Saidin, N., Zen, D., Hamida, B., Khan, S., Ahmad, H., Dimyati, K., & Harun, S. (2013). A Q-switched thulium-doped fiber laser with a graphene thin film based saturable absorber. *Laser Physics, 23*(11), 115102.

8. Saidin, N., Zen, D. I. M., Ahmad, F., Damanhuri, S. S. A., Ahmad, H., Dimyati, K., & Harun, S. W. (2014). Q-switched Thulium-doped fiber laser operating at 1900 nm using graphene based saturable absorber. Accepted on 29th October 2013*, IET Optoelectronics.*

9. Saidin, N., Zen, D. I. M., Ahmad, F., Haris, H., Ahmad, M. T., Latiff, A. A., Ahmad, H., Dimyati, K., & Harun, S. W. (2014). Q-switched thulium-doped fibre laser operating at 1900 nm using multi-walled carbon nanotubes saturable absorber. *The Journal of Engineering, 1*(1).

10. Saidin, N., Harun, S., Ahmad, H., Ali, S., Damanhuri, S., Halder, A., Paul, M., Das, S., Pal, M., & Bhadra, S. (2015). Enhancement of Thulium–Ytterbium doped fiber laser efficiency using dual-pumping method. Microwave and Optical Technology Letters, 57(2), 285-287.

Paper Presented at Conferences

1. Saidin, N., Ahmad, F., Zen, D., Hamida, B., Khan, S., Ahmad, H., Dimyati, K., & Harun, S. (2013). *All-fiber graphene passively Q-switched nanosecond Thulium doped fiber laser at 1900 nm.* Paper presented at the 2013 IEEE International Conference on Smart Instrumentation, Measurement and Applications (ICSIMA), Kuala Lumpur.

2. Saidin, N., Damanhuri, S., Ali, S., Halder, A., Ghosh, D., Pal, M., Paul, M., Bhadra, S., Harun, S., & Ahmad, H. (2013). *Comparison between the single and dual-pumping method of large mode area Yb^{3+}/Tm^{3+} co-doped air-clad fiber laser.* Paper presented at the 2013 International Conference on Technology, Informatics, Management, Engineering, and Environment (TIME-E), Bandung Indonesia.

3. Saidin, N., Damanhuri, S., Halder, A., Paul, M. C., Harun, S., Das, S., Pal, M., Bhadra, S. K., & Ahmad, H. (2012). *Wideband spectrum-sliced ASE source operating at 2 micron region based on double clad ytterbium-sensitized thulium-doped fiber.* Paper presented at the 2012 International Conference on Computer and Communication Engineering (ICCCE), Kuala Lumpur.

4. Ali, S., Saidin, N., Damanhuri, S., Harun, S., Halder, A., Paul, M. C., Ahmad, H., Das, S., Pal, M., & Bhadra, S. K. (2012). *Comparison of linear and ring lasers of thulium-ytterbium co-doped fiber.* Paper presented at the 2012 International Conference on Computer and Communication Engineering (ICCCE), Kuala Lumpur.

APPENDIX

A selection of published works are attached in this appendix

A *Q*-switched thulium-doped fiber laser with a graphene thin film based saturable absorber

2013 Laser Phys. 23 115102

(http://iopscience.iop.org/1555-6611/23/11/115102)

Laser Phys. **23** (2013) 115102 (5pp) doi:10.1088/1054-660X/23/11/115102

A *Q*-switched thulium-doped fiber laser with a graphene thin film based saturable absorber

N Saidin[1,2], D I M Zen[1,3], B A Hamida[4], S Khan[4], H Ahmad[1], K Dimyati[3] and S W Harun[1]

[1] Photonics Research Centre, University of Malaya, 50603 Kuala Lumpur, Malaysia
[2] Department of Electrical Engineering, Faculty of Engineering, University of Malaya, 50603 Kuala Lumpur, Malaysia
[3] Department of Electrical and Electronic Engineering, National Defense University of Malaysia, Kem Sungai Besi, 57000 Kuala Lumpur, Malaysia
[4] Department of Electrical and Computer Engineering, International Islamic University Malaysia, Jalan Gombak, 53100 Kuala Lumpur, Malaysia

E-mail: swharun@um.edu.my

Received 16 August 2013, in final form 28 August 2013
Accepted for publication 30 August 2013
Published 7 October 2013
Online at stacks.iop.org/LP/23/115102

Abstract
We demonstrate a simple, compact and low cost *Q*-switched thulium-doped fiber laser (TDFL) operating at 1844.1 nm by exploiting a graphene based saturable absorber (SA) in conjunction with 1552 nm pumping. The SA is fabricated by sandwiching the graphene thin film between two fiber connectors. The thin film was produced by mixing graphene flakes, synthesized by an electrochemical exfoliation process, with polyethylene oxide (PEO) solution. The TDFL generates a stable pulse train with 6.73 kHz repetition rate, 11.41 μs pulse width and 90.64 nJ pulse energy at 513 mW 1552 nm pump power. A higher performance *Q*-switched TDFL is expected to be achieved with the optimization of the SA and laser cavity.

(Some figures may appear in colour only in the online journal)

1. Introduction

Q-switched fiber lasers are of great interest because of their many applications in remote sensing, range finding, medicine, material processing, and telecommunications [1, 2]. They can be obtained through active [3] or passive techniques [4]. Compared to the ones derived via active techniques, passively *Q*-switched fiber lasers possess attractive advantages of compactness, simplicity, and flexibility in design. They have been extensively investigated using various saturable absorbers such as semiconductor saturable absorber mirrors (SESAMs) [5], and carbon nanotubes (CNTs) [6, 7]. However, the fabrication of SESAMs requires very complex and costly processes. CNT based saturable absorbers (SAs) are comparatively simple and more cost effective. Unfortunately, to operate at a particular wavelength, CNTs require bandgap tuning by controlling their diameters and chirality. Moreover, the surface tension of CNTs is too large, leading to a low damage threshold [8].

More recently, novel nano-material graphene has attracted much attention as it was reportedly used in broadband functional SAs [9]. This is due to the gapless linear dispersion of Dirac electrons in graphene which allows a broadband operation covering the wavelength range from the visible to the mid-IR. Compared with CNTs, graphene is expected to have a higher damage threshold due to its two-dimensional structure [10]. However, until now most reported works on graphene have focused on mode-locked fiber lasers [10–13] while graphene *Q*-switched fiber lasers were seldom [14–17] investigated. Recent realizations on *Q*-switched fiber lasers are mainly on the erbium-doped fiber lasers operating in the 1.5 μm region [18–20]. For instance, Luo *et al* [18] have recently reported a *Q*-switched

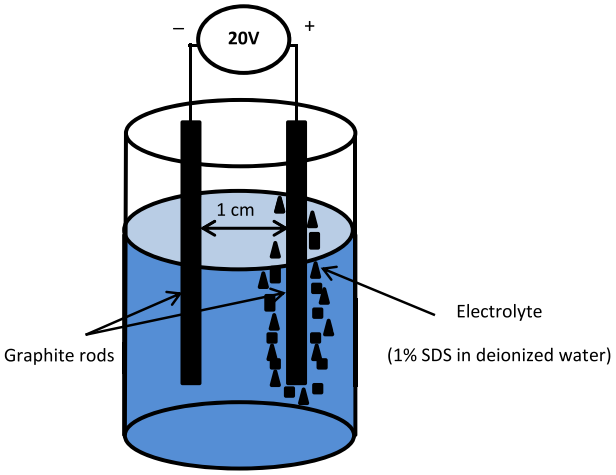

Figure 1. Electrochemical exfoliation of the graphene.

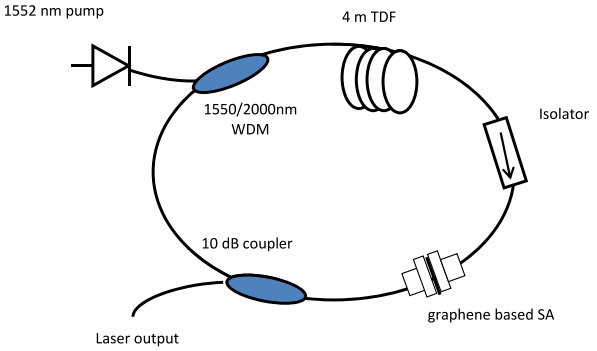

Figure 2. Experimental setup of the proposed graphene based *Q*-switched TDFL.

erbium-doped fiber laser (EDFL) using an optical deposition technique.

Thulium-doped fiber lasers (TDFL) operating in the 'eye-safe' wavelength region are useful for various applications, for example in light detection and ranging (LiDAR), differential absorption LiDAR, and as pumps for mid-IR generation. So far, only a few works on the generation of *Q*-switched fiber lasers near the 2 μm wavelength region have been reported. For instance, Wang *et al* [21] reported a *Q*-switched generation with a maximum pulse energy of 69 nJ and a repetition rate of 26 kHz using a 1560 nm CW laser source and a graphene based SA. More recently, Jiang *et al* [22] achieved a laser with a short pulse duration of 760 ns and a repetition rate of 202 kHz using graphene transferred to the highly reflective mirror as the SA. In this paper, a *Q*-switched TDFL operating near the 1900 nm region is demonstrated using a simple and low cost graphene based SA. The graphene is synthesized by electrochemical exfoliation of graphite at room temperature in 1% sodium dodecyl sulfate (SDS) aqueous solution. Graphene flakes obtained from the process are mixed with polyethylene oxide (PEO) as the host polymer to produce free standing composite thin film which acts as a passive *Q*-switcher in the TDFL ring cavity. The SA is integrated in the TDFL by sandwiching the graphene thin film between two fiber connectors, resulting in a stable pulse train with 6.73 kHz repetition rate, 11.41 μs pulse width and 90.64 nJ pulse energy at 513 mW 1552 nm pump power.

2. Experiment

Figure 1 shows the experimental setup used for producing graphene flakes from the electrochemical exfoliation process. As shown in the figure, a constant voltage difference of 20 V was applied to two graphite rod electrodes, which were placed 1 cm apart in an electrolysis cell filled with electrolyte (1% SDS in deionized water) to generate hydroxyl and oxygen radicals. The oxygen radicals corrode the graphite anode and thus create black sediments (graphene) in the solution due to the intercalation of anionic surfactant. It was observed that graphene sheets started to peel off from the anode after several minutes. The exfoliation process was continued for 2 h to obtain a stable graphene suspension in the SDS solution. The stable graphene suspension was centrifuged at 3000 rpm for 30 min to remove large agglomerates. Then, the supernatant portion of the suspension was decanted. The concentration of the centrifuged graphene was estimated from the weight of the suspension used. To prepare the PEO solution, 1 g of polyethylene oxide (PEO) (Mw = 1000 000 g mol^{-1}) was dissolved in 120 ml of deionized water. 5 ml of the graphene suspension was then mixed with 5 ml of the PEO solution to produce a polymer composite. The composite solution was dried in petri dishes at 56 °C to obtain a graphene/PEO thin film with 50 μm thickness.

Figure 2 shows the experimental setup of the proposed *Q*-switched TDFL using the fabricated graphene/PEO thin film as a passive *Q*-switcher. It consists of a 4 m long thulium-doped fiber (TDF), which is pumped by a 1552 nm laser via a 1550/2000 nm wavelength division multiplexer (WDM), an isolator, a graphene film based SA, and a 10 dB output coupler in a ring configuration. The SA is fabricated by using a tiny patch of the prepared film (2 × 2 mm^2) and sandwiching it between two FC/PC fiber connectors, after depositing index-matching gel onto the fiber ends. The insertion loss of the SA is measured to be around 3.5 dB at 1900 nm. The TDF used has core and cladding diameters of 9 μm and 125 μm respectively and Tm ion absorption of 27 dB m^{-1} at 793 nm. The high absorption allows the use of a short active gain medium. An isolator is used to ensure a unidirectional operation of the laser. The laser output is obtained via a 10 dB optical coupler located after the graphene based SA, which channels out about 10% of the oscillating light from the ring cavity. The optical spectrum analyser (OSA, Yokogawa, AQ6370B) is used for the spectral analysis of the *Q*-switched EDFL with a spectral resolution of 0.02 nm, whereas the oscilloscope (OSC, Tektronix, TDS 3052C) is used to observe the output pulse train of the *Q*-switched operation via a 460 kHz bandwidth photo-detector (Thor lab, PDA50B-EC). The total cavity length of the ring resonator is measured to be around 13.6 m.

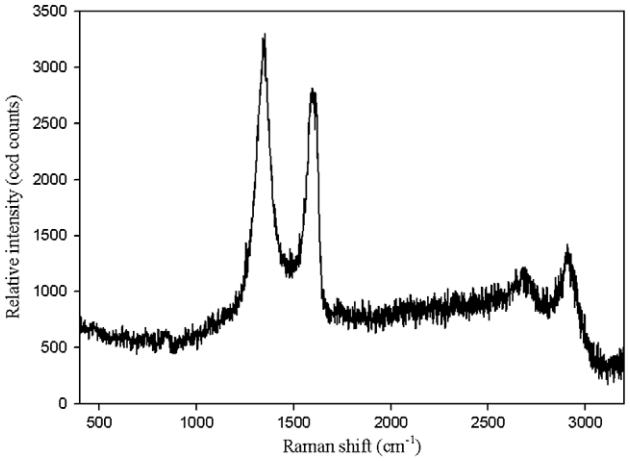

Figure 3. Raman spectrum obtained by 532 nm laser excitation on the graphene thin film, which indicates that the graphene has a multi-layer structure.

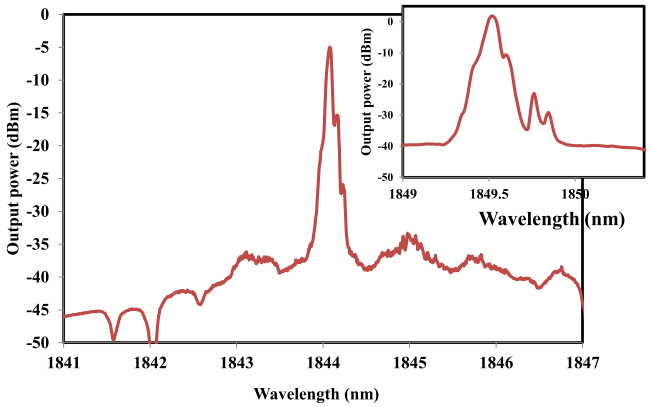

Figure 4. Output spectrum of the *Q*-switched laser.

3. Results and discussion

Raman spectroscopy was performed to confirm the presence of a graphene layer in the fabricated graphene thin film and the result is shown in figure 3. In the experiment, a 532 nm light source was used in conjunction with a charge-coupled device (CCD) camera as a detector with an exposure time of 10 s. As seen in figure 3, three prominent peaks are observed at approximately 1351 cm^{-1}, 1617 cm^{-1} and 2911 cm^{-1}, which are normally referred to as the D, G and 2D bands, respectively. The G band contributes to an E_{2g} mode of graphite and is related to the in-plane vibration of sp^2-bonded carbon atoms, while the D band is associated with the vibrations of carbon atoms with sp^3 electronic configuration of disordered graphite. The intensity ratio of the D and G bands of the graphene sheets is about 1.2, indicating the presence of defects in the graphene samples. The 2D Raman peaks change in shape, position and relative intensity with the number of graphene layers applied. The Raman spectroscopy reveals a broad 2D peak, which indicates the graphene has a multi-layer structure. In addition, we obtained a G/2D peak ratio of slightly larger than 2, which further confirmed that we had multi-layer graphene on the fabricated thin film.

Figure 4 shows the output spectrum of the *Q*-switched laser analyzed by an OSA with a resolution of 0.05 nm. In the absence of the SA in the cavity, the TDFL generates a CW laser as the pump power is set above the threshold value of 416 mW. The inset of figure 4 shows the output spectrum of the CW laser at the pump power of 416 mW, which operates at 1849.5 nm. Once the SA is inserted in the laser cavity, the laser starts to operate in a passive *Q*-switching operation as the pump power is adjusted to 513 mW. The pump threshold is relatively low compared to that of an SWNT or SESAM based *Q*-switched TDFL, mainly owing to a lower saturation intensity of the graphene. As seen in figure 4, the laser operates at wavelength 1844.1 nm with the full-width at half maximum of 0.05 nm limited by the OSA resolution and signal to noise ratio of about 29 dB. The threshold value is slightly higher and the operating wavelength shifts to a shorter wavelength by the incorporation of the SA due to the insertion loss of the SA. As the cavity loss increases, the oscillating laser shifts toward the peak absorption wavelength of the thulium fiber, which is near to 1800 nm to acquire more gain so that it can compensate the additional cavity loss.

Figure 5(a) shows the oscilloscope trace of the *Q*-switched pulse train when the pump power is fixed at the threshold value of 513 mW. There is no distinct amplitude modulation in each *Q*-switched envelope of the spectrum, which means that the self-mode locking effect on the *Q*-switching is weak. At 513 mW pump power, a stable passively *Q*-switching operation starts to occur with an average output power of 0.61 mW and a repetition rate of 6.73 kHz. The pulse energy is calculated to be around 90.64 nJ at this pump power. The pulse energy could be improved by reducing the insertion loss of the saturable absorber or by optimizing the laser cavity. Figure 5(b) shows the typical oscilloscope trace of the pulse envelope at the pump power of 513 mW. As seen in the figure, the full-width at half maximum or pulse width was obtained at 11.41 μs. Figure 6 shows the repetition rate and pulse width versus the pump power. Unlike a mode-locked fiber laser, where the repetition rate is dependent on cavity length, the repetition rate in a *Q*-switched fiber laser varies with pump power. As the pump power increases, more gain is provided to saturate the SA. Since pulse generation relies on saturation, the repetition rate increases with the pump power as shown in figure 6. When the pump power is tuned from 513 to 539 mW, the pulse train repetition rate varies from 6.73 to 24.16 kHz. On the other hand, the pulse width varies from 8.17 to 11.41 μs within the same pump power range. Further reduction in pulse width is expected when pump power increases to the point allowable by the damage threshold of the graphene based SA. A shorter cavity length using a higher dopant fiber would be an effective alternative for an even shorter pulse [23].

Figure 7 shows the average output power and pulse energy of the *Q*-switched TDFL as functions of pump power. The output power increases from 0.61 to 1.01 mW as the pump power is varied from 513 to 539 mW. On the other hand, the pulse energy reduces from 90.64 to 41.8 nJ as the pump power is increased within the same pump power range. These results indicate that graphene has great potential

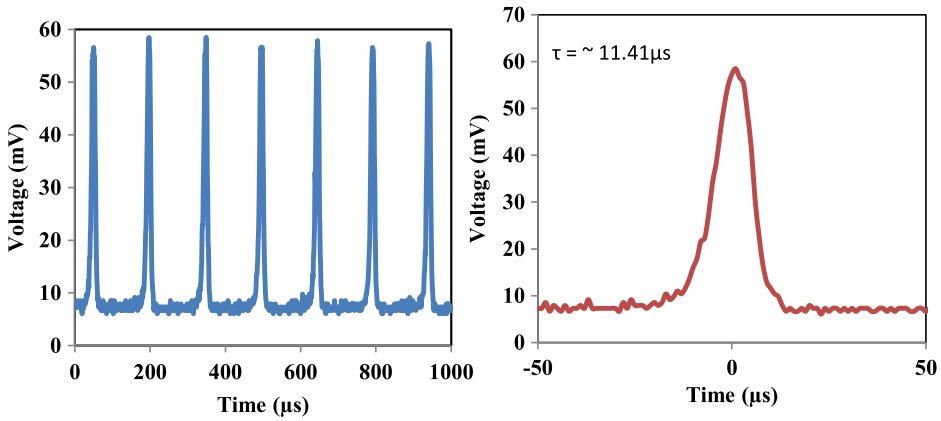

Figure 5. (a) The pulse train for the proposed TDFL with multi-layer graphene film based SA at threshold with the repetition rate of 6.73 kHz. (b) Enlarged pulse width spectrum with pulse width of 11.41 μs.

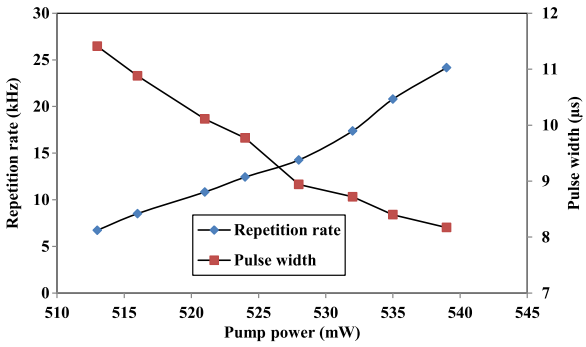

Figure 6. Repetition rate and pulse width as a function of pump power.

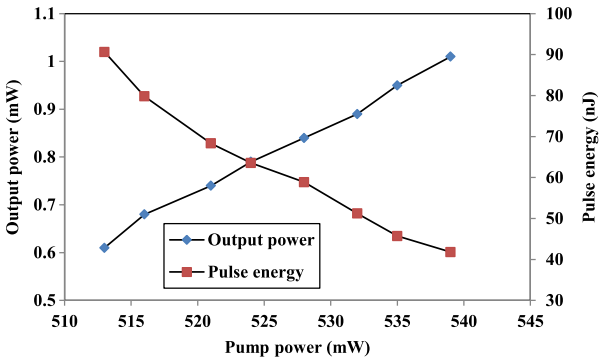

Figure 7. Output power and pulse energy versus pump power.

for superior *Q*-switching and saturable absorption compared to conventional light absorbing components when carefully employed in an appropriate laser system. The fabrication of the SA is also simple and thus the cost of the laser should be low. The simple and low cost laser is suitable for applications in metrology, environmental sensing and biomedical diagnostics.

4. Conclusion

A new all-fiber *Q*-switched ring TDFL is demonstrated based on 1552 nm pumping by employing a passive graphene thin film based SA. The graphene is fabricated via electrochemical exfoliation of graphite rod in electrolyte at room temperature and then mixed with polymer to form a free standing film with a thickness of 50 μm. The thin film is then attached to the end of a fiber ferrule with the aid of index-matching gel and connected with another clean fiber ferrule via an FC connector. The *Q*-switched TDFL has a threshold pump power of 513 mW with pulse-repetition-rate-tunable range of 6.73–24.16 kHz, and minimum pulse duration from 8.17 μs. The TDFL operates at around 1844.1 nm with an average output of 0.61 mW and maximum pulse energy of 90.64 nJ at the pump power of 513 mW. The proposed laser is expected to have many practical applications in fiber communications and sensors.

Acknowledgments

This project was funded by the Ministry of Higher Education under PRGS (Grant No. PR003-2011A) and HIRG (Grant No: UM.C/625/1/HIR/MOHE/SCI/29). B A Hamida would like to thank the International Islamic University of Malaysia for the postdoctoral fellowship.

References

[1] Koechner W 1996 *Solid-State Laser Engineering* 4th edn (Berlin: Springer)
[2] Skorczakowski M *et al* 2010 *Laser Phys. Lett.* **7** 498
[3] Andrés M V, Cruz J L, Díez A, Pérez-Millán P and Delgado-Pinar M 2008 *Laser Phys. Lett.* **5** 93
[4] Garnov S V *et al* 2007 *Laser Phys. Lett.* **4** 648
[5] Yang W, Hou J, Zhang B, Song R and Liu Z 2012 *Appl. Opt.* **51** 5664
[6] Harun S W, Ismail M A, Ahmad F, Ismail M F, Nor R M, Zulkepely N R and Ahmad H 2012 *Chin. Phys. Lett.* **29** 114202
[7] Ismail M A, Harun S W, Zulkepely N R, Nor R M, Ahmad F and Ahmad H 2012 *Appl. Opt.* **51** 8621

[8] Hasan T, Sun Z, Wang F, Bonaccorso F, Tan P H, Rozhin A G and Ferrari A C 2009 *Adv. Mater.* **21** 3874
[9] Bonaccorso F, Sun Z, Hasan T and Ferrari A C 2010 *Nature Photon.* **4** 611
[10] Zhang H, Tang D Y, Zhao L M, Bao Q L and Loh K P 2009 *Opt. Express* **17** 17630
[11] Popa D, Sun Z, Torrisi F, Hasan T, Wang F and Ferrari A C 2010 *Appl. Phys. Lett.* **97** 203106
[12] Luo Q, Wang J Z, Zhou M, Xu H Y, Cai Z P and Ye C C 2012 *Laser Phys. Lett.* **10** 229
[13] Sobon G, Sotor J and Abramski K M 2012 *Laser Phys. Lett.* **9** 581
[14] Jiang T M, Ma H F, Ren Z Y, Chen X M, Long J Y, Qi M, Shen D Y, Wang Y S and Bai J T 2013 *Laser Phys. Lett.* **10** 055103
[15] Zhang L Q, Zhuo Z, Wang J X and Wang Y Z 2012 *Laser Phys.* **22** 433
[16] Cao J, Wang H-Y, Luo A-P, Luo Z-C and Xu W-C 2012 *Laser Phys. Lett.* **9** 54
[17] Zhang L *et al* 2012 *Laser Phys. Lett.* **9** 888
[18] Luo Z Q, Zhou M, Weng J, Huang G M, Xu H Y, Ye C C and Cai Z P 2010 *Opt. Lett.* **35** 3709
[19] Yap Y K, De La Rue R M, Pua C H, Harun S W and Ahmad H 2012 *Chin. Opt. Lett.* **10** 041405
[20] Ismail M A, Ahmad F, Harun S W, Arof H and Ahmad H 2013 *Laser Phys. Lett.* **10** 025102
[21] Wang F, Torrisi F, Jiang Z, Popa D, Hasan T, Sun Z, Cho W and Ferrari A 2012 *Proc. Conf. Quantum Electronics and Laser Science*
[22] Jiang M, Ma H F, Ren Z Y, Chen X M, Long J Y, Qi M, Shen D Y, Wang Y S and Bai J T 2013 *Laser Phys. Lett.* **10** 055103
[23] Chen S *et al* 2011 *ACS Nano* **5** 1321

Thulium Bismuth Co-Doped Fiber Lasers at 1901 nm by 802 nm Pumping

Arindam Halder, N. Saidin, D. I. M. Zen, S. S. A. Damanhuri, Sulaiman Wadi Harun, Harith Ahmad, K. Dimyati, Mukul Chandra Paul, Shyamal Das, and S. K. Bhadra

***Abstract*—We demonstrate an efficient fiber laser operating at 1901.6 nm using a new Thulium Bismuth co-doped fiber (TBF) under 802 nm pumping. The TBF was fabricated using modified chemical vapor deposition process associated with optimized solution doping techniques. The TBF lasers at 1901.6 nm are obtained at a noticeably low threshold pump power of 75–92 mW using two fiber Bragg gratings in a Fabry–Perot cavity. The highest efficiency of 42.2% is achieved using a 0.4 m long TBF fiber with a core dopant concentrations (in wt%) of 0.35 Bi_2O_3, 0.9 Tm_2O_3, 3.0 Al_2O_3 and 4.0 GeO_2. Compared to the laser from a commercially available Thulium-doped fiber, the proposed laser has a significantly higher efficiency and lower threshold pump power. This is attributed to the incorporation of Bi ions in the gain medium which helps to increase the $^3F_4$ population through energy transfer processes. The maximum output power of 52.7 mW is achieved at the pump power of 195 mW.**

***Index Terms*—Chemical laser, Fabry–Perot resonators, laser.**

I. Introduction

LASERS in $\sim$2 μm spectral region have recently gathered interest for its various applications into the field of medicine, defense and spectroscopy [1]–[3]. Traditionally, these applications utilize holmium-doped crystalline YAG or YLF lasers which require cryogenic cooling or complex pumping schemes [4]. To overcome these issues, fiber lasers with kilowatt-level outputs at slightly shorter wavelengths (i.e., 1 to 1.5 μm) have been used as alternatives. 2 μm fiber laser can be achieved using either Thulium or thulium–holmium doped fibers as a gain medium [5], [6]. Thulium fiber has a broad emission in the wavelength range of 1650 to 2100 nm due to energy transition of $^3F_4 \rightarrow {}^3H_6$ and is suitable for lasing at 2 μm region.

Co-doping of Thulium with other elements such as Erbium, Ytterbium, Terbium and Bismuth has been demonstrated to improve the s-band amplification and 2 μm lasing of Thulium doped fiber (TDF). For instance, co-doping Thulium–Terbium in germanate glass was performed by Librantz *et al*. [7] to improve amplification in the 1450 nm region, i.e., s-band by depopulating F_4 via energy transfer process from Thulium to Terbium. Meanwhile, Braud *et al.* [8] capitalized the energy transfer from Ytterbium to Thulium to decrease the effective lifetime of F_4 level to generate the 1500 nm laser emission. In our earlier work, TBF was utilized to improve amplification at 1.9 μm region [9]. Besides cross relaxation process between thulium ions, TBF also provides effective energy transfer from bismuth to thulium ions that improves amplification efficiency at 1.9 μm region. Higher dopant concentration of Thulium ions can also be achieved in the co-doped fibers since clustering effect is suppressed by the presence of the co-doping ions.

Previously, many works have been reported on high power Thulium doped fiber laser (TDFL) and the Thulium-Holmium doped fiber laser utilizing double-clad fiber to achieve efficiency of around 47%–68% [10], [11]. However, there is still a lack of research works on core-pumping TDFL. In an earlier work, Geng *et al*. [12] demonstrated highly efficient diode-pumped fiber laser with 35% slope efficiency and 50 mW output power operating near 2 μm, which generated from a 2 cm long piece of highly Tm-doped germanate glass fiber pumped at 805 nm.

In this paper, an efficient TBFL operating at 1.9 μm region is experimentally demonstrated using a newly developed TBF as the gain medium for the first time. The co-doped fiber is obtained from optical preform, which was made using the conventional modified chemical vapor deposition (MCVD) process in conjunction with solution doping (SD) technique. The performance of the proposed TBFL is then compared with the one obtained using a commercial TDF. The advantage of the proposed TBFL is that it operates in eye-safe wavelength region with significantly lower pump power threshold compared to commercial TDF, where permissible free space transmission intensity can be several orders of magnitude greater than 1 μm. The novelty of this work lies on the use of core pumping silica fiber to produce a single mode laser output with high efficiency and low threshold by using a relatively short gain medium.

II. Fabrication and Characterization of the TBF

The TBF was fabricated from a lithium–alumino–germano–silicate core glass optical preform co-doped with Tm and Bi ions

Manuscript received November 22, 2013; revised January 2, 2014; accepted January 30, 2014. This work was supported in part by the Ministry of Higher Education under High Impact Research Grants UM.C/625/1/HIR/MOHE/SCI/29 and HIR000009–16001 and by the Department of Science and Technology and the Council of Scientific and Industrial Research (CSIR), Govt. of India. The work of A. Halder was supported by the CSIR through a research fellowship.

A. Halder, M. C. Paul, S. Das, and S. K. Bhadra are with the Fiber Optics and Photonics Division, CSIR-Central Glass and Ceramic Research Institute, Kolkata 700032, India (e-mail: arindam.cgcri@gmail.com; paulmukul@hotmail.com; dshyamal@cgcri.res.in; skbhadra88@gmail.com).

N. Saidin and S. S. A. Damanhuri are with the Department of Electrical and Telecommunication Engineering, University of Malaya, 50603 Kuala Lumpur, Malaysia (e-mail: insaidin@yahoo.com; sarah_damanhuri@yahoo.com).

D. I. M. Zen is with the Photonics Research Center, University of Technology, Malaysia, 81300 Skudai, Malaysia (e-mail: dimz_rmaf@yahoo.com).

S. W. Harun and H. Ahmad are with the Photonics Research Center, University of Malaya, 50603 Kuala Lumpur, Malaysia (e-mail: swharun@um.edu.my; harith@um.edc.my).

K. Dimyati is with the Department Electrical and Electronic Engineering, National Defense University of Malaysia, 57000 Kuala Lumpur, Malaysia (e-mail: kaharudin@upnm.ced.my).

Color versions of one or more of the figures in this paper are available online at http://ieeexplore.ieee.org.

Digital Object Identifier 10.1109/JSTQE.2014.2304420

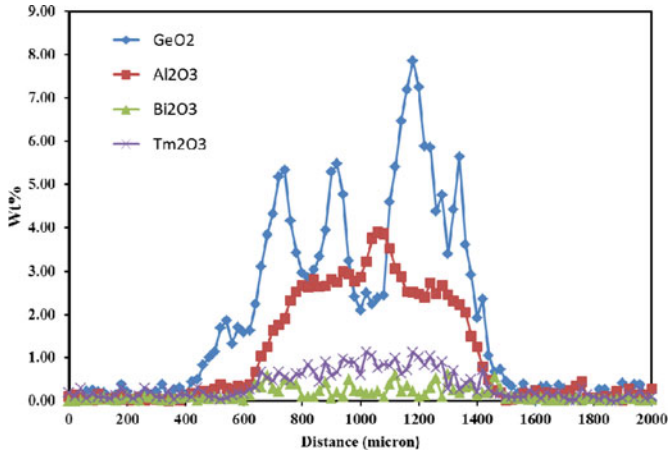

Fig. 1. EPMA plot of dopants showing a distribution of Bi_2O_3, Tm_2O_3, Al_2O_3, and GeO_2 for TB2 sample.

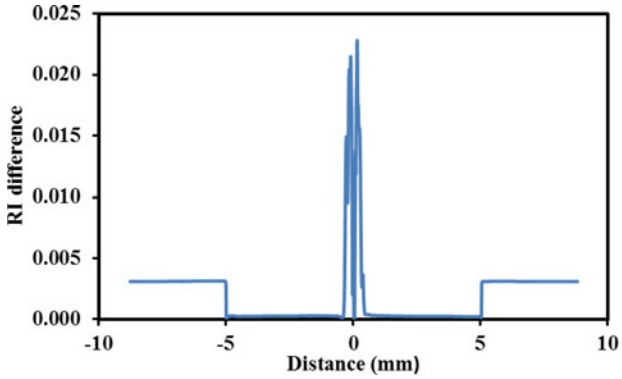

Fig. 2. Plot of RI profile for the TB2, Tm-Bi co-doped preform, which is used to fabricate TBF (TB2).

TABLE I
DOPING CONCENTRATION AND PHYSICAL CHARACTERISTICS OF THE FABRICATED TBF SAMPLES

Sample no.	Concentration of dopants into perform (wt %)	Core diameter	N.A
TB1	0.15 Bi_2O_3, 0.3 Tm_2O_3, 1.0 Al_2O_3 and 12.0 GeO_2	6.90 μm	0.21
TB2	0.35 Bi_2O_3, 0.9 Tm_2O_3, 3.0 Al_2O_3 and 4.0 GeO_2	7.20 μm	0.23
TB3	0.2 Bi_2O_3, 0.06 Tm_2O_3, 0.05 Al_2O_3 and 0.3 GeO_2	9.00 μm	0.14

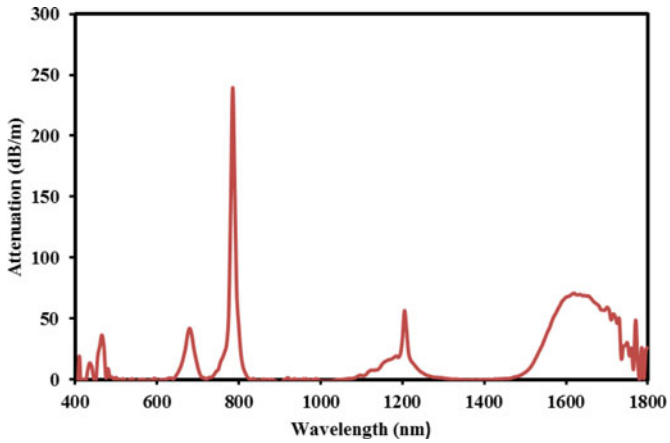

Fig. 3. Absorption spectrum of TB2 measured using a cut-back method.

using fiber drawing tower. The optical preform is fabricated through conventional MCVD process, followed by optimised SD technique. In the MCVD process, at first a pure silica glass tube with inner/outer diameter of 17/20 mm is mounted at lathe. Then the tube was collapsed by applying a high temperature of 2180 °C until its outer diameter reduces to ∼15 mm. After that a single porous unsintered SiO_2-GeO_2 soot layer is deposited inside a silica glass tube. The deposition process was carried out at temperature around 1420–1475 °C. Then the unsintered layer inside the tube was immersed into an alcoholic solution of $TmCl_3$, $Bi(NO_3)_3$, $Al(NO_3)_3$, $LiNO_3$ and 5∼% HNO_3 using a 'U' tube SD set up and kept for about 45 min to achieve uniform soaking. After the SD, the glass undergoes dehydration and oxidation processes at temperature around 900–1000 °C. The next process is sintering of the un-sintered layers by gradually increasing the temperature from 1500 to 2000 °C. After the oxidation and sintering processes, the tube is slowly collapsed to transform it into transparent optical preform. A spool of bare TBF sample coated with normal poly-acrylate resin for protection, is obtained by drawing of the preform at 2050 °C at fiber drawing tower.

Three TBF samples (TB1, TB2 and TB3) are fabricated for demonstration of TBFL operating at 1.9 μm region. Electron probe microscopic analysis (EPMA) is carried out for all samples to determine the dopant concentrations into the core glass. Fig. 1 shows the dopant concentration distribution plot obtained from the EPMA for TB2 preform sample. As shown in Fig. 1, the composition of the core-glass consists of Bi_2O_3, Tm_2O_3, Al_2O_3 and GeO_2. The dopant concentrations (in wt%) are 0.35 Bi_2O_3, 0.9 Tm_2O_3, 3.0 Al_2O3 and 4.0 GeO_2, which correspond to Bi and Tm ratio (Bi:Tm) of 1: 2.5. The contribution of Li_2O can't obtain by EPMA as it exists beyond the lower element limit of EPMA. Aluminium is used to increase the refractive index (RI) of the core compared to the cladding and to improve the solubility of the dopant material [8]. The profile of the fabricated preform was analyzed by a preform analyzer (model PKL2600, Photon Kinetics) and the generated RI profile is shown in Fig. 2. From the profile plot, the RI difference between the core and cladding can be obtained to calculate the numerical aperture (NA) of the fabricated fiber. A dip at the center of the RI profile can be observed which we believed to be affected the laser's performance. Single mode pump have the highest intensity in the middle of the core. If the RI profile of the fiber does not have the dip, the Tm^{3+} ions at the center of the core may interact with higher pump intensity producing higher intensity laser [13]. However, the imperfection leaves the Tm^{3+} ions populating outer regions of the core interacting with lower-intensity pump. The glitch may have cost us the laser efficiency. The details of the three samples are summarized in Table I.

The absorption spectrum of TB2 is also investigated using cut-back method and the result is shown in Fig. 3. The absorption bands of the TBF are obtained at 465, 680, 785, 1205, and

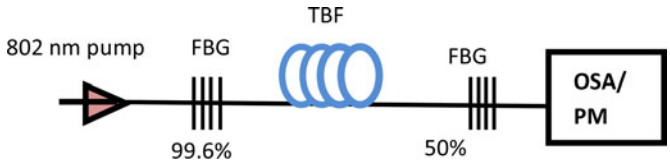

Fig. 4. Experimental setup for lasing experiments.

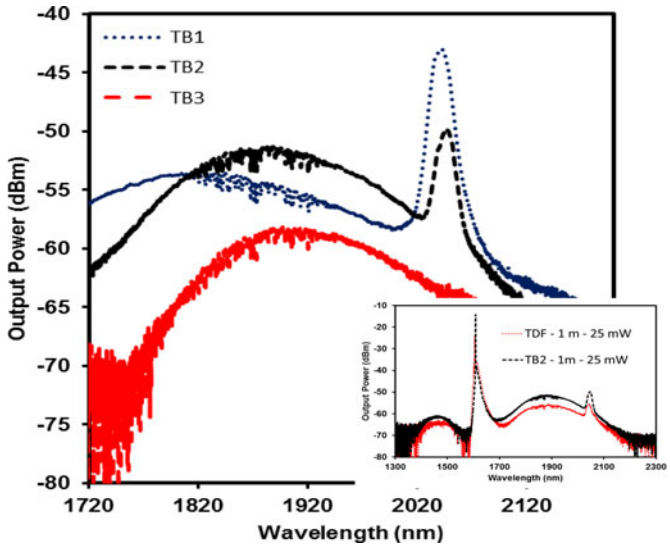

Fig. 5. ASE spectra for different TBF samples at the fixed 802 nm pump power of 25 mW. Inset shows the comparison of the ASE emission between TBF sample (TB2) and the commercial TDF.

1650 nm. It has peak attenuation of 239 dB/m at 785 nm, which is much higher than that of a commercial TDF. Since 785 nm pump laser is not commercially available, in this work, the 802 nm pump wavelength was used instead as it is the closest that we can get to 785 nm.

III. Experimental Setup

The configuration of the proposed 1.9 μm laser with the fabricated TBF as the gain medium is shown in Fig. 4. It employs two FBGs operating at the centre wavelength of 1901.6 nm to establish linear laser cavity. They have reflectivities of 99.6% and 50% with the corresponding 3 dB spectral width of 1.5 and 0.6 nm respectively. The TBF is pumped using a 802 nm laser diode at the 99.6% FBG port and the output laser is taken out from the 50% FBG port. The output spectrum and intensity of the laser are monitored by using an optical spectrum analyzer (OSA) and power meter (PM) respectively. The performance of the 1.9 μm fiber laser is also investigated by replacing the TBF with a commercial Thulium-doped fiber (Nufern, TDF) for comparison. The core diameter of the commercially available TDF is 9 μm while its NA and Thulium ion concentration are 0.15 and 0.25 wt.% accordingly.

IV. Results and Discussion

The ASE spectra of TB1, TB2 and TB3 samples under 802 nm excitations are investigated and the result is summarized in Fig. 5. In the experiment, the pump power and TBF length were

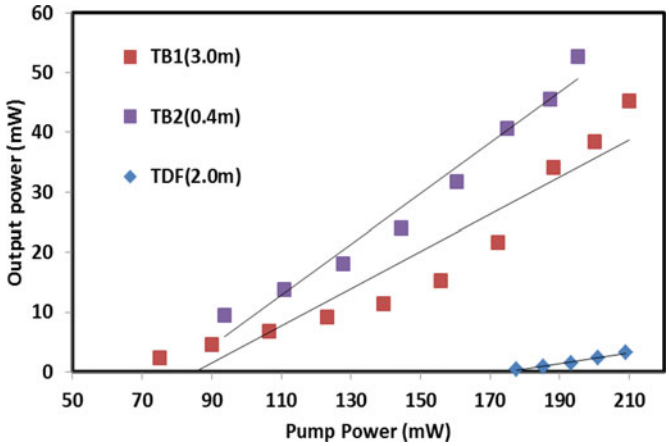

Fig. 6. Performance comparison for three different gain media of TB1, TB2, and TDF.

fixed at 25 mW and 1 m, respectively. As shown in Fig. 5, an apparent emission of the Tm: $^3F_4$ to $^3H_6$ transition at 1900 nm is observed for all TBF samples. It is also observed that TB2 exhibits the highest ASE power emission of around -51.6 dBm having centre at 1881 nm region. This is due to the high Tm^{3+} concentrations in the fiber compared with other samples as indicated in Table I. The peak ASE powers of TB1 and TB3 are obtained at -54.2 and -58.7 dBm, respectively. With TB2 as the gain medium, the 3 dB bandwidth of the ASE spectrum covers from 1801 to 1962 nm while 10 dB bandwidth covers the range from 1724 to 2076 nm as depicted in Fig. 5. Another peak observed at 2050 nm region is associated with the characteristics of the 802 nm source pump that exists even without the use of the gain medium. Inset of Fig. 5 compares the ASE of TB2 with the commercial TDF (Nufern) under 802 nm excitation when the fiber length and pump power are fixed at 1 m and 25 mW, respectively. As shown in the inset figure, both fibers generate almost similar ASE spectrum centred at 1880 nm. With the TBF, the ASE spectrum is higher by 5 dB compared to that of the commercial TDF. This is attributed to the Thulium ion concentration, which is higher in TB2 (0.9 wt%) compared to the TDF, which has a Thulium ion concentration of around 0.25 wt%. The observed emission at 1470 nm is appeared due to the active Bi: $^3P_1$ to $^3P_0$ transition as shown in the inset of Fig. 5. This confirms the occurrence of the energy transfer from active Bi to Tm^{3+} ions.

The lasing experiments were carried out for all TBF samples and the commercial TDF. The lasing was achieved at 1.9 μm for all fibers except for TB3. The optimized fiber lengths for TB1, TB2 and TDF are 3.0, 0.4, and 2.0 m, respectively for maximum efficiency of the laser generation. The experiment has been carried out using several other TDF lengths pumped by 802 nm wavelength excitation with the maximum input power of 200 mW, however no lasing has been observed due to insufficient pump to reach the threshold power. Fig. 6 shows the relationship of the output power against the pump power at the optimized fiber lengths for three different gain media (TB1, TB2 and TDF). As seen in the figures, the slope efficiencies of 31.0, 42.2 and 9.0% are obtained for the laser of TB1, TB2 and

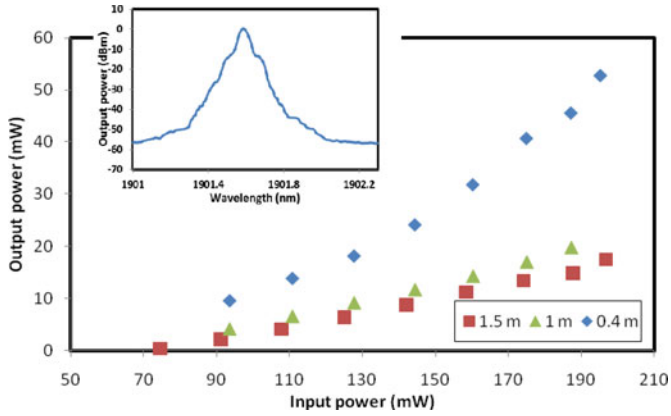

Fig. 7. Output power of the proposed TBFL against the pump power at different TBF (TB2) lengths. Inset shows the attenuated output spectrum of the laser at the maximum pump power.

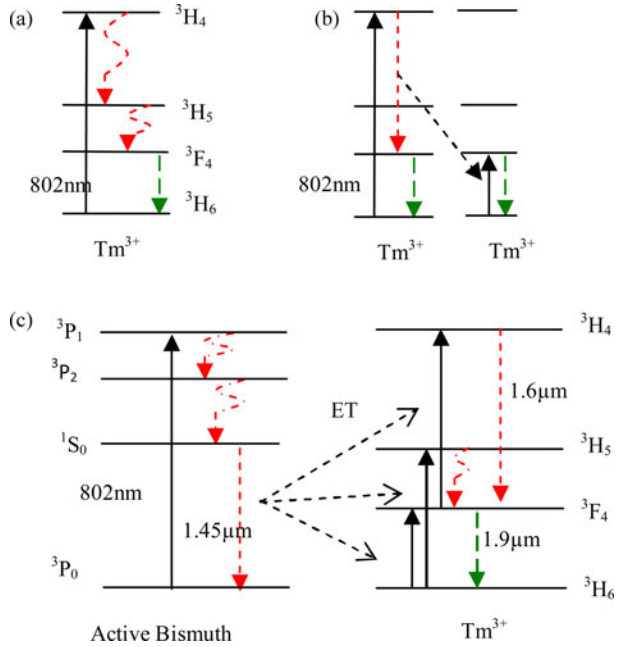

Fig. 8. Three possible energy transitions in TBF under 792 nm pumping involving (a) only $Tm3^{+}$, (b) cross relaxation between Tm^{3+}, and (c) energy transfer from Bi^{3+} to Tm^{3+}.

TDF, respectively. Compared to the TDF, both TBFs produce laser with a higher efficiency at a significantly lower threshold pump power. The threshold pump power for both TBFLs are observed to be around 75–92 mW, which is much lower than the threshold pump power of the TDFL (177 mW). The optimum length is so much shorter for TB2 compared to that of TB1 since the Thulium ion concentration in TB2 is 3 times as high. High thulium doping concentration in TB2 increases the efficiency of stepwise energy transfer such that the optimum length for lasing is comparatively shorter. To avoid clustering from the high concentration of rare earth ion, aluminium is added as host modifiers [14]. It also helps to reduce phonon energy of the core glass in the fiber, thus increases the probability of radiative emission and improves lasing efficiency.

Fig. 7 shows the relationship of the output power against the pump power at different TBF lengths. The figure shows that the efficiency of the laser increases from 13.7% to 42.2% as the length of the gain medium reduces from 1.5 to 0.4 m. At the optimal length of 0.4 m a maximum output power of 52.7 mW is achieved at the pump power of 195 mW. The proposed laser performance is higher by 7% in efficiency and 2.7 mW higher in output power in comparison to the work of Geng *et al*. [12]. Inset of Fig. 7 shows the attenuated output spectrum of the TBFL at the optimum length of 0.4 m when the 802 nm pump is fixed at 195 mW. The laser operates at 1901.6 nm, which corresponds to the center wavelength of both FBGs. Its signal to noise ratio is more than 50 dB while its 3 dB bandwidth is less than 0.02 nm (limited by the OSA resolution). It is also observed that the peak wavelength of the residual pump (802 nm) is about 17 dB lower than the peak power of the lasing wavelength (1901.6 nm). This indicates that the output power measured by a PM is mainly contributed by the lasing wavelength. The efficiency of the laser is observed to drastically decrease as the TBF length reduces below 0.4 m. In addition, the ratio of residue pump/output power is approximately 0.58 at 0.4 m. As the fiber length becomes shorter, it is observed that the residual pump power is higher than the peak laser power.

By pumping the TBF, both thulium and active bismuth ions are excited to the upper level. As shown in Fig. 8(a), thulium ion will be excited to $^3H_4$ level as it absorbs the pump photon. Then it decays non-radiatively twice so that it can occupy the $^3F_4$ level that has longer lifetime. From the $^3F_4$ level it will drop to the ground state ($^3H_6$) while emitting at 1.9 μm. Since the thulium ion doping concentration in this fiber is relatively high, Tm-Tm cross relaxation may occur [see Fig. 8(b)]. Thulium ion in ground state absorbs 802 nm photons such that it is elevated to $^3H_4$ level. When the ion in this level de-excites to $^3F_4$, instead of emitting at 1.47 μm, the energy is transferred to nearby thulium ion. The ion that resides in the ground state absorbs the donated photon to occupy the upper $^3F_4$ level which acts as metastable laser level. Both ions then drop to the ground state while emitting the 1.9 μm photons. With each absorbed pump photon, two 1.9 μm photons are produced, as shown in Fig. 8(b). On the other hand, active bismuth ion absorbs the pump photon in order to occupy the excited state of $^1S_0$. The Bismuth ion then decays irradiatively while dropping to $^3P_1$ level. From the $^3P_1$ level the ion will descend to ground state and emits at 1.45 μm. Fig. 8(c) demonstrates three possible energy transfer mechanism that may occur in this fiber. As the bismuth ion drops to the ground state from $^3P_1$ state, it donates its energy to a nearby thulium ion. The thulium ion got elevated from the ground state to $^3F_4$ level before it emits at 1.9 μm. The second possible transition is, the thulium ion is excited from $^3H_6$ to $^3H_5$ level instead, only then it will relax non-radiatively to $^3F_4$ level. The ion will de-excite to ground state emitting at 1.9 μm. The final possible electronic transition is for the nearby thulium ion from $^3F_4$ to $^3H_4$. The ion then drops to $^3F_4$ level while emitting at 1.47 μm. Two out of three energy transfer process help to increase the $^3F_4$ population and thus improves the laser efficiency compared to the conventional TDFA.

Compared to the TDFL, the proposed TBFL has shown a significantly higher efficiency due to various factors such as doping concentration and the assistance from cross relaxation and energy transfer process. The thulium ion concentration is higher in the TBF (0.90 wt.% in TB2) than the TDF, which has a Thulium ion concentration of around 0.25 wt%. The higher dopant density is possible due to the incorporation of Bismuth ions in the fiber. The Bi ions also help to increase the $^3F_4$ population and thus improve the efficiency of the laser through energy transfer processes. As also shown in Fig. 7, the pump power threshold for the proposed laser is around 92 mW for 1 m and 0.4 m TB2. As the longer length is used (1.5 m), the lower threshold 75 mW is obtained. This is due to the higher population inversion at low pump power for the longer TBF. In general, these thresholds are significantly lower than that of the TDFL, which is around 177 mW. The incorporation of active bismuth ions improves the population inversion by the energy transfer process. Other TDF lengths failed to exhibit any laser radiation. Failure to generate any laser at the other TDF lengths was due to insufficient input pump power to excite enough Tm^{3+} ions to the upper state level so that it can create a sufficient population inversion to compensate all the losses in the cavity. The performance of both TBFL and TDFL in terms of threshold and efficiency is expected to improve significantly where the pump operated at the optimum wavelength of 785 nm. The proposed TBFL could be scaled up in power if higher input pump power in 785 nm is available and better heat management is taken into account.

V. Conclusion

An efficient TBFL is demonstrated using a newly developed TBF under 802 nm pumping. The laser operates at 1901.6 nm with a lasing efficiency of 42.2% using 0.4 m long TBF with core dopant concentrations (in wt.%) of 0.35 Bi_2O_3, 0.9 Tm_2O_3, 3.0 Al_2O_3 and 4.0 GeO_2 in conjunction with a Fabry-Perot cavity with two FBGs. The efficiency is higher than that of the conventional TDFL due to the incorporation of Bi ions in the gain medium, which help to increase the $^3F_4$ population. It is found that the pump power threshold of the proposed TBFL is significantly lower (75–92 mW) compared to the laser with a commercial TDF. The maximum output power of 52.7 mW is achieved at the pump power of 195 mW.

References

[1] J. Wu, Z. Yao, J. Zong, and S. Jiang, "Highly efficient high-power thulium-doped germanate glass fiber laser," *Opt. Lett.*, vol. 32, pp. 638–640, 2007.

[2] S. W. Harun, N. Saidin, S. S. A. Damanhuri, H. Ahmad, A. Halder, M. C. Paul, S. Das, M. Pal, and S. K. Bhadra, "Fiber laser at 2 micron region using double-clad thulium/ytterbium co-doped yttria-aluminosilicate fiber," *Laser Phys. Lett.*, vol. 9, pp. 50–53, 2012.

[3] J. Geng, J. Wu, S. Jiang, and J. Yu, "Efficient operation of diode-pumped single-frequency thulium-doped fiber lasers near 2 μm," *Opt. Lett.*, vol. 32, pp. 355–357, 2007.

[4] P. A. Budni, L. A. Pomeranz, M. L. Lemons, C. A. Miller, J. R. Mosto, and E. P. Chicklis, "Efficient mid-infrared laser using 1.9-μm-pumped Ho:YAG and ZnGeP2 optical parametric oscillators," *J. Opt. Soc. Amer. B*, vol. 17, pp. 723–728, 2000.

[5] Z. Zhang, A. J. Boyland, J. K. Sahu, W. A. Clarkson, and M. Ibsen, "High-Power single-frequency thulium-doped fiber DBR laser at 1943 nm," *IEEE Photon. Technol. Lett.*, vol. 23, no. 7, pp. 417–419, Apr. 2011.

[6] R. Gumenyuk, I. Vartiainen, H. Tuovinen, and O. G. Okhotnikov, "Dissipative dispersion-managed soliton 2 μm thulium/holmium fiber laser," *Opt. Lett.*, vol. 36, pp. 609–611, 2011.

[7] A. F. H. Librantz, L. Gomes, G. Pairier, S. J. L. Ribeiro, and Y. Messaddeq, "Tm and Tm–Tb-doped germanate glasses for S-band amplifiers," *J. Luminescence*, vol. 128, pp. 51–59, 2008.

[8] A. Braud, S. Girard, J. L. Doualan, M. Thuau, R. Moncorge, and A. M. Tkachuk, "Energy-transfer processes in Yb:Tm-doped KY3F10, LiYF4, and BaY2F8 single crystals for laser operation at 1.5 and 2.3 μm," *Phys. Rev. B*, vol. 61, pp. 5280–5292, 2000.

[9] H. Fatehi, S. D. Emami, A. Zarifi, F. Z. Zahedi, S. E. Mirnia, A. Zarei, H. Ahmad, and S. W. Harun, "Analytical model for broadband thulium-bismuth-doped fiber amplifier," *IEEE J. Quantum Electron.*, vol. 48, no. 8, pp. 1052–1058, Aug. 2012.

[10] J. Wu, Z. Yao, J. Zong, and S. Jiang, "Highly efficient high-power thulium-doped germanate glass fiber laser," *Opt. Lett.*, vol. 32, no. 6, pp. 638–640, 2007.

[11] S. D. Jackson, A. Sabella, and D. G. Lancaster, "Application and development of high-power and highly efficient silica-based fiber lasers operating at 2 μm. selected topics in quantum electronics," *IEEE J. Sel. Topics Quantum Electron.*, vol. 13, no. 3, pp. 567–572, May/Jun. 2007.

[12] J. Geng, J. Wu, S. Jiang, and J. Yu, "Efficient operation of diode-pumped single-frequency thulium-doped fiber lasers near 2 μm," *Opt. Lett.*, vol. 32, no. 4, pp. 355–357, 2007.

[13] S. Emami, H. Abdul-Rashid, H. Ahmad, A. Ahmadi, and S. Harun, "Effect of transverse distribution profile of thulium on the performance of thulium-doped fibre amplifiers," *Ukr. J. Phys. Opt*, vol. 13, pp. 74–81, 2011.

[14] W. Blanc, T. L. Sebastian, B. Dussardier, C. Michel, B. Faure, M. Ude, and G. Monnom, "Thulium environment in a silica doped optical fibre," *J. Non-crystalline Solids*, vol. 354, no. 2, pp. 435–439, 2008.

Arindam Halder received the M.Sc. degree in chemistry from the University of Calcutta, Kolkata, India, in 2009. He is currently working toward the Ph.D. degree at Fiber Optics and Photonics Division, CGCRI, Kolkata. His current research interests include development of nano-engineering glass-based rare-earths-doped optical fiber for fiber laser at VIS and NIR regions.

N. Saidin received the B.E. and M.Sc. engineering degrees from the University of Malaya, Kuala Lumpur, Malaysia, in 2005 and 2010, respectively, where she is currently working toward the Ph.D. degree with the Photonics Research Center. She is also a Lecturer with the Department of Computer and Communication Engineering, International Islamic University Malaysia, Selangor, Malaysia.

D. I. M. Zen received the B.E. degree in electrical engineering from the University of Technology, Malaysia, Johor, Malaysia, in 2002, where he is currently working toward the M.Eng.Sc. degree with the Photonics Research Center. He is also an Engineering Officer with the Royal Malaysian Air Force.

S. S. A. Damanhuri received the B.E. degree in telecommunication engineering from the University of Malaya, Kuala Lumpur, Malaysia, in 2010, where she is currently working toward the M.Eng.Sc. degree.

Sulaiman Wadi Harun received the B.E. degree in electrical and electronics system engineering from the Nagaoka University of Technology, Nagaoka, Japan, and the M.Sc. and Ph.D. degrees in photonics from the University of Malaya, Kuala Lumpur, Malaysia, in 1996, 2001, and 2004, respectively. He is currently a Full Professor with the Faculty of Engineering, University of Malaya. His current research interests include fiber optics, active and passive devices.

Harith Ahmad received the Ph.D. degree in laser technology from the University of Swansea, Swansea, U.K., in 1983. He is currently a Full Professor with the Photonics Research Center in the University of Malaya, Kuala Lumpur, Malaysia.

K. Dimyati received the B.Eng. (Hons.) degree in electrical engineering, University of Malaya, Kuala Lumpur, Malaysia, in 1992, and the Ph.D. degree in photonics from the University of Wales Swansea, Swansea, U.K., in 1996. He is currently a Full Professor with the Faculty of Electrical and Electronic Engineering, National Defense University of Malaysia, Kuala Lumpur, Malaysia. His current research interests include wireless communications, optical communications, and coding theory.

Mukul Chandra Paul received the M.Sc. degree in inorganic chemistry from the University of Burdwan, Bardhaman, India, in 1989, and the Ph.D. degree in the field of development of radiation sensitive fibers for evaluation of their radiation response behavior at room temperature from the Central Glass and Ceramic Research Institute (CGCRI), Kolkata, India, in 2003. Since 1997, he has been a Research Scientist with the Fiber Optics and Photonics division of CGCRI. He has published more than 100 scientific articles in journals and conference proceedings as author and coauthor, and holds four U.S. patents on fabrication of rare-earth doped fibers. His current research interests include suitable crystalline host based PS fibers for writing FBGs and advanced rare earth doped nano-engineering host based optical fibers for high power fiber laser and up-conversion laser. Metal and transition elements doped nano-crystalline fiber for low-threshold super-continuum generation. Dr. Paul is a member of Optical Society of America and a life member of Material Research Society of India and Indian Ceramic Society. He is Editorial Board Member of the *New Journal of Glass And Ceramics*.

Shyamal Das received the B.E. and M.E. degrees in chemical engineering from Jadavpur University, Kolkata, India. He has nearly five years research experience in the field of sol gel processing. He joined the Fiber Optics and Photonics Group, Central Glass and Ceramic Research Institute, Kolkata, India, in 2006. Since then he is working on fabrication of radiation sensitive fiber, Er-doped fiber, large flattened mode fiber, thulium-doped fiber and specialty optical fiber.

S. K. Bhadra is currently a Senior Scientist at Central Glass and Ceramic Research Institute, Kolkata, India, working in the advanced areas of fiber optics. He is coordinating various national and international research projects. He has published a number of papers in international repute journals. He had four national and international patents in the last couple of years. He had been invited by international forums abroad for delivering lectures in different occasions. Dr. Bhadra became a member of the Executive Council of the Optical Society of India in 2006 and an Honorary Editor of the *Journal of Transaction Indian Ceramic Society*.

IEEE Photonics Journal
An IEEE Photonics Society Publication

1880-nm Broadband ASE Generation With Bismuth–Thulium Codoped Fiber

Volume 4, Number 6, December 2012

A. Halder
M. C. Paul
S. W. Harun
S. M. M. Ali
N. Saidin
S. S. A. Damanhuri
H. Ahmad
S. Das
M. Pal
S. K. Bhadra

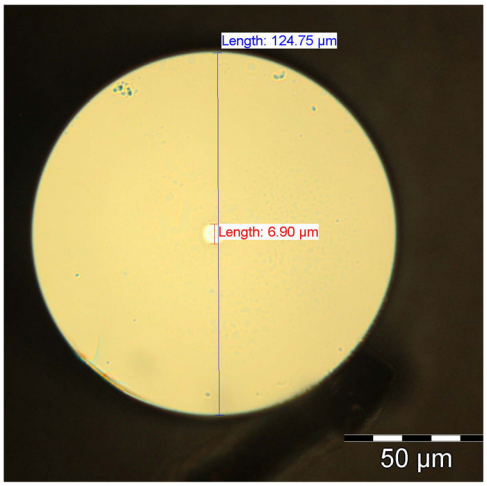

DOI: 10.1109/JPHOT.2012.2221691
1943-0655/$31.00 ©2012 IEEE

IEEE photonics SOCIETY
IEEE

1880-nm Broadband ASE Generation With Bismuth–Thulium Codoped Fiber

A. Halder,[1] M. C. Paul,[1] S. W. Harun,[2,3] S. M. M. Ali,[2] N. Saidin,[2] S. S. A. Damanhuri,[2] H. Ahmad,[3] S. Das,[1] M. Pal,[1] and S. K. Bhadra[1]

[1]Fiber Optics and Photonics Division, Central Glass & Ceramic Research Institute, CSIR, Kolkata, India
[2]Department of Electrical Engineering, Faculty of Engineering, University of Malaya, 50603 Kuala Lumpur, Malaysia
[3]Photonic Research Center, University of Malaya, 50603 Kuala Lumpur, Malaysia

DOI: 10.1109/JPHOT.2012.2221691

Manuscript received June 26, 2012; revised September 24, 2012; accepted September 25, 2012. Date of publication October 10, 2012; date of current version November 27, 2012. This work was supported by the Department of Science and Technology of the Government of India. The work of A. Halder was supported by the Council of Scientific and Industrial Research, India, under a CSIR-research fellowship. The work of S. W. Harun was supported by the University of Malaya under the HIR Grant D000009-16001.
Corresponding author: S. W. Harun (e-mail: swharun@um.edu.my).

Abstract: A broadband amplified spontaneous emission (ASE) generation in 1880-nm region is demonstrated by employing a newly developed single-mode Tm–Bi codoped fiber (TBF) in conjunction with 793-nm pumping for the first time. The TBF was obtained by drawing a preform, which was fabricated using a deposition of porous layer by the modified chemical vapor deposition (MCVD) process in conjunction with solution doping technique. The highest Bi^{3+} and Tm^{3+} concentrations of 0.35 wt.% and 0.9 wt.%, respectively, were successfully achieved to generate ASE centered at 1880-nm region. The ASE peaked at −47.2 dBm with 3-dB spectral width ranging from 1817 to 1984 nm with 1.0-m-long TBF and 200-mW 793-nm pump power, which was generated due to the transition of thulium ions from $^3F_4$ to $^3H_6$ with some assistance from bismuth to thulium ion energy transfer. The use of a secondary pump of 1550 nm is also shown to improve the ASE generation.

Index Terms: Bismuth–thulium codoped fiber, modified chemical vapor deposition (MCVD), 1.8-micron ASE source.

1. Introduction

Fiber amplified spontaneous emission (ASE) light has a broadband spectrum and can be thus used as a broadband light sources. It is developed using the emission characteristics, which depend on the energy structure of dopant ions in the glass host and pumping wavelength. The pump laser energizes the dopant ions so that spontaneously emitted light from one ion propagates along the fiber where it is amplified by the gain properties of the fiber and emitted as the ASE. Light is emitted in both forward and backward directions, relative to pump direction, but the backward ASE, or counter-pumped direction, has a higher quantum efficiency and is normally selected as the source output. Unlike lasers, ASE sources do not rely on optical feedback, and thus, the full-width half-maximum (FWHM) bandwidth of the backward ASE is generally very broad, typically greater than 10 nm. The most common fiber ASE source comprises a single-mode pump that energizes a length of Er-doped single-mode silica fiber, typically in tens of meter, to emit at 1550 nm [1], [2]. Recently, ASE sources operating around mid infrared spectral region have gained tremendous interest for possible applications in spectroscopy, gas sensing, low-coherence interferometer, and medical imaging via optical coherence tomography. Currently, commercial light-emitting diodes (LEDs) and semiconductor lasers operating

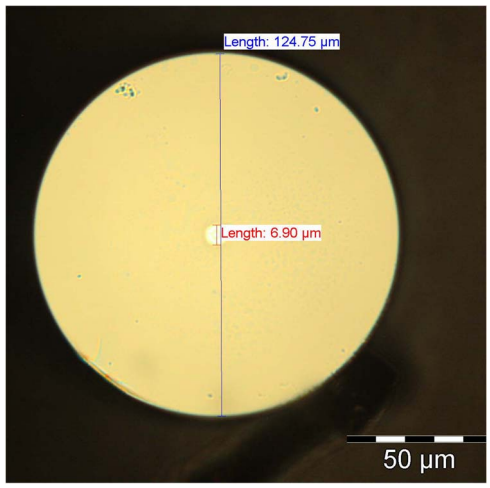

Fig. 1. Cross-sectional view of TB-a sample.

in mid-infrared region are normally used for these applications. However, the main drawbacks of these sources are its stability, which is strongly dependent on temperature, high coupling loss when connected to standard single mode fibers, and fabrication cost.

Thulium and thulium–holmium doped fibers have been demonstrated to be prospective candidates for laser systems operating at around 1900 nm [3], [4]. thulium fiber has a broad ASE between 1650 nm and 2100 nm from transition of $^3F_4 \rightarrow {}^3H_6$ and is therefore suitable to be a broadband ASE source. In this paper, ASE generation in the 1900-nm waveband is demonstrated using a Tm–Bi codoped fiber (TBF) as a gain medium for the first time. The TBF is obtained by drawing a preform, which was fabricated using a deposition of porous layer by the modified chemical vapor deposition (MCVD) process in conjunction with solution doping technique.

2. Fabrication and Characterization of Tm–Bi Codoped Optical Fiber

The Tm and Bi codoped lithium-alumino-germano-silicate (LAGS) core glass optical preform was fabricated by the MCVD process, followed by solution doping technique. A pure silica glass tube with outer/inner diameter of 20/17 mm was used for deposition of a single porous unsintered SiO_2-GeO_2 soot layer to make the preform while maintaining a suitable deposition temperature at around 1420 °C–1475 °C with the help of a single-wavelength online IR Pyrometer with an accuracy of ±5 °C. Before the deposition of the unsintered layer, the outer diameter of the tube was reduced to 15 mm by using a standard collapsing technique at a temperature around 2180 °C. This step reduced the inner surface of the tube as well, and thus, it helped reduce the loss of bismuth glass due to the thermal decomposition reaction of Bi_2O_3 at the time of collapsing. It is reported that Bi_2O_3 molecules are converted to volatile BiO and move out of the deposited core layer during sintering and collapsing [5]. Then, an alcoholic solution of $TmCl_3$, $Bi(NO_3)_3$, $Al(NO_3)_3$, $LiNO_3$, and 5∼% HNO_3 was used to soak the porous layer with for about 45 min to achieve efficient doping. After the completion of solution soaking, dehydration and oxidation processes were performed at temperature around 900 °C–1000 °C. Sintering of unsintered layers was carried out using the conventional MCVD technique by slowly increasing the temperature from 1500 °C to 2000 °C. Following the completion of sintering as well as oxidation, the tube was slowly collapsed to transform it into optical preform. The fabricated preform was then drawn at temperature of 2050 °C into a spool of optical bare fiber before it was coated with a low refractive index (1.379) polymer resin.

Three TBF samples (TB-a, TB-b, and TB-c) were fabricated for the broadband ASE generation at 1900-nm region. The cross-sectional view of one of the TBF sample (TB-a) is shown in Fig. 1. As shown in the figure, it has a circular cladding with the core and cladding diameters of 6.90 μm and 124.75 μm, respectively. The distribution pattern of dopants inside the core of the fiber is also

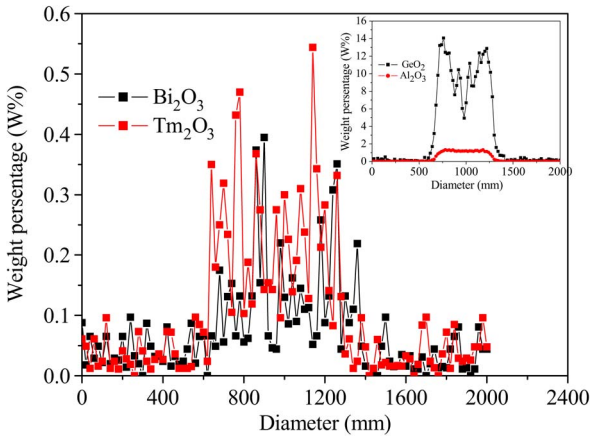

Fig. 2. EPMA plot of dopants showing a distribution of Bi_2O_3 and Tm_2O_3 for TB-a sample. Inset shows the distribution of Al_2O_3 and GeO_2.

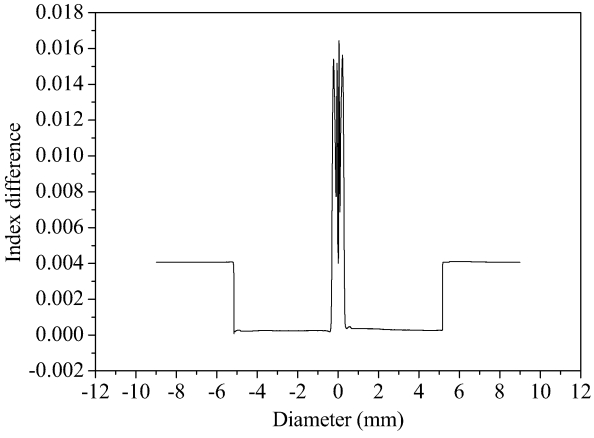

Fig. 3. A plot of RI profile for the Tm–Bi codoped preform, which is then used to fabricate TB-a.

investigated for all samples. Fig. 2 shows the distribution plot obtained from the electron probe microscopic analysis (EPMA) for TB-a. As shown in Fig. 2, the dopant concentrations (in wt.%) and compositions inside the core for TB-a are 0.15 Bi_2O_3, 0.3 Tm_2O_3, 1.0 Al_2O_3, and 12.0 GeO_2, which correspond to Bi and Tm ratio (Bi:Tm) of 1 : 2. The profile of the fabricated preform was also analyzed by a preform analyzer (PKL 2600, Photon Kinetics, USA), and the generated refractive index profile is shown in Fig. 3. From the profile plot, the RI difference between the core and cladding can be obtained to calculate the numerical aperture (NA) of the fabricated fiber. The characteristic details of the three samples are summarized in in Table 1.

3. ASE Characteristics

The proposed ASE source consists of a piece of 1-m-long TBF sample, which is forward pumped by a 793-nm laser diode at 200-mW pump power. In the experiment, 793-nm pump laser was used because it operates at one of the most efficient Tm^{3+} and Bi^{3+} absorption wavelength. Furthermore, it is easily available and cheap. The ASE emission was investigated for three different fabricated samples, as shown in Fig. 4. As seen in the figure, all three fibers emit broadband ASE at 1880-nm region. This is attributed to the 973-nm pumping, which excites both Tm^{3+} and Bi^{3+} from the ground

TABLE 1

The doping concentration and physical characteristics of the fabricated TBF samples

Sample no.	Concentration of dopants into performs (Wt%)	Core diameter	N.A.
TB-a	0.15 Bi_2O_3, 0.3 Tm_2O_3, 1.0 Al_2O_3 and 12.0 GeO_2	6.9 μm	0.21
TB-b	0.35 Bi_2O_3, 0.9 Tm_2O_3, 3.0 Al_2O_3 and 4.0 GeO_2	7.2 μm	0.23
TB-c	0.2 Bi_2O_3, 0.06 Tm_2O_3, 0.05 Al_2O_3 and 0.3 GeO_2	9.0 μm	0.14

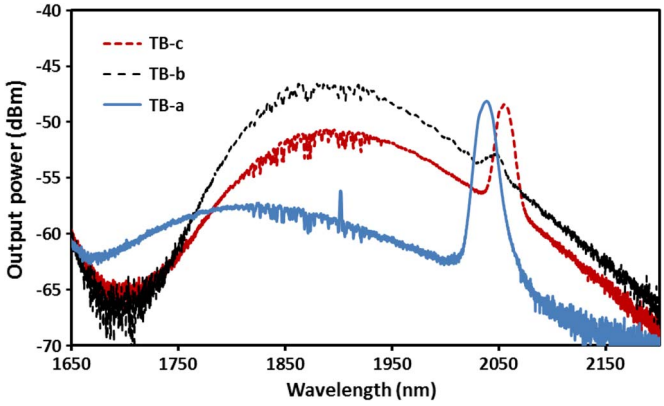

Fig. 4. ASE spectra at different TBF samples at the fixed 793-nm pump power of 200 mW.

state to the higher energy levels of $^3H_4$ and $^1S_0$, respectively. Then, the Tm^{3+} ions decay to $^3F_4$ to create a population inversion between $^3F_4$ and $^3H_4$ levels of the Tm^{3+}, which generates spontaneous emission at around 1900-nm region. After a fast decay into $^3P_2$ then to $^3P_1$ level, the Bi^{3+} ions transfer their energy to the Tm^{3+} ions via multipolar interactions. Immediately after this energy transfer, the Tm^{3+} ions move from $^3H_5$ to $^3F_4$ energy level through rapid multiphonon relaxations. This improves the amplification and ASE generation at around 1900-nm region. Another peak observed at 2050-nm region is the third-order generation light from the 793-nm laser diode. As shown in Fig. 4, TB-b exhibits the ASE power with the highest output peak of −47.2 dBm centered at 1880-nm region. The peak ASE powers of TB-c and TB-a are obtained at −51.3 dBm and −58.3 dBm, respectively. This is attributed to the gain medium of TB-b, which has the highest Tm^{3+} and Bi^{3+} concentrations compared with other samples. Using TB-b, the 3-dB bandwidth of the ASE spectrum covers from 1817 nm to 1984 nm, while 10-dB bandwidth covers from 1769 nm to 2078 nm, as depicted in Fig. 4.

Fig. 5 shows the ASE spectra of the different lengths of TB-b under 793-nm wavelength excitation when the pump power is fixed at 200 mW. In the experiment, the gain medium length was varied from 0.5 to 2.5 m. As seen in the figure, the power of the broadband ASE spectrum rises drastically as the TB-b length increases from 0.5 m to the optimum length of 1.0 m. This is attributed to the additional Tm^{3+} and Bi^{3+} from the longer length, which can absorb more pump power and emit stronger ASE light. However, the ASE power drops as the gain medium length is further increased due to saturation effect. The unused Tm^{3+} and Bi^{3+} will absorb the 1880-nm ASE and reduces the output power of the ASE spectrum. It is also observed that the peak ASE wavelength is shifted to a longer wavelength as the TB-b length increases from 1.0 m to 2.5 m. This is attributed to the shorter wavelength ASE being absorbed by the unused Tm^{3+} and Bi^{3+} and emitted at a longer wavelength and thus shifts the peak wavelength to a longer wavelength. The

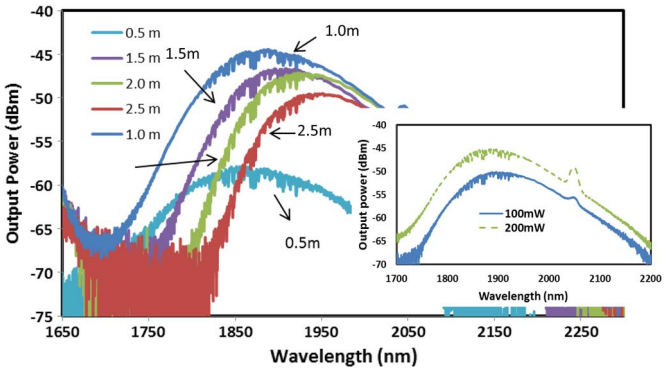

Fig. 5. ASE spectra at different TB-b lengths at the fixed 793-nm pump power of 200 mW. Inset shows the ASE spectrum obtained with 1-m-long TB-b at two different 793-nm pump powers.

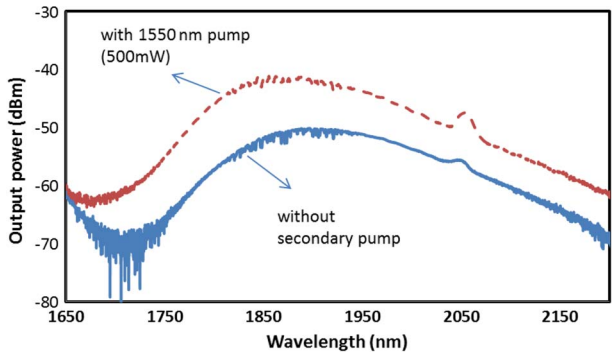

Fig. 6. ASE spectrum with and without 500 mW of 1550-nm pumping when the primary pump of 793 nm is fixed at 100 mW.

inset in Fig. 5 compares the ASE spectrum obtained at two different pumping powers of 100 mW and 200 mW when TB-b is fixed at 1.0 m. It is observed that the ASE spectrum power increases with the pump power. Further increase of pump power is expected to further raise the attainable power of the ASE spectrum.

The effect of a secondary pump of 1550 nm on the performance of the ASE spectrum was also investigated. Fig. 6 shows the ASE spectrum of the TB-b with and without a secondary pump of 1550 nm when the primary pump of 793 nm is fixed at 100 mW. As seen in the figure, the ASE power is increased by more than 10 dB at 1850-nm region as the 500-mW secondary pump is injected into the gain medium. This is due to the Tm^{3+} excitation to $^3F_4$ level, which enhances the population inversion and thus increases the output intensity of the ASE via $^3F_4 \rightarrow {}^3H_6$ transition, particularly at 1850-nm region.

4. Conclusion

ASE generation in a newly developed TBF has been demonstrated, which operates at 1880-nm region with 793-nm pumping. The gain medium has been drawn from a preform, which has been fabricated using an MCVD and solution doping processes. The fabricated TBF has the highest Bi^{3+} and Tm^{3+} dopant concentrations of 0.35 wt.% and 0.9 wt.%. The TBF has been forward pumped by a 793-nm single mode laser to generate ASE peaking at -47.2 dBm with 3-dB spectral width ranging from 1817 to 1984 nm. The ASE generation is due to the transition of thulium ion from $^3F_4$ to $^3H_6$ and enhanced by energy transfer from Bi^{3+} to Tm^{3+}. The ASE can be also improved by injecting a secondary pump at 1550 nm.

Acknowledgment

The authors acknowledge a strong support from the director and the staff members of the Central Glass and Ceramic Research Institute (CGCRI).

References

[1] H. Lin and C.-H. Chang, "High power C+L-band Erbium ASE source using optical circulator with double-pass and bidirectional pumping configuration," *Opt. Exp.*, vol. 12, no. 25, pp. 6135–6140, Dec. 2004.
[2] X. S. Cheng, H. Ahmad, and S. W. Harun, "Broadband ASE source using bismuth-based erbium-doped fibers in double-pass set-up," *Microw. Opt. Technol. Lett.*, vol. 52, no. 7, pp. 1636–1638, Jul. 2010.
[3] Z. Zhang, A. J. Boyland, J. K. Sahu, W. A. Clarkson, and M. Ibsen, "High-power single-frequency thulium-doped fiber DBR laser at 1943 nm," *IEEE Photon. Technol. Lett.*, vol. 23, no. 7, pp. 417–419, Apr. 2011.
[4] R. Gumenyuk, I. Vartiainen, H. Tuovinen, and O. G. Okhotnikov, "Dissipative dispersion-managed soliton 2μm thulium/holmium fiber laser," *Opt. Lett.*, vol. 36, no. 5, pp. 609–611, Mar. 2011.
[5] L. I. Bulatov, V. V. Dvoyrin, V. M. Mashinsky, E. M. Dianov, A. P. Suhorukov, A. A. Umnikov, and A. N. Guryanov, "Absorption and scattering in bismuth-doped optical fibers," *Bull. Russian Acad. Sci.—Phys.*, vol. 72, no. 1, pp. 98–102, Jan. 2008.

Abstract: A lasing action from a newly developed double-clad Tm^{3+}/Yb^{3+} co-doped yttria-alumino-silicate fiber (TYDF) is demonstrated based on cladding pumping technique. The TYDF used was drawn from D-shape preform, which was fabricated using a modified chemical vapor deposition (MCVD) process in conjunction with a solution doping technique. The $Tm^{3+}$and Yb^{3+} ions concentrations in this fiber are 5.55×10^{19} and 15.52×10^{19} ions/cc, respectively. The fiber laser operates at wavelength of 1948.4 and 1947.2 nm with pump power thresholds of 0.6 and 1.0 W for 915 and 940 nm pumping, respectively. The maximum output power of 10.5 mW was achieved with the 915 nm pumping at the maximum pump power of 1.5 W. It is found that the laser is more efficient with 915 nm pumping compared to 940 nm pumping.

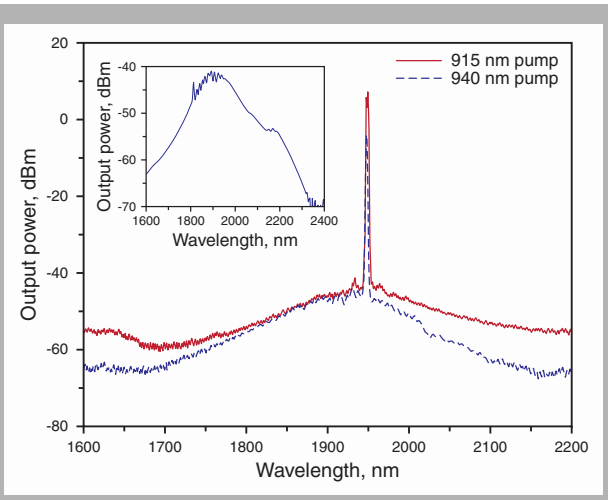

Output spectrum of the laser at different pump wavelength. Inset shows the ASE spectrum for TYDF using 0.6 W, 915 nm pumping

Fiber laser at 2 micron region using double-clad thulium/ytterbium co-doped yttria-alumino-silicate fiber

S.W. Harun, [1,2,*] *N. Saidin,* [1] *S.S.A. Damanhuri,* [1] *H. Ahmad,* [2] *A. Halder,* [3] *M.C. Paul,* [3] *S. Das,* [3] *M. Pal,* [3] *and S.K. Bhadra* [3]

[1] Department of Electrical Engineering, Faculty of Engineering, University of Malaya, 50603 Kuala Lumpur, Malaysia
[2] Photonics Laboratory, Department of Physics, University of Malaya, 50603 Kuala Lumpur, Malaysia
[3] Fiber Optics and Photonics Division, Central Glass & Ceramic Research Institute, CSIR, Kolkata, India

Received: 23 July 2011, Revised: 26 July 2011, Accepted: 29 July 2011
Published online: 1 November 2011

Key words: thulium/ytterbium co-doped fiber laser; double-clad; 2 micron laser

1. Introduction

2 μm thulium and thulium-pumped holmium laser sources are of interest for many application in the scientific, defense and medical fields [1–5]. The 2 μm radiation has a strong absorbtion in water and biological tissues and thus these lasers have a number of potential applications in the medical field. Incisions in porcine tissue and chicken breast have been recently demonstrated with a 1.98 μm continuous wave Tm-doped fiber laser (TDFL) [6,7]. Also, the penetration depth of 2 μm laser radiation matches with the subcutaneous depth of the pain nerve receptors in the skin such that the 2 μm laser makes an near-ideal source for experimental pain research as the damage on the skin surface can be minimized [8]. Recently, tissue interactions with a Q-switched TDFL have been reported [9].

The TDFL uses thulium-doped fiber as a gain medium, which exhibits a significant advantage over other rare-earth ions in that the slope efficiency can exceed the Stokes limit [10–13]. They can efficiently pumped at ~790,

* Corresponding author: e-mail: swharun@um.edu.my

~ 1200, or ~ 1600 nm [14–17]. A quantum efficiency near 2 μm can be achieved for thulium ions' $^3F_4 \rightarrow {}^3H_6$ transition because of the so-called cross-relaxation energy transfer between thulium ions. During the cross-relaxation energy transfer process, two ground-level thulium ions can be excited to the upper lasing level of the $^3F_4 \rightarrow {}^3H_6$ transition by absorbing only one pump photon near 790 nm, which means one excited Tm^{3+} ion at the $^3H_4$ level generates two Tm^{3+} ions at the $^3F_4$ upper laser level [18]. However, the availability of high-power diodes in this wavelength range is relatively poor as well as very costly. Pumping TDFs at 1200 or 1600 nm is complicated by the need for an intermediate laser source, since high-power laser diodes are not commercially available at this wavelength.

An alternative approach is to co-dope with Yb^{3+} and pump at 910 – 980 nm. Tm^{3+} has a level ($^3H_5$), which is (quasi-) resonant with the excited Yb^{3+}-level ($^2F_{5/2}$), allowing for the possibility of sensitization of TDFs with Yb^{3+} , similar to the case of ytterbium erbium doped fiber [19–20]. In this paper, a thulium ytterbium co-doped fiber laser (TYDFL) is demonstrated by using a newly developed double-clad Tm^{3+}/Yb^{3+} co-doped alumino-silicate fiber (TYDF) as a gain medium. The TYDF is obtained by drawing a D-shape preform, which has been fabricated using a deposition of porous layer by the modified chemical vapor deposition (MCVD) process in conjunction with solution doping technique. In this TYDF, pump energy is absorbed by the Yb^{3+} ions and is then transferred non-radiatively to the Tm^{3+} ions, which emit light in the 2 μm wavelength range.

2. Fabrication of TYDF

TYDF used in this experiment is drawn from a preform, which was fabricated using the MCVD and solution doping techniques. The core of the preform is a combination of alumino silicate and yttrium alumino silicate fabricated through the deposition of multiple porous phosphosilicate layers at several deposition temperature and varied pre-sintering temperatures. This large core is then doped with solution doping technique using a suitable strength of dopants precursor. In the solution doping process, phosphosilicate layer is soaked into a suitable strength of alcoholic solution of $YbCl_3{\cdot}6H_2O$, $TmCl_3{\cdot}6H_2O$, $AlCl_3{\cdot}6H_2O$ and $YCl_3{\cdot}6H_2O$ to incorporate the dopants. All co-dopants that are present in the solution go into the silica glass matrix during the sintering stage after the solution soaking process. During collapsing process, the core glass is phase separated into silica rich and silica deficient areas (Fig. 1) so that it forms a glass matrix with a combination of Tm_2O_3 and Yb_2O_3 doped yttria alumino rich and deficient phase-separated silica glass matrix. From energy-dispersive X-ray (EDX) analyzes Yb^{3+} and Tm^{3+} ions are found to be present in both regions. The concentration level of doping ions

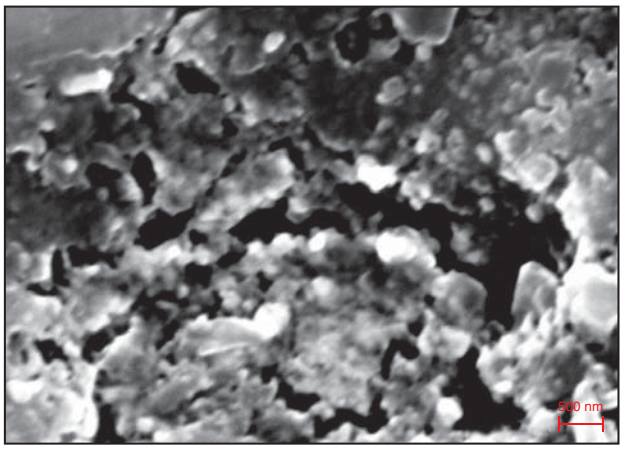

Figure 1 (online color at www.lphys.org) Scanning electron microscope picture of the core region of Tm_2O_3 and Yb_2O_3 co-doped yttria-alumino silica glass based optical preform

is controlled through the change of porosity of unsintered SiO_2 layer by manipulating the temperature, time of soaking and concentration levels of components in the solution.

Such silica glass matrix is then fabricated into a double-clad D-shaped fiber. As opposed to the conventional single mode fiber where the pump light is coupled directly into the core, the pump light travels down the fiber in the first cladding and get absorbed by the dopants, in this case the Yb ions when it overlaps with the core. The D-shape geometry of the cladding improves the pump absorption and furthermore it is cheaper to be fabricated compared to other geometries such as hexagonal and rectangular. Al ions introduced into the host network act as a silica network modifier to lower the host's phonon energy. Low phonon energy in host network will decrease non radiative loss due to multiphonon relaxation during electronic transition of $^3H_4$ to $^3H_5$ level for Tm ions, increasing blue emission intensities, which is a radiative emission. Al ions also deter clustering by distributing the rare earth ions homogenously. Tm ions have a tendency to cluster together especially at high doping concentrations and thus preventing lasing to occur due to Tm-Tm ions energy transfer. Adding a modifier into the silica network to lower its phonon energy have its drawbacks as it affects the host's environment with poor mechanical, thermal and chemical stability. Thus, a good compromise between lower phonon energy and the host's environment stability must be taken into consideration for efficient device operation. Yttrium oxide is chosen only to maximize the probability of lasing by decreasing phonon energy of glass host.

The distribution of the dopants along the whole diameter of the fabricated TYDF preform sample is analyzed using an electron probe micro-analyzer (EPMA). The polished preform sample of thickness 2.1 mm is analyzed with the maximum spatial resolution of 30 μm after applying thin graphite coating layer for elemental distribu-

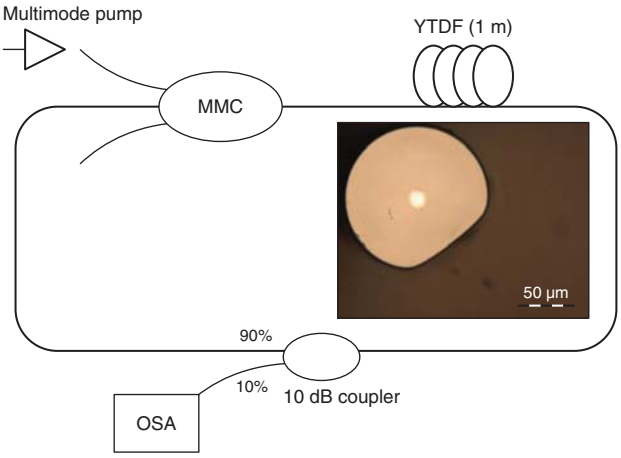

Figure 2 (online color at www.lphys.org) Schematic diagram of the experimental setup for the proposed TYDFL. Inset shows the microscopic view of the D-shaped TYDF cross-section

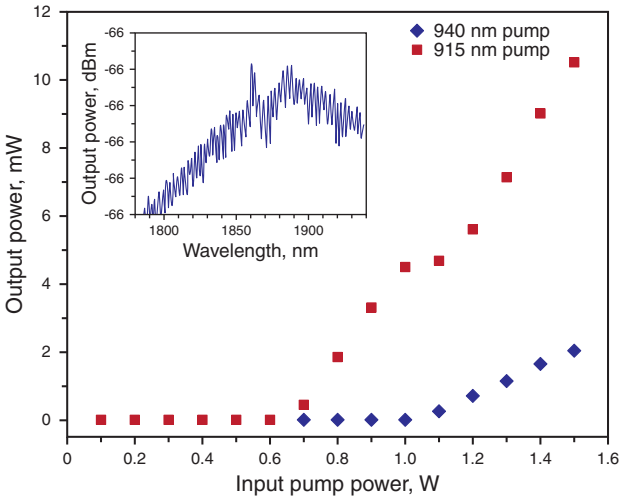

Figure 3 (online color at www.lphys.org) Laser output power at $\sim$ 1940 nm against the input pump power. Inset shows the attenuated output spectrum of the TYDFL with 980 nm pumping when the input pump power is fixed at 1.3 W

tion along the diameter of the central core. From EPMA results, it was found that the fabricated fiber has a core composition of $Al_2O_3 - Y_2O_3 - Tm_2O_3 - Yb_2O_3$ with the doping levels of Tm^{3+} and Yb^{3+} ions are measured to be around 5.55×10^{19} and 15.52×10^{19} ions/cc, respectively. NA and core diameter of the fabricated TYDF are measured to be 0.26, and 17.5 μm, respectively.

3. Experiment

The experimental setup of the proposed TYDFL is depicted in Fig. 2. It consists of a piece of the fabricated TYDF as a gain medium, a multimode combiner and a 10 dB output coupled to the optical spectrum analyzer (OSA). Inset of Fig. 2 shows the cross section of the double clad TYDF with D-shape structure and an inner cladding diameter of around 100 μm. The TYDF length is fixed at 1 m, which optimized with the pump power. A 915 nm laser diode pump is coupled into the TYDF *via* the multimode combiner. The pump source is a multimode laser diode (LD) with a center wavelength of 915 nm. The pump light is coupled into the YDF through a multimode coupler. The amplified spontaneous emission (ASE) light oscillates in the ring cavity to generate laser at 2.0 μm region. The output of the TYDFL is tapped out using a 10 dB output coupler, which allows 90% of the light to oscillate in the cavity laser and characterized by the OSA with a resolution of 0.015 nm. The experiment is repeated using other pump wavelengths of 940 and 980 nm for comparison purpose. This laser device contains no adjustable parts and can only be controlled externally by the amount of pump power that is injected.

Fig. 3 shows the output power of the proposed TYDFL against the launched pump power for two different pump wavelengths of 915 and 940 nm. As shown in the figure, lasing starts at a different threshold power depending on the TYDF lengths and the laser output is observed to linearly increase with the launched pump power. The threshold pump powers are obtained at 0.6 and 1.0 W with 915 and 940 nm pumping, respectively. A maximum output power of 10.5 mW was achieved with the 915 nm pumping at the maximum pump power of 1.5 W. The laser output showed no evidence of roll-over even at the highest output power, which was limited only by available pump power. There was no evidence of any power limitation due to nonlinear scattering, nor was any stimulated Raman scattering observed. Inset of Fig. 3 shows the output spectrum of the attenuated laser with 980 nm pumping. However, there is no lasing occurred as shown in the inset figure. The slope efficiency of 1.14% is obtained with 915 nm pumping, which is so much higher than that of 940 nm pumping. The slope efficiency is only 0.11% with 940 nm pumping. This shows that the absorption and emission cross sections of the fabricated TYDF is higher in 915 nm compared to that of two other wavelengths. The low output power mainly due to the cladding pump that provides insufficient absorption of a pump light as well as the un-optimized fiber's fabrication process.

Fig. 4 shows the output spectrum of the TYDFL at different pump wavelength with the input pump power of 1.1 W. Inset of Fig. 4 shows the ASE spectrum, which is obtained by pumping the TYDF with 915 nm laser at 0.6 W (below laser threshold). The ASE spectrum peaks at around 1900 nm with 3 dB bandwidth of around 150 nm. Consequently, the TYDFL operates at 1948.4 and 1947.2 nm with 915 and 940 nm pumping, respectively, as shown in Fig. 4. The peak power of the laser is also

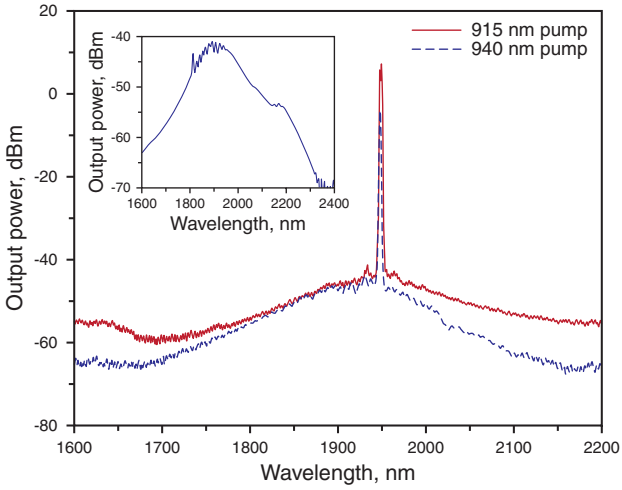

Figure 4 (online color at www.lphys.org) Output spectrum of the laser at different pump wavelength. Inset shows the ASE spectrum for TYDF using 0.6 W, 915 nm pumping

observed to be higher with 915 nm pumping compared to that of the 940 nm pumping due to the same reason as explained earlier. The peak signal-to-noise-ratios are obtained at 50 and 40 dB with 915 and 940 nm pumping, respectively. This is attributed to the population inversion which is more efficient with 915 nm pumping compared to 940 nm pumping. These results show that the 915 nm is the best pumping wavelength for the proposed TYDFL. The efficiency of the proposed TYDFL can be further improved by using a linear configuration with fiber Bragg gratings to reduce the cavity loss.

4. Conclusion

A double-clad TYDFL operating in 2 μm region is demonstrated based on cladding pumping technique using a newly developed TYDF. The fiber was drawn from D-shape preform, which was fabricated using the MCVD and solution doping processes. The fabricated fiber has Tm^{3+} and Yb^{3+} ions concentrations of 5.55×10^{19} and 15.52×10^{19} ions/cc, respectively. The fiber laser operates at wavelength of 1948.4 and 1947.2 nm with pump power thresholds of 0.6 and 1.0 W for 915 and 940 nm pumping, respectively. The maximum output power of 10.5 mW was achieved with the 915 nm pumping at the maximum pump power of 1.5 W. The slope efficiency of the laser is 1.14%, which is more efficient than 940 nm pumping. No lasing action is observed with 980 nm pumping.

Acknowledgements This work was supported by the University of Malaya under UM/MOHE HIR Grant (Account Number: D000009-16001).

References

[1] M.J.F. Digonnet (ed.), Rare-Earth-Doped Fiber Lasers and Amplifiers, 2nd ed. (CRC Press, 2001).
[2] J. Li, S.H. Yang, H.Y. Zhang, W. Xie, and C.M. Zhao, Laser Phys. **20**, 1806–1809 (2010).
[3] A.S. Kurkov, Ya.E. Sadovnikova, A.V. Marakulin, and E.M. Sholokhov, Laser Phys. Lett. **7**, 795–797 (2010).
[4] A.S.K. Sarp and M. Gülsoy, Proc. SPIE **7884**, 78840K (2011).
[5] N.M. Fried, R.L. Blackmon, and P.B. Irby, Proc. SPIE **7914**, 791402 (2011).
[6] M.C. Pierce, S.D. Jackson, P.S. Golding, B. Dickinson, M.R. Dickinson, T.A. King, and P. Sloan, Proc. SPIE **4253**, 144 (2001).
[7] M.C. Pierce, S.D. Jackson, M.R. Dickinson, and T.A. King, Laser Surg. Med. **25**, 407–413 (1999).
[8] E. Opsommer, T. Weiss, W.H.R. Miltner, and L. Plaghki, Clin. Neurophysiol. **112**, 1868–1874 (2001).
[9] A.F. El-Sherif and T.A. King, Laser Med. Sci. **18**, 139–147 (2003).
[10] A.S. Kurkov, E.M. Sholokhov, A.V. Marakulin, and L.A. Minashina, Laser Phys. Lett. **7**, 587–590 (2010).
[11] F. Wang, D.Y. Shen, D.Y. Fan, and Q.S. Lu, Laser Phys. Lett. **7**, 450–453 (2010).
[12] Y. Tian, J.Q. Zhao, W. Gao, W. Wang, and Y.Z. Wang, Laser Phys. Lett. **7**, 298–302 (2010).
[13] D.Z. Yang, W. Liu, T. Chen, W. Ye, and Y.H. Shen, Laser Phys. **20**, 1752–1755 (2010).
[14] D.C. Hanna, I.R. Perry, J.R. Lincoln, and J.E. Townsend, Opt. Commun. **80**, 52–56 (1990).
[15] T. Yamamoto, Y. Miyajima, and T. Komukai, Electron. Lett. **30**, 220–221 (1994).
[16] W.A. Clarkson, N.P. Barnes, P.W. Turner, J. Nilsson, and D.C. Hanna, Opt. Lett. **27**, 1989–1991 (2002).
[17] S.W. Harun, M.R.A. Moghaddam, and H. Ahmad, Laser Phys. **20**, 1899–1901 (2010).
[18] S.D. Jackson, Opt. Commun. **230**, 197–203 (2004).
[19] J.E. Townsend, W.L. Barnes, K.P. Jedrzejewski, and S.G. Grubb, Electron. Lett. **27**, 1958–1959 (1991).
[20] B. Peng, H. Zhang, M. Gong, and P. Yan, Laser Phys. **19**, 2019–2022 (2009).